



UvA-DARE (Digital Academic Repository)

Endothelial tip cells in culture

An in vitro approach for studies of angiogenesis

Dallinga, M.G.

Publication date

2020

Document Version

Final published version

License

Other

[Link to publication](#)

Citation for published version (APA):

Dallinga, M. G. (2020). *Endothelial tip cells in culture: An in vitro approach for studies of angiogenesis*. [Thesis, fully internal, Universiteit van Amsterdam].

General rights

It is not permitted to download or to forward/distribute the text or part of it without the consent of the author(s) and/or copyright holder(s), other than for strictly personal, individual use, unless the work is under an open content license (like Creative Commons).

Disclaimer/Complaints regulations

If you believe that digital publication of certain material infringes any of your rights or (privacy) interests, please let the Library know, stating your reasons. In case of a legitimate complaint, the Library will make the material inaccessible and/or remove it from the website. Please Ask the Library: <https://uba.uva.nl/en/contact>, or a letter to: Library of the University of Amsterdam, Secretariat, Singel 425, 1012 WP Amsterdam, The Netherlands. You will be contacted as soon as possible.

The background of the cover is a grayscale micrograph showing a dense field of endothelial cells. Overlaid on this are three distinct, colored structures: a red, elongated, and somewhat irregular structure in the upper left; a blue, jagged, and branching structure in the upper right; and a purple, highly branched and complex structure in the lower right. A semi-transparent white rectangular box is centered on the page, containing the title and author information.

ENDOTHELIAL TIP CELLS IN CULTURE
An in vitro approach for studies of angiogenesis

M.G. DALLINGA

**ENDOTHELIAL TIP CELLS IN CULTURE: AN *IN VITRO*
APPROACH FOR STUDIES OF ANGIOGENESIS**

Marchien Dallinga

Cover, layout and printing: Off Page, Amsterdam

The printing of this thesis was financially supported by the Rotterdamse Stichting Blindenbelangen, Landelijke Stichting voor Blinden en Slechtzienden, Oculenti, Rockmed, Synga, and the department of Ophthalmology, Amsterdam University Medical Center.

ENDOTHELIAL TIP CELLS IN CULTURE: AN *IN VITRO* APPROACH FOR STUDIES OF ANGIOGENESIS

ACADEMISCH PROEFSCHRIFT

ter verkrijging van de graad van doctor

aan de Universiteit van Amsterdam

op gezag van de Rector Magnificus

prof. dr. ir. K.I.J. Maex

ten overstaan van een door het College voor Promoties ingestelde commissie,

in het openbaar te verdedigen in de Aula der Universiteit

op vrijdag 4 december 2020, te 11 uur

door Marchien Geesje Dallinga

geboren te Wageningen

PROMOTIECOMMISSIE:

Promotores:	prof. dr. C.J.F. van Noorden	AMC-UvA
	prof. dr. R.O. Schlingemann	AMC-UvA
Co-promotor:	dr. I. Klaassen	AMC-UvA
Overige leden:	prof. dr. E.M.A. Aronica	AMC-UvA
	prof. dr. C.J.M. de Vries	AMC-UvA
	dr. J.W. Wilmink	AMC-UvA
	prof. dr. M.J. Jager	Universiteit Leiden
	prof. dr. C.C.W. Klaver	Erasmus Universiteit Rotterdam
	dr. P. Nowak-Sliwiska	Université de Genève

Faculteit der Geneeskunde

TABLE OF CONTENTS

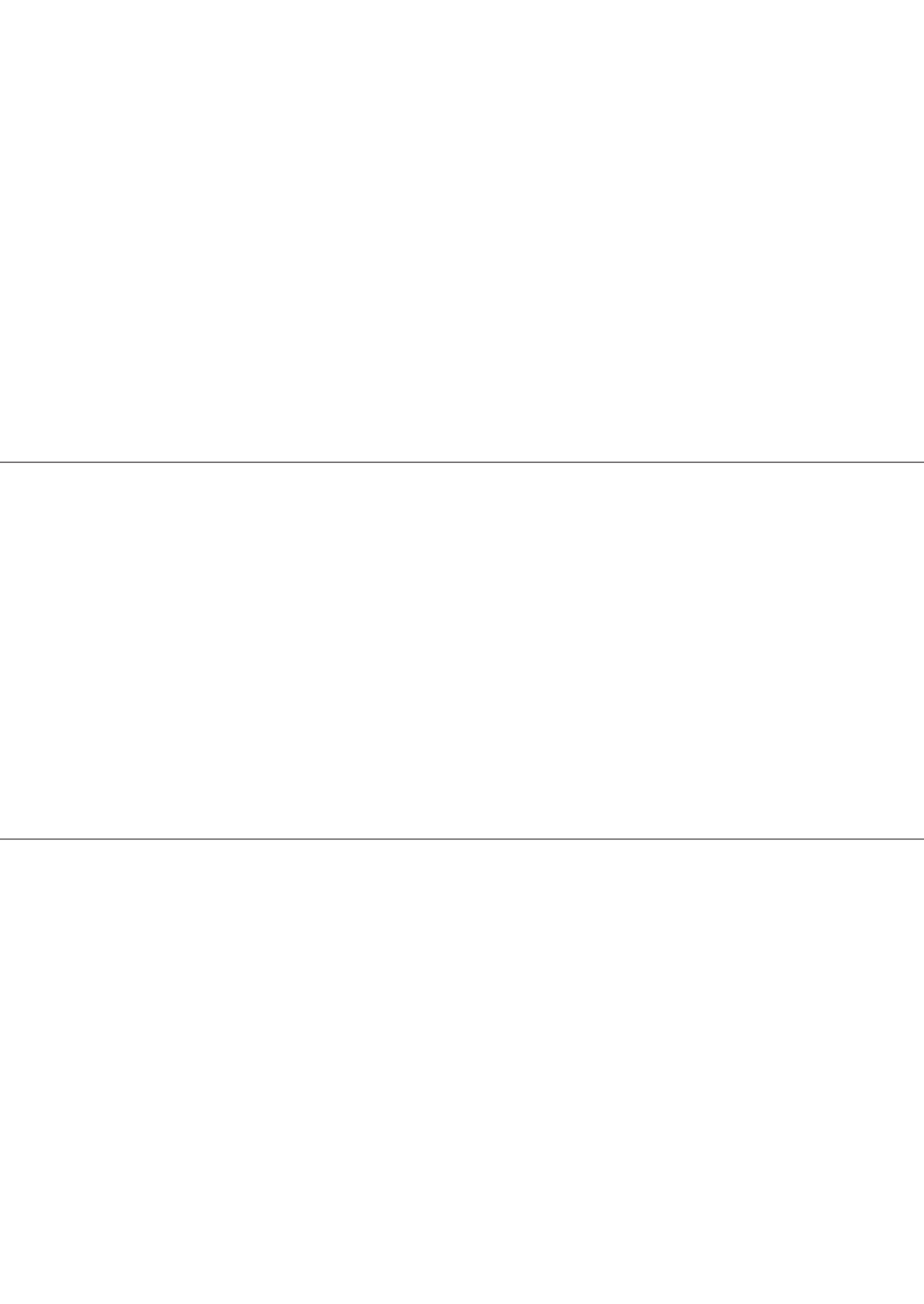
Chapter 1	Introduction	9
	1.1 Introduction and aim of the thesis	11
	1.2 Tip cells in angiogenesis	17
	1.3 Practical aspects of the study of CD34 ⁺ endothelial tip cells <i>in vitro</i>	35
	References	40
Chapter 2	Tip cell-specific proteins	45
	2.1 CD34 promotes pathological epi-retinal neovascularization in a mouse model of oxygen-induced retinopathy	47
	2.2 IGF2 and IGF1R identified as novel tip cell genes in primary microvascular endothelial cell monolayers	67
	2.3 IGF-binding proteins 3 and 4 are regulators of sprouting angiogenesis	85
	2.4 The role of the insulin-like growth factor family in endothelial tip and stalk cell biology in angiogenesis	103
	References	116
Chapter 3	Effects of angiogenesis inhibitors on endothelial tip cells <i>in vitro</i>	127
	3.1 Rapid optimization of drug combinations for the optimal angiostatic treatment of cancer	129
	3.2 Anti-angiogenic effects of crenolanib are mediated by mitotic modulation independently of PDGFR expression	147
	References	166
Chapter 4	Identification of interactions between endothelial tip cells, non-tip cells and extracellular proteins	173
	4.1 Computational screening of tip and stalk cell behavior proposes a role for apelin signaling in sprout progression	175
	4.2 Role of heparan sulfate and neuropilin 2 in VEGFA signaling in human endothelial tip cells and non-tip cells in angiogenesis	205
	4.3 Role of Sulfatase 2 in Lipoprotein Metabolism and Angiogenesis	221
	References	229
Chapter 5	Summary and Discussion	239
	5.1 Summary and Discussion	241
	References	247

Chapter 6	Appendices	249
	6.1 Samenvatting	251
	6.2 Publications	259
	6.3 Authors and contributions	265
	6.4 Portfolio	271
	6.5 Dankwoord	277
	6.6 Curriculum vitae	283





INTRODUCTION



A decorative graphic consisting of two horizontal lines, one at the top and one at the bottom. Between these lines are three gray shapes: a tall, narrow rectangle on the left with a diagonal cutout at the top-left corner, a smaller square in the center, and another tall, narrow rectangle on the right with a diagonal cutout at the top-right corner.

INTRODUCTION AND AIM OF THE THESIS

INTRODUCTION AND AIM OF THE THESIS

Blood vessel outgrowth from existing vessels, or angiogenesis, is a physiological process that can occur anywhere in the body, usually as part of wound healing processes. Since the eye is the organ with the highest oxygen demand and blood flow per unit tissue in the human body (1), it is not surprising that diseases in which the ocular vascular networks are compromised, especially in the retina, can have severe consequences for vision. Examples of such diseases include diabetic retinopathy and retinopathy of prematurity. When the retinal blood vessels cannot fulfill the oxygen demand, hypoxia will occur. The retinal tissue responds by producing growth factors that induce angiogenesis to restore the blood flow. This is a physiological response to restore tissue integrity, but it can have negative consequences as the new blood vessels may remain immature and leaky for prolonged periods, which compromises retinal function and causes vision loss. Mature blood vessels in the retina are lined by a single layer of endothelial cells that are tightly bound to each other by adherens junctions and tight junctions. The endothelial cells are supported by other cell types such as pericytes and the extracellular matrix (2). In the healthy retina, the so-called blood-retinal barrier is formed in this way. Unlike mature blood vessels, angiogenic blood vessel sprouts are immature and are adapted to the wound healing milieu, lacking tight junctions, mature pericytes and a proper extracellular matrix, which allows them to grow and make them leaky for plasma proteins.

Blood vessel sprouts are composed of specific subtypes of endothelial cells. A detailed introduction of these endothelial cell subtypes is presented in **Chapter 1.2**. In short, a blood vessel sprout is led by a tip cell that is followed by stalk cells and phalanx cells. Tip cells are characterized by the extension of filopodia, which are essential for migration towards hypoxic tissue areas. The stalk cells proliferate to allow elongation of the vessel sprout, whereas phalanx cells are furthest away from the tip cells and form the mature part of the new vessel. Because of their leading role in vessel sprouts and their unique protein expression (3-5), tip cells form an attractive selective target for anti-angiogenic therapy. Consequently, endothelial tip cells are subject of many pre-clinical studies that aim to identify specific targets for novel therapies to treat retinal diseases.

Thus far, most of the research on tip cells has been performed in animal models to identify possible selective molecular therapeutic targets in tip cells. The use of animal models should preferably be avoided as much as possible because of ethical reasons, which is why we explored the possibilities of studying tip cells *in vitro*. The Ocular Angiogenesis Group AMC has shown for the first time that tip cells can be identified in endothelial cell cultures by expression of the protein CD34 (3). In the present thesis, this *in vitro* tip cell model was used to further characterize tip cells with respect to growth factors and pathways involved. As tip cell studies *in vitro* are relatively new, practical aspects of endothelial cell cultures are highlighted in **Chapter 1.3**.

The studies presented in this thesis describe 3 approaches to study tip cells *in vitro*:

- » Identification of endothelial tip cell-specific proteins,
- » Effects of angiogenesis inhibitors on endothelial tip cells *in vitro*, and
- » Identification of interactions between endothelial tip cells, non-tip cells and extracellular proteins.

Tip cell-specific proteins

A gene/protein that is specifically expressed by tip cells and at the same time essential for the phenotype may be a very attractive therapeutic target to inhibit angiogenesis. Since other cells do not express the gene, or to a lesser extent, side effects are avoided or at least limited. In the first part of this thesis, we have explored a number of these tip cell genes. In **Chapter 2.1** we investigated the role of CD34 in a mouse model during angiogenesis in the retina driven by hypoxia. In **Chapter 2.2**, the identification of insulin-like growth factor 2 (IGF2) and insulin-like growth factor 1 receptor (IGF1R) as novel tip cell genes is described. **Chapter 2.3** further explores the roles of IGF2 and IGF1R in tip cell maintenance *in vitro* and shows that other members of the IGF protein family, the IGF binding proteins 3 and 4 (IGFBP3 and IGFBP4), are also involved in sprouting angiogenesis. **Chapter 2.4** reviews the literature on this subject and describes the role of the members of the IGF family in angiogenesis and tip cell maintenance.

Inhibitors of angiogenesis

Angiogenesis is one of the hallmarks of cancer, and has been extensively studied as a potential therapeutic target (6, 7). When a tumor grows and their size becomes larger than 1-2 mm, supply of oxygen and nutrients and removal of carbon dioxide and waste products by diffusion is not sufficient anymore. As a consequence, hypoxia occurs which induces angiogenesis to construct a blood vessel network. Therefore, the idea of inhibiting angiogenesis to prevent tumor growth was introduced by Judah Folkman and co-workers as an attractive therapeutic strategy in oncology (8). However, targeting tumor angiogenesis has never had the therapeutic impact that was expected and angiogenesis inhibitors have had only marginal success in the cancer clinic. This is possibly due to compensatory mechanisms such as vascular mimicry (9, 10) or alternative angiogenic pathways (11). Angiogenesis inhibitors have often been tested extensively to observe their effects on the overall vascular network, but the direct and specific effects on tip cells have often been largely neglected, due to the lack of adequate experimental models. **Chapter 3** of this thesis is focused on the effects of anti-angiogenic compounds on tip cells. An algorithm to determine optimal combinations of angiogenesis inhibitors is described in **Chapter 3.1**. **Chapter 3.2** describes a pre-clinical study on Crenolanib, a novel angiogenesis inhibitor that affects non-tip endothelial cells rather than tip cells.

Interactions of tip cells with their microenvironment

The tip cell and stalk cell subtypes are dynamic, reversible and interchangeable (12). The best fitting cell directs the sprout as tip cell, which makes the whole process of angiogenesis more efficient, because too many tip cells would cause the generation of too many sprouts. Interactions between different endothelial subtypes and their microenvironment play an important role in determining into which subtype a cell will differentiate. Culturing tip cells *in vitro* allowed us to isolate tip cells and stalk cells to study proteins in the microenvironment and on the cell surface that induce differentiation of the cells into a specific subtype or induce characteristics of the subtypes, as shown in **Chapter 4**. **Chapter 4.1** describes a combined *in silico* and *in vitro* study of interactions between tip cells and other endothelial cells via apelin and its receptor. In **Chapter 4.2**, the effects of extracellular matrix binding of the pro-angiogenic vascular endothelial growth factor (VEGF) on tip cells and non-tip cells are described. **Chapter 4.3** presents a review of sulfatase 2, a modulator of extracellular matrix proteins in the context of angiogenesis.

In conclusion, this thesis covers our research performed on CD34⁺ tip cells *in vitro*. It shows that studying tip cells in cultures of human endothelial cells has several important advantages over the use of animal models. These include: 1) lower costs and increased efficiency, 2) superior comparability to human diseases, and 3) lack of ethical objections of using animal models. Studying tip cells *in vitro* has increased our knowledge on tip cell regulation. Continuation of this research may result in tip cell-specific targets for future anti-angiogenic therapies, and thereby hopefully a reduction of vision loss in patients with retinal diseases involving angiogenesis.

Dallinga, Marchien G, Ocular angiogenesis group, Academic medical center, Amsterdam, The Netherlands

Boas, Sonja E M, Life sciences group, Centrum Wiskunde & Informatica, Amsterdam, The Netherlands

Klaassen, Ingeborg, Ocular angiogenesis group, Academic medical center, Amsterdam, The Netherlands

Merks, Roeland H M, Life Sciences Group, Centrum Wiskunde & Informatica, Amsterdam, The Netherlands and Mathematical Institute, Leiden University, Leiden, The Netherlands

van Noorden, Cornelis J F, Ocular angiogenesis group, Academic medical center, Amsterdam, The Netherlands

Schlingemann, Reinier O, Ocular angiogenesis group, Academic medical center, Amsterdam, The Netherlands

1.2

TIP CELLS IN ANGIOGENESIS

INTRODUCTION

Inhibition or stimulation of blood vessel formation from the pre-existing vascular network, a process called angiogenesis, has potential for therapeutic management of diseases ranging from myocardial infarction and stroke to cancer, and to ophthalmic diseases including diabetic retinopathy and age-related macular degeneration.

The search for targets for pro- and anti-angiogenic therapies has been ongoing for the last century and had a boost from the discovery of a specialized endothelial phenotype, the tip cells, that lead the growing vascular sprouts (13). The tip cell is crucial for angiogenesis, and inhibition or induction of the phenotype would theoretically be an ideal therapeutic strategy for several diseases. By targeting the tip cell only, the mature, quiescent vascular network should not be affected and remain intact. In this way, adverse side effects of therapy may remain limited.

The main driving force behind sprouting is vascular endothelial growth factor (VEGF). Targeting this protein to inhibit angiogenesis has proven to be effective in some diseases such as intestinal cancer and age-related macular degeneration, but does not have the major beneficial effect that was anticipated. It appears that inhibition of VEGF can trigger other pathways to take over stimulating angiogenesis. Furthermore, targeting VEGF can disturb the balance between angiogenesis and fibrosis in neovascular tissue, which in ophthalmic disease can have devastating effects on the visual outcome of patients. Therefore, inhibition of a specific key process, such as the genesis of tip cells or their ability to correctly lead the growing sprout, is an attractive alternative therapeutic strategy.

The current pace of research, together with new research strategies, such as the use of *in silico* prediction models and *in vitro* cell culture experiments, enables rapid expansion of our understanding of key tip cell functions.

Here we review the main characteristics of tip cells, the history of tip cell research, the key regulatory pathways involved in the generation of the tip cell phenotype, and the established and novel suitable tip cell research models.

CHARACTERISTICS

Tip cells are the leading cells of newly forming sprouts during angiogenesis (fig 1). They possess filopodia to aid migration (14-16), and show a low proliferation rate (13, 17). Tip cells prevent the trailing cells from becoming tip cells and force them to take on the more proliferative stalk cell phenotype (18), thus limiting the number of sprouts and allowing for more efficient angiogenesis. However, stochastic differences in concentrations of growth factors surrounding sprouting endothelial cells and intrinsic variability in the expression of regulating proteins such as Notch1, Dll4 and VEGFR2, enable stalk cells to overtake tip cells and take on this phenotype themselves. Theoretically, this elasticity in phenotype results in the selection of cells that are most suitable to lead a sprout and to become a tip cell as well as optimized directional guidance (12). Detailed *in silico* experiments

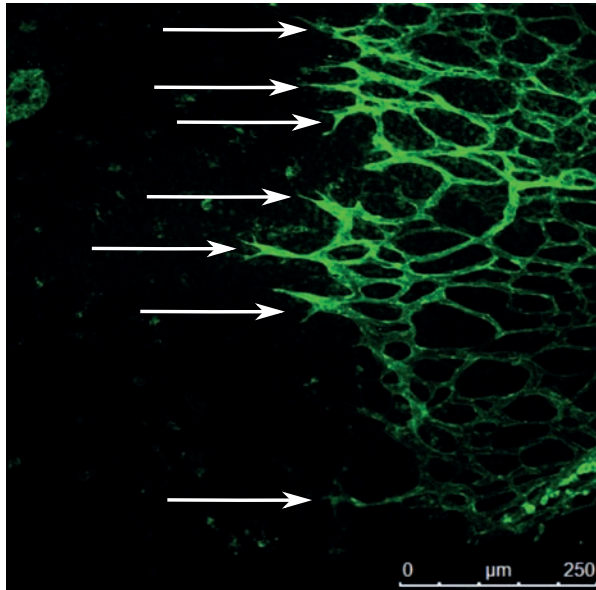
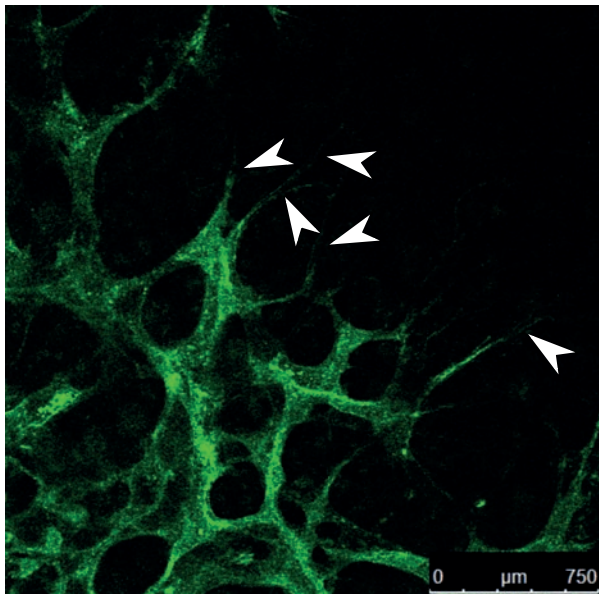
A**B**

Figure 1. Tip cells in the retina of a mouse (white arrow) at the top of newly formed capillaries during angiogenesis at 5 days after birth (P5). The capillaries are stained with Isolectin B4 (green). Higher magnification of the edge of an area in the mouse retina where tip cells at the top of newly-formed capillaries are shown to have filopodia (arrow heads). Bars are 250 μm .

on lateral inhibition have been performed by Bentley et al (19), more details about this can be found in the section on *in silico* models. Recently, it has also become clear that the metabolism of tip cells and stalk cells is different. Endothelial cells rely on glycolysis for their metabolic needs, and VEGF signalling of tip cells elevates the metabolic rate, whereas Dll4-Notch1 signalling reduces glycolysis in stalk cells (20). Cells with known phenotypical characteristics of tip cells are also present in endothelial cell cultures, where they can be identified by their selective CD34 expression (3).

DISCOVERY

Formation of blood vessels has been the subject of scientific research for over 120 years. Early studies used microscopic techniques for the analysis of blood vessel formation, including live chick embryos and transparent chambers implanted in rabbit ears (16, 21). Already then the difference between *de novo* formation of blood vessels from precursor cells and the sprouting of new blood vessels from pre-existing vessels was noticed. The former was termed vasculogenesis, whereas the latter was termed angiogenesis (16). Aspects of angiogenesis, such as the formation of loops by means of anastomosis of sprouts (21) were reported in the following decades.

Most information on angiogenesis came from research in oncology. In 1971, Judah Folkman introduced a novel theory concerning tumour growth (8). He hypothesized that the growth of tumours can be divided into two stages: stage 1, when the tumour is small (up to 2-3 mm), it receives its nutrition through diffusion from surrounding tissue, and stage 2, when the tumour becomes larger it needs its own blood vessels for its growing needs and because of the limitation of diffusion distances. According to Folkman's theory, without angiogenesis, a solid tumour no longer grows in size and cancer cells would have no access to the blood stream to metastasize. Angiogenesis was therefore presented as the promising therapeutic target (8). Even more so because endothelial cells in vessel walls are normal cells with genetically stable DNA, in contrast to cancer cells and therefore, unlike the cancer cells, they cannot become resistant to therapy (22).

This promising effect of anti-angiogenic therapy in cancer patients induced a hype. At that time, little was known about the initiation of angiogenesis, although already in 1895, Roux et al hypothesized that an increased metabolism of tissue is the stimulus for formation of new blood vessels (summarized by Sander) (23), whereas it was also suggested that the stimulus is probably a chemical substance (24). Michaelson (1948) and later Ashton (1966) proposed that in the retina such a factor 'X' was induced by hypoxia (25, 26). A breakthrough confirming the latter hypothesis was achieved in 1974 by Folkman et al., with the discovery of the first tumour angiogenic factor (TAF, supposedly this was basic fibroblast growth factor (FGF)), which induced tumour angiogenesis (27). After this initial discovery, several other pro-angiogenic growth factors were isolated, the most important of which was vascular endothelial growth factor (VEGF), initially named vascular permeability factor because of its ability to induce vascular leakage. Several

anti-VEGF therapies were developed and tested in various types of cancer. Unfortunately, these therapies were not or only mildly successful in a few types of cancer and a new strategy was needed. The cause of the lack of effects of anti-angiogenic therapy in cancer remained unclear for a number of years until the transcription factor hypoxia-inducible factor (HIF)-1 α was discovered. It then became clear that tissue hypoxia can inhibit its breakdown and induce other mechanisms besides production of pro-angiogenic factors, such as anaerobic glycolysis, increased invasion and migration, to keep cells alive under hypoxic conditions.

An alternative strategy to growth factor-directed approaches in anti-angiogenesis therapy is the targeting of the cells leading the angiogenic sprouts, the tip cells. Tip cells have a different phenotype and functions that differ from other endothelial cell phenotypes and therefore express a different set of proteins. It should therefore be possible to target only the tip cells and leave the rest of the vascular network unaffected. Although officially named in 2003, (13) a number of characteristics of tip cells, such as the filopodia (15, 16) and the difference in mitosis rate between the sprouting front and areas behind the front (17), had already been attributed to cells at the sprouting front in angiogenesis. Furthermore, tip cell-like cells had been observed in the development of the brain (termed axonal growth cones (28)), and in the tracheal system of *Drosophila melanogaster* (29). Once researchers realized that tip cells may be a therapeutic target, research accelerated and more details of the tip cell phenotype and its regulation were elucidated, including the ability of endothelial cells to switch between the phenotype of tip cells and that of stalk cells (12), and the signalling pathways involved in tip cell function, such as the VEGF pathway and signalling between tip and stalk cells involving Dll4-Notch1. Unfortunately, a specific marker for tip cells *in vivo* has not been found yet, whereas the *in vitro* marker CD34 was recently described (3).

IMPORTANT PATHWAYS

VEGF

VEGF is the major driving force behind angiogenesis. The VEGF family consists of 6 members: VEGF-A, VEGF-B, VEGF-C, VEGF-D, VEGF-E and placental growth factor (PlGF). Since VEGF-A is the major angiogenesis factor, we will mainly focus on this protein. There are 3 known receptors for VEGF: VEGFR1 (also known as FLT1), VEGFR2 (also known as FLK1 or KDR) and VEGFR3 (also known as FLT4). VEGFR2 and VEGFR3 are membrane-bound receptors with a tyrosine kinase signalling domain. VEGFR1 mainly exists in a soluble form and acts as a negative regulator of signalling induced by VEGF binding to VEGFR2 which is facilitated by the higher affinity of VEGF for VEGFR1 compared to VEGFR2 (30). In mice, the knock-out of each of the three VEGF receptors proved to be lethal at the embryonic stage due to vascular defects, illustrating the importance of all three VEGFRs (30).

Under hypoxic conditions, VEGF production is dramatically increased by stabilization of its mRNA. It can induce angiogenesis in *in vitro* models of angiogenesis, but also in *in vivo* models such as the aortic ring model and the chick chorioallantoic membrane (CAM) model. *In vivo* studies in mouse retinas have also shown its pro-angiogenic effect (13).

The importance of VEGF in physiological angiogenesis becomes apparent when either the gene or its receptors are inactivated in mice. Mice lacking one allele of either VEGF or VEGFR1 or VEGFR2 all die around post-fertilization day 9. VEGF ^{+/-} mice show a poorly developed vascular network, a defective development of blood islands, the aggregations of mesenchymal cells where vasculogenesis starts, and a defective fusion with the vascular plexus of the yolk sac (31, 32). Mice lacking VEGFR1 show endothelial cell development, but the cells fail to organize themselves into normal vascular channels, whilst mice lacking VEGFR2 failed to develop blood islands and do not show any vasculogenesis (30).

Both in embryogenesis as in adult life, VEGFR2 signalling is one of the most important initiators of sprouting angiogenesis. Processes characteristic for tip cells such as migration and the extension of filopodia are all mediated through VEGFR2 signalling (13, 30). VEGFR3 is a critical regulator of lymphangiogenesis, but is also expressed in the vasculature and is upregulated in tip cells during angiogenesis (33), suggesting a crucial additional role for its ligands VEGF-C and VEGF-D.

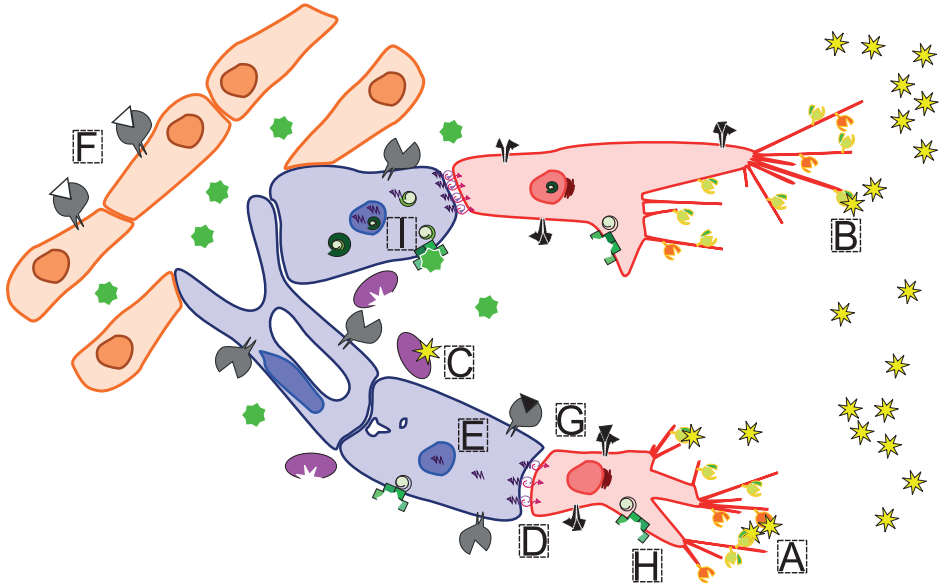
The stimulating effect of VEGF on angiogenesis is mainly exerted through its effects on tip cells. VEGFR2 and VEGFR3 are hardly present on stalk cells, whereas VEGFR1 is present in equal amounts in the microenvironment of tip cells and stalk cells (13) (fig 2A-C, enlargements A,B). In accordance, addition of VEGF to endothelial cell cultures increases the number of tip cells (3). *In silico* modelling by Bentley et al (2008) has also shown the importance of the VEGF signalling pathway for tip cell selection (12, 19).

Notch-Dll4

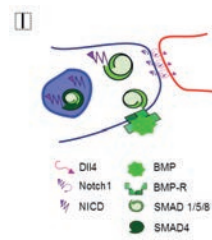
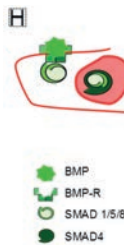
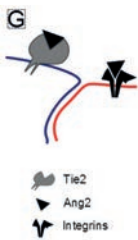
Signalling through Notch receptors (Notch 1-4) by binding its corresponding ligands (Dll1,-3,-4 and Jag 1,-2) plays a role in many developmental processes by regulation of proliferation and differentiation (34). Most important for angiogenesis are the Notch1 receptor and its ligand Dll4, which are crucial for signalling between tip cells and stalk cells and the regulation of the number of tip cells and stalk cells, a process called lateral inhibition.

The regulation of the number of tip cells is important for the correct development of a functional vascular bed. Mice with a deletion of either Dll4 or Notch1 die in utero, despite an increase in vascular sprouting and branching. Furthermore, inhibition of Dll4 in mouse tumour models resulted in a denser vascular network, but an attenuation of tumour growth and tissue perfusion (35).

During sprouting angiogenesis, Dll4 can be found on tip cells after its induction by VEGF. When Dll4 binds to the Notch1 receptor on adjacent cells (fig 2C), it is cleaved by ADAM metalloproteinases and γ -secretase, and its intracellular domain translocates to



- | | | | |
|--------|-----------|-------|------------|
| VEGFR1 | Dll4 | Ang1 | BMP |
| VEGFR2 | Notch1 | Tie2 | BMP-R |
| VEGFR3 | NICD | Ang2 | SMAD 1/5/8 |
| VEGF-A | Integrins | SMAD4 | |
| NRP1 | | | |



the nucleus where it initiates transcription of stalk cell genes, and represses transcription of tip cell genes (fig 2D-E, enlargement D) (35). Inhibition of Dll4-Notch signalling during vascular development results in increased sprouting, branching and filopodia extension, and a denser, more interconnected vascular network (18). Furthermore, expression of tip cell genes such as *Unc-5B* and *PDGF- β* is increased upon inhibition of Dll4-Notch1 signalling (18). *In vitro* data show that the number of CD34⁺ tip cells in endothelial cell cultures can be reduced by culturing on a Dll4 coated surface (3). *In silico* experiments show the complexity of the Dll4-Notch1 signalling pathway in more detail (36). All these data indicate that Dll4-Notch1 signalling reduces the number of tip cells during vascular sprouting.

See also: DOI: 10.1002/9780470015902.a0022893

Neuropilins

There are 2 known neuropilin receptors; neuropilin-1 (NRP-1) and NRP-2, each with an isoform-specific binding pattern. NRP-1 is mainly expressed on arterial endothelial cells and seems to be most crucial for angiogenesis, whereas NRP-2 is mainly expressed on venous and lymphatic endothelium and is reportedly involved in lymphangiogenesis (37). NRP-1 was initially identified as a receptor for semaphorin-3A (SEMA-3A) and as a co-receptor for VEGF-A. More recently, several other proteins have shown the capability to interact with NRP-1, amongst which fibroblast growth factor-2 (FGF-2), hepatocyte growth factor (HGF) and integrin- β 1 (37). Knock-out of NRP-1 in mice results in embryonic lethality associated with heart and vascular abnormalities as well as deficiencies in neuronal guidance. Mice lacking NRP-2 are viable, albeit smaller in size with minor abnormalities in lymphatic development. Moreover, targeted inhibition of NRP-1 by a monoclonal antibody results in disrupted angiogenesis in the mouse trachea. On the other hand, overexpression of NRP-1 in mice leads to increased blood vessel growth with leaky and haemorrhagic vessels (37).

- ◀ **Figure 2.** Overview of the key regulatory pathways for tip cell selection. Tip cells are represented in red, stalk cells in blue and the phalanx cells in orange. VEGF: VEGF-A is produced upon hypoxia, tip cells express VEGFR2 and -3, two receptors that exert the pro-angiogenic effects of VEGF. Soluble VEGFR1 is produced by stalk cells and acts as a sink for VEGF to prevent signaling in stalk cells. Neuropilins: NRP-1 acts as a co-receptor for VEGFR2 to enhance VEGF signaling. Notch1-Dll4: Dll4 is expressed by tip cells, Notch1 by stalk cells. Upon binding, Notch1 is cleaved, and the intracellular domain (NICD) is translocated to the nucleus where it recruits transcription factors to replace expression of tip cell genes by expression of stalk cell genes. Angiopoietins and Tie2: Ang1 is expressed in mature vessels and its main function is vessel stabilization. Ang2 can bind Tie2 to inhibit Ang1-mediated phosphorylation of Tie2; it also binds integrins on tip cells to enhance sprouting. BMPs and SMADs: Pro- and anti-angiogenic BMPs bind to their receptor and phosphorylate SMAD1/5/8. In tip cells, the SMAD1/5/8 complex induces polarization and migration. In stalk cells, the SMAD 1/5/8 complex forms a complex with NICD to promote the stalk cell phenotype.

NRPs interact with several proteins such as FGF and integrins. Both NRPs have distinct binding partners, for example NRP-1 can bind the VEGF isoforms VEGF-A, -B, -E and PlGF, whereas NRP-2 binds VEGF-A, -C and -D (37). Crosslinking experiments performed by Soker et al. (1998) revealed that NRP-1 can act as a co-receptor for VEGFR2, thereby enhancing VEGF-VEGFR2 signalling (38)(fig 2B, enlargement B). This is one of the possible explanations for the vital role of NRP-1 in angiogenesis. However, NRP-1 can also act in a VEGF-independent manner by promoting integrin-mediated endothelial cell adhesion to fibronectin, another essential component of angiogenesis (39). Therefore, the exact role(s) of NRPs in angiogenesis still need to be unravelled.

Angiopoietins and Tie receptors

The Tie (Tyr kinase with Ig and EGF homology domains) receptors, Tie 1 and Tie2, and their ligands, angiopoietin (Ang) 1 and 2 form an endothelial cell-specific signalling system involved in angiogenesis and vascular maturation. Ang1 and Ang2 have antagonistic roles in the activation of quiescent vessels and induction of tip cells, with Ang1 acting as stabilizer and Ang2 as an inducer of migration and tip cell behaviour. Since the function or even the ligands for Tie1 have not been identified, this receptor is not discussed here.

Ang1 was the first ligand of Tie2 to be identified. Mice lacking Ang1 have the same phenotype as Tie2^{-/-} mice (embryos die between E10.5 and 12.5 due to lack of vascular development after formation of the primary plexus), suggesting that Ang1 exclusively binds to Tie2 (fig 2F, enlargement F). Evidence suggests that Ang1 is essential for the establishment and maintenance of vessel integrity, since Ang1 controls endothelial permeability, and induces recruitment of vessel-supporting cells such as smooth muscle cells (SMCs) and pericytes. Ang1-Tie2 signalling can also function in migration by regulation of expression of matrix-degrading proteases. The outcome of Ang1-Tie2 signalling is context dependent: in an endothelial monolayer, a confluent situation, Ang1 binding results in translocation of Tie2 to cell-cell contacts (cadherins), whereas during cell spreading and migration, Ang1, either soluble or bound to a substrate, results in translocation of Tie2 to cell-matrix contacts (integrins). These different binding domains result in activation of different downstream targets (40).

Ang2, the second Tie2 ligand, was initially believed to be an antagonist for Ang1, since it binds to Tie2, but without subsequent phosphorylation of Tie2. It can also inhibit phosphorylation of Tie2 by Ang1. Mice overexpressing Ang2 have a similar phenotype as mice lacking Ang1 or Tie2, although it is more severe. Ang2^{-/-} mice have a mild phenotype, except for retinal vessels where a distinct defect in sprouting can be detected: at postnatal day 10 (P10), when a wild type retina is completely vascularised, large areas of Ang2^{-/-} retinas are without vascular coverage and have hyaloid vessels, which are normally in regression in wild type retinas at this stage, and finally no penetrating vessels to the deeper layers of the retina develop. The importance of Ang2 for sprouting is shown in mice with oxygen-induced retinopathy. In this model, mouse pups are raised in a hyperoxic

environment, which causes vessel regression in the retina. After having returned to room air, the mice develop ischemia in the retina and subsequent neovascularization (more details about this model can be found later in this review). Ang2^{-/-} mice do not show any neovascularization under these circumstances (40).

The exact roles of Ang1 or Ang2 in either tip cell or stalk cell function still has to be elucidated. In sprouting blood vessels, there is hardly any expression of Ang1, whereas Ang2 is expressed by tip cells at the sprouting front. Interestingly, Tie2 is almost completely absent in tip cells. Whilst Ang2 expression is upregulated by VEGF treatment of endothelial cells in culture, Tie2 expression diminishes as a consequence (41). The lack of phosphorylation of Tie2 after binding Ang2, together with this differential expression suggests that Ang2 is able to bind receptors other than Tie2, with integrins as a promising candidate (fig 2G, enlargement G). Ang2 is able to bind $\alpha_v\beta_3$, $\alpha_v\beta_5$ and $\alpha_5\beta_1$ integrins, albeit with lower affinity than Tie2, which are all expressed in tip cells, while Tie2 is not (41) These integrins are necessary for Ang2-induced stimulation of sprouting *in vitro*.

Bone morphogenic proteins and SMADs

Bone morphogenic proteins (BMPs) are members of the TGF- β superfamily. There are approximately 20 BMPs in total and they can either inhibit or stimulate angiogenesis. Best studied in the context of angiogenesis are BMP 2, 4, 6, 7, 9 and 10, where BMP 2, 4, 6 and 7 are pro-angiogenic and BMP 9 and 10 are anti-angiogenic (42). Furthermore, BMPs can inhibit or elicit tip cell functions such as filopodial extension formation, and they are important for the induction of the stalk cell phenotype. There are 3 types of BMP receptors: type 1 receptors (activin receptor-like kinase (ALK) 1-7), type 2 receptors (ActRIIA, ActRIIB, BMPRII, TGFBR1 and AMHR1) and type 3 co-receptors (betaglycan, endoglin or RMG-a, b, c) (43).

See also: DOI: 10.1002/9780470015902.a0002330.pub3

The basic concept of signalling of BMPs is as follows: BMPs dimerize and bind to a tetraheteromeric receptor complex composed of 2 type 1 receptor subunits, and 2 type 2 receptor subunits, whereas affinity is modulated by type 3 receptors. The kinase domain of the type 1 receptor is phosphorylated and activates downstream signalling molecules called SMADs, more specifically, BMP receptors can activate SMAD1, 5 and 8. Activated SMADs form a complex with SMAD4 and translocate to the nucleus to initiate transcription (fig 2H, enlargement H) (42). Crucial downstream targets of SMAD are the Id proteins (inhibitor of DNA binding, dominant negative helix-loop-helix protein).

BMP signalling has been implicated in angiogenesis as an important inducer of the stalk cell phenotype. Mice lacking SMAD1 and 5 die at E9.5 due to severe angiogenic defects (44). The phenotype of these mice shows normal vasculogenesis, but impaired vascular remodelling and angiogenesis. In the hindbrain, more but non-functional sprouts were formed, showing decreased proliferation. Polarization of tip cells was lost, and there was an increase in filopodial extensions, both at the sprouting tip as well as further down

the stalk. This phenotype suggests that BMP/SMAD signalling not only plays a role in the induction of a stalk cell phenotype, but also regulates polarization of tip cells and inhibits filopodial extensions.

The role in stalk cell formation was confirmed in *in vitro* experiments showing that endothelial cells devoid of SMAD1/5 prefer to have the tip cell position in sprouting assays, whereas endothelial cells overexpressing Id1 or Id3 do not show the tip cell phenotype (44). There is also cross-talk between BMP-SMAD signalling and Dll4-Notch signalling (44) (fig 2I, enlargement I). It seems that dynamic expression of any one of these pathways pushes endothelial cells towards either a tip cell or stalk cell phenotype (45).

IN VIVO, IN VITRO AND IN SILICO MODELS

Most of the studies on tip cells cited above were performed using *in vivo* experiments, employing assays such as intersegmental vessel development in zebrafish and development of retinal vessels in mice. Both assays enable visualisation of tip cells and they provide the possibility to study tip cells in both physiological and pathological settings. New models for *in vitro* and *in silico* studies are emerging, and with these the possibilities for swifter and more detailed analysis of candidate genes for tip cell function and associated mechanisms have expanded. This section covers the most frequently-used *in vivo* models as well as new techniques for *in vitro* and *in silico* studies of tip cells.

In vivo

The zebrafish is a popular model to study angiogenesis, because of the short development time, the small size and the extracorporeal development. Furthermore, mechanisms involved in vascular development are well conserved between zebrafish and humans (46). Transgenic fish expressing fluorescent tags in blood vessels enable visualization of tip cells during development. Gene-specific knock downs allow researchers to study single genes and the effect of their expression on angiogenesis in fish and chemical compounds can be administered via the water to the embryos to assess their effect (14) (fig 3a).

See also DOI: [10.1038/npg.els.0000732](https://doi.org/10.1038/npg.els.0000732)

In the mouse eye, retinal blood vessels develop after birth as a front of sprouting vessels that grows from the optic nerve in the centre of the retina towards the periphery (47) (Fig 1A-B). Behind the sprouting front, remodelling and maturation take place, enabling the analysis of the angiogenic process from an emerging tip cell up until the formation of a mature vascular network. Furthermore, the primary retinal plexus is localised superficially in the retina, enabling visualization of sprouting vessels.

To study pathological angiogenesis, the oxygen-induced retinopathy model is frequently used. This model shows many similarities with the disease retinopathy of prematurity (ROP) and is aided by the fact that formation of the retinal vasculature in the mouse takes place after birth. Seven day-old mouse pups spend 5 days in a chamber with 75% oxygen, which causes regression of part of the retinal vasculature. At day 12,

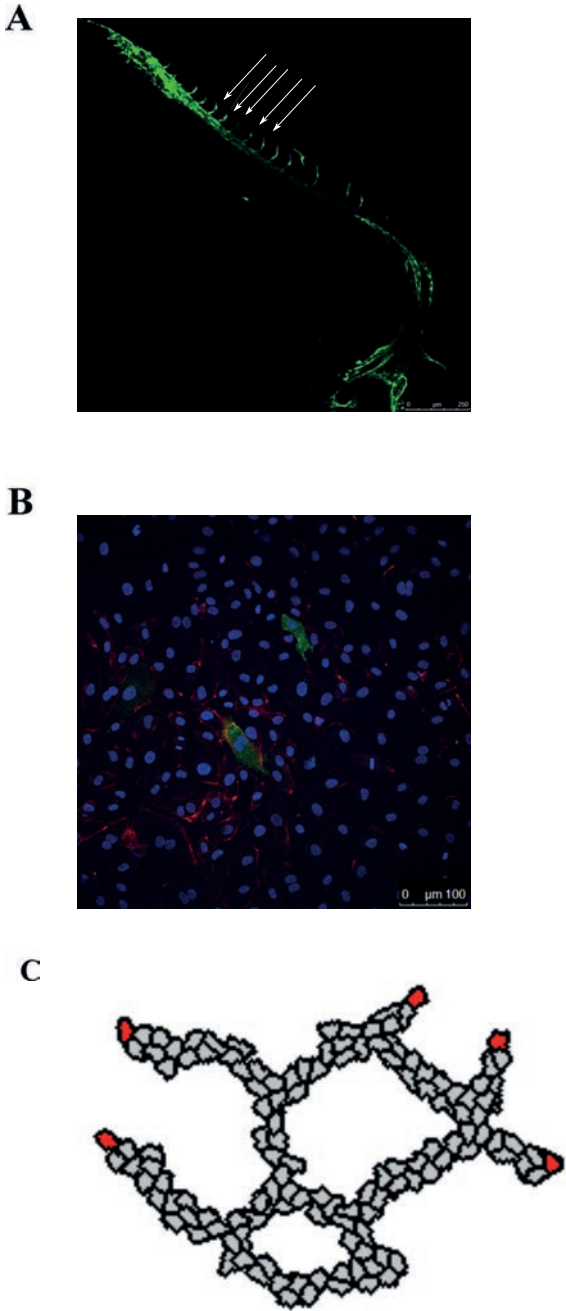


Figure 3. *In vivo*, *in vitro* and *in silico* models for angiogenesis. Fli1a-eGFP transgenic zebrafish, at 24 h post fertilization. At this stage, sprouting occurs in the intersegmental vessels (white arrows) and tip cells are present on each sprouting vessel. CD34⁺ cell in a human umbilical vein endothelial cell (HUVEC) culture. HUVECs were grown on coverslips coated with gelatin and stained for F-actin (red), CD34 (green) and DAPI (blue). *In silico* vascular network formed from a spheroid of endothelial cells by a mechanism of cell-cell contact-inhibited chemotaxis (56). Tip cells are indicated in red.

mice return to room air and the retina becomes hypoxic due to the lack of functional blood vessels. A wave of angiogenic activity occurs in response to growth factors that are produced in the hypoxic areas. The amount of neovascularization and the size of the avascular zone can be measured and quantified (48). This model can be used in mice after gene knock-out, or by the intravitreal injection of silencing RNA, or neutralizing antibodies. Other compounds, such as angiogenesis inhibitors or growth factors can also be injected into the eyes of these mice.

In vitro

Sprouting assays using either endothelial cells or stem cells have been widely used in angiogenesis studies. Recently, a subset of CD34⁺ cells that resembles tip cells as found *in vivo* was discovered in cultures of human umbilical vein endothelial cells (HUVECs) (Fig 3B) (3). These cells extend filopodia, express known tip cell genes and have a less proliferative and more migratory phenotype, identical to tip cells *in vivo*. The percentage of CD34⁺ cells can be increased by addition of VEGF to the culture and decreased by seeding cells on a Dll4-coated surface, which is in agreement with regulation of the tip cell phenotype *in vivo*. A subpopulation of tip cells is generated by HUVECs in culture, which suggests that an equilibrium exists in endothelial cell cultures. The presence of tip cells in culture implies that endothelial cell cultures, even in monolayers with contact inhibition are not quiescent, but rather in an activated, angiogenic state.

In silico

Computational models have greatly contributed to the understanding of lateral inhibition through Dll4-Notch1 and the resulting spatial patterns of tip and stalk cell differentiation. More recently, mathematical and computational models have also been used to test hypotheses on the mechanisms of tip cell overtaking and to study the function of tip cells.

Collier et al. (1996) developed the first mathematical model of pattern formation due to Dll4-Notch1 dependent lateral inhibition (49), which they studied in a system of two coupled cells, a linear array of cells and in a two-dimensional, hexagonal lattice of cells. A set of coupled ordinary differential equations (ODEs) described the level of Notch activation and the level of Delta activity in each cell. They used a simple rule to describe lateral inhibition: "the more intense the inhibition a cell receives, the weaker its ability to deliver inhibition must become" (49). This feedback loop was represented in their model by a reduction of Dll4 production in a cell upon Notch activation. Small perturbations within a monolayer of initially equivalent cells induced an alternating pattern of cells with high and low Notch activation states (stalk and tip cells respectively), a pattern often seen in experiments. They concluded that lateral inhibition with a sufficiently strong feedback can create alternating patterns of cells with high and low Delta expression.

Sprinzak et al. (2010, 2011) developed a refined ODE model of Delta-Notch signaling to study the effect of cis-interactions, the mutual inactivation of interacting

Delta and Notch of the same cell, on lateral inhibition (36, 50). The model represents a two-dimensional array of hexagonal cells. Each cell has a concentration of Notch and Delta. Sprinzak et al. showed that cis-interaction between Delta and Notch speeds up the patterning dynamics and amplifies the feedback in lateral inhibition, since down-regulation of Dll4 simultaneously increases the number of 'cis-interaction free' Notch receptors in that cell. Cis-interaction also allows for an alternative mode of feedback in which Notch production is stimulated upon Notch activation, as was found *in vivo*. Thus cis-interaction refines the regulation of tip cell selection.

Besides in tip cell selection during angiogenesis, Dll4-Notch mediated lateral inhibition plays an important role in patterning of bristles in *Drosophila* epithelium (51). Cells with high levels of Delta expression are destined to give rise to a bristle. Live imaging showed a gradual process of refinement in the late stages of lateral inhibition-mediated patterning, leading to a sparse spacing of cells with high levels of Dll4 (51). Using a model of lateral inhibition, based on the model of Collier et al. (49), Cohen et al. (51) were not able to reproduce the sparse spacing in a monolayer of epithelial cells that was geometrically similar to experimental images. Since live imaging showed that movement of the cell body contributed little to patterning refinement, Cohen et al. (2010) asked if cells might accomplish refinement with long, dynamic filopodia, which were observed to form a lateral web extending across several cell diameters at the basal side of the epithelial cells. Bristle spacing could be mimicked when the model was extended with dynamically forming filopodia that can contact and signal distant non-neighboring cells. After inhibiting filopodia dynamics the bristles differentiated more closely together both in the model and in the experiments.

Bentley et al. (2008, 2009) studied how filopodia contribute to tip cell selection during sprouting (19, 52). They developed a computational model representing a single hollow, cylindrical sprout of ten endothelial cells. In this model, the membrane of each endothelial cell is composed of agents from which a filopodium can grow. Filopodia are assumed to extend towards higher concentrations of vascular endothelial growth factor (VEGF) (19). Dll4 production is up-regulated upon VEGFR2 activation and VEGFR2 production is down-regulated by Notch1 activity (35), such that endothelial cells near higher concentrations of VEGF more likely differentiate into tip cells. Filopodial growth is stimulated by VEGF signaling, while surface extension by filopodia formation increases VEGF signaling, creating a positive feedback loop. The model predicted that tip cell patterning will stabilize faster in VEGF gradients than in uniform VEGF environments and that high VEGF levels induce oscillation of the alternating tip-stalk cell pattern. Anastomosis led by filopodia can create new cell-cell junctions with new Dll4-Notch signaling opportunities, which can make tip and stalk cells within the sprout switch fate (52).

Detailed *in vitro* and *in vivo* imaging showed that cells in the sprout regularly overtake the tip cell, indicating competition for the tip cell position (12). To study the mechanisms behind tip cell competition in more detail, Bentley et al. extended their model (53) by using

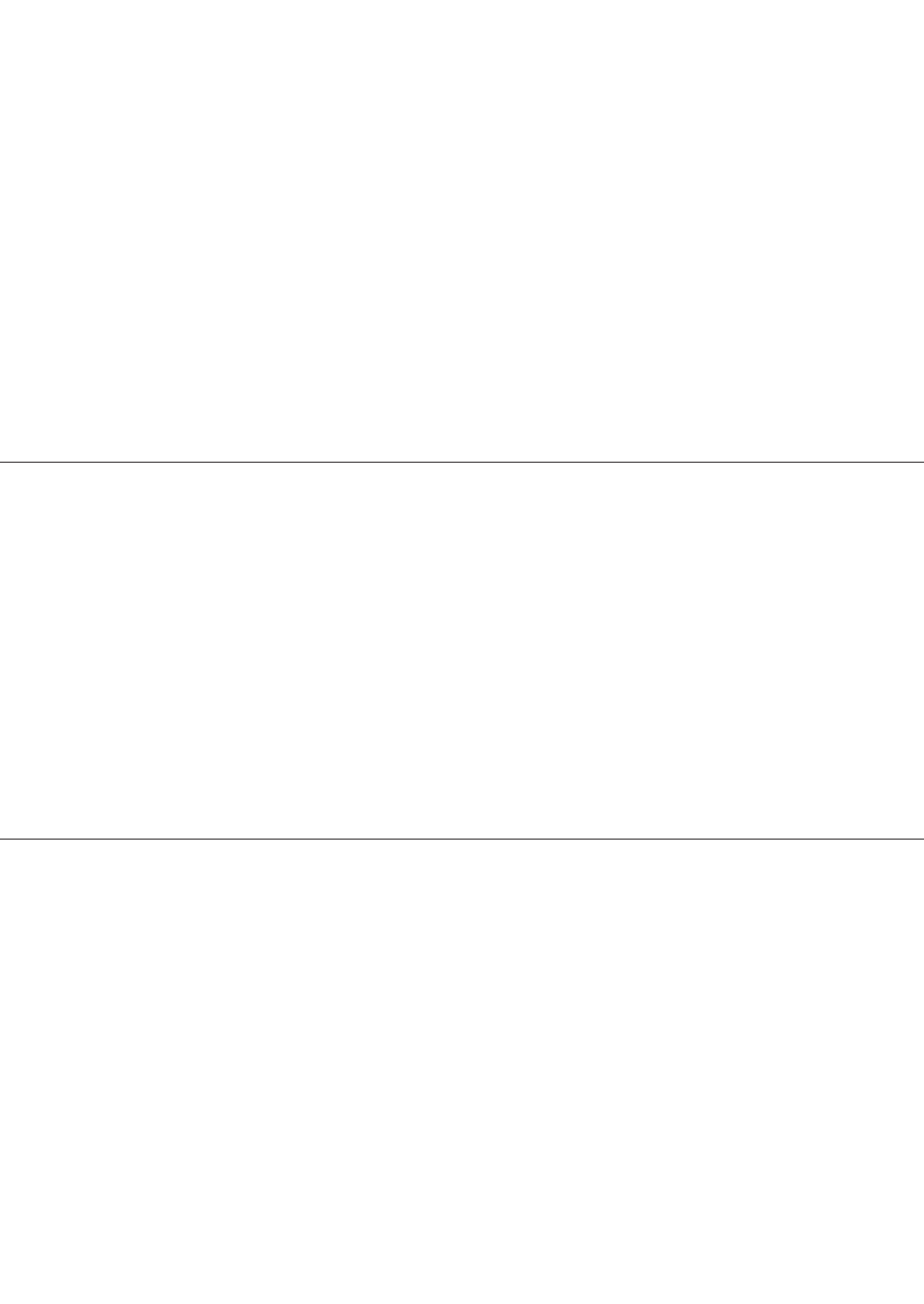
the Cellular Potts Model (CPM) (54) to represent the shape and movement of the cells, thereby explicitly modeling cell-cell adhesion and junctional reshuffling. Bentley et al. (53) hypothesized that VEGF stimulates endocytosis of vascular endothelial cadherin (VE-cadherin), thus reducing the adhesion between endothelial cells. They further assumed that Notch activity decreases extension of polarized actomyosin protrusions towards the sprout tip. Tip cell competition in the model was most in line with experimental observations and perturbations when adhesion differentially depends on VEGFR2 signaling and polarized protrusions differentially depend on Notch activity.

Although it is now well established that both tip and stalk cells are present during angiogenesis and vasculogenesis, it is not clear what biophysical properties of tip cells lead sprouts and affect the morphology of vascular networks. Palm et al. (2014) used computational modeling to address these questions (55) (fig 3C). They added a model of tip cell selection to a previously published CPM model of angiogenic sprouting and vasculogenesis (56), in which sprouts form due to cell-cell contact inhibited chemotaxis towards a compound secreted by the endothelial cells themselves (Fig 3C). Palm et al. performed large parameter sweeps and morphological analyses on the resulting vascular network, to identify “tip cell behaviors”: Tip cells move towards the sprout tip when they adhere more to the extracellular matrix than to neighboring cells, or when they are less sensitive to the secreted compound, compared to stalk cells. Tip cell selection, and the resulting switching of tip and stalk fate, localizes tip cells to the sprout tips, and thereby stabilizes the vascular network morphology at tip cell free branches.

See also: DOI: 10.1038/npg.els.0003433

CONCLUDING REMARKS

The tip cell has presented itself in the last decade as a promising target for pro- and anti-angiogenic therapies. Specific functions and complex mechanisms of regulation of the tip cell phenotype are unravelling. However, the lack of a marker for tip cells *in vivo* is a major obstacle for detailed research. The discovery of an *in vitro* marker such as CD34 will enable cell sorting to perform experiments with solitary tip cells and non-tip cells. *In silico* modelling provides another valuable approach by which important mechanisms can be elucidated which can then be confirmed in *in vitro* or *in vivo* experiments.



A large, bold, grey number '133' is positioned in the background, spanning across the middle of the page. The number is composed of three digits: a '1', a '3', and another '3'.

**PRACTICAL ASPECTS OF THE STUDY OF CD34⁺
ENDOTHELIAL TIP CELLS *IN VITRO***

Since our first publication on the discovery of CD34⁺ tip cells in endothelial cell (EC) cultures in 2012, we have gained extensive experience with this new angiogenesis model. This subchapter describes a number of important issues related to CD34⁺ EC tip cells *in vitro* as guidelines for future research.

CULTURE MEDIUM

The amount of serum used in culture medium of ECs affects the percentage of CD34⁺ tip cells. For example, human umbilical vein ECs (HUVECs) up to passage 3, as used for the experiments in this thesis, were grown in medium containing 20% total serum (10% heat-inactivated human serum and 10% fetal calf serum). The average percentage of tip cells in the HUVEC cultures at passage 3 was approximately 10%. We have performed experiments in medium containing 20% fetal calf serum, 2% human serum only, or in medium without serum. We found that the percentage of tip cells increased upon culturing in medium containing 2% human serum, but not in medium without serum. Although counter-intuitive, because serum contains many pro-angiogenic growth factors, it seems that the absolute amounts of these factors affect angiogenesis and tip cell formation.

DONORS OF PRIMARY ECS

We have performed all experiments described in this thesis with ECs from individual human donors. We did not use pooled ECs of different donors, as is the standard with commercially-available ECs. We chose this approach because of the large differences in the percentage of tip cells between donors. We hypothesize that these large differences are caused by different signalling between tip cells and stalk cells. Each donor may express different amounts of growth factors and receptors, that all surmount to an equilibrium resulting in a specific percentage of tip cells. Pooling of ECs of various donors may disturb this tip cell-stalk cell signalling and therefore disturb experimental outcomes. A downside of using ECs of individual donors is the need for correction of data which may, in turn, affect the results. We have applied the factor correction programme for this purpose (57). In short, factor correction minimalizes effects of multiplicative differences between donors or sessions by assuming that there is one level of error between unbiased donors and sessions. This procedure results in a smaller residual error than normalisation or standardisation and allows reduction of noise caused by interindividual variations between donors.

DE NOVO TIP CELL FORMATION BY DIFFERENT TYPES OF ECS

As mentioned in the previous chapters, the tip cell and stalk cell phenotypes in zebrafish are dynamic: ECs can switch from the tip cell to the stalk cell phenotype and vice versa (12). When CD34⁺ tip cells and CD34⁻ non-tip cells in human EC cultures are separated using flow-activated cell sorting (FACS), the separate populations eventually return to

the previous equilibrium of approximately 10% CD34⁺ tip cells when culture conditions are not changed (3). This means that CD34⁺ tip cells appear again in cultures of CD34⁻ cells and vice versa, suggesting that human tip cell and stalk cell phenotypes are also dynamic. In HUVEC cultures, the equilibrium of approximately 10% CD34⁺ tip cells is reached after a few days (3). However, the appearance of the first CD34⁺ cells already occurs approximately 24 hours after sorting (58), which means that 24 h is the maximum time frame for experiments using CD34⁺ and CD34⁻ HUVEC subpopulations. This time frame varies between different types of ECs, as for example in immortalized human microvascular endothelial cell-line (HMEC-1), CD34⁺ cells do not re-appear before 72 hours after sorting.

INTERPRETATION OF DATA

In our *in vitro* studies, we have only used CD34 as marker for tip cells, because other specific immunohistochemical markers of tip cells and non-tip cells are not known. This means that a measured effect on the percentages of CD34⁺ tip cells must be complemented by data on changes in the CD34⁺ cells or CD34⁻ populations separately, such as measurement of mRNA expression of other known tip cell genes, proliferation and/or apoptosis. These experiments will identify whether the observed effects are due to an effect on tip cells, on stalk cells or solely on the CD34 protein. Examples that changes in numbers of CD34⁻ cells can also affect the percentages of CD34⁺ cells are shown in Chapters 2.2 and 3.3. In Chapter 2.2 knockdown of *TIE2* resulted in increased percentages of CD34⁺ cells. Further studies showed that this was because of apoptosis of CD34⁻ cells, causing reduction in numbers of CD34⁻ cells whereas the number CD34⁺ cells remained stable. This explained the increased percentages of CD34⁺ cells. In Chapter 3.3, the percentages of CD34⁺ we measured after addition of the novel anti-angiogenesis compound Crenolanib decreased because of increased proliferation of CD34⁻ cells, causing the relative number of CD34⁺ cells to decrease, even though they were viable and present.

ADVANTAGES OF STUDYING TIP CELLS *IN VITRO*

Besides the ethical advantages over studies using laboratory animals, the *in vitro* experiments require less time and money, thus significantly reducing the costs and duration of tip cell research. Another advantage of experiments using tip cells *in vitro* is the higher accuracy of experiments. This is highlighted in chapter 2.3, in which we study the IGF family of growth factors. The presence of other IGF family members in serum of experimental animals can be a major confounder in *in vivo* studies. We eliminated noise created by serum proteins by culturing ECs in medium without serum and in this way, we discovered an essential role of the IGF-binding proteins IGFBP3 and IGFBP4 in IGF2-IGF1R-mediated maintenance of tip cells. Furthermore, tip cells and stalk cells can be studied separately *in vitro* which cannot be performed in animal models. For example, in chapter 2.1 and 2.2, we have performed sprouting experiments using spheroids of sorted

CD34⁻ and CD34⁺ cells and in chapter 2.2 and 4.2, we performed experiments in which we measured apoptosis in tip cells and stalk cells separately.

LIMITATIONS OF STUDYING TIP CELLS *IN VITRO*

1.3

There are also limitations when using CD34 as a marker for tip cells. First, CD34 is present in all endothelial cells *in vivo*, and is not only expressed on filopodial extensions of sprouts but also on the endothelial lumen of blood vessels. This means that CD34 cannot be used as tip cell marker in *in vivo* models, other than by its staining of filopodia (15). Second, the exact role of CD34 in angiogenesis is still not known. We have found that it is involved in extension of filopodia by tip cells, and that gene knockdown *in vitro* reduced the EC response to VEGF, as shown in chapter 2.1. However, knockdown of *CD34* did not affect sprouting from spheroids and no detrimental effects were found of *CD34* knockout in a mouse model of retinopathy of prematurity. This suggests that CD34 is not an essential protein for tip cells. Lastly, a marker for stalk cells or phalanx cells is not available. We have hypothesized that the CD34⁻ cell population in EC cultures consists of different angiogenic EC subtypes including stalk cells, phalanx cells and quiescent cells. When a marker of stalk cells would be available, the accuracy of experiments would increase and interpretation of the experimental results would be facilitated. For example, the studies investigating VEGF-induced proliferation presented in chapter 4.3 would greatly benefit from experiments performed on isolated stalk cells, to investigate whether their proliferation is specifically affected.

In conclusion, our *in vitro* study using CD34⁺ tip cells and CD34⁻ non-tip cells have elucidated various molecular mechanisms of angiogenesis that may become useful to develop anti-angiogenic therapies focussed on tip cells.

REFERENCES

1. Anderson B. Ocular effects of changes in oxygen and CO₂ tension. *Tr Am Ophth Soc.* 1968;66:423-74.
2. Klaassen I, Van Noorden CJ, Schlingemann RO. Molecular basis of the inner blood-retinal barrier and its breakdown in diabetic macular edema and other pathological conditions. *Prog Retin Eye Res.* 2013;34:19-48.
3. Siemerink MJ, Klaassen I, Vogels IM, Griffioen AW, Van Noorden CJ, Schlingemann RO. CD34 marks angiogenic tip cells in human vascular endothelial cell cultures. *Angiogenesis.* 2012;15(1):151-63.
4. Strasser GA, Kaminker JS, Tessier-Lavigne M. Microarray analysis of retinal endothelial tip cells identifies CXCR4 as a mediator of tip cell morphology and branching. *Blood.* 2010;115(24):5102-10.
5. del Toro R, Prahst C, Mathivet T, Siegfried G, Kaminker JS, Larrivee B, et al. Identification and functional analysis of endothelial tip cell-enriched genes. *Blood.* 2010;116(19):4025-33.
6. Hanahan D, Weinberg RA. The hallmarks of cancer. *Cell.* 2000;100:57-70.
7. Hanahan D, Weinberg RA. Hallmarks of cancer: the next generation. *Cell.* 2011;144(5):646-74.
8. Folkman J. tumor angiogenesis: therapeutic implications. *NEJM.* 1971;285(21):1182-6.
9. Maniotis AJ, Folberg R, Hess A, Seftor EA, Gardner LMG, Pe'er J, et al. Vascular channel formation by human melanoma cells *in vivo* and *in vitro*: vasculogenic mimicry. *Am J Pathol.* 1999;155(3):739-52.
10. Ayala-Dominguez L, Olmedo-Nieva L, Munoz-Bello JO, Contreras-Paredes A, Manzo-Merino J, Martinez-Ramirez I, et al. Mechanisms of Vasculogenic Mimicry in Ovarian Cancer. *Front Oncol.* 2019;9:998.
11. Abdollahi A, Folkman J. Evading tumor evasion: current concepts and perspectives of anti-angiogenic cancer therapy. *Drug Resist Updat.* 2010;13(1-2):16-28.
12. Jakobsson L, Franco CA, Bentley K, Collins RT, Ponsioen B, Aspalter IM, et al. Endothelial cells dynamically compete for the tip cell position during angiogenic sprouting. *Nat Cell Biol.* 2010;12(10):943-53.
13. Gerhardt H, Golding M, Fruttiger M, Ruhrberg C, Lundkvist A, Abramsson A, et al. VEGF guides angiogenic sprouting utilizing endothelial tip cell filopodia. *J Cell Biol.* 2003;161(6):1163-77.
14. Phng LK, Stanchi F, Gerhardt H. Filopodia are dispensable for endothelial tip cell guidance. *Development.* 2013;140(19):4031-40.
15. Schlingemann RO, Rietveld FJ, de Waal RM, Bradley NJ, Skene AJ, Davies AJ, et al. Leukocyte antigen CD34 is expressed by a subset of cultured endothelial cells and on endothelial abluminal microprocesses in the tumor stroma. *Lab Invest.* 1990;62(6):690-6.
16. Sabin FR. Preliminary Note on the Differentiation of Angioblasts and the Method by Which They Produce Blood-Vessels, Blood-Plasma and Red Blood-Cells As Seen in the Living Chick. *the anatomical record.* 1917;13.
17. Ausprunk DH, Folkman J. Migration and proliferation of endothelial cells in preformed and newly formed blood vessels during tumor angiogenesis. *Microvasc Res.* 1977;14(1):53-65.
18. Hellstrom M, Phng LK, Hofmann JJ, Wallgard E, Coultas L, Lindblom P, et al. Dll4 signalling through Notch1 regulates formation of tip cells during angiogenesis. *Nature.* 2007;445(7129):776-80.
19. Bentley K, Gerhardt H, Bates PA. Agent-based simulation of notch-mediated tip cell selection in angiogenic sprout initialisation. *J Theor Biol.* 2008;250(1):25-36.
20. Eelen G, Cruys B, Welte J, De Bock K, Carmeliet P. Control of vessel sprouting by genetic and metabolic determinants. *Trends Endocrinol Metab.* 2013;24(12):589-96.
21. Clark ER, Clark EL. Microscopic observations on the growth of blood capillaries in the living mammal. *the american Journal of Anatomy.* 1939;64(2):251-301.

22. van Noorden CJF, Meade-Tollin C, Bosman FT. The spread of cancer cells to distant sites implies a complex series of cellular abnormalities, in part, by genetic aberrations. *metastasis*. 1998;86:130-41.
23. Sander K. Wilhelm Roux and the rest: Developmental theories 1885-1895. *Roux Arch Dev Biol*. 1991;200(6):297-9.
24. Loeb J. Ueber die entwicklung vom Fishembryonen ohne kreislauf. *archiv fur die gesammte physiologie des menschen und der thiere*. 1893;54:525-31.
25. Michaelson IC. Vascular morphogenesis in the retina of the cat. *Journal of anatomy*. 1948;82(3):1948.
26. Ashton. Oxygen and the growth and development of retinal vessels. *Am J Ophthalmol*. 1966;62:412-35.
27. Folkman J. Tumor Angiogenesis Factor. *Cancer Res*. 1974;34:2109-13.
28. Sperry RW. chemoaffinity in the orderly growth of the nerve fiber patterns and connections. *P Natl Acad Sci USA*. 1963;50:703-10.
29. Zelzer E, Shilo B-Z. Cell fate choices in *Drosophila* tracheal morphogenesis. *BioEssays*. 2000;22:219-26.
30. Koch S, Claesson-Welsh L. Signal transduction by vascular endothelial growth factor receptors. *Cold Spring Harb Perspect Med*. 2012;2(7):a006502.
31. Carmeliet P, Ferreira V, Breier G, Pollefeyt S, Kieckens L, Gertsenstein M, et al. Abnormal blood vessel development and lethality in embryos lacking a single VEGF allele. *Nature*. 1996;4(380):435-9.
32. Ferrara N, Carver-Moore K, Chen H, Dowd M, Lu L, Sue O'Shea K, et al. Heterozygous embryonic lethality induced by targeted inactivation of the VEGF gene. *Nature*. 1996;38:439-42.
33. Witmer A. Vascular endothelial growth factors and angiogenesis in eye disease. *Progress in Retinal and Eye Research*. 2003;22(1):1-29.
34. Aster JC. In brief: Notch signalling in health and disease. *J Pathol*. 2014;232(1):1-3.
35. Phng LK, Gerhardt H. Angiogenesis: a team effort coordinated by notch. *Dev Cell*. 2009;16(2):196-208.
36. Sprinzak D, Lakhanpal A, Lebon L, Santat LA, Fontes ME, Anderson GA, et al. Cis-interactions between Notch and Delta generate mutually exclusive signalling states. *Nature*. 2010;465(7294):86-90.
37. Djordjevic S, Driscoll PC. Targeting VEGF signalling via the neuropilin co-receptor. *Drug Discov Today*. 2013;18(9-10):447-55.
38. Soker S, Takashima S, Miao HQ, Neufeld G, Klagsbrun M. Neuropilin-1 Is Expressed by Endothelial and Tumor Cells as an Isoform-Specific Receptor for Vascular Endothelial Growth Factor. *Cell*. 1998;92:735-45.
39. Valdembrì D, Caswell PT, Anderson KI, Schwarz JP, König I, Astanina E, et al. Neuropilin-1/GIPC1 signaling regulates alpha5beta1 integrin traffic and function in endothelial cells. *PLoS Biol*. 2009;7(1):e25.
40. Augustin HG, Koh GY, Thurston G, Alitalo K. Control of vascular morphogenesis and homeostasis through the angiopoietin-Tie system. *Nat Rev Mol Cell Biol*. 2009;10(3):165-77.
41. Felcht M, Luck R, Schering A, Seidel P, Srivastava K, Hu J, et al. Angiopoietin-2 differentially regulates angiogenesis through TIE2 and integrin signaling. *J Clin Invest*. 2012;122(6):1991-2005.
42. Wiley DM, Jin SW. Bone Morphogenetic Protein functions as a context-dependent angiogenic cue in vertebrates. *Semin Cell Dev Biol*. 2011;22(9):1012-8.
43. David L, Feige JJ, Bailly S. Emerging role of bone morphogenetic proteins in angiogenesis. *Cytokine Growth Factor Rev*. 2009;20(3):203-12.
44. Moya IM, Umans L, Maas E, Pereira PN, Beets K, Francis A, et al. Stalk cell phenotype depends on integration of Notch and Smad1/5 signaling cascades. *Dev Cell*. 2012;22(3):501-14.
45. Beets K, Huylebroeck D, Moya IM, Umans L, Zwijsen A. Robustness in angiogenesis: notch and BMP shaping waves. *Trends Genet*. 2013;29(3):140-9.
46. Dooley K, Zon LI. Zebrafish: a model system for the study of human disease. *current opinion in genetics and development*. 2000;10:252-6.

47. Fruttiger M. Development of the Mouse Retinal Vasculature: Angiogenesis Versus Vasculogenesis. *Investigative Ophthalmology and visual science*. 2002;43(2):522-7.
48. Smith LEH, Wesolowski E, McLellan A, Kostyk SK, D'Amato R, Sullivan R, et al. Oxygen-Induced Retinopathy in the Mouse. *Investigative Ophthalmology and visual science*. 1994;35:101-11.
49. Collier JR, Monk NAM, Maint PK, Lewis JH. Pattern Formation by Lateral Inhibition with Feedback] a Mathematical Model of DeltaNotch Intercellular Signalling. *journal of theoretical biology*. 1996;183:429-46.
50. Sprinzak D, Lakhapanal A, LeBon L, Garcia-Ojalvo J, Elowitz MB. Mutual inactivation of Notch receptors and ligands facilitates developmental patterning. *PLoS Comput Biol*. 2011;7(6):e1002069.
51. Cohen M, Georgiou M, Stevenson NL, Miodownik M, Baum B. Dynamic filopodia transmit intermittent Delta-Notch signaling to drive pattern refinement during lateral inhibition. *Dev Cell*. 2010;19(1):78-89.
52. Bentley K, Mariggi G, Gerhardt H, Bates PA. Tipping the balance: robustness of tip cell selection, migration and fusion in angiogenesis. *PLoS Comput Biol*. 2009;5(10):e1000549.
53. Bentley K, Franco CA, Philippides A, Blanco R, Dierkes M, Gebala V, et al. The role of differential VE-cadherin dynamics in cell rearrangement during angiogenesis. *Nat Cell Biol*. 2014;16(4):309-21.
54. Graner F, Glazier JA. Simulation of Biological Cell Sorting Using a Two-Dimensional Extended Potts Model. *physical review letters*. 1992;69(13):2013-6.
55. Palm MM, Merks RM. Vascular networks due to dynamically arrested crystalline ordering of elongated cells. *Phys Rev E Stat Nonlin Soft Matter Phys*. 2013;87(1):012725.
56. Merks RM, Perryn ED, Shirinifard A, Glazier JA. Contact-inhibited chemotaxis in de novo and sprouting blood-vessel growth. *PLoS Comput Biol*. 2008;4(9):e1000163.
57. Ruijter JM, Thygesen HH, Schoneveld OJ, Das AT, Berkhout B, Lamers WH. Factor correction as a tool to eliminate between-session variation in replicate experiments: application to molecular biology and retrovirology. *Retrovirology*. 2006;3:2.
58. Dallinga MG, Yetkin-Arik B, Kayser RP, Vogels IMC, Nowak-Sliwinska P, Griffioen AW, et al. IGF2 and IGF1R identified as novel tip cell genes in primary microvascular endothelial cell monolayers. *Angiogenesis*. 2018;21:823-36.



TIP CELL-SPECIFIC PROTEINS



Martin J. Siemerink¹,
Michael R. Hughes²,
Marchien G. Dallinga¹,
Tomek Gora¹,
Jessica Cait²,
Ilse M.C. Vogels¹,
Bahar Yetin-Arik¹,
Cornelis J.F. Van Noorden¹,
Ingeborg Klaassen¹,
Kelly M. McNagny²,
Reinier O. Schlingemann^{1#}

¹Ocular Angiogenesis Group, Department of Ophthalmology and
Department of Cell Biology and Histology, University of Amsterdam,
Academic Medical Center, Amsterdam, The Netherlands.

²Department of Medical Genetics and The Biomedical Research Centre,
University of British Columbia, Vancouver, BC, Canada.

A large, light gray, stylized number '21' is positioned in the background, spanning across the middle of the page. The number is composed of thick, rounded strokes. The '2' is on the left, and the '1' is on the right. The text is centered over the '2' and the top part of the '1'.

**CD34 PROMOTES PATHOLOGICAL EPI-RETINAL
NEOVASCULARIZATION IN A MOUSE MODEL
OF OXYGEN-INDUCED RETINOPATHY**

INTRODUCTION

Angiogenesis is the process by which vessels grow and branch from existing vessels to generate new vascular beds (reviewed in ref (1)). Physiological angiogenesis in adults is critical for wound healing, reproduction, and tissue growth and regeneration. Accordingly, insufficient or pathological angiogenesis underlies many human diseases including myocardial infarction, delayed wound healing (ulcerative disease), neurological disease, impairment of vision (proliferative retinopathies) and tumor growth and metastasis (reviewed in ref (2)). Thus, a more complete understanding of the mechanisms regulating both physiological and pathological angiogenesis may have clinical implications for the treatment of disease and advancement of regenerative therapies.

The highly organized vascular sprouts in angiogenesis are composed of distinctly differentiated endothelial cell subtypes that act in a strict hierarchical fashion (3, 4). Among these subtypes are endothelial tip cells, the leading cells of vascular sprouts that form filopodia to aid migration towards a source of growth factors such as vascular endothelial growth factor-A (VEGF-A); and, to direct adjacent endothelial cells to form and elongate the stalk of sprouting vessels (4-8). In addition, tip cells have other functions that are essential for capillary sprouting such as a specific proteolytic machinery that is required for migration and invasion into the extracellular matrix or ischemic areas (9, 10). Whether tip cell functions differ in sprouting angiogenesis under normal conditions and pathological conditions is unknown.

CD34 and podocalyxin (PODXL) are transmembrane anti-adhesive sialomucins that are ubiquitously expressed on the luminal surface of endothelial cells in capillaries (11-15). CD34 and PODXL also act as anti-adhesive molecules during lumen formation in the developing mouse aorta by maintaining or promoting the separation between contralateral apical endothelial cell lumen surfaces (16). It has been shown in *Cd34* knockout (*Cd34^{-/-}*) mice that, when expressed on blood cells, CD34 enhances the adhesion, mobility and invasiveness of hematopoietic progenitors, mast cells, and eosinophils (17-20). High expression of CD34, but not PODXL, on endothelial tip cells and their filopodia (4, 21) suggests that CD34 may play a role in angiogenesis that is specifically related to filopodia functions or architecture (7, 13, 22, 23). A role of CD34 in tumor angiogenesis was suggested by the observation that *Cd34* deletion in mice (specifically in non-hematopoietic lineages) impaired early tumor growth due to a delay in angiogenesis (24). Whether this effect is specifically related to expression of CD34 on tip cells is not known. We have found that only a subset (approximately 10%) of cultured human umbilical vein endothelial cells (HUVECs) express CD34 and this CD34-positive population has a distinct endothelial tip cell phenotype (21). We also showed that this subpopulation of CD34⁺ tip cells is actively restored when isolated CD34⁻ HUVECs are re-cultured (21). Furthermore, stimulation of HUVECs with angiogenic growth factors such as VEGF-A induced CD34 expression (25). Therefore, high CD34 expression marks endothelial cells with tip cell activity *in vitro*. However, it is not known whether CD34 has a functional role in tip cell behavior or angiogenesis in general.

In the following study, we investigated the role of CD34 in angiogenesis using *in vitro* angiogenesis models in the presence or absence of CD34-specific small interfering RNA (siRNA) and in physiological and pathological angiogenesis *in vivo* using *Cd34^{-/-}* mice. In a model of oxygen-induced retinopathy (OIR), we provide evidence that, although CD34 is not necessary for physiological retinal blood vessel development, it promotes epi-retinal tuft formation in pathological retinal angiogenesis.

MATERIALS AND METHODS

Cells and cell cultures

Immortalized human microvascular dermal endothelial (HMEC-1) cells were grown on culture flasks coated with 2% gelatin containing M199 medium (Gibco, Grand Island, NY, USA) supplemented with 5% human serum (Academisch Medisch Centrum Hospital, Amsterdam, The Netherlands), 5% fetal bovine serum (FBS) (Biowhittaker, Walkersville, MD, USA) and 1% penicillin-streptomycin-glutamine (Gibco). HMEC-1 cells between passages 30 and 40 were used for all experiments. All cells were grown in a humidified 37°C incubator with 5% CO₂.

Small interfering RNA (siRNA) transfection

HMEC-1 were transfected with either CD34-specific siRNA pool or non-targeting siRNA (Accell SMARTpool, Dharmacon, Lafayette, CA, USA). The siRNAs were transfected using the reversed-transfection method, according to the manufacturer's protocol. Cells were either collected at 72 h after transfection for RNA or spheroids, formed 52 h after transfection, were embedded in collagen gels (72 h after transfection) for sprouting assays.

FACS and flow cytometry

For flow cytometric analysis, HMEC-1 cells were labeled with anti-human podocalyxin antibody (goat pAb IgG, AF1556, R&D Systems, Minneapolis, MN, USA), anti-human CD34 antibody (mouse mAb IgG1, QBend10 clone, R&D Systems) or the appropriate isotype control antibody at the same concentrations followed by a fluorochrome-conjugated secondary antibody (Alexa Fluor® 647 chicken anti-goat IgG (A21469; ThermoFisher Scientific, Waltham, MA, USA) or fluorescein isothiocyanate (FITC) goat anti-mouse IgG (1010-02; Southern Biotech, Birmingham, AL, USA). Data was collected on an LSR II instrument (Becton Dickinson (BD), Mountain View, CA, USA) and analyzed using FlowJo v10.0.08 software (FlowJo, Ashland, OR, USA). For cell-sorting, HMEC-1 were labeled with anti-CD34 antibody (QBend10 clone; Sanquin, Amsterdam, The Netherlands) and sorted for CD34 expression on a FACSAria or FACSCanto-II instrument (Becton Dickinson, Mountain View, CA, USA) as described previously (21).

RNA isolation and gene expression analysis

Total RNA was isolated from cells using the TRIzol method (Invitrogen, Carlsbad, CA, USA). Approximately 1 μg of total RNA was used for DNase treatment (amplification grade; Invitrogen) and reverse transcription into first strand cDNA using Superscript III and oligo(dT)₁₂₋₁₈ (Invitrogen). The primers used for the CD34 quantitative PCR (qPCR) analysis were 5'-GGAGCAGGCTGATGCTGATG-3' (For); 5'-ATCCCCAGCTTTTTCAGGTCAGAT-3' (Rev). NCBI BLAST confirmed specificity of the primers. The presence of a single PCR product was verified by both the presence of a single melting temperature peak and detection of a single band of the expected size on agarose gels. Non-template controls were included to verify the method and the specificity of the primers. Mean primer efficiency was 96% \pm 3%. Real-time qPCR was performed as described previously (26), using a CFX96 real-time PCR detection system (Bio-Rad Laboratories, Hercules, CA, USA).

Spheroid-based angiogenesis model

Endothelial cells (750 cells/spheroid) were seeded in medium containing methylcellulose (Sigma-Aldrich, St Louis, MO, USA) to form spheroids (27). After 24 h, cells were embedded in collagen gel in the presence or absence of 50 ng/ml human recombinant VEGF-A (Sanquin) and allowed to sprout for 24 h. At least 8 spheroids per group were analyzed under an inverted microscope (Leica Microsystems, Mannheim, Germany) and phase contrast images were quantified using image analysis and ImageJ software (28).

Scratch assay

HMEC-1 cells were transfected with siRNAs as described above and cultured in 12-well tissue culture plates until confluent. The confluent monolayer was scraped with a 200- μl pipette tip to generate a wound and was rinsed twice with medium. Micrographs were taken at 40 \times magnification using an inverted microscope (Leica Microsystems) and phase contrast images were quantified using image analysis and ImageJ software (28).

Cell invasion assay

HMEC-1 cells were transfected with siRNAs as described above and seeded (5×10^4 cells per well) on transwell Boyden chamber inserts (8 μm pores; Corning, Lowell, MA, USA) containing a polycarbonate filter as previously described (29). Filters were pre-coated with Matrigel (BD Discovery Labware, Bedford, MA, USA) diluted 1:3 in M199 basal medium to create an artificial internal limiting membrane. Inserts containing cells were placed in M199 supplemented with 2% human serum in 24-well plates. HMEC-1 migration was stimulated by adding complete medium to the lower well of the Boyden chamber. After 24 h, membranes were washed with ice-cold phosphate-buffered saline (PBS) (Lonza, Walkersville, MD, USA) and the upper surface of the insert was swabbed to remove non-migrated cells. Cells that had migrated through the pores of the filter were either fixed in 4% paraformaldehyde (Electron Microscopy Sciences (EMS), Hatfield, PA, USA)

and stained with Hoechst or fixed with absolute methanol and stained with Giemsa. Migration was evaluated as the mean number of migrated cells in 5 high-power fields (HPF) per well (20× magnification). Each condition was assayed in triplicate and each experiment was performed at least twice.

Mice. All mice that were used in this study were backcrossed to C57Bl/6J mice for more than 12 generations. *Cd34*^{-/-} mice were generated as described previously (30). Mice were bred and maintained in specific pathogen-free conditions at the Biomedical Research Centre (The University of British Columbia (UBC), Vancouver, BC, Canada). All animal experiments were approved by UBC's animal care committee and were conducted humanely following institutional and Canadian Council on Animal Care guidelines (Protocol #A11-0289).

Oxygen-induced retinopathy model and analysis of postnatal retinal angiogenesis

The OIR model was carried out as previously described (31) with the use of a BioSpherix ProOX A chamber equipped with ProOx P110 oxygen controller (BioSpherix, Lacona, NY, USA). Postnatal day 7 (P7) pups together with their nursing dams were placed for 5 consecutive days in a 75% oxygen chamber. Litters of 8 pups or less had 1 nursing dam; those with more than 8 pups had 2 nursing dams. The chamber was only opened briefly between P7 and P12 when the nursing dams were replaced with foster dams to mitigate any adverse effects of hyperoxia on the nursing dams. At P12, the pups were returned to room air (21% oxygen). Pups were sacrificed and their eyes were collected at P12, P17 and P21. In addition, mouse eyes were collected from pups raised at room temp at P1, P3, P5, P7, P9 and P25 as a control.

Eyes were fixed for 30 min in 4% paraformaldehyde prepared in PBS. Retinas were dissected, fixed overnight in 4% paraformaldehyde at 4°C, dehydrated in methanol and stored in methanol at -20°C. Before immunofluorescence analysis, retinal whole-mounts were rehydrated, permeabilized in PBS containing 1% bovine serum albumin (BSA) (Sigma-Aldrich) and 0.5% Triton X-100 (Sigma-Aldrich) at 4°C overnight and washed with PBS. Retinal whole-mounts were blocked in PBlec (PBS (pH 6.8) with 1% Triton X-100, 0.1 mM CaCl₂, 0.1 mM MgCl₂, 0.1 mM MnCl₂ (all from Sigma-Aldrich)), and incubated with AF488-labeled or AF594-labeled lectin from *Bandeiraea simplicifolia* (isolectin B4) (Invitrogen) in PBlec at 4°C overnight. After extensive washing in PBS, the retinas were either flat mounted in Vectashield (Vector, Burlingame, CA, USA) or processed for multiple labeling, using primary antibodies directed against mouse CD34 (clone RAM34; eBioscience, San Diego, CA, USA) or mouse PODXL (clone 192704, R&D Systems). Secondary antibodies used were cyanine-3 (Cy3)-labeled donkey anti-goat and Cy3-labeled goat anti-rat, respectively (Jackson ImmunoResearch Laboratories Inc, West Grove, PA, USA). Images were taken using a wide-field fluorescence microscope or confocal microscope (Leica Microsystems). In control eyes, filopodia at the vascular front

were analyzed in 20 microscopic fields selected randomly from 5 retinas per group of mice (mutants or wild type littermates) and quantified using image analysis and ImageJ software (28). For the OIR model, the retinal avascular areas and neovascularization areas were quantified using Adobe Photoshop CS4 software according to a published protocol (28, 32).

Statistical analysis

Values are given as mean values \pm SD or SEM, as indicated. Data are represented as averages of independent experiments, performed in duplicate or triplicate. Statistical analyses were performed using the Student's t-test and P-values < 0.05 were considered to indicate statistically significant differences.

RESULTS

CD34 silencing does not impair sprouting angiogenesis *in vitro*

We previously reported that CD34 marks cells with an endothelial “tip cell” phenotype and gene expression pattern in cultures of HUVEC (21). To evaluate a possible functional role of CD34 in endothelial cells during angiogenesis, we carried out *in vitro* experiments using HMEC-1. Similar to HUVEC (21), approximately 9-10% of HMEC-1 express high levels of CD34 (Fig 1A, right panel). To test the functional contribution of CD34⁺ and CD34⁻ cells to sprouting, we generated spheroids of FACS-isolated populations of CD34⁺ or CD34⁻ HMEC-1 cells and embedded them in collagen gels in the presence or absence of VEGF-A. After 24 h, CD34⁺ sorted HMEC-1 showed a significant increase in the number of sprouts (but not sprout length) in response to VEGF-A, as did spheroids composed of unsorted HMEC-1 cells. The CD34⁻ HMEC-1 spheroids were unresponsive to VEGF-A (Fig 1A and 1B). This shows that VEGF-A-responsive angiogenic sprouting activity in HMEC-1 cultures is associated with the CD34⁺ population.

Although VEGF-A induced sprouting activity is associated with the CD34-expressing HMEC-1 population, it is possible that CD34 is simply a marker of “tip” like cells but does not serve a functional role. Therefore, to further investigate a possible functional role of CD34 in HMEC-1 sprouting angiogenesis or migration activity *in vitro*, we silenced CD34 expression in HMEC-1 using siRNA. Although only 10% of HMEC-1 in culture are positive for CD34, all cells express the closely related sialomucin podocalyxin (PODXL) (Fig 2A). Both CD34 and PODXL are widely expressed at the luminal plasma membrane of vascular endothelial cells. Knockdown of CD34 by siCD34 was confirmed at the mRNA transcript level by qPCR (Fig 2B, left panel). Notably, knockdown of CD34 did not alter gene expression of *PODXL* (Fig 2B, right panel). Flow cytometric analysis confirmed suppression of CD34 protein expression on the plasma membrane in the presence or absence of exogenous VEGF-A (Fig 2C).

To explore whether CD34 gene ablation affects endothelial cell sprouting, migration and invasion, we performed three separate *in vitro* assays. First, we repeated the spheroid-

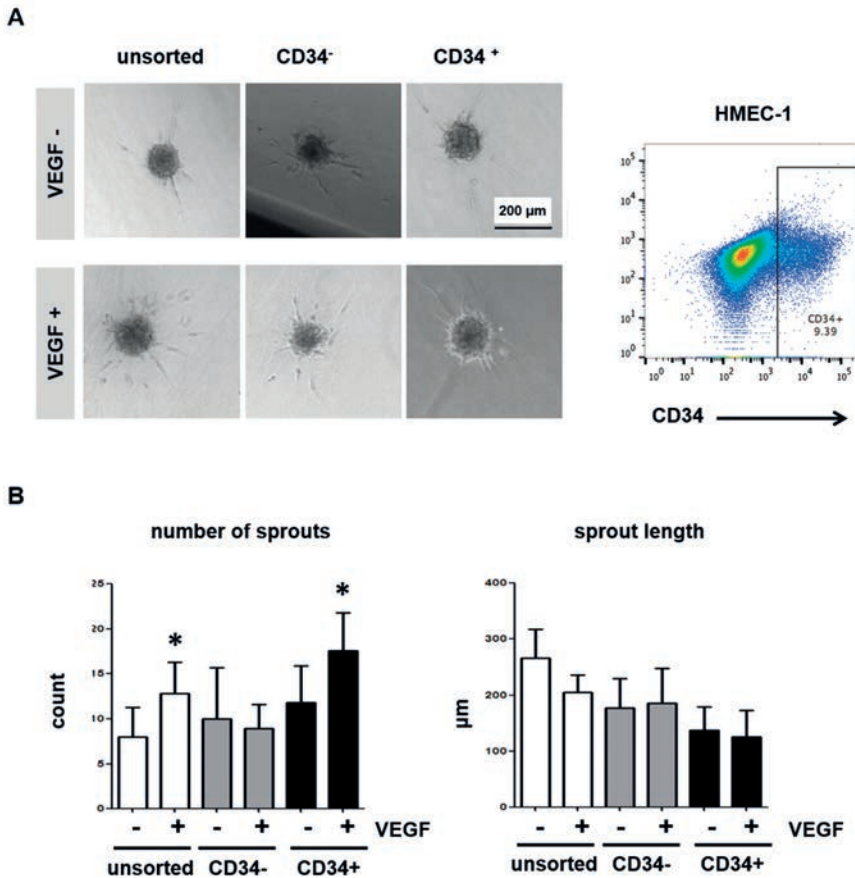


Figure 1. The CD34⁺ fraction of HMEC-1 cultures contains the VEGF-induced angiogenic sprouting activity. **(A, left panel)** Representative images of spheroids that were generated from HMEC-1 were either unsorted or FACS-sorted, based on CD34 cell surface expression (CD34⁻ and CD34⁺ populations). Spheroids were embedded in collagen gel supplemented with (+) or without (-) VEGF. Scale bar = 200 µm. **(A, right panel)** Flow cytometry dot plot demonstrating gating for HMEC-1 sorting based on CD34 expression. **(B)** The number of sprouts per spheroid and the mean sprout length were quantified using Image J. Error bars represent standard deviation. * Significantly different from unstimulated control (VEGF-) with $P < 0.05$.

based sprouting assay as described in Figure 1 using siCD34 transfected HMEC-1. Silencing of CD34 expression increased the number of sprouts per spheroid marginally (1.3-fold) in the absence of exogenous VEGF-A. However, spheroids in which CD34 was silenced did not respond to VEGF-A stimulation (**Fig 3A**). No significant differences were observed for sprout length when comparing spheroids silenced for CD34 with control spheroids (**Fig 3A**) and the results are in line with spheroids of FACS-isolated populations of CD34⁺ or CD34⁻ HMEC-1 cells. Second, we performed a wound closure (scratch) assay using siCD34 transfected HMEC-1. This experiment showed that silencing of CD34 did not alter

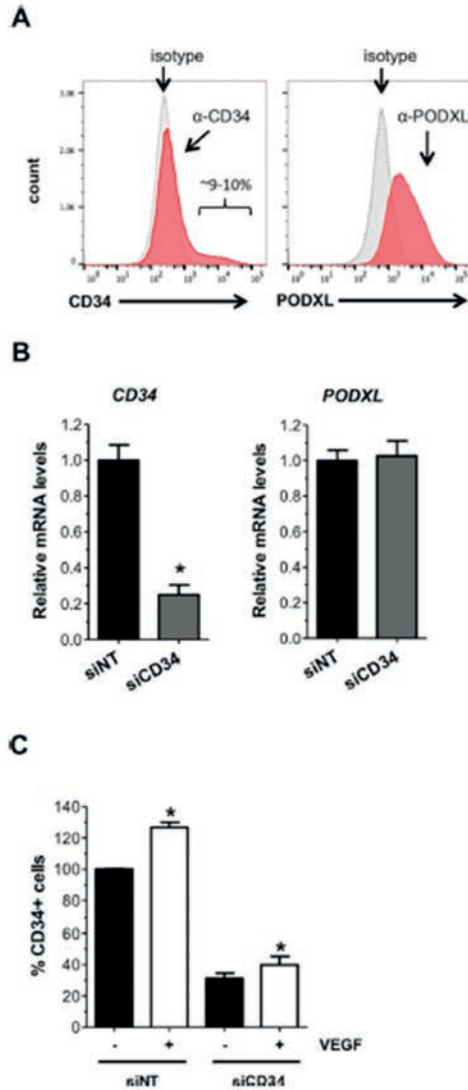
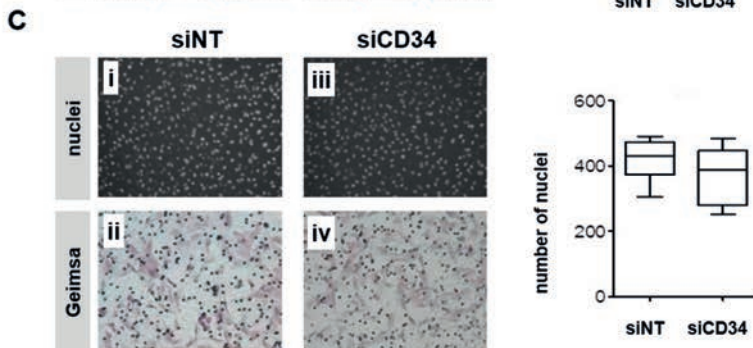
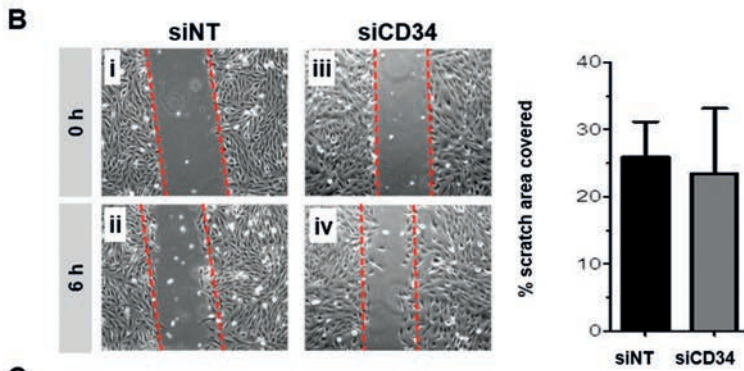
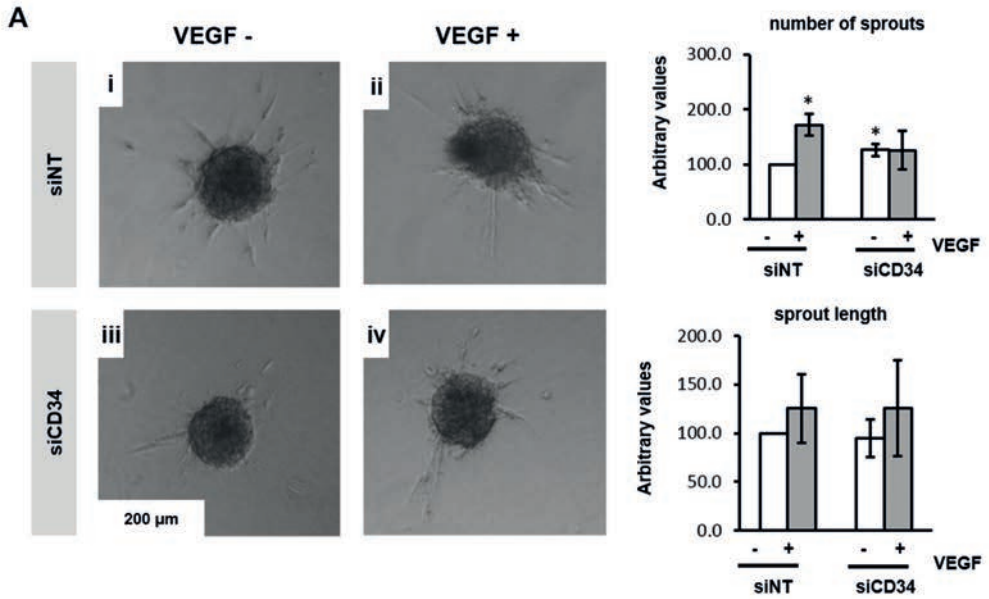


Figure 2. Silencing of CD34 expression in HMEC-1. (A) Representative histograms showing the intensity of anti-CD34 (left panel) or anti-podocalyxin (right panel) labeling of HMEC-1 cells compared to an isotype control (grey peak). (B) Quantitative PCR (qPCR) analysis of CD34 and PODXL mRNA levels and (C) flow cytometric analysis of CD34 protein expression on the membrane of HMEC-1 72 h after transfection with CD34-targeting (siCD34) or non-targeting (NT) (siNT) siRNA. Stimulation with VEGF induced CD34 plasma membrane expression in both siNT-treated and siCD34 treated HMEC-1 cells. However, CD34 expression in siCD34-treated HMEC-1 was less than 30% as compared to expression levels in siNT-treated cells. *Significantly different from non-stimulated cells with $P < 0.05$.



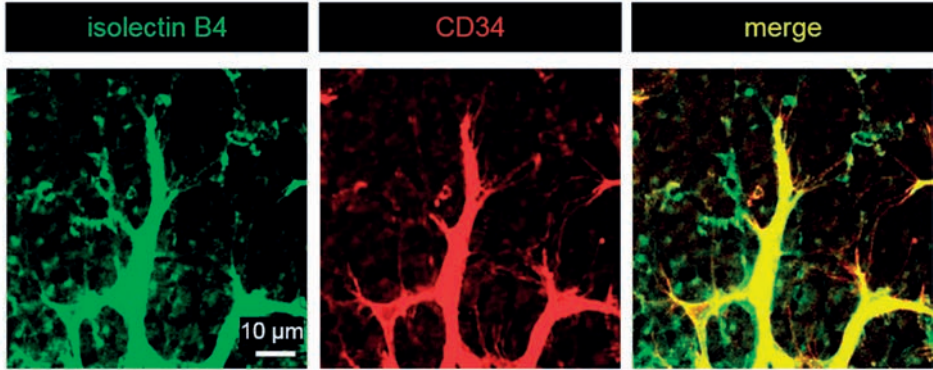
HMEC-1 migration (**Fig 3B**). Third, we seeded siCD34 transfected HMEC-1 into Boyden chambers containing membranes pre-coated with Matrigel to mimic the extracellular matrix of endothelium. Silencing of CD34 did not affect the level of HMEC-1 invasion after 20 hours in this assay (**Fig 3C**). Thus, although silencing of CD34 results in a marginal increase in spheroids sprouting, the most important result seems to be that HMEC-1 without CD34 expression do not respond to VEGF-A, although a basic level of sprouting is still intact. Migration and invasion of HMEC-1 were not affected by silencing of CD34. Migration and invasion of HMEC-1 were not affected by silencing of CD34.

CD34 is expressed on endothelial tip cells and tip cell filopodia *in vivo*

Since our *in vitro* assays suggested that CD34 has a role in regulating VEGF-induced sprouting activity, we next wished to determine whether CD34 has a role in sprouting angiogenesis *in vivo*. In retinal angiogenesis, blood vessels are formed in an organized and directional manner and offer a controlled and physiological model to study angiogenesis *in vivo*. Our first objective was to determine the expression pattern of CD34 in the mouse retina during postnatal vessel development. Immunohistochemistry of whole-mount retinas harvested from P5 mouse pups showed that CD34 and PODXL are expressed on the vasculature in the developing retina. Although CD34 expression is limited to a select population in HUVEC and HMEC-1 cultures, CD34 is more widely expressed throughout microvasculature in humans and is expressed on filopodial of angiogenic tip cells during active angiogenesis (21). Likewise, we found that in the developing retinal vessels of neonatal mice, CD34 is expressed on the filopodial extensions of tip cells at the angiogenic vessel front in addition to the expression throughout the advancing sprouts, phalanx and the lumen of the vessel stalk (**Fig 4A**). The distribution pattern of CD34 on endothelial cells in angiogenic tissues was similar to that of isolectin B4 (an endothelial marker used to visualize endothelial tip cells and their filopodia) (**Fig 4A**) (6, 7, 33-36). Notably, PODXL is expressed only within the stalk (and phalanx) region of vessels and is absent from

- ◀ **Figure 3.** Effect of CD34 silencing on sprouting, cell migration and invasion. (**A, left panel**) Representative images of spheroids that were generated from HMEC-1, transfected with either a non-targeting siRNA (siNT) or siCD34 and subsequently embedded in collagen gel in the presence or absence of VEGF-A. (**A, right panel**) Spheroids were analyzed at 24 h after embedding and the number of sprouts per spheroid and average sprout length were quantified using image J. Results were expressed relative to values of siNT transfected cells without VEGF. (**B, left panel**) siNT- and siCD34-transfected HMEC-1 were grown until confluent. Scratches were made using a pipette tip and images were taken at 0 and 6 h after scratching. (**B, right panel**) The percentage of width of the scratch filled with cells was quantified over time. (**C, left panel**) Representative images of HMEC-1 transfected with siNT or siCD34, located at the lower side of the Boyden filter after invasion through Matrigel visualized by DNA staining (i,iii) or Giemsa (ii,iv) staining at 20 h after seeding. (**C, right panel**) Cells invading the Matrigel were quantified by counting the number of nuclei per microscopic field. Error bars represent standard deviation; *Significantly different from siNT control with $P < 0.05$.

A



B

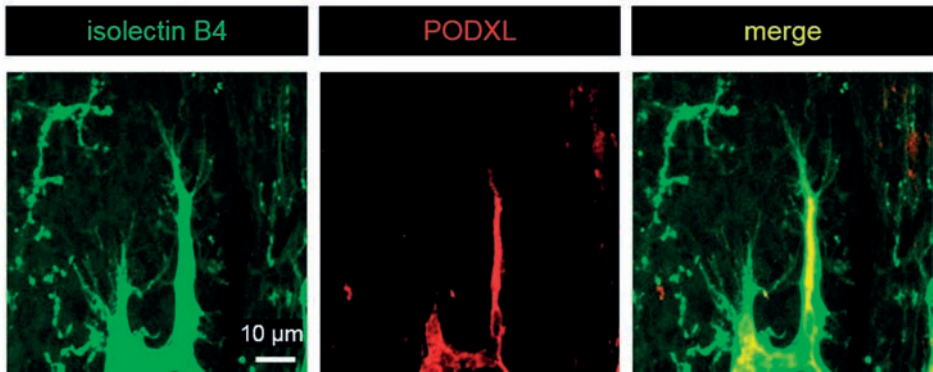


Figure 4. Endothelial tip cell filopodia in developing retinal vessels express CD34 but not podocalyxin. Immunofluorescence staining of retinal whole-mounts of wild type (Wt) mice at P5. Both CD34 and podocalyxin (PODXL) are expressed on developing vasculature. CD34 but not podocalyxin is expressed on endothelial tip cell filopodia. Isolectin B4 staining (green) was used to visualize tip cell filopodia. Scale bar = 10 μm .

the filopodia (**Fig 4B**). These findings suggest that CD34 and PODXL have non-redundant functions in vascular endothelia.

CD34 deletion reduces the number of tip cell filopodia without perturbing retinal vasculature development

Since CD34 is an anti-adhesive molecule, we hypothesized that CD34 reduces adhesion of filopodia to the extracellular matrix or membranes of other cells, thereby facilitating extension of tip cell filopodia. To test this hypothesis, we examined the morphologic features of tip cells during retinal development under normoxic conditions in wild type and *Cd34*^{-/-} mice. Detailed analysis of the vascular front revealed that filopodia density was reduced by 30% in *Cd34*^{-/-} mice at P5 as compared to wild type mice (**Fig 5**).

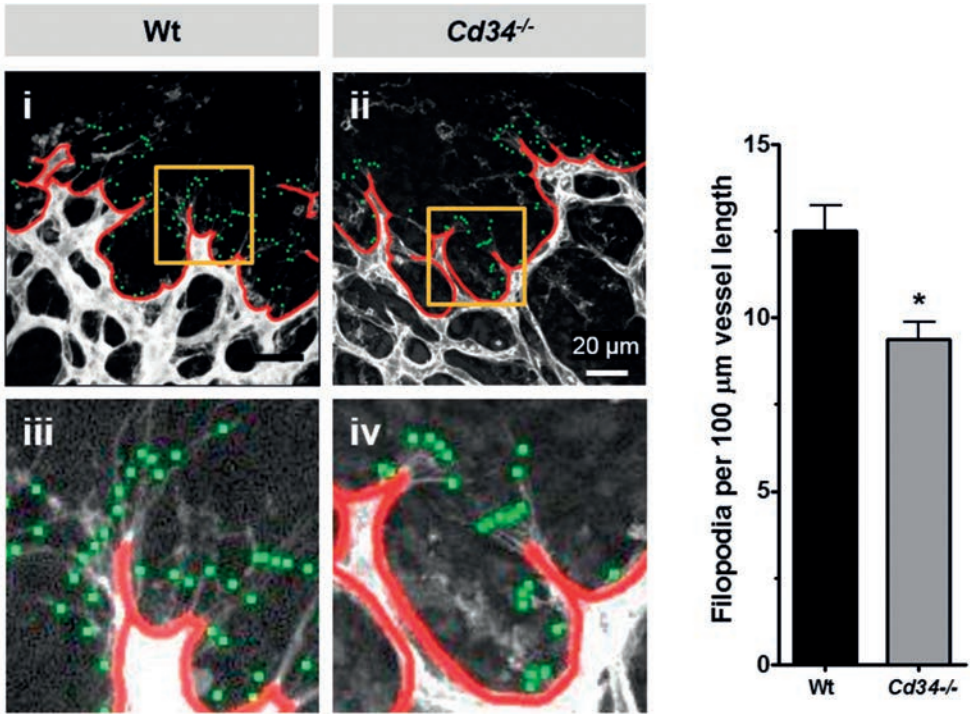


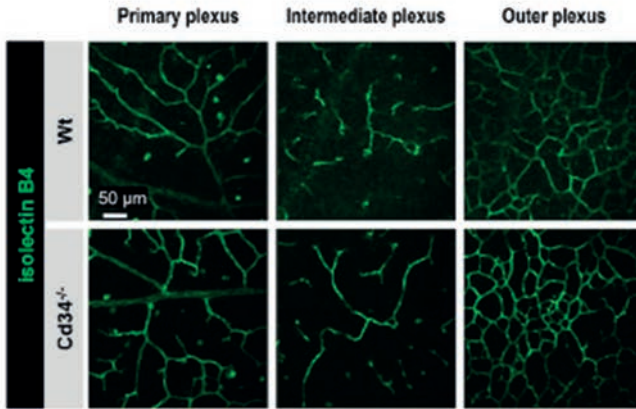
Figure 5. CD34 deletion reduces the number of endothelial tip cell filopodia. (A) Whole-mount isolectin B4 staining showing the angiogenic front of wild type (Wt) (i,iii) and *Cd34*^{-/-} (ii,iv) mouse retinas at P5. Scale bar (i,ii) = 20 μm. Tip cell filopodia were marked (green dots) and normalized to vessel length (red lines, see insets iii, iv). (A, right panel) Quantification of filopodia per 100 μm vessel length. Error bars represent standard errors of the mean. * Significantly different from wild type with P < 0.05.

To determine whether the reduction density of filopodia in *Cd34*^{-/-} mice has consequences for the physiological development of retinal vessels, we studied the retinal vasculature in normoxic wild type and *Cd34*^{-/-} mice at P25 (Fig 6A), when the superficial, intermediate and outer vascular plexus vessels are fully mature. Isolectin B4 staining of retinas of *Cd34*^{-/-} mice revealed no abnormalities in development in any of the retinal vascular plexus layers.

Although we did not detect PODXL expression on tip cell filopodia of advancing retinal vessels in wild type mice, it is possible that, in the absence of CD34, PODXL is expressed as a compensatory mechanism. However, immunohistochemistry of whole-mount retinas revealed no difference in PODXL expression on the vasculature in the developing retinas of wild type and *Cd34*^{-/-} mice. Moreover PODXL staining was not detected in filopodia at the angiogenic front in *Cd34*^{-/-} mice (Fig 6B).

From this we concluded that, although the CD34 enhances formation of filopodia at the angiogenic front of retinal vessels, CD34 is dispensable for vascularization of the mouse

A



B

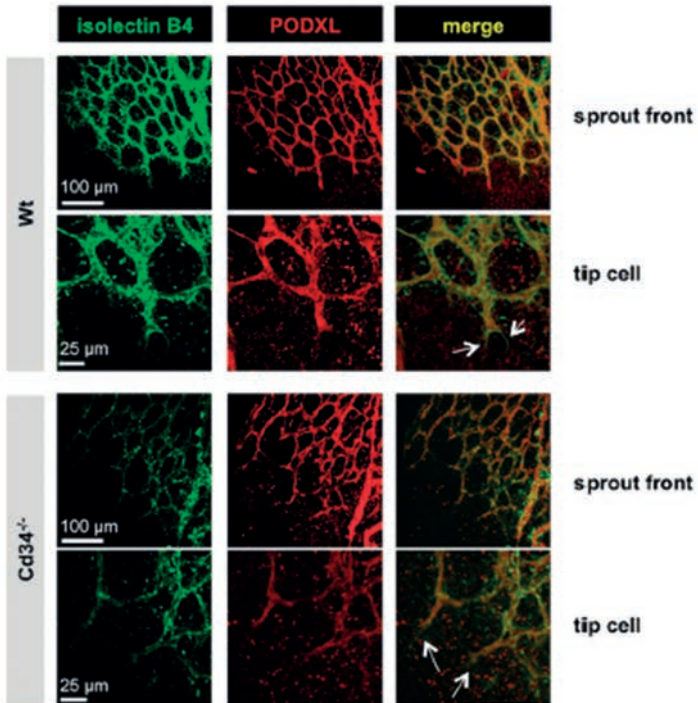


Figure 6. Retinal vessels develop normally in *Cd34*^{-/-} mice under normoxic conditions and podocalyxin is not expressed on tip cells in developing retinal vessels in *Cd34*^{-/-} mice. (A) Isolectin B4 staining (green) of retinal whole-mounts of wild type (Wt) and *Cd34*^{-/-} mice under normoxic conditions at P25. The plexuses of retinal vessels in both the inner and outer retina are similar in Wt and *Cd34*^{-/-} mice at P25. Scale bar = 50 µm. (B) Immunofluorescence staining of podocalyxin (PODXL, red) and isolectin B4 (green) of whole-mounts of retinas harvested from wild type (Wt) and *Cd34*^{-/-} mice at P5. The arrows in the merge (yellow) indicate tip cell filopodia that stain with isolectin B4 but do not co-express podocalyxin. Podocalyxin is not expressed on endothelial tip cell filopodia in either wild type (Wt) or *Cd34*^{-/-} mice. Scale bars = 100 mm (sprout front) or 25 mm (tip cell).

retina. In addition, PODXL does not compensate for loss of CD34 expression during retinal angiogenesis. These data suggest that CD34 expression marks endothelial tip cells during retinal angiogenesis, but it is not functionally required for vessel development in the retina.

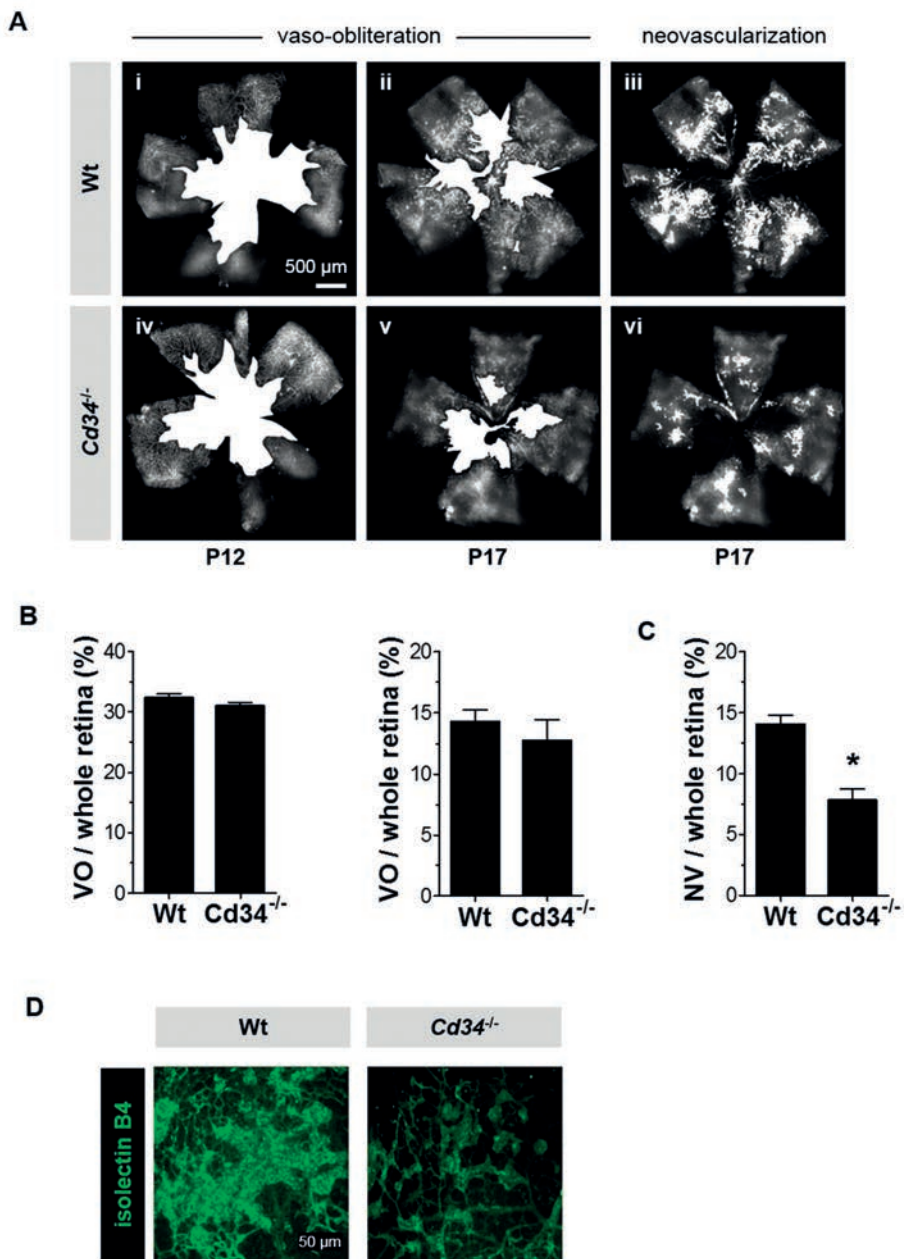
CD34 is involved in epi-retinal neovascularization but is dispensable for restoration of retinal vasculature following vaso-obliteration.

We next used the OIR model to determine whether ablation of *Cd34* impairs pathological retinal neovascularization. The OIR model is an acute bi-phasic model of pre-retinal neovascularization associated with ischemia in the retina that develops after a period of experimental hyperoxia. In the first phase, P7 mouse pups are exposed to a high oxygen concentration (75% O₂) for 5 days (P7-P12) to cause retinal vaso-obliteration in the central posterior retina (37). In the second phase, pups are returned to normoxia where the relatively low oxygen concentration of 21% causes hypoxia and consequent excessive angiogenesis beyond the retina into the vitreous. Endothelial cell migration and invasion through the inner limiting membrane (the boundary between the neuroretina and the vitreous cavity) is an early phase of the formation of pathological neovascular tufts that expand beyond the retina in the OIR model.

We first analyzed the degree of vaso-obliteration in *Cd34*^{-/-} and wild type pups after 5 days of hyperoxia (P12) and found that exposure to hyperoxia resulted in a significantly reduced number of retinal capillaries especially in the central area (Fig 7A) but the extent of vaso-obliteration was identical in wild type and *Cd34*^{-/-} mice at P12 and P17 (Fig 7A and 7B). However, the ratio of the area of pre-retinal neovascularization to the total retinal area was significantly lower at P17 in *Cd34*^{-/-} mice (7.8%) as compared to wild type mice (14.0%) (Fig 7C). Furthermore, confocal images of P17 OIR retinas labeled with isolectin B4 revealed that epi-retinal tufts in wild type mice aggregated as large continuous areas of neovascularization whereas in *Cd34*^{-/-} mice, the considerably smaller tufts did not aggregate (Fig 7D). At P25, vaso-obliteration or neovascularization was not detected in OIR-treated wild type or *Cd34*^{-/-} mice and both genotypes appeared to have recovered the retinal vasculature at this stage (data not shown). Thus, in a model of pathological angiogenesis, the absence of CD34 reduces epi-retinal vessel tuft formation, a process that contributes to vision impairment in human retinopathies.

DISCUSSION

Earlier studies showed that CD34 is actively regulated on vascular endothelial cells and that angiogenic factors play a role in this regulation (7, 12, 13, 16, 21-23, 27, 38). The role of VEGF in CD34 expression on endothelial cells *in vitro* has been controversial with studies showing that it either downregulates (12, 38) or upregulates (21, 27) expression. We hypothesized that the anti-adhesive function of CD34 is relevant in angiogenesis during invasion of endothelial tip cells through the basal lamina and other



extracellular matrix structures. This hypothesis was borne out as we previously found that CD34 enhances adhesion, mobility and invasiveness of hematopoietic progenitors, mast cells, and eosinophils (17-20). The observation of high expression of CD34 on endothelial tip cells and their filopodia suggests a similar molecular function (7, 13, 21-23). Adhesive and anti-adhesive interactions between cell surface proteins and individual components of the vascular basal lamina determine the number and the behavior of endothelial tip cells during angiogenesis [42]. We showed that sprouting angiogenesis activity in HMEC-1 cultures is enhanced in the CD34⁺ fraction of HMEC-1 cells, and silencing of CD34 expression in HMEC-1 cells inhibits their response to exogenous VEGF-A. Migration is a key characteristic of tip cells. However, we did not find any effect of silencing of CD34 on HMEC-1 invasion or migration *in vitro*. We conclude that the absence of CD34 prevents VEGF-induced angiogenic sprouting *in vitro*, but does not limit endothelial cell migration or invasion *in vitro*.

During developmental angiogenesis in the mouse retina, CD34 is expressed on filopodia of endothelial tip cells in a distribution pattern similar to that of isolectin B4 (22). We show that ablation of CD34 in mice reduces the formation of filopodia in retinal tip cells by approximately 30% during developmental retinal angiogenesis. However, this reduction in filopodia was not sufficient to cause a loss of vessel density in the fully developed retinas in *Cd34*^{-/-} mice. This is consistent with observations by Sawamiphak et al [43] who report that reduction of filopodial density by at least 50% is needed to attenuate vessel density in the retina and Phng et al [8] who show that filopodia are dispensable for angiogenesis [8, 43]. Because we have previously shown that PODXL is a potent inducer of microvillus formation in epithelial cells [14] and because microvilli and filopodia share many structural similarities and molecular components, we considered the possibility that PODXL compensates for the loss of CD34 in the formation of endothelial tip cell filopodia. However, we did not detect PODXL expression on filopodia at the retinal vessel front in either wild type or *Cd34*^{-/-} mice.

We found that CD34 did not impair physiological retinal angiogenesis aimed to restore the vasculature due to OIR. However, CD34 ablation impaired pathological epi-retinal tuft formation in the OIR model. Intriguingly, Budd et al. showed that reduced numbers of endothelial tip cell filopodia corresponded to a reduced intravitreal but not intra-retinal

- ◀ **Figure 7.** Loss of CD34 limits formation of pathological neovascularization in oxygen-induced retinopathy (OIR). (A) Representative retinal images showing total retinal area and regions of vaso-oblivation (VO) in OIR model for wild type (Wt) and *Cd34*^{-/-} mice at P12 and P17 and neovascularization (NV) at P17. Scale bar = 50 μm (B) Ratios of VO to total retinal area indicated no significant difference in VO between wild type and *Cd34*^{-/-} mice. (C) At P17, neovascularization was significantly decreased in *Cd34*^{-/-} mice as compared to wild type mice (*P < 0.01). Error bars represent standard deviation. * Significantly different from wild type with P < 0.05. (D) Isolectin B4 labeling of retinas harvested at P25 after OIR revealed that epi-retinal tufts in wild type mice aggregated as large continuous areas of neovascularization whereas in *Cd34*^{-/-} mice, the considerably smaller tufts did not aggregate. Scale bar = 50 μm.

vascularization [44]. Therefore, it is possible that the diminished number of filopodia in retinal tip cells in *Cd34*^{-/-} mice hampered intravitreal invasion. This suggests that CD34 has a functional role in VEGF-mediated vessel growth.

2.1

CONCLUSION

In conclusion, our study shows that CD34 is important for the formation of vascular sprouts and filopodia but CD34 does not appear to be essential for the development of an intact retinal vascular network. However, the absence of CD34 limits invasion of vessels into the vitreous and formation of epi-retinal tufts in the OIR model, which suggests that CD34 is involved in the pathological neovascularization causing vision loss in proliferative retinopathies.

ACKNOWLEDGEMENTS

We thank Drs. W. Song and F. Cai (Department of Psychiatry, Faculty of Medicine, University of British Columbia (UBC)) for use of their mouse oxygen incubator. We are grateful to Dr. Jennifer Baker for her helpful suggestions and critical reading of the manuscript. MJS was supported by the Dutch Cancer Society (KWF) (KWF-stagebeurs voor academici). MRH and JC were supported by a PDF-summer studentship from the Centre for Blood Research at UBC. This work was partially funded by a Grant-in-Aid from the Heart and Stroke Foundation of Canada (to KMM). KMM is a Michael Smith Foundation for Health Research Senior Scholar.

Marchien G. Dallinga¹,
Bahar Yetkin-Arik¹,
Richelle P. Kayser¹,
Ilse M.C. Vogels¹,
Patrycja Nowak-Sliwinska²,
Arjan W. Griffioen³,
Cornelis J.F. van Noorden^{1,4},
Ingeborg Klaassen¹,
Reinier O. Schlingemann^{1,5}

¹ Ocular Angiogenesis Group, Departments of Ophthalmology and Medical Biology, Amsterdam University Medical Centers, Academic Medical Center, Amsterdam, The Netherlands.

² School of Pharmaceutical Sciences, University of Geneva, Geneva, Switzerland.

³ Angiogenesis Laboratory, Department of Medical Oncology, Amsterdam University Medical Centers, VU University Medical Center, Amsterdam, The Netherlands.

⁴ Department of Genetic Toxicology and Cancer Biology, National Institute of Biology, Ljubljana, Slovenia

⁵ Department of Ophthalmology, University of Lausanne, Jules-Gonin Eye Hospital, Fondation Asile des Aveugles, Lausanne, Switzerland



**IGF2 AND IGF1R IDENTIFIED AS NOVEL TIP
CELL GENES IN PRIMARY MICROVASCULAR
ENDOTHELIAL CELL MONOLAYERS**

INTRODUCTION

New blood vessel sprouting is led by tip cells, a transdifferentiated phenotype of endothelial cells (ECs) induced by pro-angiogenic factors including vascular endothelial growth factor (VEGF) (39, 40). *In vivo*, the tip cell phenotype is characterized by extension of filopodia, enhanced migratory propensity and mitotic quiescence (39, 41). Tip cells differ in various aspects from the more proximal, proliferating stalk cells and the maturing phalanx cells (40), and express a distinct set of genes (42, 43). Until recently, progress in research on tip cells has been slow because of the need to use laboratory animals, as an *in vitro* model of tip cells was lacking. However, we have identified tip cells in monolayer HUVEC cultures employing CD34 as a marker (44). *In vivo*, CD34 is expressed throughout the body at the luminal side of endothelial cells of small blood vessels and umbilical veins and on filopodia of tip cells (12), but we have shown that in monolayers of HUVECs that have been passaged at least 3 times, approximately 10% of the cells express high levels of CD34. Moreover, these CD34-positive HUVECs have a distinct phenotype, with striking similarities when compared to tip cells *in vivo*, including CD34⁺ filopodia-like extensions, mitotic quiescence and expression of tip cell genes (44, 45).

As validation of our *in vitro* model for tip cells, we investigated first whether CD34⁺ tip cells are also present in monolayer cultures of primary human microvascular endothelial cells (hMVECs), as angiogenesis *in vivo* is initiated in microvessels (46). In addition, we studied the effects on CD34⁺ tip cells of silencing of two known tip cell genes, the growth factor angiopoietin-2 (*ANGPT2*) and the receptor tyrosine kinase with immunoglobulin-like and EGF-like domains 1 (*TIE1*), both of which were shown by us previously to have higher mRNA expression levels in CD34⁺ tip cells (44). *ANGPT2* is involved in angiogenesis and interacts with the actin cytoskeleton to induce migration (47). Silencing of *ANGPT2* in mouse models of angiogenesis results in absence of tip cells at the front of new vessel sprouts in mouse retinas (48). *TIE1* is an orphan receptor, which is expressed on tip cells and a subset of stalk cells, and which is involved in survival signaling in stalk cells (49).

Then, we explored the role in angiogenesis of two novel tip cell genes identified by us on the basis of differential expression in microarrays of CD34⁺ and CD34⁻ HUVECs, insulin-like growth factor 2 (*IGF2*) and insulin-like growth factor-1 receptor (*IGF1R*) (6). Both genes belong to the IGF family of growth factors, which consists of the ligands IGF1 and IGF2, the receptors IGF1R, IGF2R and insulin receptor (*INSR*) and at least 7 IGF binding proteins (IGFBPs). IGF2 binds to and signals through IGF1R and the other IGF receptors. In earlier studies, knockdown of IGF2 and IGF1R inhibited angiogenesis in developing mice and zebrafish (50-52), but a specific role of these proteins in tip cells has not yet been reported. Here, we used our tip cell model to further characterize the role in angiogenesis of these novel tip cell genes.

MATERIALS & METHODS

Cell cultures

Primary human umbilical vein endothelial cells (HUVECs) were isolated from umbilical cords (obtained from the Department of Gyneacology, Academic Medical Center, Amsterdam, The Netherlands), as described earlier [16], and grown in M199 basal medium (Gibco, Grand Island, NY, USA) supplemented with 10% heat inactivated human serum (obtained from the Department of Oncology, Academic Medical Center, Amsterdam, The Netherlands), 10% fetal bovine serum (Gibco), and 1% penicillin-streptomycin-glutamine (Gibco). HUVEC cultures were incubated with antibodies directed against CD31/PECAM-1 (1:100; eBioscience, Vienna, Austria) to check the purity of the endothelial cells. Human microvascular endothelial cells (hMVECs), a kind gift of Dr. P. Koolwijk (VU University Medical Center, Amsterdam, The Netherlands), were cultured with 50% HUVEC medium and 50% EBM-2 medium (Lonza, Basel, Switzerland) and cells were characterized as previously described [17]. HUVECs and hMVECs were cultured in 2% gelatin-coated (Millipore, Billerica, MA, USA) T75 culture flasks at 37°C and 5% CO₂. Experiments were performed with confluent HUVEC at passage 3 cells and hMVEC at passage 9-10 cells of at least 3 different donors. Subjects gave informed consent for the use of tissues or serum and samples were stored anonymously. Cells were treated with recombinant human VEGF-A (R&D Systems, Minneapolis, MN, USA), IGF2 (ProSpec, Rehovot, Israel), bFGF (Sanquin, Amsterdam, The Netherlands) or DLL4 (R&D Systems) as indicated.

Immunocytochemistry

Cells were cultured on gelatin-coated coverslips (Thermo Scientific, South Logan, UT, USA) for 72 h when treated with siRNA or until confluent for spheroids and sorting experiments. Cells were fixed in freshly-made 4% paraformaldehyde in phosphate-buffered saline (PBS, Lonza) for 15 min at room temp, and then blocked in PBS containing 10% bovine serum albumin (BSA; Sigma-Aldrich, St. Louis, MO, USA) and 0.5% Triton X-100 (Sigma) for 1 h at room temperature. Next, cells were incubated with a primary antibody against CD34 (diluted 1:100, clone MD34.2; Sanquin) for 2 h and a secondary anti-mouse Alexa488 antibody (Life Technologies, Carlsbad, CA, USA) and phalloidin (Life Technologies) to stain for F-actin for 1 h.

DLL4 coating

Culture flasks were coated according to Harrington *et al.* (53) using 0.2% gelatin in PBS, with 1 µg/mL of either recombinant human DLL4 (R&D systems) or BSA for 24 h before the cells were seeded. After cells were cultured for 24 h, flow cytometric analysis was performed.

Determination and selection of tip cells

For determining the percentage of tip cells, cells were harvested using TrypLE (Gibco), fixed in 4% paraformaldehyde in PBS for 15 min at room temp and incubated with anti-CD34-phycoerythrin antibody (diluted 1-100; anti-CD34-PE; clone QBend-10, Thermo Scientific, Waltham, MA, USA) for 30 min at room temperature. Cells were analyzed flow cytometrically using a FACSCalibur (Becton Dickinson, Franklin Lakes, NJ, USA) and FlowJo 6.4.7 software (Tree Star, San Carlos, CA, USA). The FITC channel was used to detect autofluorescence. Non-stained and non-treated cells were used as negative controls. For cell sorting experiments, cells were sorted on the basis of CD34 expression with anti-CD34-PE on a Sony SH800z cell sorter (Sony Biotechnology, Surrey, UK). CD34⁺ cells were cultured for 6 or 24 h, and then cells were fixed, stained and analyzed using flow cytometry as described above.

Apoptosis

Cellular apoptosis was assessed by measuring binding of annexin-V conjugated with FITC, following manufacturer's instructions (Molecular Probes, catalog number: V13242, Eugene, OR, USA) in combination with staining for CD34 to discriminate apoptosis in tip and non-tip cells.

RNA isolation and quantitative PCR

Total RNA was isolated from cells using the TRIzol method according to the manufacturer's instructions (Invitrogen, Carlsbad, CA, USA). An amount of 1 µg RNA was used for DNase I treatment (amplification grade; Invitrogen) and reverse transcribed into cDNA using the Maxima First Strand cDNA Synthesis Kit (Thermo Scientific). Real-time quantitative PCR (RT qPCR) was performed using a CFX96 real-time PCR detection system (Bio-Rad Laboratories, Hercules, CA, USA) as described previously (Siemerink et al. 2012). Primer details are presented in **Supplementary Table 1**. NCBI BLAST confirmed the specificity of the primers. The presence of a single PCR product was verified by both the presence of a single melting temperature peak and detection of a single band of the expected size on agarose gels. Non-template controls were included to verify the method and the specificity of the primers. PCR products that did not show a single melting temperature peak were excluded from analysis. Ct values were converted to arbitrary absolute amounts ($2^{-Ct} \times 1E^{12}$) and expressed as fold change as compared to controls. Expression data was normalized to tyrosine 3-monooxygenase/tryptophan 5-monooxygenase activation protein zeta (YWHAZ) mRNA levels.

siRNA knockdown

HUVECs and hMVECs were transfected with 25 nM of either a non-targeting small interfering RNA (siNT) or a gene-specific siRNA and 2.5 µg/mL Dharmafect 1 transfection agent (Dharmacon, Lafayette, CO, USA). The cells were transfected during 6 h using

the reversed transfection method according to the manufacturer's instructions. Transfection efficiency was checked at the mRNA level and was considered acceptable when expression was reduced by at least 70% after 72 h.

2.2

Spheroid-based sprouting assay

Spheroid experiments were performed with siRNA-transfected cells or cells that were sorted on the basis of CD34 expression. HUVECs transfected with siRNA were harvested after 48 h and 750 cells per spheroid were seeded in methylcellulose (Sigma-Aldrich, Buchs, Switzerland) containing M199 medium and 2% human serum to allow spheroid formation (27). Cells sorted according to CD34 expression were immediately seeded in the same manner. After 18 h, the spheroids were embedded in collagen gels containing 0.5% human serum and, when indicated, treated with VEGF-A (25 ng/mL) or IGF2 (50 ng/mL), and were allowed to sprout for 24 h. Images were taken using a phase-contrast microscope and the number of sprouts and average sprout length per spheroid were analyzed using the Neuron-J plug-in package of Image-J software (28). Spheroid experiments were performed with HUVECs, since hMVECs did not sprout in this experimental setup.

Statistics and data correction

To correct for differences between donors, data from flow cytometry and spheroid experiments were corrected using the Factor Correction program as described previously (54). Statistical analysis was performed using a Student's t-tests.

Chicken chorioallantoic membrane assay

The anti-angiogenic efficacy of a custom si*IGF2* (Dharmacon) was tested in the CAM model (55) via topical administration (each time 25 ml), between embryo development day (EDD) 7 and 8 once daily. Control eggs (blank) received 25 ml of HEPES (4-(2-hydroxyethyl)-1-piperazineethanesulfonic acid) buffer (Gibco) or 25 ml of non-targeting control siRNA (siNT) (Eurogentec, Liege, Belgium, SR-C2000-005) premixed with HEPES buffer and transfection reagent (DharmaFECT-1; Dharmacon). At EDD 9, the *in ovo* CAMs were visualized by means of FITC-dextran (20 kDa, 25 mg/mL; Sigma-Aldrich) epi-fluorescence angiography (56) and subsequently analyzed by an image-processing quantification method as described previously (57). Briefly, on the basis of FITC-dextran fluorescence angiography the skeleton overlay of the vascular network was placed on top of the vascular network and branching points/mm² were calculated.

Zebrafish morpholino experiments

Zebrafish experiments were performed with the approval of the Animal Ethics Committee of the University of Amsterdam and in compliance with the Association for Research in Vision and Ophthalmology (ARVO) statement for the Use of Animals in Ophthalmic

and Vision Research. *Tg(Fli1a:eGFP)* transgenic zebrafish embryos were injected with morpholino oligonucleotides against *IGF2a* or *IGF2b* that were designed and tested previously (52, 58). For each gene, a 6-base pair mismatch control was used, and a p53 morpholino as a control for non-specific activation by morpholino injection. After 24 and 30 h, the chorion was manually removed and zebrafish were mounted in 0.5% agarose gels and analyzed using confocal microscopy. Details of morpholino sequences are shown in **Supplementary Table 1**.

RESULTS

Human microvascular endothelial cell cultures contain CD34⁺ tip cells

We have previously identified CD34 as a marker for tip cells in monolayer cultures of HUVECs (44), which are of macrovascular origin. hMVECs are primary cells of microvascular origin, and derived from the endothelial cell types which generate new vessels *in vivo*, and may therefore be physiologically more relevant for studies of angiogenesis. To study whether tip cells are also present in monolayer cultures of hMVECs, we analyzed CD34 expression with flow cytometry and confocal microscopy, using anti-CD34 antibodies. This revealed a population of CD34⁺ hMVECs with filopodia-like extensions (**Fig. 1a**) of approximately 10% (**Fig. 1b**).

Freshly-isolated HUVECs and hMVECs express CD34 on all cells ((59, 60), but the percentage of CD34⁺ cells gradually tapers with increasing passage numbers until an equilibrium has been reached which is maintained for several passages. In HUVEC cultures, the equilibrium is reached at passage 3, whereas in hMVEC cultures the equilibrium is reached at passage 9. We examined whether CD34 expression in hMVECs either marks newly generated tip cells or identifies cells that have retained their phenotype since isolation. For this purpose, we sorted and cultured CD34⁻ hMVECs and found that between 6 and 24 h after the CD34⁻ cells were plated a new fraction of CD34⁺ cells appeared (**Fig. 1c-e**). This suggests that CD34⁺ cells develop *de novo* in CD34⁻ hMVEC cultures.

Next, we determined whether VEGF, DLL4 and bFGF would change tip cell differentiation, as measured by the percentage of tip cells in hMVECs, in a similar manner as was reported for these factors tip cells *in vivo*. In the developing mouse retina, VEGF stimulates tip cell formation (39), whereas DLL4 inhibits the tip cell phenotype (61, 62) and bFGF induces proliferation of blood vessels (63). In hMVEC cultures, VEGF significantly increased the percentage of CD34⁺ cells (**Fig. 1f**). In contrast, DLL4 and bFGF significantly decreased the percentage of CD34⁺ cells (**Fig. 1f, g**).

Analysis of mRNA expression of genes that have been associated with a tip cell phenotype in the developing mouse retina and zebrafish embryos (39, 42, 43, 64-72), showed that 13 out of the 14 genes have significantly higher expression levels in CD34⁺ than in CD34⁻ hMVECs (**Fig. 1h**).

These experiments show that CD34⁺ hMVECs are phenotypically and genotypically similar to tip cells *in vivo*.

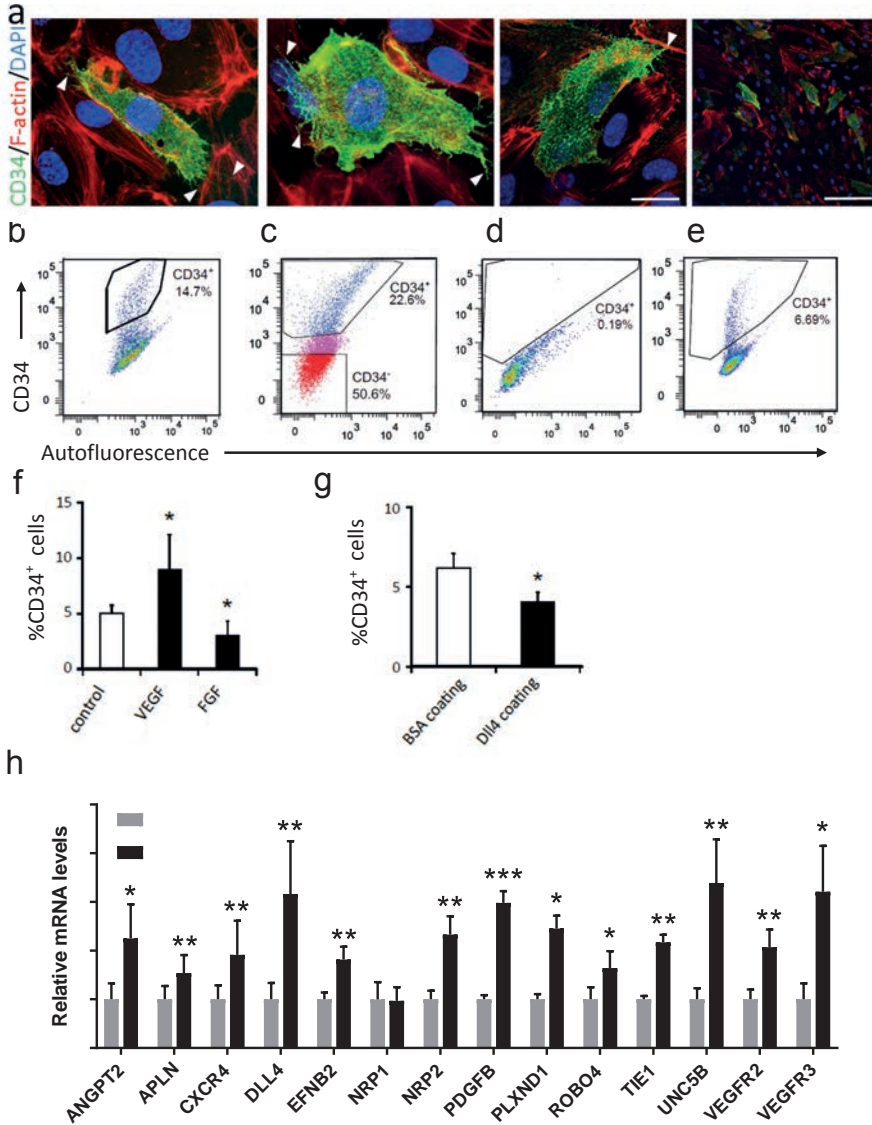


Figure 1. Human microvascular endothelial cell cultures contain CD34⁺ tip cells. (a) Identification of tip cells by staining with anti-CD34 (green), F-actin (phalloidin, red) and nuclei (DAPI, blue) in hMVECs. Representative examples are shown. Arrowheads indicate filopodia-like extrusions on CD34⁺ cells. Scale bar represents 25 μ m (first 3 images) and 100 μ m (last image). (b) HMVECs were analyzed for CD34 expression by flow cytometry. (c-e) Re-expression of CD34 in hMVECs after cell sorting. CD34⁻ cells (shown in c) were cultured and CD34 expression was analyzed after 6 h (d) and 24 h (e). (f-g) The effect of exposure to VEGF or bFGF (f) and DLL4 (g) on the percentage of CD34⁺ tip cells. BSA was used as a control for DLL4. * $p < 0.05$ as compared to control. Data are shown as the mean \pm standard deviation after factor correction ($n=3$). (h) Fold change in mRNA expression levels of known tip cell genes in CD34⁺ hMVECs as compared to CD34⁻ hMVECs. Graph shows fold change of expression in CD34⁺ cells as compared to CD34⁻ cells after factor correction ($n=5$). * $p < 0.05$, ** $p < 0.01$, *** $p < 0.001$.

Knockdown of ANGPT2 expression inhibits tip cell differentiation and sprouting

As a further validation of our *in vitro* tip cell model, we investigated whether knockdown of the expression of known tip cell genes would affect the percentage of tip cells similar as was reported *in vivo*. For this purpose, we chose *ANGPT2* and *TIE1*. Knockdown of *Angpt2* was reported to reduce the number of tip cells at the retinal sprouting front in the developing mouse retina (48, 73) and knockdown of the orphan receptor *Tie1* in mouse retinas resulted in stalk cell apoptosis (49). Previously published microarray data (Geo Accession: GSE 34850) showed that *ANGPT2* and *TIE1* mRNA levels were significantly higher in CD34⁺ HUVECs than in CD34⁻ cells (44), which could be confirmed for hMVECs by qPCR as well (Fig. 1h).

Knockdown of *ANGPT2* expression by siRNA reduced the percentages of CD34⁺ tip cells significantly in hMVECs (Fig. 2a), but not in HUVECs (Fig. 2b). However, in the HUVEC spheroid-based sprouting model, sprout numbers and average sprout length were significantly decreased after knockdown of *ANGPT2* expression (Fig. 2c, d), and resulted in a disturbance of the actin cytoskeleton, in which the number of short radial stress fiber-like actin bundles was increased (Fig. 2g).

Knockdown of *TIE1* expression resulted in a significant increase in the CD34⁺ tip cell fraction in HUVECs (1.7-fold; Fig. 2a) and HMVECs (1.6-fold; Fig. 2b). The number of sprouts in the HUVEC spheroid model was marginally decreased (Fig. 2c), whereas sprout length was unaffected (Fig. 2d). Immunocytochemical staining of CD34 and F-actin showed that knockdown of *TIE1* expression did not result in morphological changes in HUVECs (Fig. 2g). After *TIE1* knockdown, apoptosis in CD34⁻ cells was higher (22.3%) than in siNT-treated HUVECs (11.1%), whereas in CD34⁺ HUVECs the percentage of apoptotic cells was much lower (1.4%) with no difference as compared to siNT control (Fig. 2e, f). This indicates that at least part of the measured increase in tip cell percentage after *TIE1* knockdown was due to apoptosis of the CD34⁻ non-tip cells.

Together, we show that by using our *in vitro* tip cell model, we were able to reproduce observations reported on tip cells after *ANGPT2* and *TIE1* knockdown *in vivo*.

Expression of IGF2 and IGF1R are essential for tip cell maintenance

Our microarray data of HUVECs showed that mRNA expression levels of *IGF2* were 45-fold higher in CD34⁺ cells as compared to CD34⁻ cells [6]. In addition, expression levels of *IGF1R*, a receptor for IGF2, were 2.1-fold higher in CD34⁺ cells (44). IGF2 is known to stimulate angiogenesis *in vitro*, and increased IGF2 mRNA expression was found in vascular tufts in the retina of mice in the oxygen induced retinopathy model [39] and in human vascular tumors such as hemangiomas (50, 74, 75). To investigate whether IGF2 is specifically involved in tip cell fate, we performed knockdown of *IGF2* and *IGF1R* expression in hMVECs and HUVECs, which resulted in decreased percentages of CD34⁺ tip cells (Fig. 3a, b) and reduced numbers of sprouts per spheroid (Fig. 3c). Knockdown

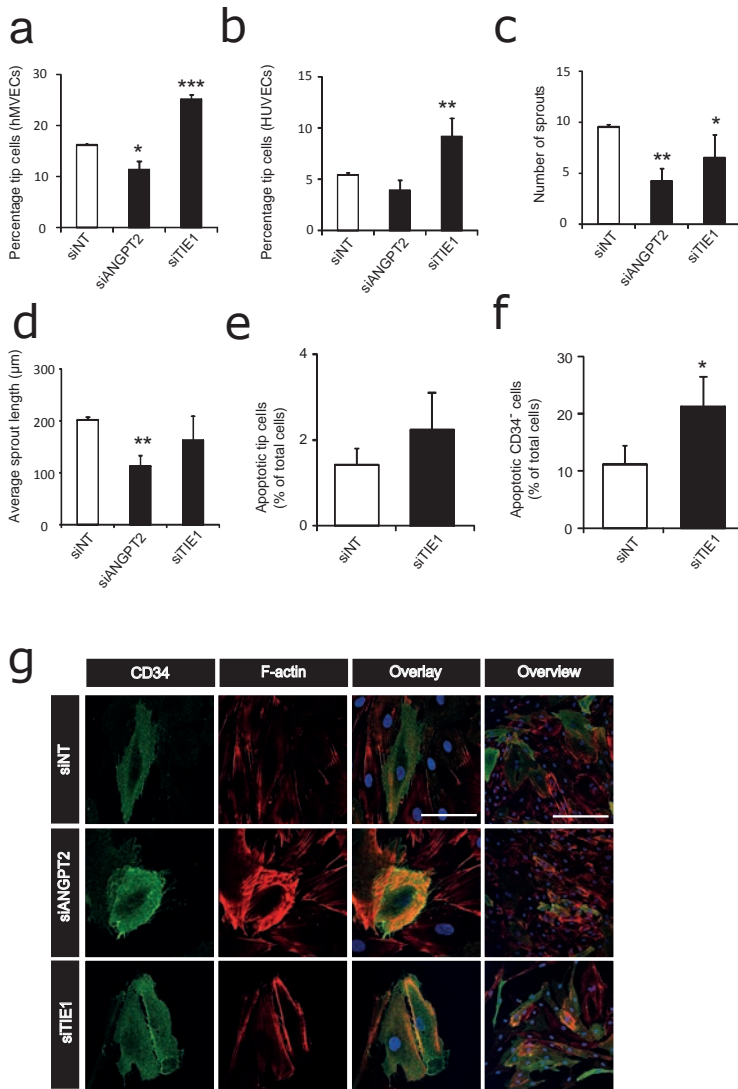


Figure 2. Effects of *ANGPT2* and *TIE1* knockdown on CD34⁺ tip cells and CD34⁻ non-tip cells *in vitro*. (a, b) Effect of knockdown of *ANGPT2* and *TIE1* expression on percentages of CD34⁺ tip cells. Bars show percentages of CD34⁺ hMVECs (a) and HUVECs (b) as detected by flow cytometry after treatment with non-targeting siRNA (siNT), *siANGPT2* or *siTIE1*. (c, d) Quantification of numbers of sprouts (c) and average sprout length (d) of spheroids composed of HUVECs treated with siNT, *siANGPT2* or *siTIE1*. (e, f) Percentages of apoptotic cells as detected by flow cytometry after treatment of HUVECs with siNT or *siTIE1*. Staining for CD34 was performed in combination with annexin-V staining of apoptotic CD34⁺ tip cells (e) and CD34⁻ cells (f). Data in a-f are shown as the mean \pm standard deviation after factor correction. * $p < 0.05$, ** $p < 0.01$, *** $p < 0.001$ as compared to siNT ($n=3$). (g) Analysis of CD34⁺ tip cell morphology after knockdown of *ANGPT2* and *TIE1* expression. Staining of CD34 (green), F-actin (phalloidin, red) and nuclei (DAPI, blue) in hMVECs and overlay images of higher and lower magnification. Note the cortical F-actin staining in the cells treated with *siANGPT2*. Scale bars represent 50 μm (first 3 columns) and 100 μm (last column).

of expression of *IGF2* but not of *IGF1R* reduced sprout length (Fig. 3d). Knockdown of *IGF1R* expression increased the intensity of F-actin staining in hMVECs in all cells. Knockdown of *IGF2* seemed to increase the intensity of F-actin staining in all cells as well, but most strongly in CD34⁺ cells (Fig. 3e).

To investigate the effects of exogenous IGF2 on the percentage of tip cells and sprouting, we exposed HUVECs to IGF2 (50 ng/ml) in both models. Addition of IGF2 did not alter the CD34⁺ fraction in HUVEC cultures (Fig. 3f), but did increase the number of sprouts per spheroid (Fig. 3g-h). Next, we determined the effects of IGF2 on sprouting from spheroids composed of sorted CD34⁻ cells, CD34⁺ cells and unsorted human microvascular endothelial cells (HMEC-1s). We used the immortalized cell line HMEC-1 for these experiments, as the timespan before appearance of *de novo* generated CD34⁺ tip cells in CD34⁻ cultures is over 72 hours in HMEC-1 cells, but only 24 hours in hMVECs and HUVECs. Lack of expression of CD34 protein was confirmed by immunocytochemistry on HMEC-1 spheroids after completion of the experiment (data not shown). Similar to spheroids of unsorted cells, in spheroids of CD34⁺ cells the number of sprouts was increased by VEGF and by IGF2. In contrast, spheroids composed of CD34⁻ cells had less sprouts per spheroid and did not respond to VEGF or IGF2 (Fig. 3h, i). We performed an apoptosis assay to determine whether the effects seen on tip cell percentage and sprouting were due to apoptosis (Supplementary Fig. 1). Treatment with siIGF2 resulted in higher ($p < 0.05$) percentages of apoptotic cells in the tip cell (10%) and CD34⁻ cell (19%) fractions, respectively, as compared to siNT (5% and 8%, respectively). Treatment of HUVECs with siIGF1R did not alter the percentage of apoptotic cells as compared to siNT.

To further investigate the role of IGF2 in angiogenesis, we knocked down IGF2 expression *in vivo*, using the developing chorioallantoic membrane model in chicken embryos (57) and zebrafish embryos, respectively. In the CAM model, silencing of *IGF2* resulted in a 2-fold reduction in number of vascular branching points per mm² (Fig. 4a, b), in larger avascular areas in between vessels, and in irregular vascular caliber (Fig. 4b). Gene silencing of the two zebrafish IGF2 isoforms (*IGF2A* and *IGF2B*) using morpholinos in zebrafish embryos resulted in disturbed angiogenesis, albeit with a different phenotype for each isoform (Fig. 4c, d). *IGF2A* silencing caused delayed sprouting of intersegmental vessels (ISVs) after 24 h, and absence of filopodia at 30 h post-fertilization (Fig. 4c, d). Silencing of *IGF2B* resulted in chaotic sprouting of ISVs after 24 h and 30 h with some ISVs developing slower than their neighbors, and reduced numbers of filopodia (Fig. 4c, d).

DISCUSSION

In the present study we show that primary microvascular endothelial cells, hMVECs, contain a subset of CD34⁺ tip cells. This finding is similar to our earlier finding of CD34⁺ tip cells in macrovascular HUVEC cultures and immortalized ECs as HMEC-1 and RF24 [6], suggesting that the formation of tip cells in endothelial cell cultures is a general

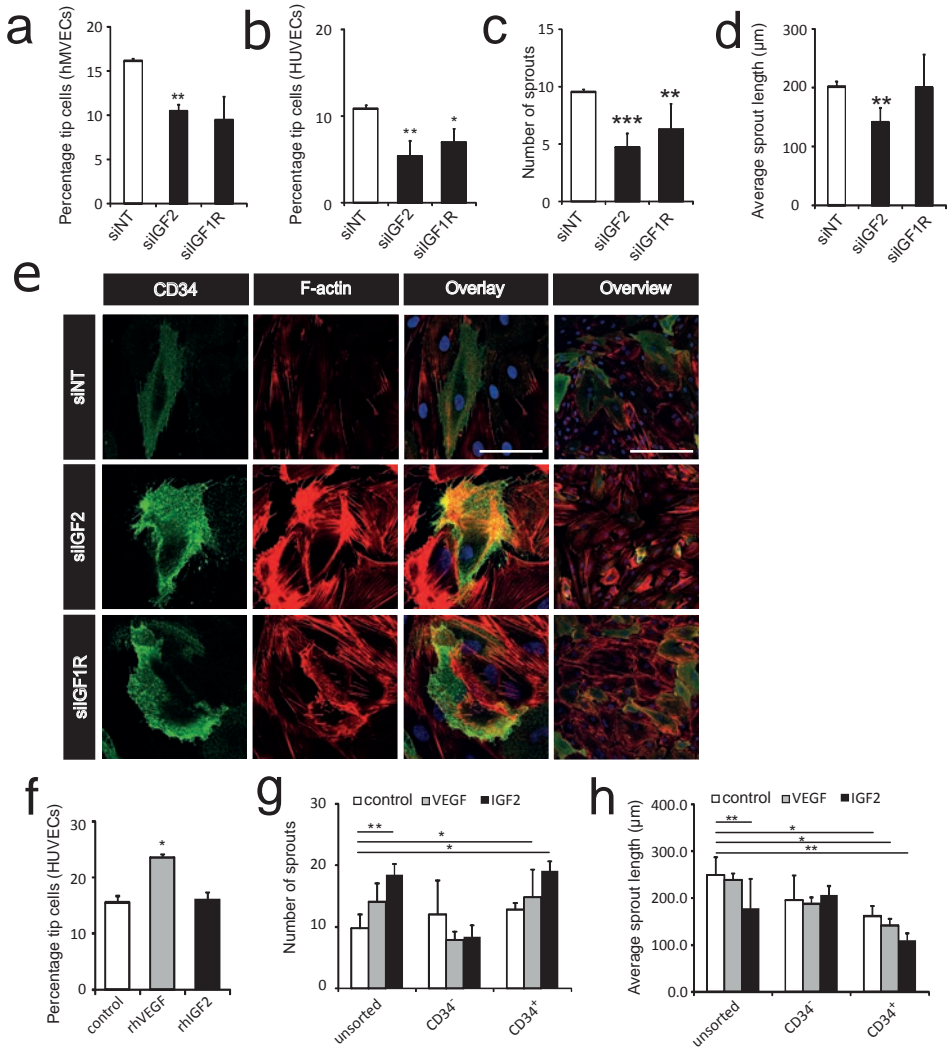


Figure 3. IGF2 and IGF1R are essential for CD34⁺ tip cell fate. **(a, b)** Effect of knockdown of *IGF2* and *IGF1R* expression on percentages of CD34⁺ tip cells. Bars show percentages of CD34⁺ hMVECs **(a)** and HUVECs **(b)** treated with siNT, *siIGF2* or *siIGF1R* as detected by flow cytometry. **(c, d)** Quantification of numbers of sprouts **(c)** and average sprout length **(d)** of spheroids composed of HUVECs after treatment with siNT, *siIGF2* or *siIGF1R*. **(e)** Analysis of CD34⁺ tip cell morphology after knockdown of *IGF2* and *IGF1R* expression. Staining of CD34 (green), F-actin (phalloidin, red) and nuclei (DAPI, blue) in hMVECs. Scale bars represent 50 μm (first 3 columns) and 100 μm (last column). **(f)** Effect of rhIGF2 on CD34⁺ HUVEC tip cell percentages. Bars shows CD34⁺ tip cells, of HUVECs treated with either 25 ng/mL BSA, 25 ng/mL VEGF-A or 50 ng/mL rhIGF2 as detected by flow cytometry. **(g, h)** Effects of VEGF and IGF2 on the number of sprouts **(g)** and average sprout length **(h)** in spheroids consisting of CD34⁺ tip cells or CD34⁻ non-tip cells HMEC-1 cells. Data in a-d and f-h are shown as mean ± standard deviation after factor correction. * $p < 0.05$, ** $p < 0.01$, *** $p < 0.001$ as compared to control.

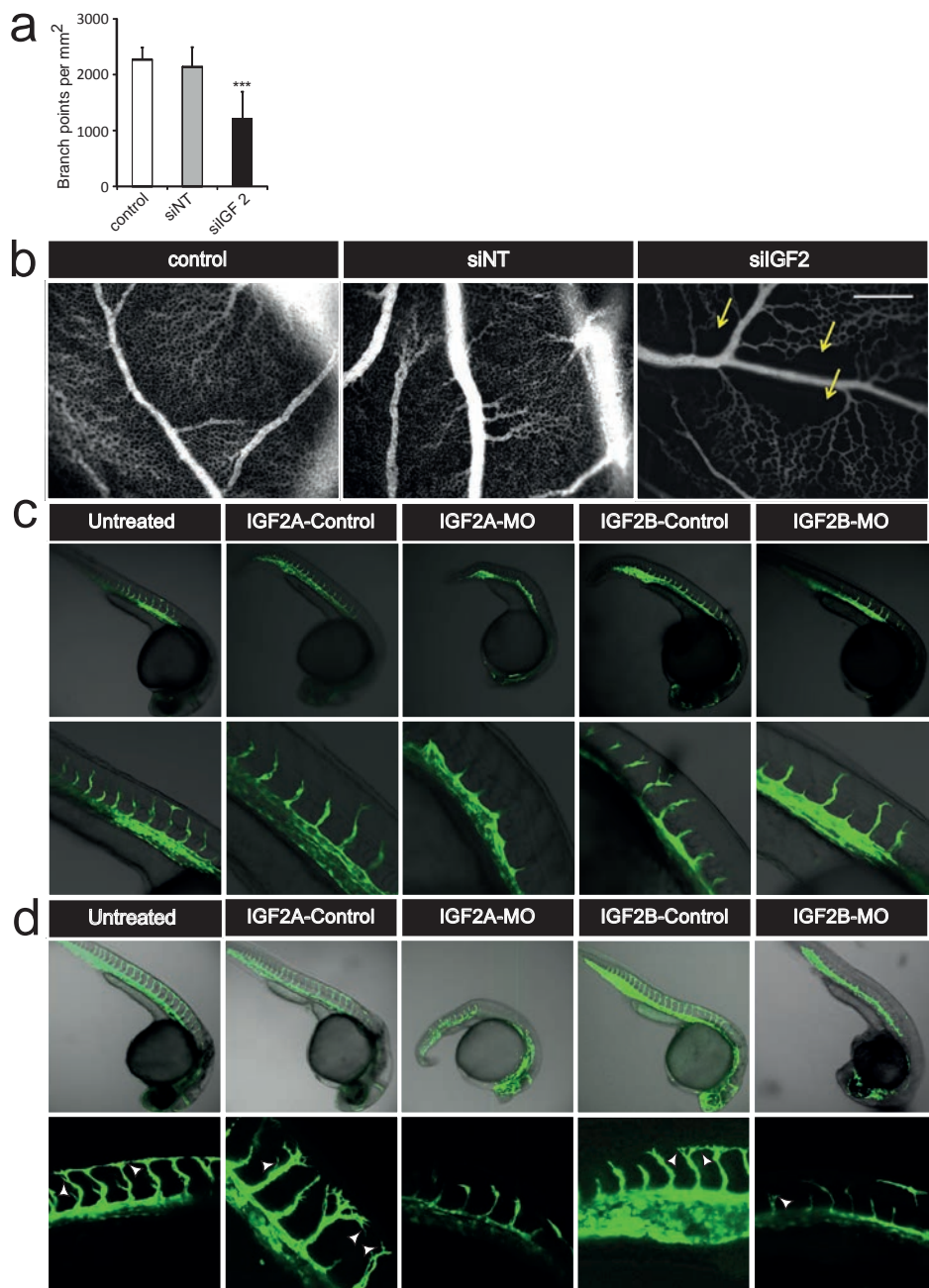


Figure 4. IGF2 is essential for sprouting in the chicken chorioallantoic membrane and zebrafish embryos. (a) Quantification of number of branching points/mm² comparing untreated membranes and membranes treated with siNT or with *siIGF2* in the chicken chorioallantoic membrane (CAM). *** $p < 0.001$ as compared to control as well as siNT treatment. (b) Representative images of the vascular network in CAMs of chicks that were treated with siNT or *siIGF2* and untreated control. Arrows indicate non-vascularized areas in the vascular network. Scale bar represents 500 μ m. (c, d) ▶

- ▶ Representative images of *Tg(fli1a-eGFP)* zebrafish embryos at 24 h (c) and 30 h (d) after injection of either a morpholino targeting *Igf2a* (IGF2A-MO) or *Igf2b* (IGF2B-MO) or a 6-base pair mismatch control morpholino for each gene (IGF2A-CON and IGF2B-CON, respectively). Untreated zebrafish embryos are shown as a control. Arrowheads indicate filopodia.

2.2

phenomenon. We found that knockdown of the expression of two known tip cell-specific genes, *ANGPT2* and *TIE1*, had the same effects on tip cell fate *in vitro* as has been reported on the basis of *in vivo* studies. In addition, employing our model, we identified IGF2 and IGF1R to be highly expressed in CD34⁺ tip cells and we showed that these molecules are essential for tip cell fate and function *in vitro* and for angiogenesis *in vivo*. Together, these results further contribute to the acceptance of our *in vitro* tip cell model as a valid model. The use of our model will help to gain insight into new cellular and molecular mechanisms that are of importance in tip cell biology.

CD34 identifies tip cells in human microvascular endothelial cell cultures

CD34 is ubiquitously expressed on the luminal surface of endothelial cells of small blood vessels, but also has a striking presence on filopodia of tip cells *in vivo* (12, 76). Although all endothelial cells express CD34 directly after isolation, after a certain number of passages CD34 expression is reserved to a small fraction of cells, (59, 60) which we here identify as tip cells *in vitro*. Since CD34 expression re-appeared within 24 h in cultures of CD34⁻ hMVECs that were sorted by FACS, we conclude that these cells are generated *de novo* in endothelial cell cultures. Immunocytochemistry showed that CD34⁺ hMVECs *in vitro* have filopodia-like extensions that are positive for CD34, similar to the extensions of tip cells in sprouting vascular fronts in mouse retina and in human colon carcinoma *in vivo* (39, 45, 77). Stimulation of hMVECs with VEGF and DLL4 resulted in increased and decreased tip cell percentages, respectively, mimicking the regulatory effects on tip cells of these factors *in vivo* (39, 61, 62). Finally, analysis of mRNA expression levels of the genes known to be higher expressed in tip cells compared to stalk cells *in vivo*, demonstrated that these genes are also expressed at significantly higher levels in CD34⁺ cells than in CD34⁻ hMVECs.

Similar findings were previously demonstrated in our study of CD34⁺ cells in HUVECs [6]. In addition to the presently reported results in hMVECs, in HUVECs TNF α was shown to reduce the fraction of CD34⁺ tip cells, and CD34⁺ cells showed a higher capacity in cell migration and a much lower proliferation rate than CD34⁻ cells [6]. Genome-wide mRNA profiling analysis of CD34⁺ cells demonstrated enrichment for biological functions related to angiogenesis and migration, whereas CD34⁻ cells were enriched for functions related to proliferation. Furthermore, gene set enrichment analysis (GSEA) showed that our gene set and gene sets of other studies comprising the transcriptional profile of tip cells (42, 43, 53) were highly correlated.

Taken together, we conclude that the CD34⁺ fraction in endothelial cell cultures can be used to study what molecular mechanisms determine formation of the tip cell phenotype, their behavior and their gene expression. However, careful evaluation of experimental results is required to ascertain whether the outcome is due to positive effects on the CD34⁺ fraction, or rather by negative effects on the CD34⁻ fraction, or by a direct effect on CD34 itself. We have taken this into account in our present experiments. For example, bFGF reduced the percentage of CD34⁺ tip cells in hMVECs. Since bFGF is reported to stimulate endothelial cell proliferation during angiogenesis (63, 78) and CD34⁺ cells have a low proliferation rate, we interpreted the reduced percentage of CD34⁺ cells to be a result of increased proliferation of CD34⁻ cells, rather than of a direct downregulation of the numbers of CD34⁺ tip cells. However, the effect on cell proliferation should be further confirmed in experiments with FACS sorted CD34⁺ and CD34⁻ cells exposed to bFGF. As another example, knockdown of *TIE1* increased the fraction of CD34⁺ cells. However, silencing of *TIE1* in developing mouse retinas causes increased apoptosis of stalk cells (49). Similarly, in our study, knockdown of *TIE1* *in vitro* caused increased apoptosis of CD34⁻ but not of CD34⁺ cells. Therefore, we conclude that apoptosis of CD34⁻ cells upon knockdown of *TIE1* most likely contributes to or explains the observed increase in the fraction of CD34⁺ cells.

Knockdown of ANGPT2 inhibits endothelial cell sprouting

We studied the effects of ANGPT2 and TIE1 silencing on CD34⁺ tip cells to further validate our *in vitro* tip cell model as a tool to study genes enriched in tip cells, and to further study the role of these two genes in tip cell biology. Mice lacking *ANGPT2* have decreased numbers of tip cells at the sprouting front in the developing retinal vasculature, and severely impaired angiogenesis (48, 73). ANGPT2 binds to integrins that interact with the actin cytoskeleton, and thus may play a role in regulating cell migration (48, 79). Our experiments *in vitro* revealed decreased tip cell percentages and decreased sprouting from spheroids upon knockdown of *ANGPT2*. Furthermore, the actin skeleton of cells treated with *siANGPT2* was disturbed. Since tip cells and stalk cells can switch phenotype (41), and as it has been hypothesized that the best-equipped cells become tip cells (41, 80), we hypothesize that knockdown of *ANGPT2* decreases migration of endothelial cells, which renders them unsuitable to become tip cells. Phenotype switching of neighboring non-tip cells would require migratory abilities to enable cells to reach the sprouting front (81). Since neighboring cells also lack *ANGPT2* and are thus impaired in their migratory abilities, these cells would be unable to take over the tip cell phenotype, which causes the tip cell fraction to decrease and sprouting to be reduced.

IGF2 and IGF1R are essential for tip cell fate

We used our *in vitro* tip cell model as a tool to identify and characterize novel tip cell specific genes. From our microarray data [6], that comprised of more than 400

differentially expressed genes, we selected *IGF2*, a gene with one of the highest difference in mRNA levels in CD34⁺ cells as compared to CD34⁻ cells, and one of its receptors, *IGF1R*, which is also significantly higher expressed in CD34⁺ cells. On the basis of previous studies of knockdown of *IGF2* and *IGF1R* expression, it appeared that both proteins are important for angiogenesis *in vivo* and *in vitro*. This importance is reflected by reduced neovascularization in oxygen-deprived retinas, reduced mRNA expression in growing vascular tufts in developing mouse retinas, impaired angiogenesis in zebrafish embryos, and reduced sprouting in *in vitro* models of angiogenesis upon knockdown of *IGF2* and *IGF1R* (50-52). Downstream pathways of IGF2 and IGF1R include pathways that are important for tip cells, such as phosphatidylinositol 3-kinases (PI3K), a kinase that promotes cell migration (82-84). However, a specific role in tip cells has not yet been reported for either protein. We show here that IGF2 is essential for maintenance of the tip cell phenotype, as knockdown of IGF2 expression reduced the percentage of CD34⁺ tip cells, which could not be explained by tip cell-specific apoptosis, since the percentages of apoptotic cells were higher in CD34⁻ cells than in CD34⁺ tip cells (19% and 10% respectively). IGF2 was also shown to be essential for angiogenesis, since knockdown of IGF2 expression reduced the number and length of sprouts in the spheroid assay. The role of IGF2 in angiogenesis was further supported by our *in vivo* experiments in the CAM assay and zebrafish, which show that sprouting in the absence of *IGF2* mRNA is chaotic and irregular.

Our experiments using spheroids composed of sorted CD34⁺ cells, CD34⁻ cells or mixed populations of cells show that stimulation with IGF2 increased the number of sprouts in CD34⁺ spheroids and in spheroids composed of mixed populations, but not in CD34⁻ spheroids. This suggests that IGF2 mainly acts on tip cells, which is confirmed by the staining for F-actin: disturbances in the actin skeleton upon knockdown of *IGF2* occurred mainly in tip cells. On the other hand, stimulation with exogenous IGF2 did not increase the fraction of tip cells cultured in monolayers, suggesting that the effects on sprouting of exogenous IGF2 may be dependent on other growth factors present in the gel in which the spheroids grow. Thus, our results suggest that IGF2 alone does not induce *de novo* tip cell formation, but that endogenous IGF2 is necessary to maintain the tip cell phenotype, probably in an autocrine fashion.

IGF1R binds all ligands of the IGF family of growth factors: IGF1, IGF2 and insulin (INS) (85). IGF1 and INS also play a role in angiogenesis, as has been shown *in vivo* and *in vitro* (86-89). In the present study, we showed that tip cell percentages and sprouting are reduced upon knockdown of *IGF1R*, and that the actin skeleton is disturbed in all cells. This further supports the essence of the IGF family of growth factors, including IGF2, in tip cell formation and sprouting angiogenesis. We will further explore the underlying molecular mechanisms in future experiments.

CONCLUSIONS

In addition to the identification of tip cells in HUVECs, HMEC-1 cells and RF24 cells, CD34 marks tip cells in cultures of hMVECs. This suggests that the existence of tip cells in endothelial cell cultures is a general phenomenon. Studying CD34⁺ tip cells *in vitro* can improve our understanding of tip cell biology by identifying proteins that are essential for tip cells, as shown for ANGPT2 and TIE1. Finally, we provide evidence that IGF2 and IGF1R are novel tip cell proteins, and show that they are essential for maintenance of the tip cell phenotype.

Supplementary information is available here:

<https://link.springer.com/article/10.1007/s10456-018-9627-4>

Marchien G. Dallinga¹,
Yasmin I. Habani¹,
Richelle P. Kayser¹,
Cornelis J.F. Van Noorden^{1,2},
Ingeborg Klaassen¹,
Reinier O. Schlingemann^{1,3}

¹ Ocular Angiogenesis Group, Departments of Ophthalmology and Medical Biology, Amsterdam Cardiovascular Sciences, Cancer Center Amsterdam, Amsterdam UMC, University of Amsterdam, Meibergdreef 9, Amsterdam, The Netherlands.

² Department of Genetic Toxicology and Cancer Biology, National Institute of Biology, Ljubljana, Slovenia

³ Department of Ophthalmology, University of Lausanne, Jules Gonin Eye Hospital, Fondation Asile des Aveugles, Lausanne, Switzerland.

A large, light grey number '2.3' is centered on the page, spanning across two horizontal lines. The number is composed of a large '2', a small '3' as a decimal, and another large '3'.

**IGF-BINDING PROTEINS 3 AND 4 ARE
REGULATORS OF SPROUTING ANGIOGENESIS**

INTRODUCTION

Sprouting angiogenesis is a complex process that involves endothelial cell differentiation, proliferation and migration. It is initiated by an array of growth factors such as vascular endothelial growth factor (VEGF) (39). We have recently reported that insulin-like growth factor 2 (IGF2) and insulin-like growth factor 1 receptor (IGF1R) are essential for sprouting angiogenesis, because they enable maintenance of the tip cells, the leading cells in vessel sprouts (90, 91). Here, we have analyzed the role of other IGF family members in sprouting angiogenesis.

The IGF family consists of 2 ligands, IGF1 and IGF2, that can bind to 3 receptors, IGF1R, IGF2R and insulin receptor (INSR), which activates downstream signaling pathways such as the phosphatidylinositide 3-kinase (PI3K) and mitogen-activated kinase-like protein (MAPK) pathways, which are pro-angiogenic (85). IGF1R and INSR can bind both IGF1 and IGF2, IGF2R can bind only IGF2 and inhibits its signaling (84, 92). IGF1R and INSR both form homodimers as well as heterodimers that can bind both IGF ligands with similar binding affinity (93-95). The IGF family also comprises 6 high-affinity and at least 4 low-affinity IGF-binding proteins (IGFBPs) that regulate bioavailability and degradation of IGF ligands (96). For an overview of this complex interacting multicomponent network, we refer to Massoner *et al.* (97).

IGF2 and its family members have been linked to the process of angiogenesis in general (85, 98). For example, levels of IGF1 and IGF2 in vitreous in the eye increase upon hypoxia, and IGF2 expression is upregulated in the growth phase of capillary hemangiomas (74, 75, 99). Furthermore, experiments in mice have shown that IGF family members, including IGF1R, INSR and IGF2 are located in neovascular tufts in hypoxic retinas (74). Although there are differences in activation of downstream signaling, a clear overlap for IGF1R and INSR signaling has been shown as well. This overlap includes pathways involved in angiogenesis such as the MAPK and PI3K pathways (97, 100), and it was recently published that INSR plays an important role in angiogenesis in tumors (97, 100, 101).

However, specific information about the exact role of IGF family members in sprouting angiogenesis was lacking until recently, when we reported that IGF2 and IGF1R are involved in tip cell maintenance and sprouting angiogenesis by means of a local autocrine growth-regulating signaling axis (90). We now present evidence that suggests that other IGF family members besides IGF2 and IGF1R are involved in this process as well.

Serum contains significant concentrations of both IGF ligands as well as IGFBPs. IGF1 is produced by hepatocytes in the liver, whereas IGF2 is produced in the liver but also in various other tissues such as bone and placenta (102, 103). Both ligands are transported in the circulation after complex formation with IGFBP3 and acid-labile subunit (ALS). The latter protein is also produced in the liver and reduces bioavailability and degradation of IGFs in the blood (104-108).

In the present study, we have determined the impact of serum on *in vitro* sprouting angiogenesis of HUVECs and studied the effects of IGFBP3 and IGFBP4, which are both

present in significant concentrations in the circulation and therefore in serum. In the past, serum and vitreous levels of IGFBP3 have been positively correlated with angiogenesis and proliferative retinopathy (109), whereas IGFBP4 levels have been negatively correlated with angiogenesis (110-112). Furthermore, in a previous study we noted that IGFBP4 is highly expressed in CD34⁺ tip cells when compared to non-tip cells *in vitro* (44).

We show here that serum affects IGF2 and IGF1R functions *in vitro*, and that IGFBP3 and IGFBP4 are likely candidates for these effects, by regulating sprouting angiogenesis via IGF2 binding.

MATERIALS & METHODS

Cell cultures

Primary human umbilical vein endothelial cells (HUVECs) were isolated from umbilical cords (obtained from the Department of Gynecology, Academic Medical Center, Amsterdam, The Netherlands), as described previously (113). HUVECs were cultured in M199 basal medium (Gibco, Grand Island, NY, USA) supplemented with 10% heat-inactivated human serum (obtained from the Department of Oncology, Academic Medical Center, Amsterdam, The Netherlands), 10% fetal bovine serum (Gibco), and 1% penicillin-streptomycin-glutamine (Gibco). Subjects gave informed consent for the use of tissues or serum and samples were stored anonymously. HUVEC cultures were incubated with antibodies directed against CD31/PECAM-1 (1:100; eBioscience, Vienna, Austria) to check the purity of the endothelial cells. HUVECs were cultured in 2% gelatin-coated (Millipore, Billerica, MA, USA) T75 culture flasks at 37°C and 5% CO₂. Experiments were performed with confluent HUVECs at passage 3 of at least 3 donors. Subjects gave informed consent for the use of tissues and/or serum and samples were stored anonymously. To determine the effects of increased extracellular protein concentrations, cells were treated with recombinant human IGF2, IGF1, IGFBP3, IGFBP4 (Prospec, Rehovot, Israel) or INS (Actrapid, Novo Nordisk, Sweden) as indicated. To determine the effect of serum proteins on IGF2-IGF1R interactions, we performed experiments in the presence and absence of serum. Addition of VEGF (R&D Systems, Minneapolis, MN, USA) in a concentration of 25 ng/mL was necessary to reduce apoptosis and to maintain sprouting from spheroids in the absence of serum. Experiments in the presence of serum were performed without additional VEGF.

siRNA knockdown

HUVECs were transfected with 25 nM of either a non-targeting small interfering RNA (siNT) or a gene-specific siRNA and 2.5 µg/mL Dharmafect 1 transfection agent (Dharmacon, Lafayette, CO, USA). Custom duplexes or company-selected smartpools were used as shown in **Supplemental Table 1**. Cells were transfected during 6 h using the reversed transfection method according to the manufacturer's instructions. Transfection efficiency was checked at the mRNA level (**Supplemental Fig. 1a**) and was considered acceptable when expression was reduced by at least 70% after 72 h. To rule out cytotoxic effects by

siRNA treatment, we performed MTT assays as described below. No negative effects on cell viability were observed (**Supplemental Fig. 1c**).

Cell viability assay

To test the effect of siRNA inhibition on cell viability, an MTT [3-(4,5-dimethylthiazol-2-yl)-2,5-diphenyl-tetra-zolium bromide] assay (Promega) was used, according to the manufacturer's instructions. Absorbance was measured photometrically at 570 nm using a microplate reader (VersaMax, Sunnyvale, CA, USA).

2.3

RNA isolation and quantitative PCR

Total RNA was isolated from cells using the TRIzol method according to the manufacturer's instructions (Invitrogen, Carlsbad, CA, USA). An amount of 1 μ g RNA was used for DNase-I treatment (amplification grade; Invitrogen) and reversely transcribed into cDNA using the Maxima First Strand cDNA Synthesis Kit (Thermo Scientific, Waltham, MA, USA). Real-time quantitative PCR (RT qPCR) was performed using a CFX96 real-time PCR detection system (Bio-Rad Laboratories, Hercules, CA, USA) as described previously (44). Primer details are presented in **Supplemental Table 1**. NCBI BLAST confirmed the specificity of the primers. The presence of a single PCR product was verified by both the presence of a single melting temperature peak and detection of a single band of the expected size on agarose gels. Non-template controls were included to verify the method and the specificity of the primers. PCR products that did not show a single melting temperature peak were excluded from analysis. Ct values were converted to arbitrary absolute amounts ($2^{-Ct} \times 1E^{12}$) and expressed as fold change as compared to controls. Expression data was normalized to YWHAZ (tyrosine 3-monooxygenase/tryptophan 5-monooxygenase activation protein zeta) mRNA levels.

Spheroid-based sprouting assay

Spheroid experiments were performed with siRNA-transfected or untreated HUVECs. Transfected HUVECs were harvested after 48 h, untreated cells were harvested when confluent. Cells (750 per spheroid) were seeded in methylcellulose (Sigma-Aldrich, Buchs, Switzerland) containing M199 medium and 2% human serum to allow spheroid formation with the use of the hanging drop method (27, 114). After 18 h, the spheroids were embedded in collagen gels containing either 2% serum or VEGF-A (25 ng/mL) and when indicated exogenous IGF1 (30 ng/mL), IGF2 (50 ng/mL), insulin (10 μ M), IGFBP3 (30 ng/mL) or IGFBP4 (40 ng/mL), and were allowed to sprout for 24 h. Images were taken using a phase-contrast microscope. Sprout numbers were counted using the NeuronJ plugin of ImageJ (28) and sprout length was measured in pixels and converted into μ m. For live microscopy, spheroids were incubated at 37 °C in an atmosphere containing 5% CO₂ and imaged every 10 min for 24 h under an inverted phase-contrast microscope (Leica; 10x objective).

Determination and selection of tip cells

To determine the fraction of tip cells, HUVECs were harvested using TrypLE (Gibco), fixed in 4% paraformaldehyde in PBS for 15 min at room temp and incubated with anti-CD34-phycoerythrin antibody (diluted 1-100; anti-CD34-PE; clone QBend-10; Thermo Scientific) for 30 min at room temperature. Cells were analyzed flow cytometrically using a FACSCalibur (Becton Dickinson, Franklin Lakes, NJ, USA) and FlowJo 6.4.7 software (Tree Star, San Carlos, CA, USA). The FITC channel was used to detect autofluorescence. Non-stained and non-treated cells were used as negative controls.

3D angiogenic sprouting model combined with siRNA knockdown

A 3D angiogenesis model was used as described previously (115). Briefly, collagen type I (R&D systems) was patterned in the microfluidic channel, followed by a 24 h coating with fibronectin (10 µg/ml; Sigma-Aldrich) solution in PBS at 37 °C and 5% CO₂. Meanwhile, the HUVECs were first transfected with 25 nM siNT or siIGF2 and 2.5 µg/mL DharmaFECT 1 transfection agent (Dharmacon, Lafayette, CO, USA). The cells were transfected for 6 h using the reversed transfection method according to the manufacturer's instructions and cultured in 12-wells plates. The efficiency of *IGF2* knockdown was checked by qPCR in parallel cultures that were treated in similar medium conditions (**Supplemental Fig. 1b**) and was considered acceptable when expression was reduced by at least 70% after 72 h. After 24 h, the transfected HUVECs were seeded in one of the adjacent channels in a concentration of 2·10⁷ cells/ml in EGM2 medium (PromoCell). The cells were cultured for 3 days to form a confluent microvessel. Sprouting was induced by supplementing EGM2 media with VEGF (50 ng/ml; Peprotech, Rocky Hill, NJ, USA) and S1P (0.5 µM; Sigma) for 2 days. The sprouting microvessels were fixed using 4% PFA for 15 min, permeabilized for 15 min using 0.2% Triton-X100 and stained for nuclei using Hoechst (1:2000), F-actin using phalloidin (1:200) and anti-CD34 (1:50; clone MD34.2, Sanquin, Amsterdam, The Netherlands) at room temp. Images were acquired using a confocal microscope (Leica TCS SP8 DLS) using a 10X dry objective (NA 0.5) with a 2.0 digital zoom and images were acquired in the DAPI, AF488 and TexasRed channels. The line average was set at 6 and the imaging resolution at 2048 x 2048 pixels. Images were acquired from a total of 8 sites with 10% overlap per well. The max projections were stitched in LAS X (Leica Application Suite software)(116).

Statistics and data correction

To correct for differences between donors, data from flow cytometry and spheroid experiments were corrected using the Factor Correction program as described previously (54). Statistical analysis was performed using a Student's t-tests. Triplicate experiments were performed in HUVEC cultures of at least 3 different donors.

RESULTS

Sprouting angiogenesis *in vitro* is dependent on IGF2 and is affected by serum components

In our previous study, we found that *IGF2* mRNA is enriched in CD34⁺ tip cells as compared to non-tip cells, and that knockdown of *IGF2* gene expression by siRNA leads to a reduction in the fraction of tip cells in endothelial cell cultures, and in reduced sprouting from spheroids (90). Now, we verified this finding in a novel 3-dimensional angiogenesis model (115) after knockdown of *IGF2* by siRNA. Whereas CD34⁺ tip cells were easily identified in sprouts after non-targeting siRNA (siNT), the existence of CD34⁺ tip cells was hardly found after knockdown of *IGF2* (Fig. 1). Sprouting did occur after *IGF2* knockdown, but was reduced in number and length (Fig. 1e-g, i-k) as compared to siNT treated cells (Fig. 1a-c). In addition, cells with filopodial-like extensions were observed, but the length of these extensions was reduced (Fig. 1d',h', l').

In our previous study, experiments were performed in the presence of serum, which contains factors such as VEGF, bFGF, IGF1, IGF2 and IGFbps, all of which may interfere with IGF2 signaling (85). In the present study, we compared the effects of *IGF2* knockdown, and that of the addition of exogenous IGF2, on sprouting from HUVEC spheroids in the presence or absence of 20% serum to assess the effects of serum factors (Fig. 2). To maintain sprouting and reduce HUVEC apoptosis, it was necessary to add VEGF to HUVECs cultured in the absence of serum.

Spheroids sprouted less when treated with *siIGF2*. Knockdown of *IGF2* in the presence of serum resulted in a decreased number of sprouts by 1.8-fold, whereas knockdown of *IGF2* in the absence of serum reduced the number of sprouts even by 5.5-fold (Fig. 2a). Knockdown of *IGF2* reduced sprout length to a similar extent in both conditions (1.3-fold versus 1.2-fold, respectively; Fig. 2b, c), whereas spheroids in serum-free conditions produced marginally longer sprouts than in the presence of serum.

To further explore the effects of serum components, we followed sprout formation from HUVEC spheroids by using live-cell imaging. We found that spheroids in the presence of serum and VEGF displayed a coordinated process of sprout initiation and elongation (Movie 1). Knockdown of *IGF2* in the presence of serum resulted in failure of sprout formation: endothelial cells attempted to form sprouts, but rapidly returned into the spheroid (Movie 2). Together, these results suggest that IGF2 is necessary for initiation of sprouting, and that its effects are significantly affected by the presence of serum components.

Next, we determined the effects of exogenous IGF2 in the presence or absence of serum on sprouting angiogenesis. Addition of IGF2 resulted in an increased number of sprouts in the presence of serum (1.9-fold) and to a lesser extent in serum-free conditions (1.2-fold) (Fig. 2d). Sprout length was significantly reduced in the presence of serum and IGF2 (1.4-fold), whereas in the absence of serum sprouts were longer, independent from exogenous IGF2 (Fig. 2e). IGF2 increased the number of sprouts per spheroid in

the absence of serum in the presence of VEGF, without affecting sprout length (Fig. 2f). No cytotoxicity was observed after different periods in the presence of IGF2 in serum-free conditions (Supplemental Fig. 1d).

2.3

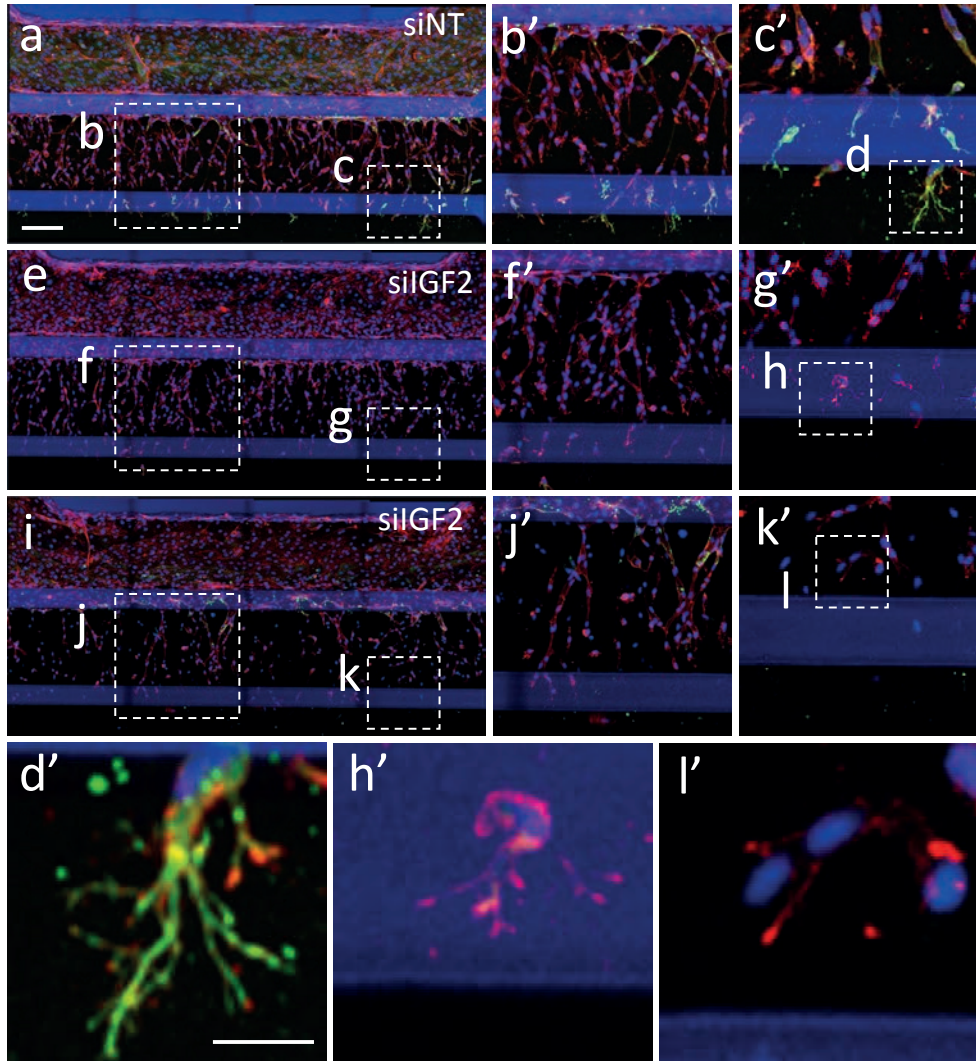


Figure 1. Knockdown of IGF2 results in a reduced number of CD34⁺ tip cells in a 3D angiogenic sprouting model. HUVECs were transfected with non-targeting (siNT) siRNA (a-d) or siRNA against *IGF2* (siIGF2) (e-l). Angiogenic sprouts are stained for CD34 (green), F-actin (red) and nuclei (blue). Note the absence of CD34⁺ tip cells in *siIGF2* treated cells. Magnifications are shown and indicated in the corresponding overview images. Long filopodial extensions are present in siNT treated cells (d'), whereas filopodia-like extensions in *siIGF2* treated cells were much shorter (h', l'). Representative images of triplicate experiments are shown. Scale bars, 100 μ m (overview a) and 20 μ m (magnification d').

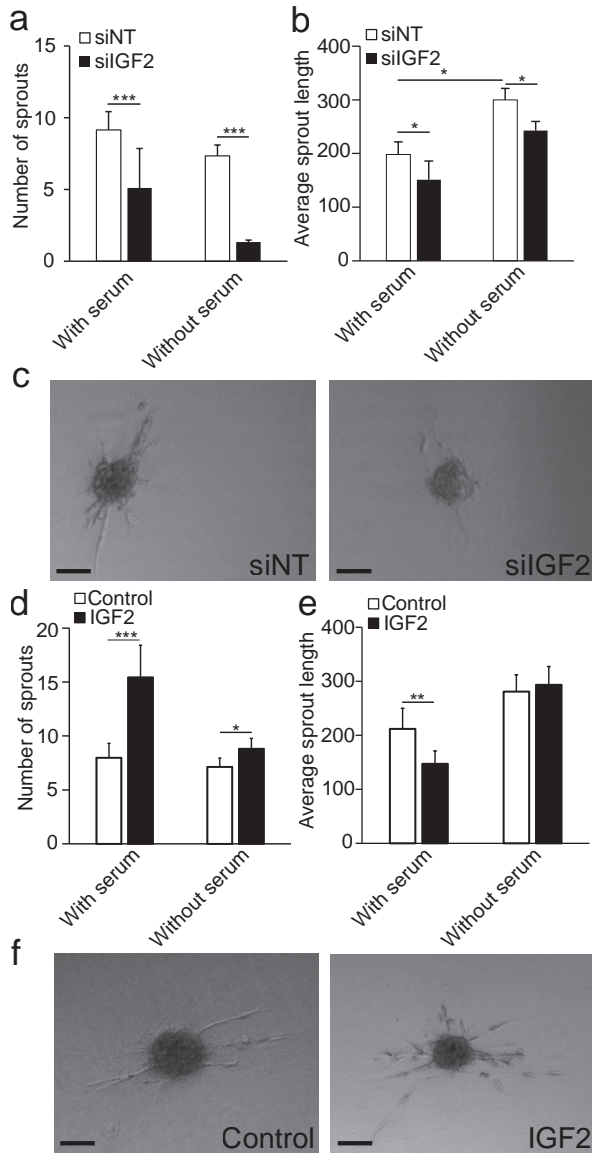


Figure 2. Angiogenic sprouting is dependent on the presence of IGF2 and serum. HUVECs were cultured in the presence or absence of 20% serum and in the presence of either siNT or *siIGF2* (a-c) or in the presence or absence of IGF2 (d-f). **a** Number of sprouts and **b** average length of sprouts (μm) per spheroid after knockdown of *IGF2* in the presence or absence of serum; **c** corresponding representative images. Scale bars represent 200 μm . **d** Number of sprouts and **e** average length of sprouts (μm) per spheroid cultured in the presence or absence of exogenous IGF2 in the presence or absence of serum and **f** corresponding representative images. Scale bars represent 200 μm . Data of sprout number and length are shown as the mean \pm standard deviation after factor correction. Medium of spheroids cultured in the absence of serum was supplemented with VEGF to maintain sprouting and to reduce EC apoptosis. * $P < 0.05$, ** $P < 0.01$, *** $P < 0.001$ as compared to control or siNT treatment using a Student's t-test ($n=3$).

2.3

IGFBP4 is an inhibitor of IGF2-induced sprouting

To find possible interaction partners of IGF2 in angiogenesis, we determined mRNA expression of IGF family members using microarrays in CD34⁺ tip cells and non-tip cells (44). IGF1 is not expressed by HUVECs (Fig. 3), and will therefore be absent when HUVECs are cultured in the absence of serum, which indicates that in our HUVEC model, IGF1 is not necessary for sprouting angiogenesis. Expression of all receptors of the IGF family was significantly higher in CD34⁺ tip cells than in CD34⁻ cells (Fig. 3), whereas expression of IGFBP3 was similar in tip cells and non-tip cells, and expression of IGFBP4 was significantly higher in tip cells (Fig. 3).

IGFBP4 is an IGF-binding protein that inhibits sprouting (110). To investigate whether IGFBP4 interacts with IGF2 and affects sprouting from spheroids, we performed siRNA-mediated knockdown of *IGFBP4* in the presence or absence of exogenous IGF2 under serum-free conditions but in the presence of VEGF. Knockdown of *IGFBP4* increased the number of sprouts but reduced the average sprout length both in the presence and absence of exogenous IGF2 (Fig. 4a, b). Simultaneous knockdown of *IGFBP4* and *IGF2*

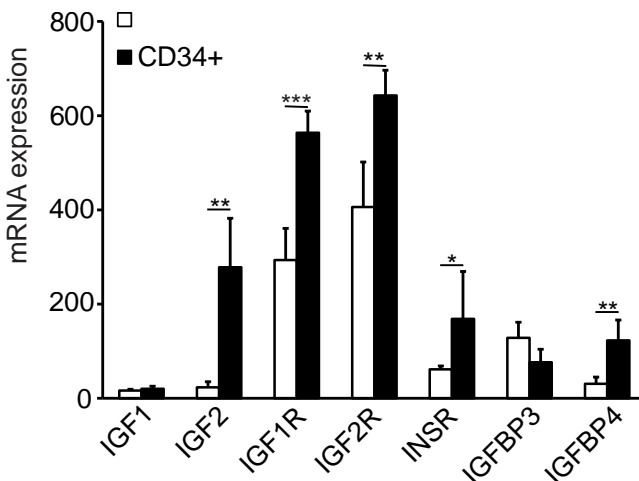


Figure 3. mRNA expression of IGF family members in tip cells and non-tip cells. Relative mRNA expression levels of *IGF1*, *IGF2*, *IGF1R*, *IGF2R*, *INSR*, *IGFBP3* and *IGFBP4* in CD34⁺ HUVEC tip cells and CD34⁻ HUVECs. Data are presented as normalized intensity values of mRNA expression as measured by microarray analysis as described previously (44). * P<0.05, ** P<0.01, *** P<0.001 as compared to control or siNT treatment using a Student's t-test (n=3).

greatly diminished the number of sprouts as compared to knockdown of *IGFBP4* alone, but the number of sprouts was still slightly higher compared to knockdown of *IGF2* alone (Fig. 4c, d).

Exogenous *IGFBP4* significantly reduced the number sprouts per spheroid (Fig. 4d). Addition of exogenous *IGF2* increased the number of sprouts by 1.4-fold in the absence

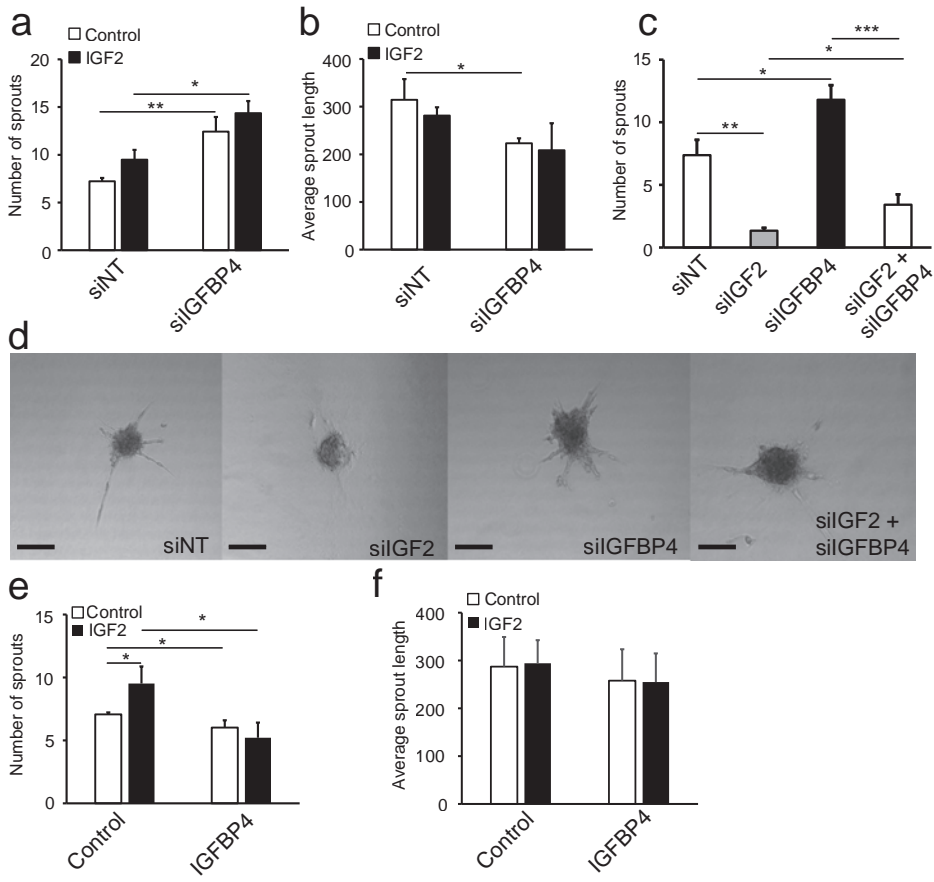


Figure 4. IGFBP4 inhibits IGF2-induced sprouting angiogenesis. HUVECs were cultured in the absence of serum and in the presence of either siNT or *siIGFBP4* and/or *siIGF2* (a-d) or in the presence or absence of *IGFBP4* and/or *IGF2* (e-f). **a** Number of sprouts and **b** average length of sprouts (μm) per spheroid after knockdown of *IGFBP4* in the presence or absence of exogenous *IGF2*. **c** Number of sprouts per spheroid after knockdown of *IGFBP4* and/or *IGF2*. **d** Representative images of spheroids cultured in the absence of serum, but in the presence of VEGF and either siNT, *siIGF2* and/or *siIGFBP4*. Scale bars represent 200 μm . **e** Number of sprouts and **f** average length of sprouts (μm) per spheroid in the presence and absence of exogenous *IGFBP4* and/or exogenous *IGF2*. Medium of the spheroids was supplemented with VEGF to maintain sprouting and to reduce EC apoptosis. Data of sprout numbers and length are shown as the mean \pm standard deviation after factor correction. * $P < 0.05$, ** $P < 0.01$, *** $P < 0.001$ as compared to control or siNT treatment using a Student's t-test ($n = 3$).

of IGFBP4, but not in its presence (Fig. 4e). Sprout length was not affected by exogenous IGFBP4 or IGF2 (Fig. 4f).

Together, these results show that IGFBP4 inhibits IGF2-induced sprouting from spheroids.

IGFBP3 is involved in sprouting angiogenesis and maintenance of the tip cell phenotype

2.3

IGFBP3 is a serum component that has been associated with angiogenesis, with both pro- and anti-angiogenic roles reported (109). To test whether it is involved in IGF2-induced sprouting, we performed siRNA-mediated knockdown of *IGFBP3* in the absence of serum but in the presence of VEGF, which resulted in a strong reduction in the number of sprouts as compared with treatment with siNT and to some extent in sprout length, irrespective of the presence of exogenous IGF2 (Fig. 5a-c). Addition of exogenous IGFBP3 did not significantly change the number of sprouts and did not affect sprout length (Fig. 5d,e). These results show that inhibition of *IGFBP3* strongly reduces the number of sprouts per spheroid, whereas exogenous IGFBP3 did not induce additional sprouting from spheroids, similar to the effects of silencing IGF2 or addition of exogenous IGF2, respectively.

To study whether the effects of IGFBP3 on sprouting are due to direct effects on tip cells, we performed siRNA-mediated knockdown of *IGFBP3* in HUVEC cultures and measured the percentages of CD34⁺ tip cells, which were significantly decreased upon knockdown (Fig. 5f).

We conclude that IGFBP3 is an important co-factor in sprouting angiogenesis and tip cell maintenance.

Inhibition of INSR, but not inhibition of IGF2R, reduces sprouting angiogenesis

Previously, we have shown that knockdown of *IGF1R* reduces sprouting *in vitro* (90). When studying the other receptors of the IGF family, we found that knockdown of INSR significantly decreased the number of sprout per spheroid but not their length, whereas knockdown of *IGF2R* did not change the number or length of sprouts (Fig. 6a-c). HUVEC spheroids were cultured in the absence of serum but in the presence of VEGF, after treatment with siNT, *siINSR* or *siIGF2R*.

The addition of exogenous IGF1 or INS also did not result in significant changes in sprouting from spheroids, as neither the number nor length of the sprouts changed (Fig. 6d, e).

DISCUSSION

This study confirms the previously identified crucial role of IGF2 in sprouting angiogenesis, and shows that the IGF binding proteins IGFBP3 and IGFBP4 have positive and negative regulatory roles in the function of IGF2 in sprouting angiogenesis, respectively. We have summarized our results in graphical form in Supplemental Fig. 2.

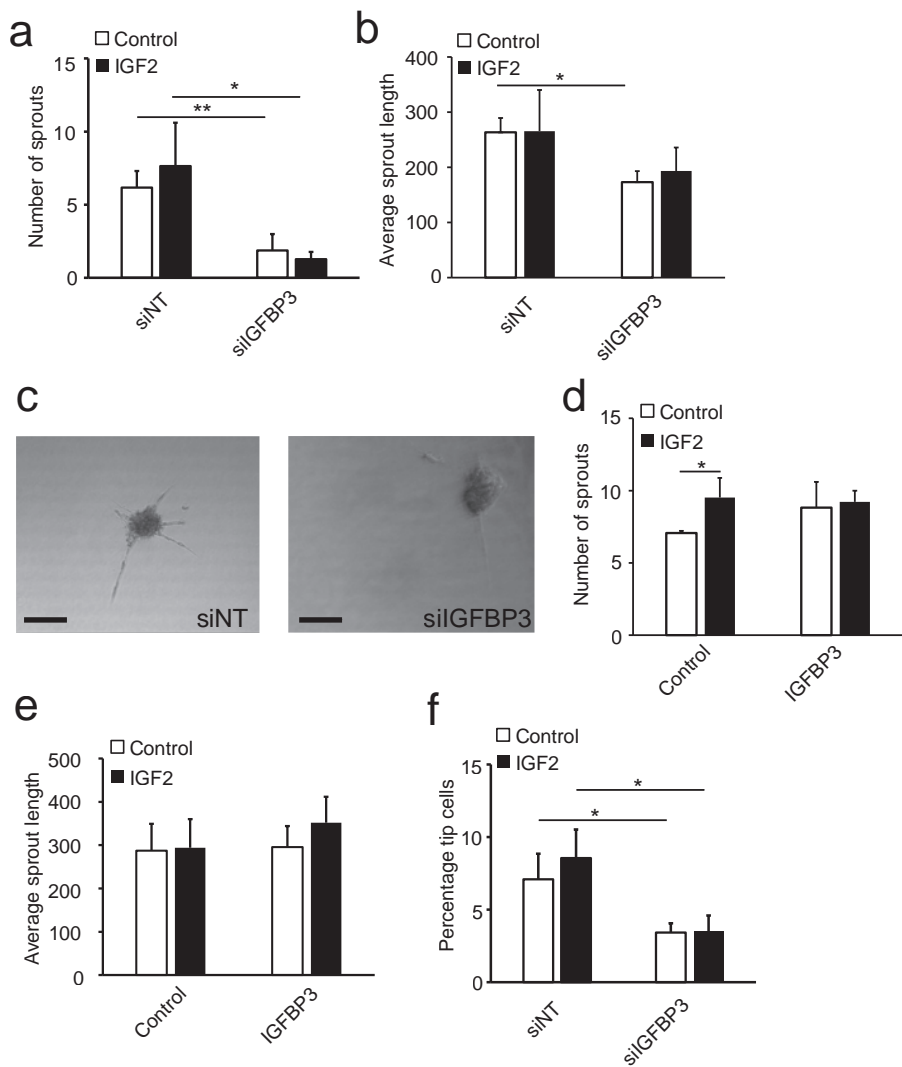


Figure 5. IGFBP3 is essential for IGF2-mediated sprouting angiogenesis. HUVECs were cultured in the absence of serum and in the presence of either siNT, *siIGFBP3* or *siIGF1R* (a-c, f) and in the presence or absence of exogenous IGF3 and/or IGF2 (d, e). a Number of sprouts and b average length of sprouts (μm) per spheroid after knockdown of *IGFBP3* in the presence or absence of exogenous IGF2; c corresponding representative images. Scale bars represent 200 μm. d Number of sprouts and e average length of sprouts (μm) per spheroid in the presence and absence of exogenous IGFBP3 and/or exogenous IGF2. f Flow cytometric analysis of the percentages of CD34⁺ tip cells in HUVEC cultures in the presence or absence of *siIGFBP3* and in the presence or absence of exogenous IGF2. Medium of spheroids was supplemented with VEGF to maintain sprouting and to reduce EC apoptosis. Data of sprout numbers and length are shown as the mean ± standard deviation after factor correction. Flow cytometric data are presented as average percentages of CD34⁺ HUVECs. * P<0.05, ** P<0.01 as compared to control or siNT treatment using a Student's t-test (n=3).

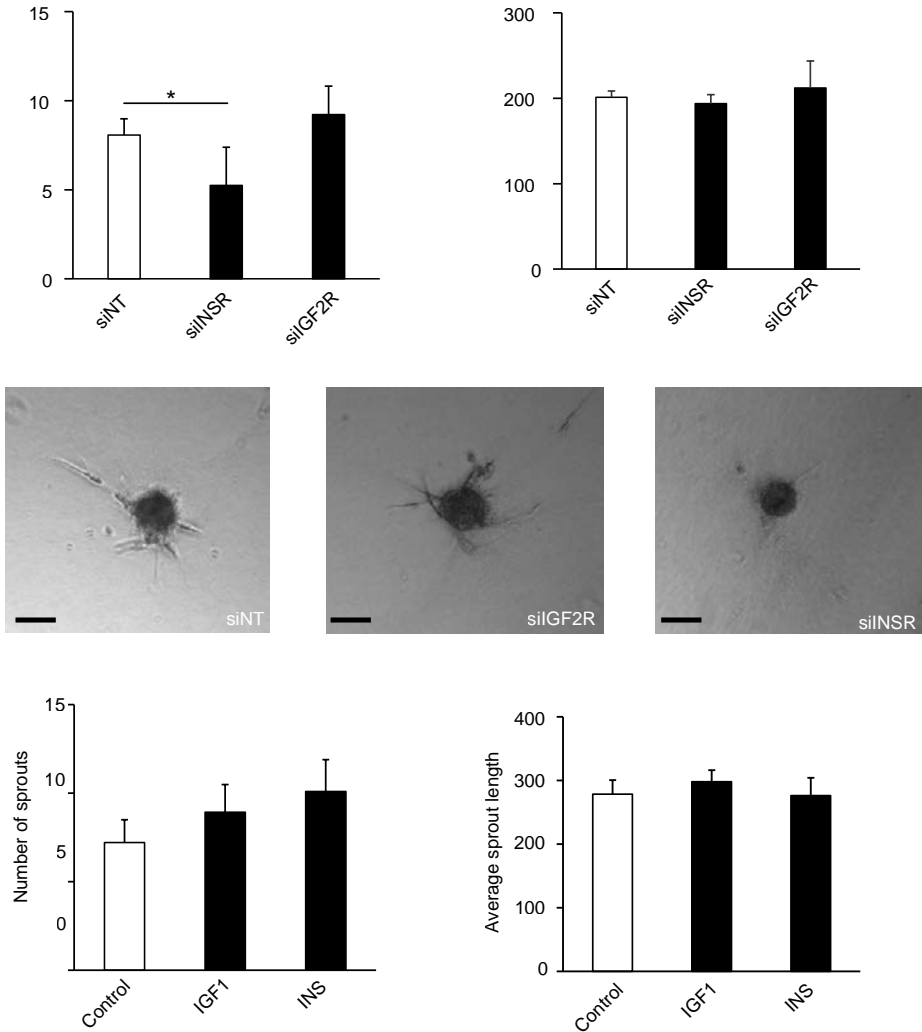


Figure 6. Involvement of other receptors besides IGF1R on sprouting angiogenesis. HUVECs were cultured in the absence of serum and in the presence of either siNT, *siIGF2R* or *siINSR* and in the presence or absence of exogenous IGF2. **a** Number of sprouts and **b** average length of sprouts (μm) per spheroid after knockdown of *IGF2R* or *INSR*; **c** corresponding representative images. Scale bars represent 200 μm. **d** Numbers of sprouts and **e** average length of sprouts (μm) per spheroid in the presence or absence of IGF1 or INS. Medium of spheroids was supplemented with VEGF to maintain sprouting and to reduce EC apoptosis. Data of sprout numbers and length are shown as the mean ± standard deviation after factor correction. * $P < 0.05$ as compared to control or siNT treatment using a Student's t-test ($n=3$).

In a novel 3D angiogenesis model, we verified a role of IGF2 in sprouting angiogenesis. For the first time, we have applied this model in combination with siRNA-mediated knockdown. Previously we have reported this model in standard conditions (117),

showing CD34-specific staining of endothelial tip cells. In siNT treated cells, a similar staining for CD34 was found, whereas in cells treated with *siIGF2*, CD34-staining was virtually absent. Although sprouting was still occurring after *IGF2* knockdown, it was reduced in number and length. Knockdown efficiency is difficult to check in this model, but showed more than 80% reduction in *IGF2* mRNA levels in parallel culture plates in similar experimental conditions. Together these experiments show additional evidence for the important role of IGF2 in sprouting angiogenesis.

The purpose of this study was to identify members of the IGF protein family other than IGF2 and IGF1R that play a role in sprouting angiogenesis, based on experimental models of angiogenesis *in vitro*. As serum contains significant levels of IGF1, IGF2 and IGFBPs (85, 105, 106), we compared sprouting angiogenesis of HUVECs *in vitro* in the presence or absence of 20% serum. We observed that in the absence of serum knockdown of *IGF2* affected sprouting more markedly than in the presence of serum, most likely due to the presence of IGF2 in serum. Live-cell imaging showed that IGF2 is necessary for the initiation of sprouting (90), and that in the absence of IGF2, tip cells emerge from spheroids but do not have the capacity to maintain their phenotype for sprouting. These findings indicate that local levels of IGF2, produced by the tip cells, are essential for efficient sprouting.

The most likely other candidate proteins present in serum for local regulation of IGF2 signaling are the IGFBPs, which regulate IGF bioavailability, and of which IGFBP3 and IGFBP4 have the highest affinities for IGF2 (118). In addition, IGFBP4 is highly expressed in tip cells [28]. We indeed found that IGFBP3 and IGFBP4 expression in tip cells affected IGF2 signaling, in a positive and negative fashion, respectively.

It has been hypothesized that IGFBP4 acts as an extracellular reservoir for IGF1 and IGF2 (112). IGFBP4 binds and inhibits the activity of these IGF ligands. Local degradation of IGFBP4 releases the IGF ligand, which then becomes available for receptor binding and activation of downstream signaling (119). Our study is in agreement with this hypothesis, as our interpretation of our data is that IGFBP4 is mainly produced by tip cells to regulate local concentrations of IGF2, which by itself maintains the tip cell phenotype and enhances sprouting angiogenesis. IGFBP3, on the other hand, forms a complex with ALS and either IGF1 or IGF2, and acts as a carrier of these ligands to prevent their degradation (120, 121). It has been reported that IGFBP3 has pro- and anti-angiogenic roles (122), but we have found a clear stimulatory role of IGFBP3 in sprouting angiogenesis. It has been reported that IGFBP3 can bind to the cell surface, which induces conformational changes that decrease the IGF-binding affinity to IGFBP3, but increases affinity of IGF ligands for IGF1R (123, 124), thereby enhancing downstream signaling.

We also investigated whether the other ligands and receptors of the IGF family played a role in sprouting angiogenesis. Since expression of IGF1 is barely detectable in HUVECs and was absent in serum-free medium, we conclude that it did not contribute. This is consistent with the literature, since it was found that addition of IGF1 to HUVECs contributed to vessel maintenance and not to angiogenesis (87). This conclusion is also in

agreement with the role of IGF1 in retinopathy of prematurity, which is a disease in infants in which neovascularization of retinal vessels does not occur until serum concentrations of IGF1 have reached a threshold (86, 125). Only when serum IGF1 levels are high, retinal blood vessels are being formed and cause damage to the retina.

Exogenous INS also did not affect sprouting angiogenesis, but knockdown of INSR reduced sprouting angiogenesis. INSR exists as two splice variants: INSR-A and INSR-B, of which the INSR-A isoform has recently been shown to be important in tumor angiogenesis, and preferably binds IGF2 (100). Our INSR knockdown experiments show reduced sprouting and also reduced effects of IGF2 on sprouting angiogenesis. Our findings, in combination with data in the literature, indicate that (1) INSR is involved in angiogenesis in mice and chicken (51, 101) and (2) INSR and IGF1R can form heterodimers to mediate downstream signaling (51, 126). Therefore, we conclude that INSR is involved in IGF2-induced sprouting angiogenesis, together with or independent of IGF1R. On the other hand, IGF2R acts as an extracellular sink for IGF2 (84, 92, 127). However, the lack of effect of *IGF2R* knockdown on sprouting from spheroids indicates that its role in sprouting angiogenesis is not strong.

Limitations of this study include the lack of *in vivo* experiments to support our *in vitro* findings. It would be interesting to study tip cells *in vivo* in, for example, mouse retinas to confirm our *in vitro* data. Experiments showing the presence of IGF2 around tip cells with the use of *in situ* hybridization would add evidence to our hypothesis of IGF2 being locally produced to maintain the tip cell phenotype. We have so far not managed to show the presence of IGF2 *in vivo*, which may be due to its very small molecular size of 7.5 kDa. Another concern is the comparison of concentrations of growth factors and binding proteins that we used in our experiments and their serum equivalents. For VEGF, the concentration that we used in the serum-free experiments (25 ng/mL) was similar to the concentration in medium supplemented with 20% human serum (22-45 ng/mL) (128-130). However, the concentrations of IGF2 and IGFBP3 were relatively low in our experimental setup as compared to medium supplemented with 20% serum and especially that of IGFBP3 (108, 131-133). A comparison of these concentrations can only be performed with caution because of the interactions between these proteins and other IGF family members (97). In the circulation, virtually all IGF1 and IGF2 is bound to IGFBP3 and ALS and to a lesser extent to IGFBP4 (85). This means that higher concentrations in serum do not mean that more protein is available. Furthermore, production of IGF2 by endothelial cells is limited, and thus the low concentrations of IGF2 and IGFBP3 that we applied in our experimental setup should be sufficient. Others have shown significant effects of IGFBP3 at the concentration that we used (109). We applied a high concentration of exogenous IGFBP4 (40 ng/mL) when compared to medium with 20% serum (8 ng/mL on average (132)) to show that IGFBP4 had no effects on sprouting.

CONCLUSION

Our findings suggest that the IGF family has a major role in sprouting angiogenesis and tip cell maintenance, partly by autocrine mechanisms. Tip cells secrete IGF2, which maintains their phenotype and allows sprouting angiogenesis by signaling via IGF1R and INSR, but not via IGF2R, and tip cells secrete the IGF2 inhibitor IGFBP4, which acts as a negative local regulator, while tip cells and non-tip cells secrete IGFBP3, acting as a positive local regulator of the IGF2-induced tip cell maintenance and sprouting angiogenesis orchestrated by tip cells.

ACKNOWLEDGEMENTS

Microscopy and flow cytometry experiments were performed at the Core Facility Cellular Imaging, Department of Medical Biology of the Academic Medical Centre, Amsterdam, The Netherlands. The authors were supported by the following foundations: MGD, RPK, CJFvN, IK, ROS: Landelijke Stichting voor Blinden en Slechtienden, Algemene Nederlandse Vereniging Ter Voorkoming Van Bindheid, Stichting Blindenpenning, Novartisfonds, and the ODAS stichting, that contributed through UitZicht (Grant UitZicht 2013-12). Other grants were provided by Rotterdamse Stichting Blindenbelangen (Grant B20130006), and Stichting Nederlands Oogheekundig Onderzoek (Grant 2013-04).

Supplementary information is available here:

<https://link.springer.com/article/10.1007/s11033-020-05339-0>

M.G. Dallinga¹,
I. Klaassen¹,
C.J.F. van Noorden^{1,2},
R.O. Schlingemann^{1,3}

¹ Ocular Angiogenesis Group, Departments of Ophthalmology and Medical Biology, Amsterdam Cardiovascular Sciences, Cancer Center Amsterdam, Amsterdam UMC, University of Amsterdam, Amsterdam, The Netherlands.

² Department of Genetic Toxicology and Cancer Biology, National Institute of Biology, Ljubljana, Slovenia

³ Department of Ophthalmology, University of Lausanne, Jules Gonin Eye Hospital, Fondation Asile des Aveugles, Lausanne, Switzerland.



**THE ROLE OF THE INSULIN-LIKE GROWTH
FACTOR FAMILY IN ENDOTHELIAL TIP AND
STALK CELL BIOLOGY IN ANGIOGENESIS**

INTRODUCTION

Recently, we reported that members of the IGF family are involved in maintenance of the endothelial tip cell phenotype during angiogenesis (90, 134). Here, we review the literature on the role of members of the IGF family, such as IGF ligands, IGF receptors and IGF binding proteins (IGFBPs), in angiogenesis in general and the recent contributions in tip cell and stalk cell biology specifically.

When metabolic needs of tissues exceed oxygen and nutrient levels that are supplied by the existing vascular network, the tissues produce growth factors such as vascular endothelial growth factor (VEGF). These induce differentiation of endothelial cells (ECs) of existing blood vessels in the vicinity into specialized sub-phenotypes (39, 91). The first EC phenotype that emerges is the tip cell, the leading cell of each newly-formed sprout (Fig 1A,B)(39). Its key characteristics are limited proliferation, extension of filopodia to aid migration (77), cell-specific metabolism (80, 117, 135) and regulatory effects on following stalk cells (62, 136). Stalk cells proliferate and consequently elongate the vessel sprout (39), and they form the vascular lumen, develop tight junctions to limit diffusion out of and into the newly-formed vessel lumen, and recruit and interact with supporting cells such as pericytes, which aid maturation of the new sprout (Fig 1)(91). The third distinct EC phenotype identified is the phalanx cell, which is mainly involved in vessel maturation (137). The differentiation into tip and stalk cells is reversible: tip cells can become stalk cells and vice versa as the ECs compete for the tip cell position, aided by stochastic differences in gene expression and varying concentrations of growth factors which can cause a phenotypic switch (41, 81). Once an EC has taken on the tip cell phenotype, it enhances its role by inhibiting the transition of stalk cells into a tip cell phenotype via Delta-like ligand-4 (DLL4)-Notch signaling (138).

CD34 is a protein expressed on the luminal membrane of resting ECs throughout the body, and on filopodia of angiogenic sprouts (45). In addition, it has been identified as an *in vitro* marker of tip cells in EC cultures, as shown in Fig 1D (44, 45, 90, 114). Expression of CD34 by EC tip cells in monolayer cultures has enabled the study of the role of individual IGF family members in the regulation of the tip cell phenotype. Employing this approach, we have demonstrated that IGF2, IGF1 receptor (IGF1R) and IGFBP3 and 4 are all regulators of the tip cell phenotype, and play a role in maintenance of this phenotype (90, 134). Our studies showed that in the absence of IGF2, ECs are unable to form persistent vascular sprouts, which greatly inhibits angiogenesis *in vitro* and *in vivo* (90, 134). IGF1R was shown to be the main receptor involved in this process, whereas IGFBP3 and 4 act as local regulators. Here, we present an overview of the IGF protein family in the context of angiogenesis, and address different ways in which the IGF family members play a role by their involvement in the regulation of the tip cell phenotype.

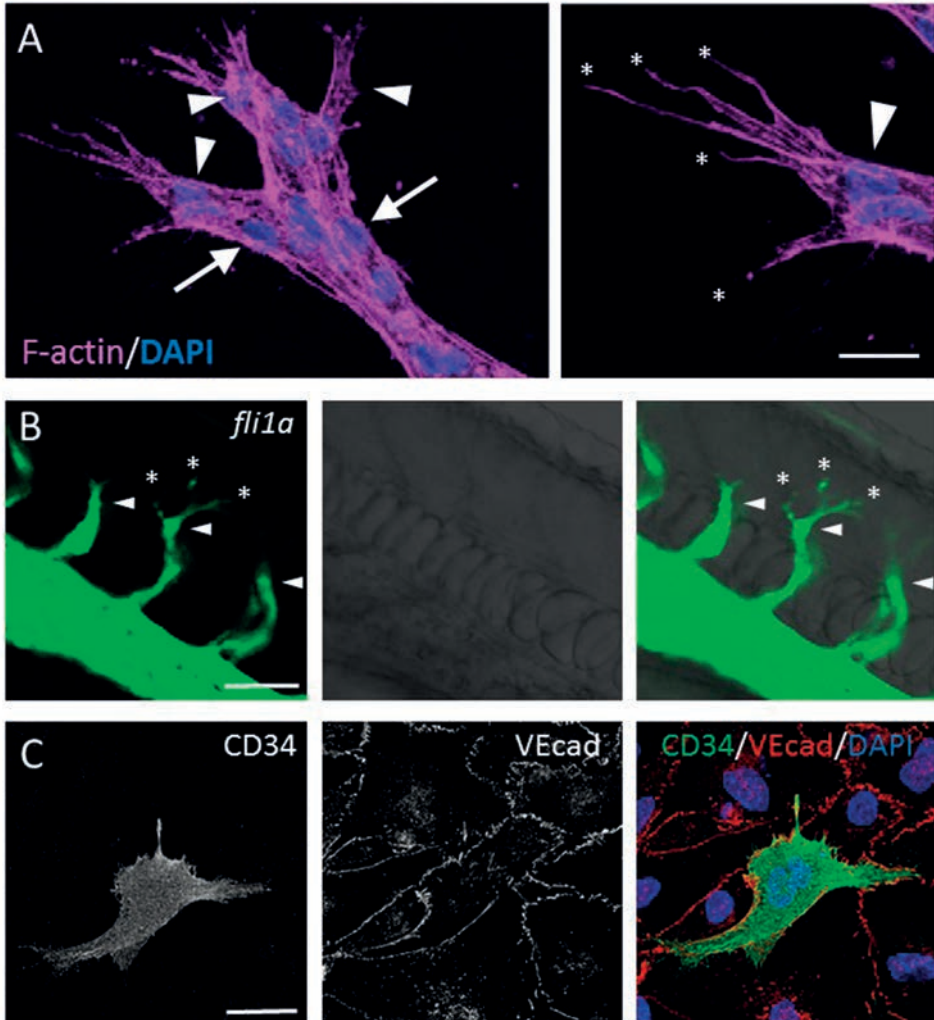


Figure 1. Tip cell morphology. (A) Tip cells in an *in vitro* spheroid-based sprouting model after F-actin (phalloidin, violet) staining and DAPI staining of nuclei (blue). Tip cells (arrow heads), stalk cell (arrows) and filopodia (*) are indicated. Scale bar = 20 μ m. (B) Tip cells in growing zebrafish intersegmental vessels. *Tg(fli1a-eGFP)* zebrafish embryos 24 h after insemination, imaged with confocal (left panel), phase contrast (middle panel) and combination microscopy. Tip cells are indicated by asterisks (*). Scale bar is 100 μ m. (C) A single CD34⁺ tip cell (green) in a monolayer culture of human umbilical vein ECs that was stained for the VEcadherin (grey) staining and DAPI staining of nuclei (blue). Scale bar = 30 μ m.

IGF PROTEIN FAMILY

The IGF protein family comprises 2 ligands, IGF1 and IGF2, 3 receptors, IGF1R, IGF2R and the insulin receptor (INSR), and 10 IGF-binding proteins (IGFBPs) (85, 139, 140). The ligands IGF1 and IGF2 are essential pre- and postnatal growth factors that affect cell differentiation, cell proliferation and growth of various tissues, amongst others (85, 120). The three receptors play different roles in the regulation of tissue growth and cellular metabolism (85, 120), although their downstream signaling pathways are overlapping. The IGFBPs fine-tune IGF signaling, by prolonging the half-life of the ligands in the circulation and/or by regulating their bioavailability (120, 139, 140).

IGF ligands

The IGF family consists of two single chain ligands with a structural overlap of 70%, called IGF1 and IGF2. Insulin is also structurally related, and shares 50% similarity with IGF2, but is not an official member of the IGF family (92, 141). The IGFs are small proteins, both with a molecular mass of 7.5 kDa (84, 142). There are considerable levels of the IGF proteins present in plasma, which originate from the liver and act in an endocrine manner. In plasma, the IGFs are bound in a complex containing IGFBP3 or IGFBP5 and an acid-labile subunit (ALS), in a 1:1:1 ratio (100, 118, 143). The function of these complexes is to prevent uncontrolled efflux of IGFs from plasma into tissues, thereby regulating bioavailability and prolonging protein half-life (143, 144). The most prominent IGF in human serum is IGF2, which has concentrations that are several fold higher than that of IGF1 (100). The IGF proteins are also produced locally in tissues, where they can act as autocrine or paracrine messengers (145). Examples of tissues and cell types that are capable of IGF production are retinal cells, the ovarian tissue, fetal and uterine ECs, chondrocytes and connective tissue (92, 118, 145). Local production of IGFs also occurs in tumor tissue and consequently potentially render these tissues independent of plasma growth factors for cell proliferation.

IGF1 and IGF2 have been found to be associated with angiogenesis in studies initiated by observations in a patient suffering from pathological angiogenesis in the eye as a result of proliferative diabetic retinopathy. The patient experienced a pituitary gland infarction during pregnancy, causing loss of production of growth hormone, IGF1 and IGF2 that coincided with spontaneous regression of the neovascularization in the retina (146). Since then, the involvement of IGF1 and IGF2 in angiogenesis has been further elucidated and the IGF family is now considered to be an important target for anti-angiogenic therapy (98, 101), which is reflected by several clinical trials in which IGF2 or IGF1R are inhibited by novel compounds designed to treat various types of cancer (**Table 1**).

In the eye, diseases with retinal angiogenesis, such as diabetic retinopathy and ROP, have also been associated with IGF proteins. For example: vitreous levels of IGF1, IGF2, IGFBP1 and IGFBP3 are elevated in patients with diabetic retinopathy (147), a retinal disease characterized by neovascularization and vascular dysfunction. In retinopathy of

Table 1. Clinical trials on IGF2 or IGF1R inhibition registered at the U.S. National Library of Medicine

Title	Intervention	Phase	NCT number
Effects of resveratrol on serum IGF2 among African American women	Inhibition of IGF2 by resveratrol in breast cancer	N/A	NCT04266353
A trial of Dalotuzumab in combination with Irinotecan versus Cetuximab and Irinotecan for participants with metastatic rectal cancers (mRC)	Dalotuzumab (MK-0646, inhibition of IGF1R) treatment in combination with Irinotecan versus Cetuximab and Irinotecan for patients with metastatic rectal cancers (mRC) expressing high IGF-1/low IGF-2 Levels	2	NCT01371695
Radiation therapy, Paclitaxel, and Carboplatin in treating patients with high-risk endometrial cancer	Combining radiation therapy, paclitaxel, and carboplatin in treating patients with high-risk endometrial cancer with secondary measurement of the effects on serum IGF protein levels	2	NCT01041027
A study of Robatumumab (SCH 717454, MK-7454) in combination with different treatment regimens in pediatric participants with advanced solid tumors	Safety, tolerability and dose-finding of robatumumab when administered in combination with temozolomide and irinotecan (Arm A); or cyclophosphamide, doxorubicin, and vincristine (Arm B), or ifosfamide and etoposide (Arm C). (Robatumumab inhibits IGF ligand binding, IGF-stimulated receptor phosphorylation and human tumor cell proliferation)	1/1B	NCT00960063
A dose-escalation study to evaluate the safety, tolerability, and antitumor activity of MEDI-573 in subjects with advanced solid tumors	A Phase 1, Multicenter, Open-label, Single-arm, Dose-escalation Study to Evaluate the Safety, Tolerability, and Antitumor Activity of MEDI-573, a Fully Human Monoclonal Antibody Directed Against Insulin-like Growth Factors I and II, in Subjects With Advanced Solid Tumors Refractory to Standard Therapy or for Which No Standard Therapy Exists	1	NCT00816361

prematurity (ROP), pathological angiogenesis develops in the eyes of premature infants. After premature birth, IGF1 plasma levels fall since these depend on maternal production *in utero*. It was shown that ROP does not occur when IGF1 plasma levels are below 30 ng/mL, but only develops when they rise after the initial decline post-partum (125, 148). Further evidence gathered *in vivo* supports an important role of IGFs in angiogenesis. In oxygen-induced retinopathy, a mouse model of hypoxia-induced retinal angiogenesis, increased *Igf2* mRNA expression levels were demonstrated in neovascular retinal tufts (74), whereas mice treated with antagonists of growth hormone (GH) that reduced *Igf1* and *Igf2* plasma levels, were protected against pathological retinal neovascularization (146). Zebrafish lacking *Igf2* exhibited abnormal sprouting of the intersegmental vessels as well as other vascular developmental disorders (52, 58). *In vitro*, effects of IGF2 on angiogenesis were observed in tube-formation assays (87, 92, 149), as well as in spheroid-based assays (90, 134).

We recently reported that these findings may be explained by specific functions of IGF2, which may be especially important for the maintenance of the endothelial tip cell phenotype during angiogenesis. We have shown that siRNA-mediated knockdown of *IGF2* gene expression reduced the percentage of CD34⁺ tip cells in EC cultures, as well as angiogenic sprouting of EC spheroids (90). When the transcriptome of CD34⁺ tip cells in EC cultures is compared with CD34⁻ non-tip cells (44), the *IGF2* gene is one of the most highly differentially expressed genes. On the other hand, *IGF1* is expressed at very low levels in EC cultures and differences in expression levels between CD34⁺ tip cells and CD34⁻ non-tip cells were not observed (44). Furthermore, IGF1 has no effect on the sprouting of EC spheroids nor does it affect the fraction of tip cells in EC cultures (134). Therefore, we concluded that IGF2 is essential for the tip cell phenotype, whereas IGF1 does not play a significant role in tip cell biology. The pivotal role of IGF1 plasma levels in patients with ROP seems to be contradictory in this case. However, experiments using cultures ECs showed that IGF1 plays a role in stabilization of new vessels rather than in their formation (87). In the context of ROP, it may mean that newly formed retinal blood vessels regress in the absence of proper IGF1 plasma concentrations.

IGF receptors

IGF1 and IGF2 can both bind to IGF1R and INSR, whereas only IGF2 can bind to IGF2R (84). IGF1R is the best studied IGF receptor, and generates most of the relevant downstream signals after ligand binding, as is described below. It is highly expressed in sprouting retinal vessels (150), and *Igf1r* knockdown in mice was shown to reduce pathological ocular angiogenesis (51). As mentioned above, IGF1R has been identified as an important target for anti-angiogenic therapy, and there are ongoing trials investigating novel inhibiting compounds (Table 1) (98). INSR activates similar downstream pathways as IGF1R, partly by forming heterodimeric IGF1R-INSR receptors (84, 122, 151). Knockdown of *Insr* *in vivo* also inhibits pathological ocular angiogenesis in mice (51).

The main role of IGF2R is reduction of the effects of IGF2 by binding and clearance of extracellular IGF2 (84, 92, 127, 151). This role is supported by the finding that mice lacking IGF2R grow faster and show lethal cardiac defects (152), which is consistent with a human disease named Beckwith-Wiedemann, in which a lack of *IGF2* imprinting induces excess levels of IGF2 (153). Typical features of this disease include organomegaly, anterior abdominal wall defects, gigantism, facial malformations, hypoglycemia, capillary naevus flammeus, neonatal hypoglycemia, cardiovascular defects. Patients also have a higher prevalence of Wilms tumor, a highly vascularized kidney tumor. Vascularization of the tumor is inversely correlated with patient survival (154). Excessively high IGF2 levels are also found during the growth phase of infantile hemangioma, a benign, well-vascularized vascular tumor (75). Together, these observations emphasize that poor control of IGF2 levels leads to unbalanced angiogenesis in human diseases.

In cultured ECs, mRNA expression levels of all three receptors are significantly higher in endothelial CD34⁺ tip cells than in non-tip cells (134). We have reported that knockdown of *IGF1R* *in vitro* had similar effects as inhibition of IGF2, leading to a reduced fraction of CD34⁺ tip cells in EC cultures, as well as reduced sprouting from EC spheroids (90). Knockdown of *INSR* also causes a significantly reduced percentage of CD34⁺ tip cells and sprouting from EC spheroids (134). Knockdown of *IGF2R* increased the percentage of tip cells, which is in line with its inhibitory role described above, but did not affect sprouting from EC spheroids *in vitro*. Based on these data, we conclude that IGF2 binding to IGF1R and to less extent INSR is involved in the maintenance of the tip cell phenotype (134). It seems that IGF2R can regulate these effects of IGF2 on tip cell maintenance, without affecting sprouting angiogenesis (134).

IGF-binding proteins

There are 6 high-affinity IGFbps (IGFBP1-6) and at least 4 low-affinity IGFbps (IGFBP7-10) (96). IGFbps regulate bioavailability of IGF ligands in a positive or negative fashion (151). Little is known about the low-affinity IGFbps. Of interest, IGFBP8 is also known as CTGF or CCN2, and is involved in fibrosis and wound healing responses, and in the angio-fibrotic switch in patients with diabetic retinopathy (155, 156). IGFBP3 and IGFBP4 are the most critical members of this family in the regulation of angiogenesis and tip cell maintenance, and are discussed here.

IGFBP3 is the main carrier of IGFs in the circulation, where it forms a complex with acid-labile subunit (ALS) in a 1:1:1 ratio that increases the half-life of IGFs in plasma, but inhibits their bioavailability (120, 121). Mice lacking *Igfbp3* do not show defects in their phenotype (96), but the addition of IGFBP3 to Matrigel plugs transplanted in mice increased vascular growth (157), which suggests a pro-angiogenic role. This is supported by the fact that in human vitreous, levels of IGFBP3 are elevated in diabetic retinopathy (147, 149). It has been shown that IGFBP3 can both decrease and increase binding to IGF1R on the cellular membrane of ECs by the IGF ligands and that intracellular signaling depends on cell surface binding of IGFBP3 (120). *In vitro* studies have shown that IGFBP3

in combination with IGF2 maintains the tip cell phenotype, and that it induces sprouting angiogenesis from EC spheroids (134, 157). Together, these data suggest that IGFBP3 is pro-angiogenic by increasing IGF2-induced tip cell maintenance.

IGFBP4 appears to have an opposite role. Mice lacking *Igfbp4* show mild growth retardation (96). *In vitro* studies have shown that IGFBP4 inhibits IGF1-induced, but not VEGF-induced angiogenesis (110), and we have shown that it specifically reduces maintenance of the tip cell phenotype by IGF2 (134). IGFBP4 is expressed more abundantly by CD34⁺ tip cells than by CD34⁻ non-tip cells, and inhibits the effects of IGF2 on tip cells, sprouting from spheroids and tube formation (134, 158). These data suggest that IGFBP4 is produced by tip cells to act as a negative regulator of local IGF2 levels in order to optimize sprouting.

IGF FAMILY MEMBERS AND TIP CELL PROPERTIES

Tip cells have functional and morphological characteristics that distinguish them from the other EC subtypes, stalk cells and phalanx cells during angiogenesis. The characteristics affected by IGF signaling include tip cell migration, regulation of the tip cell phenotype, tip cell metabolism and signaling via the phosphatidylinositol 3-kinase (PI3K) pathway, which are discussed below.

Tip cell migration

EC migration occurs through rearrangements of the cytoskeleton, initiated by GTPase activation via several pathways (159). First, VEGF activates the GTPases cell division cycle 42 (CDC42) and Rac family small GTPase 1 (RAC1), which induce migration (160, 161). Second, activation of Rho guanine nucleotide exchange factor 12 (ARHGEF12, also known as LARG) induces activation of Rho GTPases through binding of IGF1 or IGF2 to IGF1R to initiate the formation of stress fibers, which are necessary for migration (Fig 2) (159, 162, 163). In line with this, we have shown that knockdown of *IGF2* and *IGF1R* causes major cytoskeletal changes (90). The cytoskeletal changes were found in both CD34⁺ tip cells and CD34⁻ non-tip cells upon knockdown of *IGF1R*, but only in tip cells upon knockdown of *IGF2*. Moreover, knockdown of *IGF1R* and *IGF2* decreased sprouting from EC spheroids *in vitro*. These findings suggest that IGF2 and IGF1R are involved in tip cell migration through cytoskeletal rearrangements.

Regulation of the tip cell phenotype

DLL4 and NOTCH1 suppress the tip cell phenotype in adjacent endothelial stalk cells (61, 62, 136, 164). A simplified representation is that tip cells express more DLL4 on their cell membranes than stalk cells (91). Upon binding to DLL4, NOTCH1 in stalk cells is cleaved and the NOTCH1 intracellular domain (NICD) is transported to the nucleus to initiate gene transcription (91). Downstream signals initiated by binding of DLL4 to NOTCH1 include increased expression of proliferation-associated genes and decreased expression of genes

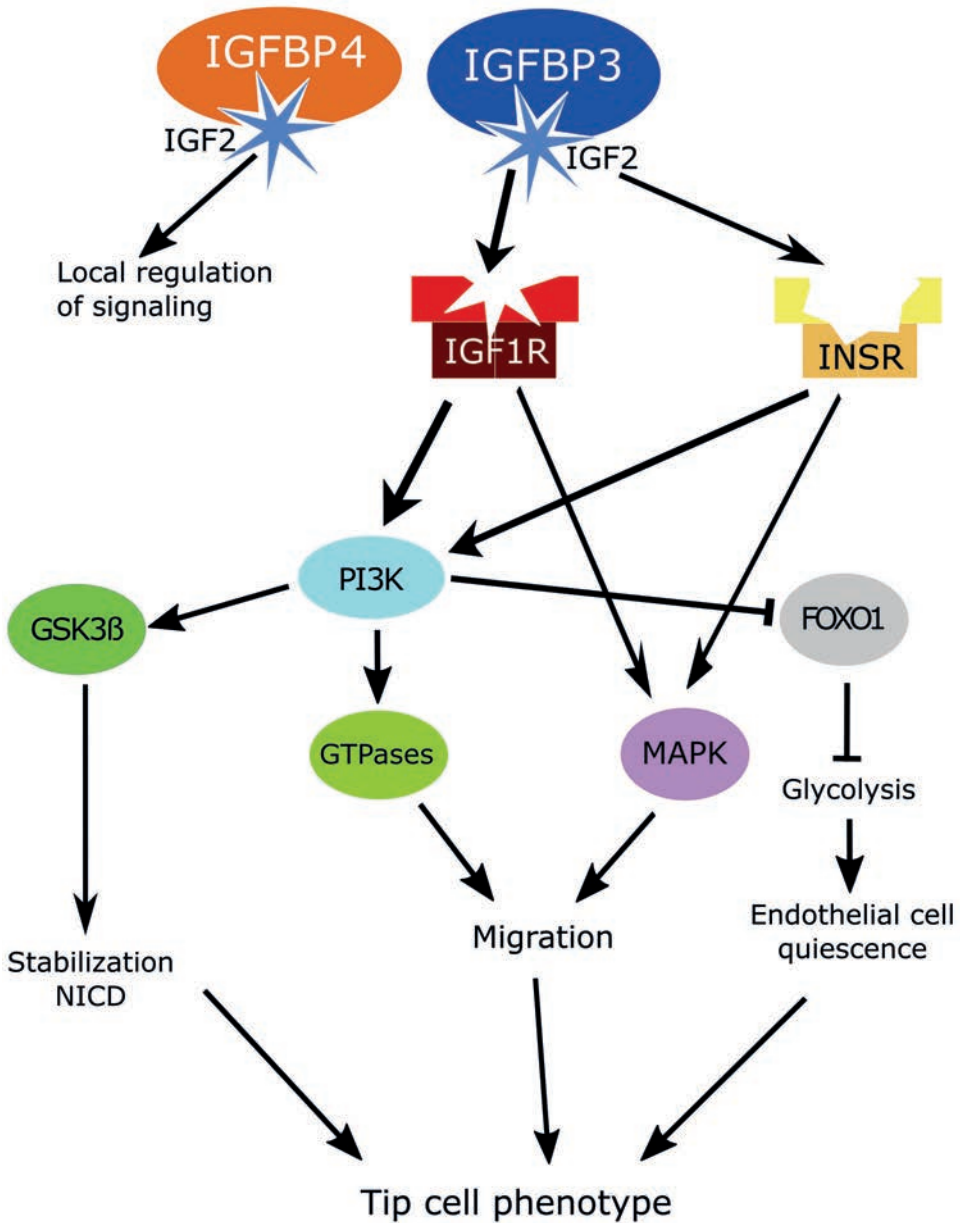


Figure 2. IGF2-induced tip cell maintenance. Overview of tip cell signaling by the IGF family. Binding of IGF2 to its receptors is inhibited by IGFBP4. IGFBP3 is essential for tip cell signals induced by binding of IGF2 to IGF1R. Binding of IGF2 to INSR induces similar signaling pathways as binding of IGF2 to IGF1R and forms heterodimers with IGF1R. The main downstream effectors is PI3K. Activated PI3K regulates GSK3 β and GTPases and inhibits FOXO1. Activation of GSK3 β prolongs the half-life of the NOTCH1-intracellular domain to stabilize the tip and stalk cell phenotypes and enhance sprouting efficiency. Activation of GTPases result in cytoskeletal changes necessary for migration. Inhibition of FOXO1 is essential for cell metabolism. In concert, activation of these pathways maintains a tip cell phenotype.

associated with the tip cell phenotype (62). This signaling cascade causes downregulation of the tip cell phenotype to increase sprouting efficiency. Dysregulation of expression of either DLL4 or NOTCH1 induces severely disrupted sprouting: mice lacking *Dll4* die *in utero* due to severe vascular defects (165, 166) and tumor growth in mice was severely hampered by *Dll4* blockade due to deregulated angiogenesis (77, 167, 168). The mice in these studies exhibited excessive, non-productive angiogenesis.

GSK3 β is a downstream effector of IGF2-IGF1R-PI3K signaling which has been shown to prolong the half-life of NICD (169, 170), enhancing the effects of DLL4-NOTCH1 signaling. We observed that knockdown of *IGF2* or *IGF1R* reduces the ability of tip cells to maintain their phenotype (90). A plausible explanation is that knockdown of *IGF2* and *IGF1R* reduces the IGF2-IGF1R-PI3K-GSK3 β signaling cascade and thus decreases the half-life of NICD, which subsequently causes tip cells to lose their dominance over the adjacent stalk cells and failure to maintain the tip cell phenotype (Fig 2).

VEGF is the most important inducer of angiogenesis and formation of tip cells (39). Tip cells have higher expression of VEGFR2 and VEGFR3 (68, 171). Binding of VEGF to one of these receptors increases tip cell percentages and sprouting (44, 171). IGF2 and IGF1 are capable of inducing mRNA and protein expression of VEGF and vice versa (172-174). Counter-intuitively, IGFBP3 and IGFBP4 are both capable of inhibiting VEGF-induced angiogenesis (110, 175, 176), which contradicts the angiogenesis-inducing effects by IGFBP3 found by us and others (121, 134, 157).

Tip cell metabolism

The importance of EC metabolism in angiogenesis has become clear in recent years: glycolysis is increased in angiogenic ECs (80), and several metabolic genes have been discovered that link EC metabolism to cellular processes. For example, pyruvate kinase M2 (PKM2) induction by AKT regulates the glycolytic rate in cancer cells (177) and regulates junction dynamics of retinal ECs during angiogenesis (178). It has been shown that IGF1-IGF1R signaling induces PKM2 expression (177), but whether IGF2-IGF1R signaling also induces PKM2 expression is unknown.

Recently, the differential metabolism of angiogenic EC subtypes was studied by our group, and we showed that tip cells are less glycolytic than stalk cells, but instead respond in a more flexible manner to metabolic stress. We hypothesized that such metabolic flexibility allows rapid adaptation of tip cells to hypoxic or glucose-deprived environments in tissues (117). In this context, an important transcription factor that inhibits glycolysis is FOXO1 (179). When FOXO1 is active, it reduces glycolysis and induces mitochondrial respiration in ECs (180), a phenomenon opposite to the situation in angiogenesis, where ECs are assumed to be dependent on glycolysis for their energy supply (80). Inhibition of FOXO1 is therefore considered essential to enable ECs to form vessels sprouts (180). Amongst the protein signaling pathways that can inhibit FOXO1 are the AKT, Sirtuin 1 (SIRT1) and PI3K pathways (179, 181, 182), and IGF2-IGF1R signaling was also reported

to inhibit FOXO1 by activating this PI3K pathway (**Fig 2**) (183). However, the role of IGF2 in this context is still debated, since it has also been reported that IGF2 stimulates FOXO1 under certain circumstances (183, 184). The precise regulation of FOXO1 in tip cells has yet to be uncovered, and whether IGF2 plays a role in its inhibition to allow tip cells to maintain their flexible metabolism will have to be studied in future research.

2.4

Signaling via the PI3K pathway

The PI3K pathway is one of the major pathways activated by signaling via IGF1R, and this may have an important role in tip cell biology in angiogenesis. PI3Ks are central regulators in many intracellular signaling pathways resulting in, amongst others, enhanced angiogenesis, metabolism and migration (83, 185). Many of the signaling pathways that regulate the tip cell phenotype eventually converge in signaling through PI3Ks. PI3Ks inhibit or induce other signaling pathways by phosphorylating various types of phosphatidylinositol lipid substrates. The primary target of PI3K is AKT, which is phosphorylated by pyruvate dehydrogenase kinase 1 (PDK1) after activation of PI3K (185, 186). Because of their essential role, specific PI3Ks have been selected as therapeutic targets to inhibit pathological angiogenesis (186).

For IGF1 or IGF2, PI3K pathway activation is a major effect of signaling via IGF1R binding (82, 84), and a systems biology study showed that PI3K is one of the main pathways induced by IGF2 in chondrocytes (170). Many of the downstream signaling pathways induced or inhibited by PI3K are essential for proper functioning of tip cells (**Fig 2**). Inhibition of PI3K in mice results in chaotic angiogenic sprouting with reduced EC motility and impaired junction formation (187). It has, therefore, been suggested that PI3K serves as a hub for many pro-angiogenic signaling pathways (188).

IGF2-IGF1R-induced maintenance of the tip cell phenotype via PI3K has not been directly shown yet. There are, however, several clues that PI3K is the key regulator of IGF2-induced tip cell maintenance, and that it is involved in all three tip cell characteristics described above. First, it has been shown that IGF2-induced activation of PI3K results in induction of GTPases (170, 189). Second, GSK3 β is a downstream effector of IGF1R-PI3K signaling which has been shown to prolong the half-life of NICD (169, 190). And third, it has been shown that IGF signaling inhibits FOXO1, although there are also contradictory reports that IGF signaling enhances FOXO1 under certain circumstances, underlining the complexity of IGF signaling (83, 184, 187).

Based on the described effects of PI3K in signaling, and the fact that activation by IGF2-IGF1R binding has been confirmed, we conclude that it is likely that PI3K is the central signaling pathway involved in IGF2-induced tip cell maintenance.

CONCLUSION

Taken together, IGF2 appears to be a major local autocrine regulator of the maintenance of tip cell fate, and of essential functions of tip cells (Fig 2). The main effects involved are induced via activation of PI3K by binding of IGF2 to IGF1R. The presence of IGFBP3 is essential for transduction of this signal, whereas IGFBP4 acts as an inhibitor and regulator of these IGF2 effects. This complex local regulation process may ensure maintenance of the tip cell phenotype long enough for proper sprout formation.

REFERENCES

1. Chung AS, Ferrara N. Developmental and pathological angiogenesis. *Annual review of cell and developmental biology*. 2011;27:563-84.
2. Carmeliet P, Jain RK. Molecular mechanisms and clinical applications of angiogenesis. *Nature*. 2011;473(7347):298-307.
3. Herbert SP, Stainier DY. Molecular control of endothelial cell behaviour during blood vessel morphogenesis. *NatRevMolCell Biol*. 2011;12(9):551-64.
4. Siemerink MJ, Klaassen I, Van Noorden CJ, Schlingemann RO. Endothelial tip cells in ocular angiogenesis: potential target for anti-angiogenesis therapy. *JHistochemCytochem*. 2013;61(2):101-15.
5. Schlingemann RO. Role of growth factors and the wound healing response in age-related macular degeneration. *Graefes ArchClinExpOphthalmol*. 2004;42(1):91-101.
6. Gerhardt H, Golding M, Fruttiger M, Ruhrberg C, Lundkvist A, Abramsson A, et al. VEGF guides angiogenic sprouting utilizing endothelial tip cell filopodia. *JCell Biol*. 2003;161(6):1163-77.
7. Schlingemann RO, Rietveld FJ, de Waal RM, Bradley NJ, Skene AJ, Davies AJ, et al. Leukocyte antigen CD34 is expressed by a subset of cultured endothelial cells and on endothelial abluminal microprocesses in the tumor stroma. *Lab Invest*. 1990;62(6):690-6.
8. Phng L-K, Stanchi F, Gerhardt H. Filopodia are dispensable for endothelial tip cell guidance. *Development*. 2013;140(19):4031-40.
9. Arroyo AG, Iruela-Arispe ML. Extracellular matrix, inflammation, and the angiogenic response. *Cardiovasc Res*. 2010;86(2):226-35.
10. Koziol A, Gonzalo P, Mota A, Pollan A, Lorenzo C, Colome N, et al. The protease MT1-MMP drives a combinatorial proteolytic program in activated endothelial cells. *FASEB J*. 2012;26(11):4481-94.
11. Baumhueter S, Dybdal N, Kyle C, Lasky LA. Global vascular expression of murine CD34, a sialomucin-like endothelial ligand for L-selectin. *Blood*. 1994;84(8):2554-65.
12. Fina L, Molgaard HV, Robertson D, Bradley NJ, Monaghan P, Delia D, et al. Expression of the CD34 gene in vascular endothelial cells. *Blood*. 1990;75(12):2417-26.
13. Ito A, Nomura S, Hirota S, Suda J, Suda T, Kitamura Y. Enhanced expression of CD34 messenger-RNA by developing endothelial cells of mice. *Lab Invest*. 1995;72(5):532-8.
14. Nielsen JS, McNagny KM. CD34 is a key regulator of hematopoietic stem cell trafficking to bone marrow and mast cell progenitor trafficking in the periphery. *Microcirculation*. 2009;16(6):487-96.
15. Testa JE, Chastina A, Oh P, Li Y, Witkiewicz H, Czarny M, et al. Immunotargeting and cloning of two CD34 variants exhibiting restricted expression in adult rat endothelia *in vivo*. *Am J Physiol Lung Cell Mol Physiol*. 2009;297(2):L251-L62.
16. Strilic B, Kucera T, Eglinger J, Hughes MR, McNagny KM, Tsukita S, et al. The molecular basis of vascular lumen formation in the developing mouse aorta. *Developmental Cell*. 2009;17(4):505-15.
17. Blanchet MR, Maltby S, Haddon DJ, Merckens H, Zbytniuk L, McNagny KM. CD34 facilitates the development of allergic asthma. *Blood*. 2007;110(6):2005-12.
18. Blanchet MR, Gold M, Maltby S, Bennett J, Petri B, Kubes P, et al. Loss of CD34 leads to exacerbated autoimmune arthritis through increased vascular permeability. *J Immunol*. 2010;184(3):1292-9.
19. Drew E, Merzaban JS, Seo W, Ziltener HJ, McNagny KM. CD34 and CD43 inhibit mast cell adhesion and are required for optimal mast cell reconstitution. *Immunity*. 2005;22(1):43-57.
20. Maltby S, Wohlfarth C, Gold M, Zbytniuk L, Hughes MR, McNagny KM. CD34 is required for infiltration of eosinophils into the colon and pathology associated with DSS-induced ulcerative colitis. *Am J of Pathol*. 2010;177(3):1244-54.

21. Siemerink MJ, Klaassen I, Vogels IMC, Griffioen AW, Van Noorden CJF, Schlingemann RO. CD34 marks angiogenic tip cells in human vascular endothelial cell cultures. *Angiogenesis*. 2012;15(1):151-63.
22. Wood HB, May G, Healy L, Enver T, Morriss-Kay GM. CD34 expression patterns during early mouse development are related to modes of blood vessel formation and reveal additional sites of hematopoiesis. *Blood*. 1997;90(6):2300-11.
23. Young PE, Baumhueter S, Lasky LA. The sialomucin CD34 is expressed on hematopoietic cells and blood vessels during murine development. *Blood*. 1995;85(1):96-105.
24. Maltby S, Freeman S, Gold MJ, Baker JHE, Minchinton AI, Gold MR, et al. Opposing roles for CD34 in B16 melanoma tumor growth alter early stage vasculature and late stage immune cell infiltration. *Plos One*. 2011;6(4):e18160.
25. Korff T, Kimmina S, Martiny-Baron G, Augustin HG. Blood vessel maturation in a 3-dimensional spheroidal coculture model: direct contact with smooth muscle cells regulates endothelial cell quiescence and abrogates VEGF responsiveness. *FASEB J*. 2001;15(2):447-57.
26. Klaassen I, Hughes JM, Vogels IM, Schalkwijk CG, Van Noorden CJ, Schlingemann RO. Altered expression of genes related to blood-retina barrier disruption in streptozotocin-induced diabetes. *Experimental eye research*. 2009;89(1):4-15.
27. Korff T, Augustin HG. Integration of endothelial cells in multicellular spheroids prevents apoptosis and induces differentiation. *J Cell Biol*. 1998;143(5):1341-52.
28. Chieco P, Jonker A, De Boer BA, Ruijter JM, Van Noorden CJ. Image cytometry: protocols for 2D and 3D quantification in microscopic images. *Prog Histochem Cytochem*. 2013;47(4):211-333.
29. Shankar S, Chen Q, Srivastava RK. Inhibition of PI3K/AKT and MEK/ERK pathways act synergistically to enhance antiangiogenic effects of EGCG through activation of FOXO transcription factor. *J Mol Signal*. 2008;3:7.
30. Suzuki A, Andrew DP, Gonzalo JA, Fukumoto M, Spellberg J, Hashiyama M, et al. CD34-deficient mice have reduced eosinophil accumulation after allergen exposure and show a novel crossreactive 90-kD protein. *Blood*. 1996;87(9):3550-62.
31. Smith LE, Wesolowski E, McLellan A, Kostyk SK, D'Amato R, Sullivan R, et al. Oxygen-induced retinopathy in the mouse. *Invest Ophthalmol Vis Sci*. 1994;35(1):101-11.
32. Connor KM, Krah NM, Dennison RJ, Aderman CM, Chen J, Guerin KI, et al. Quantification of oxygen-induced retinopathy in the mouse: a model of vessel loss, vessel regrowth and pathological angiogenesis. *Nature Protocols*. 2009;4(11):1565-73.
33. Hughes S, Yang HJ, Chan-Ling T. Vascularization of the human fetal retina: Roles of vasculogenesis and angiogenesis. *Invest OphthalmolVisSci*. 2000;41(5):1217-28.
34. Klosovskii BN, Zhukova T. [Effect of colchicine on remote phases of growing capillaries in the brain]. *ArkhPatol*. 1963;35(3):38-44.
35. Marin-Padilla M. Early vascularization of the embryonic cerebral cortex: Golgi and electron microscopic studies. *JComp Neurol*. 1985;241(2):237-49.
36. Schoefl GI. Studies on inflammation. III. Growing capillaries: Their structure and permeability. *Virchows ArchPatholAnatPhysiol KlinMed*. 1963;337:97-141.
37. Stahl A, Connor KM, Sapieha P, Chen J, Dennison RJ, Krah NM, et al. The mouse retina as an angiogenesis model. *Invest OphthalmolVisSci*. 2010;51(6):2813-26.
38. Hellwig SM, Damen CA, van Adrichem NP, Blijham GH, Groenewegen G, Griffioen AW. Endothelial CD34 is suppressed in human malignancies: role of angiogenic factors. *Cancer Lett*. 1997;120(2):203-11.
39. Gerhardt H, Golding M, Fruttiger M, Ruhrberg C, Lundkvist A, Abramsson A, et al. VEGF guides angiogenic sprouting utilizing endothelial tip cell filopodia. *J Cell Biol*. 2003;161(6):1163-77.
40. Siemerink MJ, Klaassen I, Van Noorden CJ, Schlingemann RO. Endothelial tip cells in ocular angiogenesis: potential target for anti-angiogenesis therapy. *J Histochem Cytochem*. 2013;61(2):101-15.

41. Jakobsson L, Franco CA, Bentley K, Collins RT, Ponsioen B, Aspalter IM, et al. Endothelial cells dynamically compete for the tip cell position during angiogenic sprouting. *Nat Cell Biol.* 2010;12(10):943-53.
42. del Toro R, Prahst C, Mathivet T, Siegfried G, Kaminker JS, Larrivee B, et al. Identification and functional analysis of endothelial tip cell-enriched genes. *Blood.* 2010;116(19):4025-33.
43. Strasser GA, Kaminker JS, Tessier-Lavigne M. Microarray analysis of retinal endothelial tip cells identifies CXCR4 as a mediator of tip cell morphology and branching. *Blood.* 2010;115(24):5102-10.
44. Siemerink MJ, Klaassen I, Vogels IM, Griffioen AW, Van Noorden CJ, Schlingemann RO. CD34 marks angiogenic tip cells in human vascular endothelial cell cultures. *Angiogenesis.* 2012;15(1):151-63.
45. Schlingemann RO, Rietveld FJ, de Waal RM, Bradley NJ, Skene AI, Davies AJ, et al. Leukocyte antigen CD34 is expressed by a subset of cultured endothelial cells and on endothelial abluminal microprocesses in the tumor stroma. *Lab Invest.* 1990;62(6):690-6.
46. Clark ER, Clark EL. Microscopic observations on the growth of blood capillaries in the living mammal. *the american Journal of Anatomy.* 1939;64(2):251-301.
47. Bezuidenhout L, Zilla P, Davies N. Association of Ang-2 with integrin beta 2 controls Ang-2/PDGF-BB-dependent upregulation of human peripheral blood monocyte fibrinolysis. *Inflammation.* 2009;32(6):393-401.
48. Felcht M, Luck R, Schering A, Seidel P, Srivastava K, Hu J, et al. Angiopoietin-2 differentially regulates angiogenesis through TIE2 and integrin signaling. *J Clin Invest.* 2012;122(6):1991-2005.
49. Savant S, La Porta S, Budnik A, Busch K, Hu J, Tisch N, et al. The Orphan Receptor Tie1 Controls Angiogenesis and Vascular Remodeling by Differentially Regulating Tie2 in Tip and Stalk Cells. *Cell Rep.* 2015;12(11):1761-73.
50. Kim KW, Bae SK, Lee OH, Bae MH, Lee MJ, Park BC. Insulin-like growth factor II induced by hypoxia may contribute to angiogenesis of human hepatocellular carcinoma. *Cancer Res.* 1998;58(2):348-51.
51. Kondo T, Vicent D, Suzuma K, Yanagisawa M, King GL, Holzenberger M, et al. Knockout of insulin and IGF-1 receptors on vascular endothelial cells protects against retinal neovascularization. *J Clin Invest.* 2003;111(12):1835-42.
52. Hartnett L, Glynn C, Nolan CM, Grealay M, Byrnes L. Insulin-like growth factor-2 regulates early neural and cardiovascular system development in zebrafish embryos. *Int J Dev Biol.* 2010;54(4):573-83.
53. Harrington LS, Sainson RC, Williams CK, Taylor JM, Shi W, Li JL, et al. Regulation of multiple angiogenic pathways by Dll4 and Notch in human umbilical vein endothelial cells. *Microvasc Res.* 2008;75(2):144-54.
54. Ruijter JM, Thygesen HH, Schoneveld OJ, Das AT, Berkhout B, Lamers WH. Factor correction as a tool to eliminate between-session variation in replicate experiments: application to molecular biology and retrovirology. *Retrovirology.* 2006;3:2.
55. Nowak-Sliwinska P, Segura T, Iruela-Arispe ML. The chicken chorioallantoic membrane model in biology, medicine and bioengineering. *Angiogenesis.* 2014;17(4):779-804.
56. Weiss A, Ding X, van Beijnum JR, Wong I, Wong TJ, Berndsen RH, et al. Rapid optimization of drug combinations for the optimal angiostatic treatment of cancer. *Angiogenesis.* 2015;18(3):233-44.
57. Nowak-Sliwinska P, van Beijnum JR, van Berkel M, van den Bergh H, Griffioen AW. Vascular regrowth following photodynamic therapy in the chicken embryo chorioallantoic membrane. *Angiogenesis.* 2010;13(4):281-92.
58. White YA, Kyle JT, Wood AW. Targeted gene knockdown in zebrafish reveals distinct intraembryonic functions for insulin-like growth factor II signaling. *Endocrinology.* 2009;150(9):4366-75.

59. Delia D, Lampugnani MG, Resnati M, Dejana E, Aiello A, Fontanella E, et al. CD34 expression is regulated reciprocally with adhesion molecules in vascular endothelial cells *in vitro*. *Blood*. 1993;91(4):1001-8.
60. Hellwig SMM, Damen CM, van Adrichem NPH, Blijham GH, Groenewegen G, Griffioen AW. Endothelial CD34 is suppressed in human malignancies: role of angiogenic factors. *Cancer Letters*. 1997;120:203-11.
61. Suchting S, Freitas C, le Noble F, Benedito R, Breant C, Duarte A, et al. The Notch ligand Delta-like 4 negatively regulates endothelial tip cell formation and vessel branching. *Proc Natl Acad Sci U S A*. 2007;104(9):3225-30.
62. Hellstrom M, Phng LK, Hofmann JJ, Wallgard E, Coultas L, Lindblom P, et al. Dll4 signalling through Notch1 regulates formation of tip cells during angiogenesis. *Nature*. 2007;445(7129):776-80.
63. Javerzat S, Auguste P, Bikfalvi A. The role of fibroblast growth factors in vascular development. *Trends Mol Med*. 2002;8(10):483-9.
64. Gerhardt H, Ruhrberg C, Abramsson A, Fujisawa H, Shima D, Betsholtz C. Neuropilin-1 is required for endothelial tip cell guidance in the developing central nervous system. *Dev Dynam*. 2004;231(3):503-9.
65. Sawamiphak S, Seidel S, Essmann CL, Wilkinson GA, Pitulescu ME, Acker T, et al. Ephrin-B2 regulates VEGFR2 function in developmental and tumour angiogenesis. *Nature*. 2010;465(7297):487-91.
66. Tammela T, Zarkada G, Nurmi H, Jakobsson L, Heinolainen K, Tvorogov D, et al. VEGFR-3 controls tip to stalk conversion at vessel fusion sites by reinforcing Notch signalling. *Nat Cell Biol*. 2011;13(10):1202-13.
67. Wang Y, Nakayama M, Pitulescu ME, Schmidt TS, Bochenek ML, Sakakibara A, et al. Ephrin-B2 controls VEGF-induced angiogenesis and lymphangiogenesis. *Nature*. 2010;465(7297):483-6.
68. Witmer AN, van Blijswijk BC, Dai J, Hofman P, Partanen TA, Vrensen GF, et al. VEGFR-3 in adult angiogenesis. *J Pathol*. 2001;195(4):490-7.
69. Witmer A. Vascular endothelial growth factors and angiogenesis in eye disease. *Progress in Retinal and Eye Research*. 2003;22(1):1-29.
70. Lu X, Noble FI, Yuan L, Jiang Q, Lafarge Bd, Sugiyama D, et al. The netrin receptor UNC5B mediates guidance events controlling morphogenesis of the vascular system. *Nature*. 2004;432:179-86.
71. Koch AW, Mathivet T, Larrivee B, Tong RK, Kowalski J, Pibouin-Fragner L, et al. Robo4 maintains vessel integrity and inhibits angiogenesis by interacting with UNC5B. *Dev Cell*. 2011;20(1):33-46.
72. Martyn U, Schulte-Merker S. Zebrafish neuropilins are differentially expressed and interact with vascular endothelial growth factor during embryonic vascular development. *Dev Dynam*. 2004;231(1):33-42.
73. Maisonpierre PC. Angiopoietin-2, a Natural Antagonist for Tie2 That Disrupts *in vivo* Angiogenesis. *Science*. 1997;277(5322):55-60.
74. Lofqvist C, Willett KL, Aspegren O, Smith AC, Aderman CM, Connor KM, et al. Quantification and localization of the IGF/insulin system expression in retinal blood vessels and neurons during oxygen-induced retinopathy in mice. *Invest Ophthalmol Vis Sci*. 2009;50(4):1831-7.
75. Ritter MR, Dorrell MI, Edmonds J, Friedlander SF, Friedlander M. Insulin-like growth factor 2 and potential regulators of hemangioma growth and involution identified by large-scale expression analysis. *Proc Natl Acad Sci U S A*. 2002;99(11):7455-60.
76. Siemerink MJ, Hughes MR, Dallinga MG, Gora T, Cait J, Vogels IM, et al. CD34 promotes pathological epi-retinal neovascularization in a mouse model of oxygen-induced retinopathy. *PLoS One*. 2016;11(6):e0157902.
77. Phng LK, Stanchi F, Gerhardt H. Filopodia are dispensable for endothelial tip cell guidance. *Development*. 2013;140(19):4031-40.

78. Schweigerer L, Neufeld G, Friedman J, Abraham JA, Fiddes JC, Gospodarowic D. Capillary endothelial cells produce basic fibroblast growth factor, a mitogen that promotes their own growth. *Nature*. 1987;325:257-9.
79. Carlson TR, Feng Y, Maisonpierre PC, Mrksich M, Morla AO. Direct cell adhesion to the angiopoietins mediated by integrins. *J Biol Chem*. 2001;276(28):26516-25.
80. De Bock K, Georgiadou M, Schoors S, Kuchnio A, Wong BW, Cantelmo AR, et al. Role of PFKFB3-driven glycolysis in vessel sprouting. *Cell*. 2013;154(3):651-63.
81. Palm MM, Dallinga MG, van Dijk E, Klaassen I, Schlingemann RO, Merks RM. Computational screening of tip and stalk cell behavior proposes a role for apelin signaling in sprout progression. *PLoS One*. 2016;11(11):e0159478.
82. Riedemann J, Macaulay VM. IGF1R signalling and its inhibition. *Endocr Relat Cancer*. 2006;13 Suppl 1:S33-43.
83. Graupera M, Potente M. Regulation of angiogenesis by PI3K signaling networks. *Exp Cell Res*. 2013;319(9):1348-55.
84. Harris LK, Westwood M. Biology and significance of signalling pathways activated by IGF-II. *Growth Factors*. 2012;30(1):1-12.
85. Bach LA. Endothelial cells and the IGF system. *J Mol Endocrinol*. 2015;54(1):R1-13.
86. Hellstrom A, Carlsson B, Niklasson A, Segnestam K, Boguszewski M, De La Cerda L, et al. IGF-1 is critical for normal vascularization of the human retina. *J Clin Endocr Metab*. 2002;87(7):3413-6.
87. Jacobo SM, Kazlauskas A. Insulin-like growth factor 1 (IGF-1) stabilizes nascent blood vessels. *J Biol Chem*. 2015;290(10):6349-60.
88. Nakao-Hayashi J, Ito H, Kanayasu T, Morita I, Murota S. Stimulatory effects of insulin and insulin-like growth factor I on migration and tube formation by vascular endothelial cells. *Atherosclerosis*. 1992;92:141-9.
89. Grant MB, Mames RN, Fitzgerald C, Ellis EA, Aboufrikha M, Guy J. Insulin-like growth factor I acts as an angiogenic agent in rabbit cornea and retina: comparative studies with basic fibroblast growth factor. *Diabetologia*. 1993;36:282-91.
90. Dallinga MG, Yetkin-Arik B, Kayser RP, Vogels IMC, Nowak-Sliwinska P, Griffioen AW, et al. IGF2 and IGF1R identified as novel tip cell genes in primary microvascular endothelial cell monolayers. *Angiogenesis*. 2018;21:823-36.
91. Dallinga MG, Boas SEM, Klaassen I, Merks RHM, van Noorden CJF, Schlingemann RO. Tip cells in angiogenesis. *eLS*. 2015:1-10.
92. Herr F, Liang OD, Herrero J, Lang U, Preissner KT, Han VK, et al. Possible angiogenic roles of insulin-like growth factor II and its receptors in uterine vascular adaptation to pregnancy. *J Clin Endocrinol Metab*. 2003;88(10):4811-7.
93. Soos MA, Siddle K. Immunological relationships between receptors for insulin and insulin-like growth factor I. *J Biochem*. 1989;263:553-63.
94. Moxham CP, Duronio V, Jacobs S. Insulin-like Growth Factor I Receptor B-Subunit Heterogeneity. *Journal of Biological Chemistry*. 1989;264(22):13238-44.
95. Kasuya J, Benjamin Paz I, Maddux BA, Goldfine ID, Hefta SA, Fujita-Yamaguchi Y. Characterization of Human Placental Insulin-like Growth Factor-I/Insulin Hybrid Receptors by Protein Microsequencing and Purification1. *J Biochem*. 1993(32):13531-6.
96. Efstratiadis A. Genetics of mouse growth. *Int J Dev Biol*. 1998;42(7):955-76.
97. Massoner P, Ladurner-Rennau M, Eder IE, Klocker H. Insulin-like growth factors and insulin control a multifunctional signalling network of significant importance in cancer. *Br J Cancer*. 2010;103(10):1479-84.
98. van Beijnum JR, Pieters W, Nowak-Sliwinska P, Griffioen AW. Insulin-like growth factor axis targeting in cancer and tumour angiogenesis - the missing link. *Biol Rev Camb Philos Soc*. 2016.

99. Guidry C, Feist R, Morris R, Hardwick CW. Changes in IGF Activities in Human Diabetic Vitreous. *diabetes*. 2004;53:2428-35.
100. LeRoith D, Roberts CT. The insulin-like growth factor system and cancer. *Cancer Letters*. 2003;195(2):127-37.
101. Nowak-Sliwinska P, van Beijnum JR, Huijbers EJM, Gasull PC, Mans L, Bex A, et al. Oncofetal insulin receptor isoform A marks the tumour endothelium; an underestimated pathway during tumour angiogenesis and angiostatic treatment. *Br J Cancer*. 2019;120(2):218-28.
102. Correia da Silva G, Bell SC, Pringle JH, Teixeira N. Expression of mRNA Encoding Insulin-Like Growth Factors I and II by Uterine Tissues and Placenta During Pregnancy in the Rat. *Mol Reprod Dev*. 1999;53:294-305.
103. Tollefsen SE, Sadow JL, Rotwein P. Coordinate expression of insulin-like growth factor II and its receptor during muscle differentiation. *proc Natl Acad Sci U S A*. 1989;86:1543-7.
104. Lee CY, Rechler MM. Formation of 150-kDa binary complexes if Insulin-like growth factor binding protein-3 and the acid-labile subunit *in vitro* and *in vivo*. *Prog Growth Factor Res*. 1995;6:241-51.
105. Wang J, Li Y, Deng M, Jiang H., Guo L, Zhou J, et al. Serum insulin-like growth factor-1 and its binding protein 3 as prognostic factors for the incidence, progression, and outcome of hepatocellular carcinoma: a systematic review and metaanalysis. *oncotarget*. 2017;8(46):81098-108.
106. Gao Y, Katki H, Graubard B, Pollak M, Martin M, Tao Y, et al. Serum IGF1, IGF2 and IGFBP3 and risk of advanced colorectal adenoma. *Int J Cancer*. 2012;131(2):E105-13.
107. Greenall SA, Bentley JD, Pearce LA, Scoble JA, Sparrow LG, Bartone NA, et al. Biochemical characterization of individual human glycosylated pro-insulin-like growth factor (IGF)-II and big-IGF-II isoforms associated with cancer. *J Biol Chem*. 2013;288(1):59-68.
108. Espelund U, Gronbaek H, Villadsen GE, Simonsen K, Vestergaard PF, Jorgensen JO, et al. The Circulating IGF System in Hepatocellular Carcinoma: The Impact of Liver Status and Treatment. *Growth Horm IGF Res*. 2015;25(4):174-81.
109. Chang KH, Chan-Ling T, McFarland EL, Afzal A, Pan H, Baxter LC, et al. IGF binding protein-3 regulates hematopoietic stem cell and endothelial precursor cell function during vascular development. *Proc Natl Acad Sci U S A*. 2007;104(25):10595-600.
110. Contois LW, Nugent DP, Caron JM, Cretu A, Tweedie E, Akalu A, et al. Insulin-like growth factor binding protein-4 differentially inhibits growth factor-induced angiogenesis. *J Biol Chem*. 2012;287(3):1779-89.
111. Smith YE, Toomey S, Napoletano S, Kirwan G, Schadow C, Chubb AJ, et al. Recombinant PAPP-A resistant insulin-like growth factor binding protein 4 (dBP4) inhibits angiogenesis and metastasis in a murine model of breast cancer. *BMC Cancer*. 2018;18(1):1016.
112. Ryan AJ, Napoletano S, Fitzpatrick PA, Currid CA, O'Sullivan NC, Harmey JH. Expression of a protease-resistant insulin-like growth factor-binding protein-4 inhibits tumour growth in a murine model of breast cancer. *Br J Cancer*. 2009;101(2):278-86.
113. van der Schaft DWJ, Toebes EAH, Haseman JR, Mayo KH, Griffioen AW. Bactericidal/permeability-increasing protein (BPI) inhibits angiogenesis via induction of apoptosis in vascular endothelial cells. *Blood*. 2000;96(1):176-81.
114. Nowak-Sliwinska P, Alitalo K, Allen E, Anisimov A, Aplin AC, Auerbach R, et al. Consensus guidelines for the use and interpretation of angiogenesis assays. *Angiogenesis*. 2018.
115. van Duinen V, Zhu D, Ramakers C, van Zonneveld AJ, Vulto P, Hankemeier T. Perfused 3D angiogenic sprouting in a high-throughput *in vitro* platform. *Angiogenesis*. 2019;22(1):157-65.
116. Preibisch S, Saalfeld S, Tomancak P. Globally optimal stitching of tiled 3D microscopic image acquisitions. *Bioinformatics*. 2009;25(11):1463-5.
117. Yetkin-Arik B, Vogels IMC, Neyazi N, van Duinen V, Houtkooper RH, van Noorden CJF, et al. Endothelial tip cells *in vitro* are less glycolytic and have a more flexible response to metabolic stress than non-tip cells. *Sci Rep*. 2019;9(1):10414.

118. Cohick WS, Clemmons DR. The insulin-like growth factors *Annu Rev Physiol.* 1993;55:131-53.
119. Conover CA, Bale LK, Overgaard MT, Johnstone EW, Laursen UH, Fuchtbauer EM, et al. Metalloproteinase pregnancy-associated plasma protein A is a critical growth regulatory factor during fetal development. *Development.* 2004;131(5):1187-94.
120. Cohick WS, Clemmons DR. The insulin-like growth factors. *Annu Rev Physiol.* 1993;55:131-53.
121. Ranke MB. Insulin-like growth factor binding-protein-3 (IGFBP-3). *Best Pract Res Clin Endocrinol Metab.* 2015;29(5):701-11.
122. Chao W, D'Amore PA. IGF2: epigenetic regulation and role in development and disease. *Cytokine Growth Factor Rev.* 2008;19(2):111-20.
123. Clemmons DR, Busby W, Clarke JB, Parker A, Duan C, Nam TJ. Modifications of insulin-like growth factor binding proteins and their role in controlling IGF actions. *Endocrine journal.* 1998;45 Suppl:S1-8.
124. De Mellow JSM, Baxter RC. Growth Hormone-dependent insulin-like growth factor (IGF) binding protein both inhibits and potentiates IGF-1 stimulated DNA synthesis in human skin fibroblasts. *Biochem Biophys Res Commun.* 1988;156(1):199-204.
125. Hellstrom A, Perruzzi C, Ju M, Engstrom E, Hard AL, Liu JL, et al. Low IGF-I suppresses VEGF-survival signaling in retinal endothelial cells: direct correlation with clinical retinopathy of prematurity. *Proc Natl Acad Sci U S A.* 2001;98(10):5804-8.
126. Belfiore A, Frasca F, Pandini G, Sciacca L, Vigneri R. Insulin receptor isoforms and insulin receptor/insulin-like growth factor receptor hybrids in physiology and disease. *Endocr Rev.* 2009;30(6):586-623.
127. Ludwig T. Roles for mannose-6-phosphate receptors in lysosomal enzyme sorting, IGF-II binding and clathrin-coat assembly. *TRENDS IN CELL BIOLOGY.* 1995;5:202-6.
128. Cigrovski Berkovic M, Cacev T, Catela Ivkovic T, Marout J, Ulamec M, Zjadic-Rotkvic V, et al. High VEGF serum values are associated with locoregional spread of gastroenteropancreatic neuroendocrine tumors (GEP-NETs). *Mol Cell Endocrinol.* 2016;425:61-8.
129. Hayran Y, Lay I, Mocan MC, Bozduman T, Ersoy-Evans S. Vascular endothelial growth factor gene polymorphisms in patients with rosacea: A case-control study. *Journal of the American Academy of Dermatology.* 2019;81(2):348-54.
130. Ren H, Shao Y, Ma X, Yang M, Liu Y, Wang Q. Expression levels of serum vasohibin-1 and other biomarkers in type 2 diabetes mellitus patients with different urinary albumin to creatinine ratios. *J Diabetes Complications.* 2019;33(7):477-84.
131. Ji Y, Wang Z, Chen H, Zhang L, Zhuo F, Yang Q. Serum from Chronic Hepatitis B Patients Promotes Growth and Proliferation via the IGF-II/IGF-IR/MEK/ERK Signaling Pathway in Hepatocellular Carcinoma Cells. *Cell Physiol Biochem.* 2018;47(1):39-53.
132. Kubasiak JC, Seder CW, Pithadia R, Basu S, Fhied C, Phillips WW, et al. Value of circulating insulin-like growth factor-associated proteins for the detection of stage I non-small cell lung cancer. *J Thorac Cardiovasc Surg.* 2015;149(3):727-34 e1-3; discussion 34.
133. Kalledsoe L, Dragsted LO, Hansen L, Kyro C, Gronbaek H, Tjonneland A, et al. The insulin-like growth factor family and breast cancer prognosis: A prospective cohort study among postmenopausal women in Denmark. *Growth Horm IGF Res.* 2019;44:33-42.
134. Dallinga MG, Habani YI, Kayser RP, Van Noorden CJF, Klaassen I, Schlingemann RO. IGF-binding proteins 3 and 4 are regulators of sprouting angiogenesis. *Mol Biol Rep.* 2020;47:2561-72.
135. Yetkin-Arik B, Vogels IMC, Nowak-Sliwinska P, Weiss A, Houtkooper RH, Van Noorden CJF, et al. The role of glycolysis and mitochondrial respiration in the formation and functioning of endothelial tip cells during angiogenesis. *Sci Rep.* 2019;9(1):12608.
136. Lobov IB, Renard RA, Papadopoulos N, Gale NW, Thurston G, Yancopoulos GD, et al. Delta-like ligand 4 (Dll4) is induced by VEGF as a negative regulator of angiogenic sprouting. *Proc Natl Acad Sci U S A.* 2007;104(9):3219-24.

137. Mazzone M, Dettori D, Leite de Oliveira R, Loges S, Schmidt T, Jonckx B, et al. Heterozygous deficiency of PHD2 restores tumor oxygenation and inhibits metastasis via endothelial normalization. *Cell*. 2009;136(5):839-51.
138. Jakobsson L, Bentley K, Gerhardt H. VEGFRs and Notch: a dynamic collaboration in vascular patterning. *Biochem Soc Trans*. 2009;37(Pt 6):1233-6.
139. Bach LA. IGF-binding proteins. *J Mol Endocrinol*. 2018;61(1):T11-T28.
140. Slater T, Haywood NJ, Matthews C, Cheema H, Wheatcroft SB. Insulin-like growth factor binding proteins and angiogenesis: from cancer to cardiovascular disease. *Cytokine Growth Factor Rev*. 2019;46:28-35.
141. Stewart CEH, Rotwein P. Growth, differentiation and survival: multiple physiological functions for insulin-like growth factors. *physiological reviews*. 1996;76(4).
142. Rinderknecht E, Humbel RE. Amino-terminal sequences of two polypeptides from human serum with nonsuppressible insulin-like and cell-growth-promoting activities: evidens for structural homology with insulin B chain. *P Natl Acad Sci USA*. 1976;73(12):4379-83.
143. Zapf J, Futo E, Peter M, Froesch ER. Can "Big"insuling-like growth factor II in serum of tumore patients account for the development of extrapancreatic tumor hypoglycemia? *J Clin Invest*. 1992;90:2574-84.
144. Firth SM, Baxter RC. Cellular actions of the insulin-like growth factor binding proteins. *Endocr Rev*. 2002;23(6):824-54.
145. McAvoy JW, Chamberlain G. Growth factors in the eye. *Prog Growth Factor Res*. 1990;2:29-43.
146. Smith LE. Essential Role of Growth Hormone in Ischemia-Induced Retinal Neovascularization. *Science*. 1997;276(5319):1706-9.
147. Klaassen I, de Vries EW, Vogels IMC, van Kampen AHC, Bosscha MI, Steel DHW, et al. Identification of proteins associated with clinical and pathological features of proliferative diabetic retinopathy in vitreous and fibrovascular membranes. *PLoS One*. 2017;12(11):e0187304.
148. Spranger J, Buhnen J, Jansen V, Krieg M, Meyer-Schwickerath R, Blum WF, et al. Systemic levels contribute significantly to increased intraocular IGF-I, IGF-II and IGF-BP3 [correction of IFG-BP3] in proliferative diabetic retinopathy. *Hormone and metabolic research = Hormon- und Stoffwechselforschung = Hormones et metabolisme*. 2000;32(5):196-200.
149. Kim JH, Park SW, Yu YS, Kim KW, Kim JH. Hypoxia-induced insulin-like growth factor II contributes to retinal vascularization in ocular development. *Biochimie*. 2012;94(3):734-40.
150. Lambooi A, van Wely KHM, Lindenbergh-Kortleve DJ, Kuijpers RWAM, Mike Kliffen M, Mooy CM. Insulin-like Growth Factor-I and its Receptor in Neovascular Age-Related Macular Degeneration. *Investigative Ophthalmology and visual science*. 2003;44(5):2192-8.
151. Ocrant I, Fay CT, Permelee J. Expression of Insulin and Insulin-like growth factor receptors and binding proteins by retinal pigment epithelium. *exp eye res*. 1991;52:581-9.
152. Eggenschwiler J, Ludwig T, Fisher P, Leighton PA, Tilghman SM, Efstratiadis A. Mouse mutant embryos overexpressing IGF-II exhibit phenotypic features of the Beckwith-Wiedemann and Simpson-Golabi-Behmel syndromes. *Genes & Development*. 1997;11(23):3128-42.
153. Weksberg R, Shuman C, Beckwith JB. Beckwith-Wiedemann syndrome. *Eur J Hum Genet*. 2010;18(1):8-14.
154. Ozluk Y, Kilicaslan I, Gulluoglu MG, Ayan I, Uysal V. The prognostic significance of angiogenesis and the effect of vascular endothelial growth factor on angiogenic process in Wilms' tumour. *Pathology*. 2006;38(5):408-14.
155. Van Geest RJ, Lesnik-Oberstein SY, Tan HS, Mura M, Goldschmeding R, Van Noorden CJ, et al. A shift in the balance of vascular endothelial growth factor and connective tissue growth factor by bevacizumab causes the angiofibrotic switch in proliferative diabetic retinopathy. *Br J Ophthalmol*. 2012;96(4):587-90.
156. Klaassen I, van Geest RJ, Kuiper EJ, van Noorden CJ, Schlingemann RO. The role of CTGF in diabetic retinopathy. *Exp Eye Res*. 2015;133:37-48.

157. Granata R, Trovato L, Lupia E, Sala G, Settanni F, Camussi G, et al. Insulin-like growth factor binding protein-3 induces angiogenesis through IGF-I- and SphK1-dependent mechanisms. *Journal of thrombosis and haemostasis : JTH*. 2007;5(4):835-45.
158. Gealekman O, Gurav K, Chouinard M, Straubhaar J, Thompson M, Malkani S, et al. Control of adipose tissue expandability in response to high fat diet by the insulin-like growth factor-binding protein-4. *J Biol Chem*. 2014;289(26):18327-38.
159. Hasan SS, Siekmann AF. The same but different: signaling pathways in control of endothelial cell migration. *Curr Opin Cell Biol*. 2015;36:86-92.
160. Garrett TA, van Buul JD, Burrigide K. VEGF-induced Rac1 activation in endothelial cells is regulated by the guanine nucleotide exchange factor Vav2. *Exp Cell Res*. 2007;313(15).
161. Lamalice L, Houle F, Jourdan G, Huot J. Phosphorylation of tyrosine 1214 on VEGFR2 is required for VEGF-induced activation of Cdc42 upstream of SAPK2/p38. *Oncogene*. 2004;23(2):434-45.
162. Taya S, Inagaki N, Sengiku H, Makino H, Iwamatsu A, Urakawa I, et al. Direct interaction of insulin-like growth factor-1 receptor with leukemia-associated RhoGEF. *J Cell Biol*. 2001;155(5):809-20.
163. Shields SK, Nicola C, Chakraborty C. Rho guanosine 5'-triphosphatases differentially regulate insulin-like growth factor I (IGF-I) receptor-dependent and -independent actions of IGF-II on human trophoblast migration. *Endocrinology*. 2007;148(10):4906-17.
164. Vega R, Carretero M, Travasso RDM, Bonilla LL. Notch signaling and taxis mechanisms regulate early stage angiogenesis: A mathematical and computational model. *PLoS Comput Biol*. 2020;16(1):e1006919.
165. Krebs LT, Shutter JR, Tanigaki K, Honjo T, Stark KL, Gridley T. Haploinsufficient lethality and formation of arteriovenous malformations in Notch pathway mutants. *Genes Dev*. 2004;18(20):2469-73.
166. Gale NW, Dominguez MG, Noguera I, Pan L, Hughes V, Valenzuela DM, et al. Haploinsufficiency of delta-like 4 ligand results in embryonic lethality due to major defects in arterial and vascular development. *Proc Natl Acad Sci U S A*. 2004;101(45):15949-54.
167. Noguera-Troise I, Daly C, Papadopoulos NJ, Coetsee S, Boland P, Gale NW, et al. Blockade of Dll4 inhibits tumour growth by promoting non-productive angiogenesis. *Nature*. 2006;444(7122):1032-7.
168. Ridgway J, Zhang G, Wu Y, Stawicki S, Liang WC, Chantery Y, et al. Inhibition of Dll4 signalling inhibits tumour growth by deregulating angiogenesis. *Nature*. 2006;444(7122):1083-7.
169. Foltz DR, Santiago MC, Berechid BE, Nye JE. Glycogen Synthase Kinase-3 Modulates Notch Signaling and Stability. *Curr Biol*. 2002;12:1006-11.
170. Hamamura K, Zhang P, Yokota H. IGF2-driven PI3 kinase and TGFbeta signaling pathways in chondrogenesis. *Cell Biol Int*. 2008;32(10):1238-46.
171. Tammela T, Zarkada G, Wallgard E, Murtomaki A, Suchting S, Wirzenius M, et al. Blocking VEGFR-3 suppresses angiogenic sprouting and vascular network formation. *Nature*. 2008;454(7204):656-60.
172. Miele C, Rochford JJ, Filippa N, Giorgetti-Peraldi S, Van Obberghen E. Insulin and insulin-like growth factor-I induce vascular endothelial growth factor mRNA expression via different signaling pathways. *J Biol Chem*. 2000;275(28):21695-702.
173. Kwon YW, Kwon KS, Moon HE, Park JA, Choi KS, Kim YS, et al. Insulin-Like Growth Factor-II Regulates the Expression of Vascular Endothelial Growth Factor by the Human Keratinocyte Cell Line HaCaT. *J Invest Dermatol*. 2004;123:152-8.
174. Lee SR, Kim SH, Chae HD, Kim CH, Kang BM. Influence of vascular endothelial growth factor on the expression of insulin-like growth factor-II, insulin-like growth factor binding protein-2 and 5 in human luteinized granulosa cells. *Gynecol Endocrinol*. 2012;28(11):917-20.
175. Moreno MJ, Ball M, Andrade MF, McDermid A, Stanimirovic DB. Insulin-like growth factor binding protein-4 (IGFBP-4) is a novel anti-angiogenic and anti-tumorigenic mediator secreted by dibutyl cyclic AMP (dB-cAMP)-differentiated glioblastoma cells. *Glia*. 2006;53(8):845-57.
176. Franklin SL, Ferry RJ, Jr., Cohen P. Rapid insulin-like growth factor (IGF)-independent effects of IGF binding protein-3 on endothelial cell survival. *J Clin Endocrinol Metab*. 2003;88(2):900-7.

177. Salani B, Ravera S, Amaro A, Salis A, Passalacqua M, Millo E, et al. IGF1 regulates PKM2 function through Akt phosphorylation. *Cell Cycle*. 2015;14(10):1559-67.
178. Gomez-Escudero J, Clemente C, Garcia-Weber D, Acin-Perez R, Millan J, Enriquez JA, et al. PKM2 regulates endothelial cell junction dynamics and angiogenesis via ATP production. *Sci Rep*. 2019;9(1):15022.
179. Sengupta A, Kalinichenko VV, Yutzey KE. FoxO1 and FoxM1 transcription factors have antagonistic functions in neonatal cardiomyocyte cell-cycle withdrawal and IGF1 gene regulation. *Circ Res*. 2013;112(2):267-77.
180. Wilhelm K, Happel K, Eelen G, Schoors S, Oellerich MF, Lim R, et al. FOXO1 couples metabolic activity and growth state in the vascular endothelium. *Nature*. 2016;529(7585):216-20.
181. Oellerich MF, Potente M. FOXOs and sirtuins in vascular growth, maintenance, and aging. *Circ Res*. 2012;110(9):1238-51.
182. Gross DN, van den Heuvel AP, Birnbaum MJ. The role of FoxO in the regulation of metabolism. *Oncogene*. 2008;27(16):2320-36.
183. Evans-Anderson HJ, Alfieri CM, Yutzey KE. Regulation of cardiomyocyte proliferation and myocardial growth during development by FOXO transcription factors. *Circ Res*. 2008;102(6):686-94.
184. Mu X, Qi W, Liu Y, Zhou J, Li Y, Rong X, et al. IGF-II-mediated downregulation of peroxisome proliferator-activated receptor-gamma coactivator-1alpha in myoblast cells involves PI3K/Akt/FoxO1 signaling pathway. *Mol Cell Biochem*. 2017;432(1-2):199-208.
185. Samakova A, Gazova A, Sabova N, Valaskova S, Jurikova M, Kyselovic J. The PI3k/Akt pathway is associated with angiogenesis, oxidative stress and survival of mesenchymal stem cells in pathophysiologic condition in ischemia. *Physiol Res*. 2019;68(Suppl 2):S131-S8.
186. Wu W, Zhou G, Han H, Huang X, Jiang H, Mukai S, et al. PI3Kdelta as a Novel Therapeutic Target in Pathological Angiogenesis. *Diabetes*. 2020;69(4):736-48.
187. Angulo-Urarte A, Casado P, Castillo SD, Kobialka P, Kotini MP, Figueiredo AM, et al. Endothelial cell rearrangements during vascular patterning require PI3-kinase-mediated inhibition of actomyosin contractility. *Nat Commun*. 2018;9(1):4826.
188. Soler A, Angulo-Urarte A, Graupera M. PI3K at the crossroads of tumor angiogenesis signaling pathways. *Mol Cell Oncol*. 2015;2(2):e975624.
189. Michaelis UR. Mechanisms of endothelial cell migration. *Cell Mol Life Sci*. 2014;71(21):4131-48.
190. Espinosa L, Ingles-Esteve J, Aguilera C, Bigas A. Phosphorylation by glycogen synthase kinase-3 beta down-regulates Notch activity, a link for Notch and Wnt pathways. *J Biol Chem*. 2003;278(34):32227-35.



**EFFECTS OF ANGIOGENESIS INHIBITORS ON
ENDOTHELIAL TIP CELLS *IN VITRO***



Andrea Weiss, MSc^{1,2},
Xianting Ding, PhD³,
Judy R. van Beijnum, PhD²,
leong Wong PhD⁴,
Tse J. Wong²,
Robert H. Berndsen^{1,2},
Olivier Dormond MD, PhD⁵,
Marchien Dallinga, MD⁶,

Li Shen, PhD⁷,
Reinier O. Schlingemann, MD, PhD⁶,
Roberto Pili, MD, PhD⁷,
Chih-Ming Ho, PhD⁴,
Paul J. Dyson, PhD¹,
Hubert van den Bergh, PhD¹,
Arjan W. Griffioen, PhD^{2*},
Patrycja Nowak-Sliwinska, PhD, DSc^{1,2}

¹ Institute of Chemical Sciences and Engineering, Swiss Federal Institute of Technology, 1015, Lausanne, Switzerland.

² Department of Medical Oncology, VU University Medical Center, 1007 MB, Amsterdam, The Netherlands.

³ Med-X Research Institute, School of Biomedical Engineering, Shanghai Jiao Tong University, 200030, Shanghai, China.

⁴ Department of Mechanical and Aerospace Engineering, University of California, 90095, Los Angeles, CA, USA.

⁵ Department of Visceral Surgery, Centre Hospitalier Universitaire Vaudois, 1011, Lausanne, Switzerland.

⁶ Ocular Angiogenesis Group, Departments of Ophthalmology and Cell Biology and Histology, Academic Medical Center, 1100 DD, Amsterdam, The Netherlands.

⁷ Department of Medicine, Roswell Park Cancer Institute, 14263, Buffalo, NY, USA.



**RAPID OPTIMIZATION OF DRUG
COMBINATIONS FOR THE OPTIMAL
ANGIOSTATIC TREATMENT OF CANCER**

INTRODUCTION

Anti-angiogenic therapies are routinely used in the treatment of various cancers (1-3). Their contribution to the prolongation of patient survival, however, is often limited mainly due to disease and patient heterogeneity (4, 5), toxicity (6), induction of metastasis (7) and drug resistance (8). Redundancy of growth factor signaling pathways makes angiogenesis a robust physiological function (9, 10), where targeting multiple pathways with drug combinations may be necessary for efficient therapy. Combination strategies may thus lead to enhanced efficacy (11, 12) with limited side effects (13) and reduced probability of developing drug resistance (14, 15).

Combinations of anti-angiogenic drugs have often resulted in significant clinical toxicity (16), even when designed to target complementary pathways (17). This is because drugs to be combined are frequently selected based on their success as single agents (18) and tend to be used in combination at their maximum tolerated single agent doses, thus increasing the risk of toxicity and resistance (19). When trying to identify an optimal combination starting from, for instance 10 drugs at 5 doses, one will have to test nearly 10 million (5^{10}) combinations. To overcome this challenge, we employed a feedback system control (FSC) technique to rapidly identify the most powerful drug combinations with minimal experimental effort (20) (Supplementary Methods). In combination with the differential evolution (DE) algorithm (21) an iterative approach of experimental testing in an endothelial cell viability assay and mathematical analysis (a process of selection, where only the permutations which improve the system's response are maintained), drove the system to converge towards an optimal solution, i.e. maximal inhibition of endothelial cell growth. Although others have tried to optimize drug combinations (22-25), see Supplementary Methods, the advantage of our approach is that FSC is phenotypically driven, i.e. no mechanistic information is required in order to rapidly identify experimentally verifiable optimal drug combinations (20).

The aim of the present study was to find an optimal low-dose, synergistic anti-angiogenic drug combination using the FSC technology, and to validate this drug combination in preclinical tumor models. The FSC technique, together with a second-order linear regression model to allow for elimination of less effective drugs, resulted in the optimal low-dose combination containing erlotinib (EGFR inhibitor (26)), RAPTA-C (histone inactivator (27)), and BEZ-235 (a dual PI3K/mTOR inhibitor (28)). This final drug combination synergistically inhibited ECRF24 viability, while having minimal effects on non-endothelial cell types. We successfully translated this *in vitro* optimized drug combination to inhibit tumor growth in two preclinical tumor models.

MATERIALS AND METHODS

Cell viability, migration, and apoptosis assay.

Cell viability and migration assays were performed as previously described. Cells were seeded in a 96-well culture plate at a density of $2.5-10 \times 10^3$ cells/well. Cells were

incubated with drugs for 72 h (for drug acquisition and cells and culture conditions, see Supplementary Methods). Drugs were premixed in culture medium and applied at the doses provided in Table 1. Cell viability was assessed using the CellTiter-Glo luminescence assay (Promega, Madison, WI, USA). For migration assays ECRF24 and 786-O were seeded in 96-well cell culture plates (3×10^4 cells/well) 24 h prior to making the scratch (Peira Scientific Instruments, Beerse, Belgium). Drugs were premixed in culture medium and applied at doses indicated in Supplementary Fig. S2A. Images were automatically captured on a Leica DMI3000 microscope (Leica, Rijswijk, Netherlands) at 5x magnification with Universal Grab 6.3 software (DCILabs, Keerbergen, Belgium). Scratch sizes were determined at $t=0h$ and $t=7h$ using Scratch Assay 6.2 (DCILabs), and values reported represented the absolute closure of the scratch (initial subtracting the final scratch area). Apoptosis was measured after drug exposure, trypsinization and incubation with propidium iodide (PI, 20 $\mu g/ml$) in DNA extraction buffer (29), by flow cytometry. Tip cells were flow cytometrically quantified by CD34 (30) staining and morphology was studied *in vivo* using the CAM assay (31) (see Supplementary Methods).

The Feedback System Control (FSC) technique and data modeling

The feedback system control (FSC) technique was employed as previously described (32, 33). FSC was implemented using the differential evolution (DE) algorithm (34) and two separate optimizations were performed with the cellular outputs of ECRF24 cell viability (proliferation) and migration assays. Nineteen drug combinations were tested per iteration and 10 iterations were performed in each optimization until a plateau in the best output value was reached. For dilutions and culture conditions see Supplementary Methods.

Table 1. Drug dose values used in the *in vitro* cell viability assays.

	Drug	Dose(μM)		
		3 (ED_{10}) ^a	2 (ED_5) ^b	1 (ED_0) ^c
1.	anginex	1.80 ^d	0.76	0.13
2.	bevacizumab	15.00	10.00	1.00
3.	axitinib	1.00	0.30	0.01
4.	erlotinib	2.00	0.50	0.10
5.	anti-HMGB1 Ab	0.17	0.09	0.02
6.	sunitinib	0.50	0.10	0.05
7.	anti-vimentin Ab	0.26	0.17	0.09
8.	RAPTA-C	5.00	1.00	0.05
9.	BEZ-235	0.005	0.001	0.0005

^a dose 3, representing ED_{10} , is the dose where 10% of the maximal response was observed.

^b dose 2, representing ED_5 is the dose where 5% of the maximal response was observed.

^c dose 1, representing ED_0 , is the dose representing half the maximal concentration where no effect was observed.

^d concentrations throughout the table are in μM .

The cells were incubated in 50 μ l of each combination for 72h in the viability assay or for 7h in the migration assay.

Second-order linear regression models were generated using the data obtained from each optimization. Data were modeled using real concentration values and both concentration values and cell viability output data were transformed using the z-score function in Matlab. For detailed description see Supplementary Methods.

Human ovarian carcinoma grown on the chicken chorioallantoic membrane (CAM)

Human ovarian carcinoma tumors were implanted on the CAM as previously described (35). On embryo development day (EDD) 7, 1×10^6 A2780 carcinoma cells were prepared as a spheroid in a 25 μ l hanging drop and were transplanted onto the CAM surface 3 h after preparation. Treatment began 3 days after tumor implantation (EDD10) when vascularized tumors were visible. Drug combinations were freshly prepared and administered as a 20 μ l intravenous injection. Treatment was performed twice and tumor growth was monitored and measured daily, (volume = width² x length x 0.52).

3.1

Colorectal carcinoma xenograft model

Female Swiss nu/nu mice ages 6-8 weeks were obtained from Charles River (weight 20-30 grams). Mice were inoculated in the right flank with 100 μ l DMEM with 1 million LS174T cells. LS174T cells were obtained from ECACC, Salisbury, UK where (authentication by STR PCR) and were used within 6 months of resuscitation. Palpable tumors were present within 3-5 days, at which time treatment was initiated. Mice were treated daily by oral gavage and i.p. injection as indicated (Table 2), and were monitored daily for tumor size and body weight (see Supplementary Methods).

Immunohistochemistry

CD31 stainings (SZ31, Dianova, Hamburg, Germany) were performed using donkey anti-rat biotinylated secondary antibodies (Jackson, Suffolk, UK) and streptavidin-HRP (Dako, Glostrup, Denmark), and visualized by 3,3'-diaminobenzidine (DAB, see Supplementary Methods).

Statistical analysis

Values are given as mean values \pm standard deviation. Statistical analysis was performed using a two-sided student's t-test and the two-way ANOVA assay. * $p < 0.05$, and ** $p < 0.01$ were considered statistically significant.

RESULTS

Selection of drug combinations by the FSC technique.

Nine drugs targeting a broad spectrum of endothelial cell signaling pathways (Supplementary Fig. S1; Supplementary Methods) were selected for FSC-based screening

Table 2. Drug dose values used for *in vivo* assays.

Treatment ^b	Compounds ^a				% CTRL ± SEM ^c
	3 (axitinib)	4 (erlotinib)	8 (RAPTA-C)	9 (BEZ-235)	
CAM (µg/kg)					
I	0	29	615	0.04	41±9.0
II	0	29	307	0.04	51±14
VI	0	2.9	307	0.04	32±4.0
VII	18	29	230	0.02	13±6.0
VIII	0	29	307	0	47±14
Mice (mg/kg)					
VI	0	15	40	10	24±14
VIII	0	5	40	0	84±16
4 ₁	0	5	0	0	102±25
4 ₂	0	15	0	0	94±34
4 _{opt}	0	50	0	0	29±9.0
8 ₂	0	0	40	0	90±17
8 _{opt}	0	0	100	0	58±9.0
9 ₄	0	0	0	10	77±12
9 _{opt}	0	0	0	30	33±14

^a Corresponding dose of each compound for single drug and combination therapy. Compounds are represented as numbers 3, 4, 8 or 9, representing axitinib, erlotinib, RAPTA-C or BEZ-235, respectively. Drug doses are provided in µg/kg for the CAM model and mg/kg in the mouse model.

^b Administered treatment, either a single drug represented by the drug number (3, 4, 8, 9) and the dosage level indicated as a subscript, or drug combinations represented by the letters I-VIII.

^c The respective tumor growth inhibition efficacy represented as a percentage of the control (±SEM).

(Fig. 1A): anginex (1), bevacizumab (2), axitinib (3), erlotinib (4), anti-HMGB1 Ab (5), sunitinib (6), anti-vimentin Ab (7), RAPTA-C (8), BEZ-235 (9). Single drug dose-response curves were generated for both cell viability (example for sunitinib provided, Fig. 1B) and migration, using *in vitro* bioassays (Supplementary Fig.S 2A). The optimization was carried out with each compound at four low doses. The highest concentration, dose 3 or ED₁₀, was the dose where 10% of the maximal response was observed, dose 2 or ED₅, where 5% of the maximal response was observed, dose 1 or ED₀, represented half the maximal dose where no effect was observed, and dose 0, where no drug was present (Table 1). The boxplot in Fig. 1C provides the median and interquartile ranges of the output results by the drug combinations identified by the end of each iterative cycle of the FSC optimization. After 10 iterations of 19 drug mixtures, the optimization goal was reached, i.e. no further improvement of the lowest output efficacy could be achieved, indicating that the maximum activity (approx. 70% inhibition) had been reached.

The data obtained were used to build a second-order stepwise linear regression model (36) (Supplementary Methods) to determine the relative importance of the individual

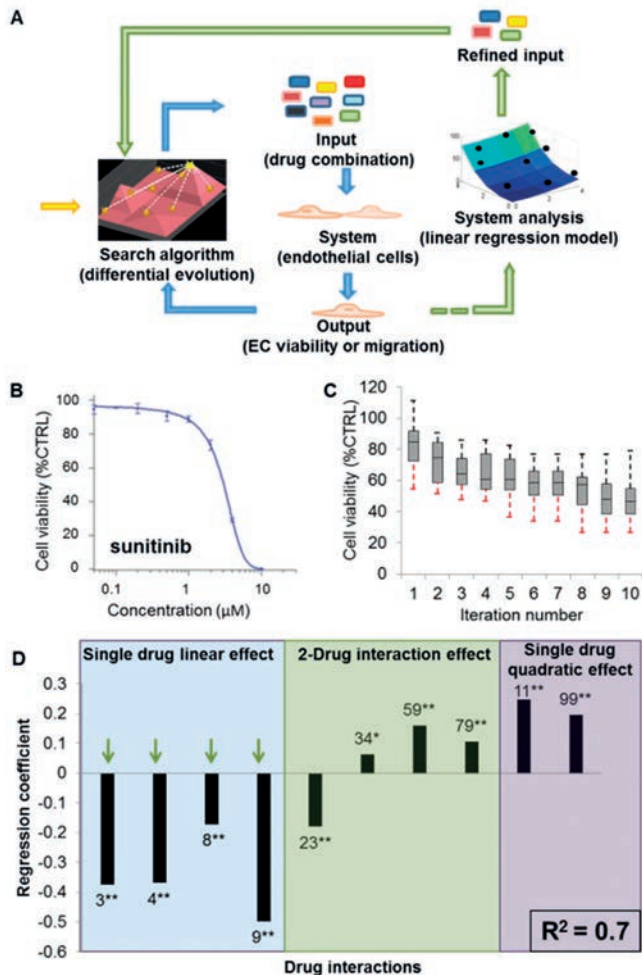


Figure 1. Optimization of the inhibition of endothelial cell viability. (A) Schematic diagram of the FSC technique loop (blue arrow loop) and modeling (green arrow loop) used for *in vitro* drug optimization. FSC starts with randomly selected drug combinations (yellow arrow) and implements an algorithm guided closed-loop feedback search to iteratively optimize the results of an *in vitro* cell assay (blue arrows). Once a plateau in the output is reached, the data obtained from the optimization is used to model the system, analyze drug interactions and eliminate certain drugs (green arrows). Using a refined set of drugs, the drug combination is again optimized with FSC (blue arrows). (B) Dose-response curve of sunitinib for cell viability bioassay. (C) Output results (*in vitro* EC viability, represented as a percentage of the control) for the 10 iterations of the FSC optimization performed. Box plots provide median and interquartile ranges of the cell response to the 19 best drug combinations identified by the end of each iterative cycle of the FSC optimization. Dotted lines, representing maximum and minimum (red) output values, showed no improvement of the best-optimized combination over iterations 8-10. (D) Regression coefficients obtained from the stepwise linear regression model generated with the data obtained from the optimization described above. The coefficient of determination (R^2) is provided in the bottom right of the graph. Green arrows indicate single drug contributions which significantly inhibit EC viability. *indicates p-value < 0.05 and ** indicates p-value < 0.01.

drugs. This model generated regression coefficients (Fig. 1D) corresponding to single drug linear effects (left panel), two-drug pair-wise interaction effects (middle panel), and single drug quadratic effects (right panel). Compounds with the largest negative regression coefficients, i.e. axitinib, erlotinib, RAPTA-C and BEZ-235, inhibited ECRF24 viability most effectively (Fig. 1D, green arrows).

In a parallel approach, we also investigated the best drug combinations for ECRF24 migration inhibition. Even though single drugs generally showed a stronger response in the cell migration assay (Supplementary Fig. S2A), the process of migration was less affected, reaching a maximum effect of 40% inhibition (Supplementary Fig. S3B). The optimization of EC migration inhibition was not further pursued. Yet, regression analysis also revealed the strongest single drug linear and quadratic contributions for erlotinib, RAPTA-C and BEZ-235.

Refined search leads to further optimized synergistic drug combinations.

Subsequently, a second FSC-based optimization was performed with the above-selected compounds, i.e. axitinib (**3**), erlotinib (**4**), RAPTA-C (**8**) and BEZ-235 (**9**), each now considered at five drug doses with a maximum activity of 25% at the highest dose (Fig. 2A; single drug effects in Supplementary Fig. S3). The strongest synergistic activity (i.e. combination index (CI) <1) was observed for combinations containing **4+8+9** (combinations labeled I, II, IV, V, VI, Fig. 2A (remaining results in Supplementary Fig. S4) or only **4+8** (labeled VIII). Two of the effective combinations identified, III and VII, showed antagonism (CI>1), and both contained axitinib (**3**).

Linear regression modeling of data showed the single drug linear contributions of all compounds, as well as the single drug quadratic effect of **4**, to be significant (Fig. 2B, green arrows). Response surfaces (Fig. 2C) provide a visual representation of the relationship between the system output (EC viability) and the varying dose of only two drugs in the combination. Interestingly, surfaces containing **3** (bottom row) show that **3** does not enhance the combination efficacy (red). Note that the response surfaces are rather smooth, indicating that moderate changes in the doses of single drugs near the optimal output in the range of experimental conditions investigated do not result in significant output changes.

Selected optimized drug combinations exhibit enhanced endothelial cell specificity.

The optimized drug combinations I-VIII (Fig. 2A) and corresponding single drugs were tested for viability of different cell types and shown in comparison to ECRF24 (Fig. 3A and Supplementary Fig. S5). The activity in ECRF24 was confirmed in primary ECs (HUVEC, Fig. 3A), and was much stronger than that of non-malignant cell types (HDFa and PBMC) and tumor cells, indicating an enhanced EC specificity. Combinations I-VIII only modestly

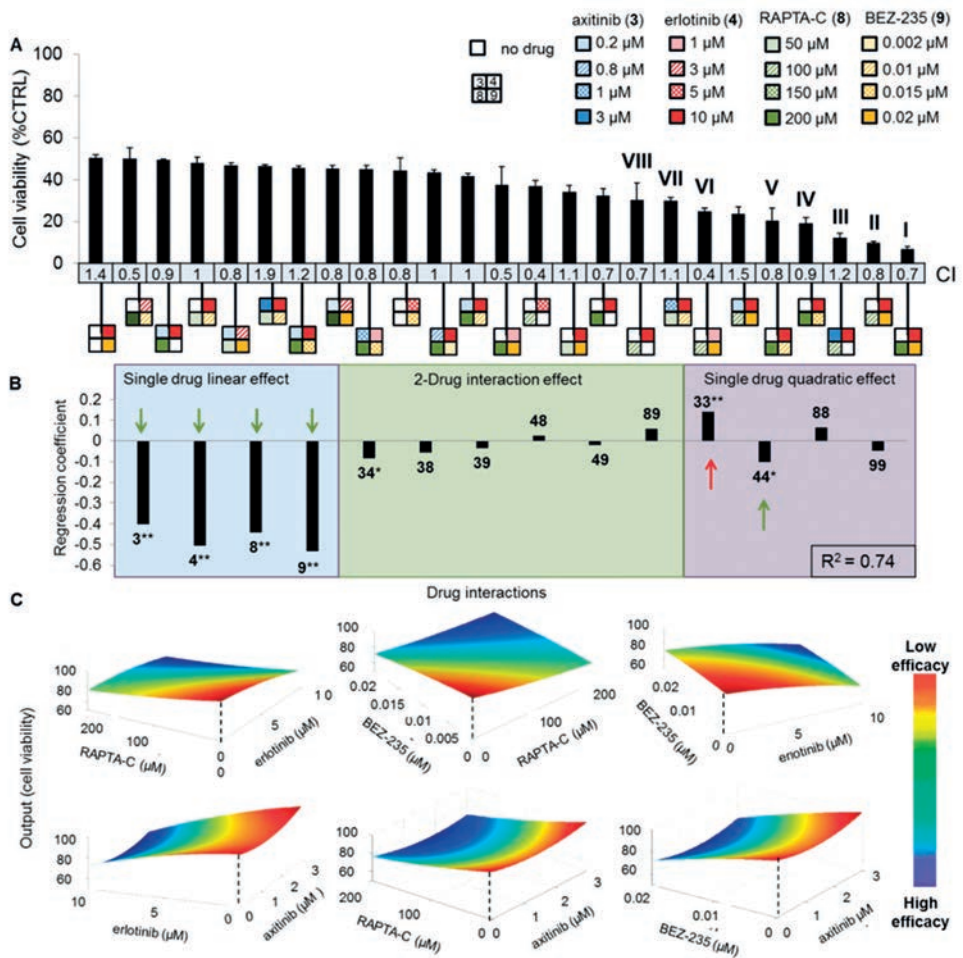
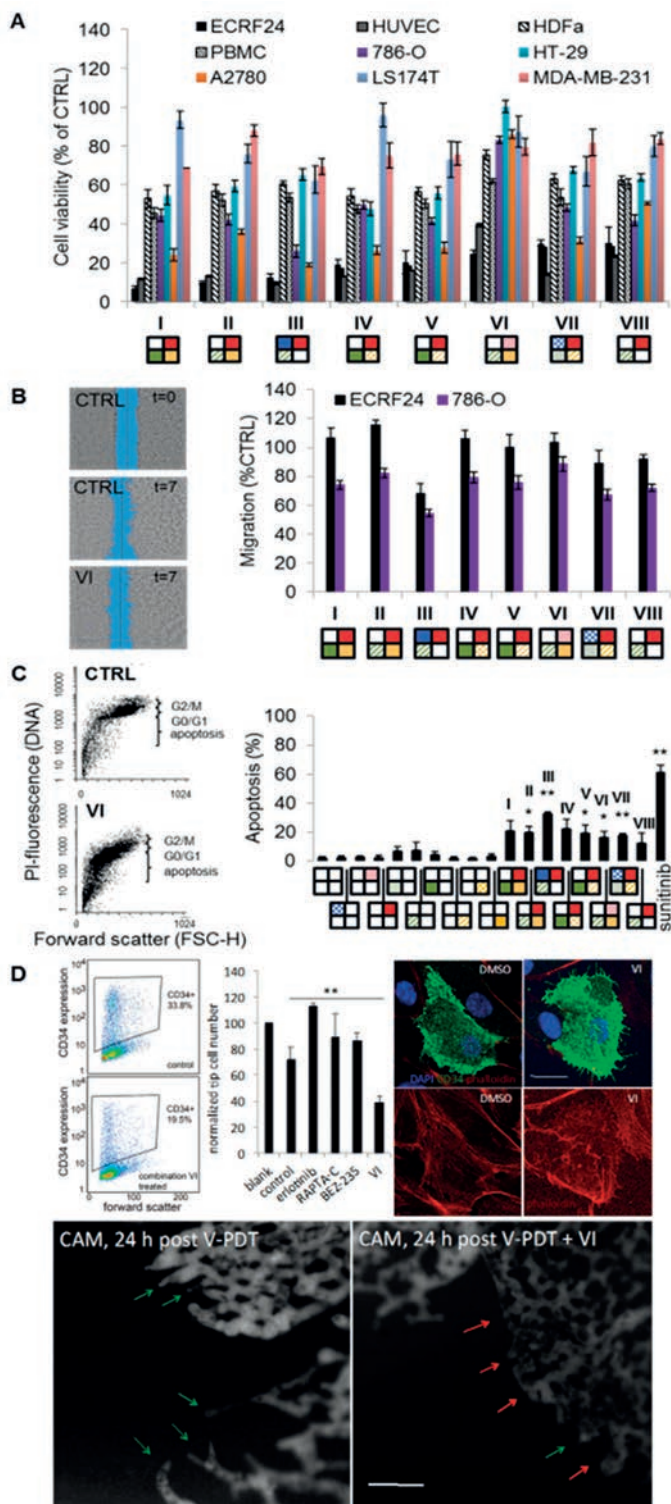


Figure 2. Identification of the optimal four-drug combinations for the inhibition of ECRF24 viability. (A) Efficacy of the best combinations identified to inhibit ECRF24 viability, using the concentrations of each drug presented in the legend at the top right. Best performing combinations resulting in 50% or more inhibition are shown, with their corresponding combination index (CI) values calculated using CompuSYN®, indicating synergistic (CI<1), additive (CI=1) or antagonistic (CI>1) interactions. The square icons present the specific combinations, where each position in the square and color corresponds to a specific drug (i.e. axitinib (3) in blue, erlotinib (4) in red, RAPTA-C (8) in green, and BEZ-235 (3) in yellow) and the concentrations (in μM) of each compound are represented by the different patterns. The most promising combinations, labeled I-VIII, represent a mean of at least 2 independent experiments, with 3 replications each, and error bars represent the SEM. (B) Regression coefficients for the second-order linear regression model generated based on the data from the optimization of the refined four-drug combination. The green arrows indicate significant regression terms which inhibit cell viability while the red arrow indicates terms which stimulates cell activity. (C) Response surfaces show the effect on the system output of varying the concentration of two drugs, while the concentration of the other two drugs remains fixed. Note the smoothness of the curves, indicating that moderate changes in the dosing of a single drug do not result in major output differences. * indicates significance p-value < 0.05 and ** p-value < 0.01.



affected cell motility (Fig. 3B). Several combinations (II, III, V, VI, VII) induced apoptosis in 20-30% of ECRF24 cells (Fig. 3C). Interestingly, optimal combination VI reduced the number of CD34⁺ tip cells *in vitro* (30), as well as the number of tip cells in an *in vivo* angiogenesis model (31) (Fig. 3D)

Successful translation of optimal drug combinations into *vivo* cancer models.

A2780 tumors, transplanted on the chorioallantoic membrane of the chicken embryo, were treated with combinations I, II, VI, VII and VIII. Doses (subsequently identified by a subscript) were translated to this model maintaining the drug dose ratios and taking into account the single drug efficacy in this model (Table 2, Supplementary Methods). Drug combination VII (3₃+4₄+8₁+9₂) synergistically (CI=0.66) inhibited tumor growth by 87% (*p<0.03, Fig. 4A). Based on results in Fig. 3a this activity could be due to the dual action on both ECRF24 and A2780 cells. Combination VI (4₁+8₂+9₄) synergistically inhibited tumor growth by 68% (Fig. 4A and 4C, **p<0.002, CI=0.34) through mainly anti-angiogenic activity (compare Fig. 3A). Of note, none of these doses inhibited tumor growth significantly when applied individually (Fig. 4B). As group VII experienced weight loss (Fig. 4D, **p<0.004), it was not further examined. Microvessel density (MVD) assessment (Fig. 4E) revealed that control tumors were well vascularized. MVD was

◀ **Figure 3.** Validation of the best drug combinations. The effects of the most promising drug combinations (I-VIII from Fig. 2) were tested on the viability of the following non-malignant and cancerous cell lines: primary EC (HUVEC), adult human dermal fibroblasts (HDFa), human *peripheral blood mononuclear cells* (PBMCs), and five human tumor cell lines, i.e. A2780 ovarian adenocarcinoma, 786-O renal cell carcinoma, MDA-MB-231 breast adenocarcinoma and LS174T and HT-29 colorectal carcinomas and (A) on the migration of ECRF24 and 786-O cells. Images on the left show an example of migration assay, where a scratch is made in a cell monolayer at t=0 and the relative closure of this scratch is measured after 7 hours. (C) Effects of individual compounds and combinations on ECRF24 apoptosis induction. Images show the analysis of the DNA content by flow cytometry, after fixation of the cells in 70% ethanol, a DNA extraction step, and staining with PI for cells in the control (CTRL) and combination VI group. * indicates significance p-value < 0.05 and ** indicates significance p-value <0.01 with student t-test. Values represent the mean of at least 2 independent experiments with 3 replications each, and error bars represent the SEM. (D) Combination therapy VI inhibits tip cells *in vitro* and *in vivo*. FACS analysis show the decrease of CD34⁺ cells VI treated in HUVEC cultures, which is quantified in the bar graph and compared to single drug treatments. CD34⁺ tip cells treated with VI present with a clearly different cellular organization of the actin fibers stained with phalloidin as compared to control cells, compatible with decreased migratory activity. Bar stands for 25 μm. The FITC-dextran fluorescence (FITC-dextran, 20 kDa, 20 ml, 25 mg/ml, Sigma-Aldrich) angiographies below show the chicken chorioallantoic membrane (CAM) capillary plexus at the edges of the Visudyne®-photodynamic therapy (V-PDT; 5 J/cm² and 35 mW/cm² at 420 ± 20 nm) treated zones 24 h post V-PDT, where the tip cells form the leading edge of the sprouting vasculature (green arrows). A major lack of sprouting tip cells (red arrows) is visible after treatment V-PDT with immediate of combination VI.

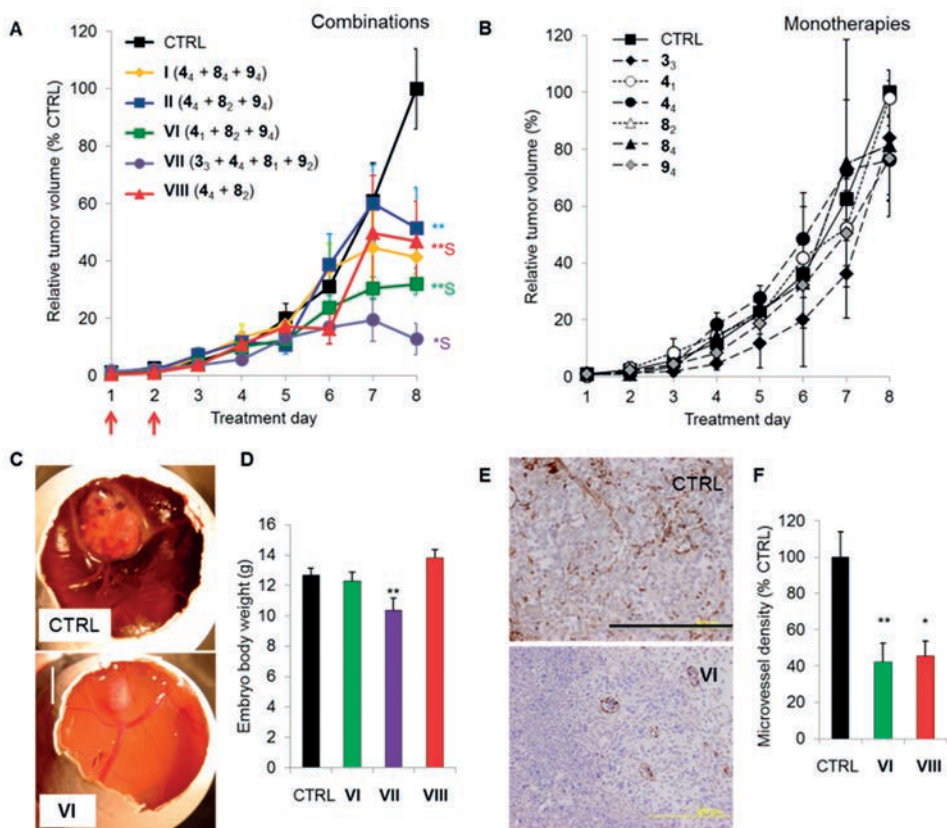


Figure 4. Inhibition of A2780 tumor growth on the CAM by the optimal drug combinations. Growth curves of A2780 tumors grafted on the CAM ($n=10$) showing tumor volume as a function of treatment day for various drug combinations (A) and single drug treatments (B). 'S' indicates synergy. Compounds were freshly premixed and administered i.v. on treatment days 1 and 2 (red arrows in A). Data points represent the average tumor volume as a percentage of the final control tumor volume per experiment. (C) Representative images of vehicle (CTRL) and combination VI treated tumors. (D) Mean embryo body weight on the last experiment day for selected treatment groups. (E) Representative images of CD31 stained tumor sections are shown. The bar in the lower right of the image represents 0.2 mm. The whole image was linearly adjusted for brightness and contrast. (F) Microvessel density quantification measured as the number of vessels per mm^2 and represented as a percentage of the control (CTRL). *indicates p -value < 0.05 and ** indicates p -value < 0.01 student t-test. Error bars represent the SEM. $N=3$ for condition 4₁. $N=5-11$ for all other groups.

50-60% lower in tumors treated with VI (** $p < 0.008$) and VIII (* $p = 0.01$, Fig. 4F). Based on these data, VI was selected as the most promising combination.

Combinations VI and VIII were studied in athymic mice grafted with human LS174T colorectal adenocarcinoma. Drug doses were adapted to this model based on single drug tumor growth inhibition efficacy (Supplementary Methods). Mice were treated with vehicle (CTRL), VI (4₂+8₂+9₄), and VIII (4₁+8₂) (Fig. 5A and Table 2). VI and VIII

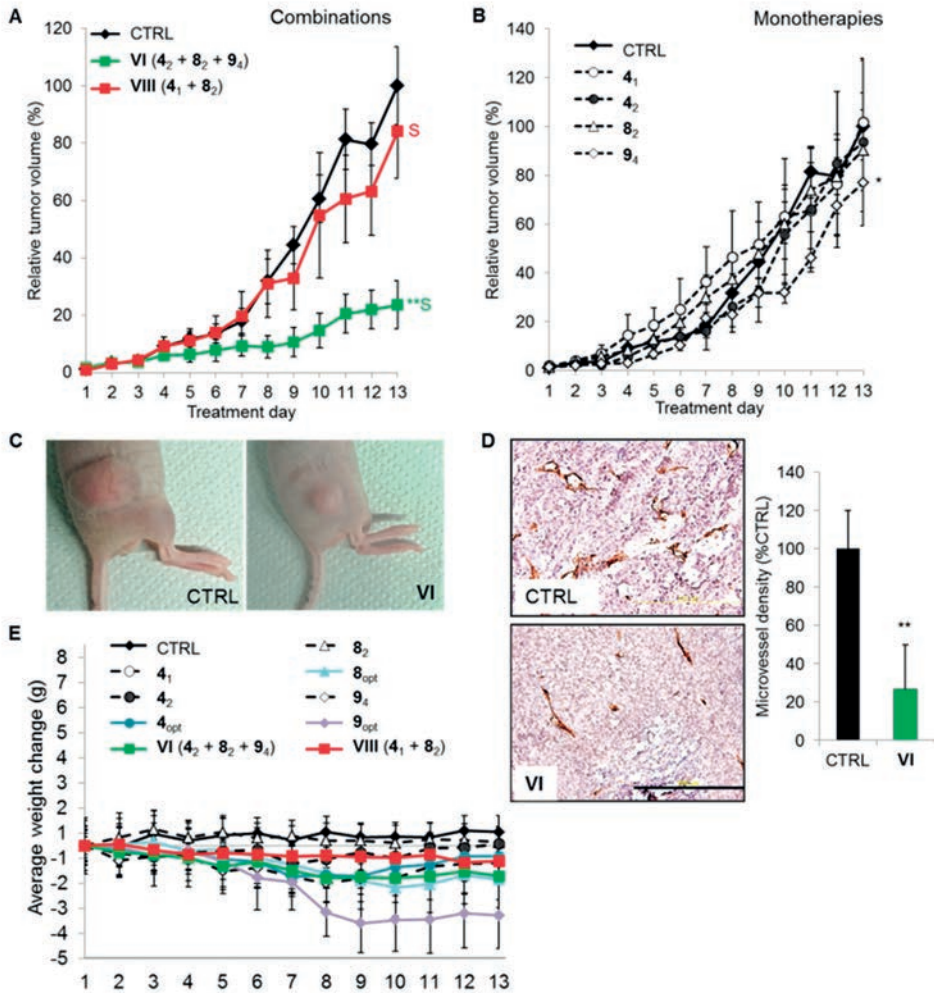


Figure 5. Inhibition of LS174T tumor growth in athymic mice by the optimal drug combinations. (A) LS174T tumors grafted subcutaneously in athymic Swiss nu/nu mice and treated daily with the drug combinations as listed in Table 2. (B) Inhibition of tumor growth by single compounds at indicated doses. Data points represent the average tumor volume as a percentage of the final CTRL volume per experiment and error bars represent the SEM; N=3-9. * $p < 0.05$ and ** $p < 0.01$ (two-way ANOVA). 'S' indicates synergy ($CI < 1$). (C) Representative images of vehicle treated (CTRL) and tumors treated with drug combination VI on the last experiment day. (D) Representative images of immunohistochemical staining for the EC marker CD31 and corresponding quantification of microvessel density, measured as the number of vessels per mm^2 and presented as a percentage of the CTRL. Results show significantly reduced microvessel density in tumors treated with VI. The bar in the lower panel image represents 0.2 mm and is valid for both images. The whole images were linearly adjusted for brightness and contrast. (b) Body weight change during the experiment. * $p < 0.05$ and ** $p < 0.01$ (student t-test). 4 (erlotinib), 8 (RAPTA-C) and 9 (BEZ-235). The error bars represent the SEM.

inhibited tumor growth significantly by $76\% \pm 14$ ($**p < 0.0001$, $CI = 0.56$) and $16\% \pm 16$ ($CI = 0.73$), respectively (Fig. 5A). Drugs applied individually inhibited tumor growth only marginally, by 6% (4_2), 10% (8_2) or 23% (9_4) ($*p < 0.013$, Fig. 5B). Interestingly, since the LS174T cell line was not sensitive to VI (Fig. 3A), effective tumor inhibition (Fig. 5A and 5C) was attributed to the inhibition of angiogenesis. MVD assessment indicated that VI suppressed angiogenesis by approximately 80% ($**p < 0.001$), compared to control tumors (Fig. 5D). No significant weight loss was recorded in either of the combinations tested (Fig. 5E). In contrast, individual compounds administered at optimal monotherapy doses, capable of effective tumor growth inhibition (Supplementary Fig. S6C) resulted in considerable body weight loss.

DISCUSSION

The FSC technique was used to navigate through the large parametric space of nine compounds, each considered at four doses, aiming for an optimal angiostatic drug combination. Using a simple *in vitro* endothelial cell (EC) viability bioassay as the output, an optimal low-dose drug combination containing axitinib (3), erlotinib (4), RAPTA-C (8) and BEZ-235 (9) was found. The most efficient of these combinations was also effectively inhibiting cancer in two *in vivo* animal models. We observed that (i) while some drugs showed synergistic interactions, others showed additive or even antagonistic behavior, (ii) the observed synergy was drug dose ratio dependent, (iii) the combination of angiostatic drugs enhanced endothelial specificity, (iv) screening on EC migration did not identify highly efficient drug combinations, and (v) *in vitro* optimized anti-angiogenic drug combinations translated to anti-angiogenic anti-cancer effects *in vivo*.

We previously demonstrated that multi-drug effects can be expressed by a quadratic relationship of the drug-drug interactions (37), which was confirmed in bacterial systems (38). Here, we have further demonstrated that the response surface for the whole range of drugs and drug doses applied can be expressed as a second-order equation that can be used to formulate optimal drug combinations. The results of this regression modeling (Supplementary Methods) permitted us to eliminate sunitinib (6) a compound which is known to have a similar target profile as axitinib (3) (note that both inhibit signaling of VEGF and PDGF (39)). The exclusion of sunitinib over axitinib appears justifiable, as axitinib is known to be a more selective TKI with stronger affinity for the same targets (39). Similarly, the exclusion of bevacizumab (2) was expected, as it is known that EC do not use VEGF as an autocrine growth factor and tumor angiogenesis is mainly driven by tumor produced VEGF.

The four drugs with significant inhibitory single drug linear contributions to cell viability were compounds axitinib, erlotinib, RAPTA-C and BEZ-235 (Fig. 1D). In terms of intracellular signaling, this combination of drugs appears to make sense in retrospect. EGFR targeting by erlotinib and VEGFR targeting by axitinib result in inhibition of two largely synergistic and widely used cellular signaling pathways, i.e. the PI3K/AKT/mTOR

and the ras/raf/MEK/MAPK(or ERK) signaling pathway, respectively. Since mTORC1 and mTORC2 belong to the PI3K/AKT pathway, one would expect that both signaling pathways are inhibited by EGFR and VEGFR inhibitors. It is also expected that a drug that targets histone proteins, such as RAPTA-C (40), can reinforce the angiostatic effect, as intervention with histone-DNA interactions is known to be angiostatic from the many reports on histone deacetylase inhibitors (41-43). mTOR and EGFR inhibitors have already been identified as a synergistic combination in various cancer cell types (44, 45), despite clinically observed toxicity (46, 47).

Based on the analysis of the response surfaces of the second order linear regression model generated from the four-drug optimization data (Fig. 2C) and embryo weight loss observed in the CAM model (Fig. 4D), axitinib was eliminated from further investigation. Thus, the optimal drug combination containing erlotinib, RAPTA-C and BEZ-235 was identified. It allowed for dose reductions of 5-, 11-, and 6-fold, respectively, as compared to the equivalent single drug doses efficiencies. Interestingly, enhanced EC specificity was observed for the combinations when compared to the individual compounds. This is another indication that the parallel blocking of multiple angiogenesis pathways can result in synergism for the angiostatic outcome. Simultaneous targeting of different signaling pathways may limit the probability of cells to develop acquired resistance (14).

The migration-based optimization screen failed to reach effective combinations (Supplementary Fig. S3B). This may suggest that proliferation is more dominant in the process of angiogenesis than cell migration, which was also proposed by others (48). The same may also be reflected by clinical trials, where proliferation inhibitors (such as sunitinib and BEZ-235) were more successful than migration inhibitors (the $\alpha_v\beta_3$ inhibitor cilengitide (49) and the $\alpha_5\beta_1$ antibody volociximab (50)).

The optimal drug mixture inhibited tumor growth by approximately 80%, most likely by an inhibitory effect on angiogenesis. Although the detailed mechanism of combination therapy still needs to be understood, the induction of apoptosis as well as the inhibition of tip cells show part of the effector mechanism. Targeting of tip cells may be another attractive strategy as these cells are indispensable for sprouting angiogenesis. The results provide a promising option for future clinical anti-angiogenic applications.

One might expect that the differences in pharmacokinetics between the components of the drug mixture may interfere with obtaining good results *in vivo*. Our results imply that (i) the best drug combinations found show smooth response surfaces (Fig. 2C, i.e. moderate changes in drug ratios do not significantly change the output), (ii) response surfaces, giving a mathematical description of the magnitude of the interaction for all drug pairs, confirmed *in vivo* treatment outcome (compare Fig. 2C and Fig. 5A), and (iii) EC viability observed *in vitro* seems to be a relatively good parameter for translation to vascular density reduction and tumor growth inhibition *in vivo*.

The current study shows that FSC applied *in vitro* can be used for the fast and reliable identification of potent, low-dose angiostatic drug combinations *in vivo*. It is likely that

combining the optimal anti-angiogenic compounds with other treatment strategies may lead to even better cancer treatment outcomes. The impact of the method also lies in the fact that it can be applied, e.g. for finding drug mixtures directly targeting tumor cells. In conclusion, designing effective, synergistic and specific multi-component drug combinations may become a key approach in developing new therapies for cancer and other diseases.

3.1

ACKNOWLEDGMENTS

We would like to thank Prof. Dean Ho (UCLA) and Prof. Michel Aguet (EPFL) for critical reviewing the manuscript.

FUNDING

The project is partially supported by Swiss Federal Institute of Technology (EPFL to PNS), Center for Translational Molecular Medicine (CTMM to AWG), The Netherlands; European Union (PIEF-GA-2013-626797 to PNS), Union for International Cancer Control (ICRET-13-080 to PNS), and the National Natural Science Foundation of China (81301293 to XD).

CONFLICT OF INTEREST

The authors declare that they have no competing interests.

Supplementary information is available here:

<https://link.springer.com/article/10.1007/s10456-015-9462-9>

Robert H. Berndsén^{1,2},
Cédric Castrogiovanni³,
Andrea Weiss¹,
Magdalena Rausch¹
Marchien G. Dallinga⁴,
Marijana Miljkovic-Licina⁵,
Ingeborg Klaassen⁶,
Patrick Meraldi^{3,4},
Judy R. van Beijnum²
Patrycja Nowak-Sliwinska^{1,4*}

¹ Molecular Pharmacology Group, School of Pharmaceutical Sciences, University of Lausanne and University of Geneva, Rue Michel-Servet 1211, Geneva, Switzerland;

² Angiogenesis Laboratory, Department of Medical Oncology, Cancer Center Amsterdam, Amsterdam UMC – location VUmc, VU University Amsterdam, De Boelelaan 1117, Amsterdam, The Netherlands;

³ Department of Cell Physiology and Metabolism, University of Geneva Medical School, Geneva, Switzerland;

⁴ Translational Research Center in Oncohaematology, Rue Michel-Servet 1211, Geneva, Switzerland;

⁵ Department of Pathology and Immunology, University of Geneva Medical School, Switzerland;

⁶ Ocular Angiogenesis Group, Departments of Ophthalmology and Medical Biology, Amsterdam Cardiovascular Sciences, Cancer Center Amsterdam, Amsterdam UMC, University of Amsterdam, Meibergdreef 9, Amsterdam, The Netherlands

The background features large, light grey numbers '3.2' that are partially obscured by the text. The number '3' is on the left, a small decimal point is in the center, and the number '2' is on the right. Two thin horizontal lines cross the page, one above and one below the text.

**ANTI-ANGIOGENIC EFFECTS OF CRENOLANIB
ARE MEDIATED BY MITOTIC MODULATION
INDEPENDENTLY OF PDGFR EXPRESSION**

BACKGROUND

Targeting angiogenesis currently is a well-established approach in cancer therapy. Key players in the process of angiogenesis include vascular endothelial growth factor receptor (VEGFR)-, fibroblast growth factor receptor (FGFR)- and TIE2 receptor signaling (51). The role of platelet-derived growth factor receptor (PDGFR) signaling in angiogenesis is not fully defined although it has been reported to contribute to angiogenesis and other mechanisms including cell growth, differentiation and migration (52, 53). Studies on the effects of PDGFR signaling on angiogenesis in both *in vivo* and *in vitro* models, as well as its contribution to the recruitment of pericytes in tumors (54), suggest an important role in the development and maintenance of functional vasculature (55).

In order to improve anti-angiogenic therapy it is important to identify drugs that target angiogenesis. For instance, combination of specific drugs that target angiogenesis via non-parallel pathways may increase clinical efficacy (56). Furthermore, detailed knowledge of the mechanism of action and identification of cell types that are affected by specific drugs can help design more effective treatment approaches. Although most tyrosine kinase inhibitors (TKIs) have been developed to target either one or a small number of signaling pathways it is becoming more clear that such drugs have a significant amount of off-target interactions (57). This may result in unexpected efficacy in less obvious tumor types on the one hand and insight in mechanisms of drug toxicities on the other hand.

Crenolanib was designed as a specific and selective PDGFR inhibitor (58), though more recently it was shown to also target FLT3 (59). It was first clinically tested in a phase I dose escalation study in patients with advanced solid tumors in 2009 and was considered safe and well tolerated (58). Currently, the efficacy of crenolanib is being evaluated in clinical trials for several indications including gliomas with PDGFR- α amplifications (NCT02626364), esophageal cancer (NCT03193918), relapsed/refractory FLT3 mutated-positive acute myeloid leukemia (AML; NCT02298166) and gastrointestinal stromal tumors (GIST; NCT02847429).

Given the proposed importance of PDGF(R) in vascular homeostasis, in this study, we set out to investigate the effects of crenolanib on endothelial cells (EC) in comparison to tumor cells and fibroblasts. We show that crenolanib strongly affects EC migration and sprout length, partly by differentially affecting endothelial tip cells. In addition, crenolanib affects mitosis and induced apoptosis. *In silico* approaches provided supporting evidence for these alternative pathways that crenolanib may act on to induce these effects. We further show that crenolanib inhibits pericyte recruitment that hampers formation of capillary like networks. *In vivo*, this resulted in inhibited tumor growth, accompanied by a significant reduction in microvessel density (MVD).

MATERIALS AND METHODS

Compounds

Crenolanib was purchased from Selleck Chemicals (Houston, Texas, USA) and was dissolved in sterile DMSO at a concentration of 10 mg/ml. Aliquots were stored in -80°C and thawed prior to each experiment. The maximum DMSO percentage was 0.1% and showed negligible activity in the performed assays and was used as control (CTRL).

Cells

Immortalized human vascular endothelial cells (ECRF24) were cultured in flasks coated with 0.2% gelatin and grown in medium containing 50% DMEM and 50% RPMI-1640 (Life Technologies, Carlsbad, CA, USA), supplemented with 10% fetal bovine serum (FBS) and 1% penicillin/streptomycin (Life Technologies). Human ovarian carcinoma cells (A2780) and Human Dermal Fibroblasts adult (HDFa) were cultured in DMEM supplemented as described above. Human umbilical vein endothelial cells (HUVEC) were harvested from umbilical cords and cultured in RPMI-1640 medium supplemented with 10% human serum, 10% FBS, 1% penicillin/streptomycin and 2 mM L-glutamine (60).

Cell viability and endothelial cell sprouting assay

For cell viability experiments, cells were seeded in 96-well cell culture plates at a density of 5×10^3 cells/well (HUVEC) or 10×10^3 cells/well (ECRF24 and A2780) and grown for 24 hours (61). After the administration of test compounds, cells were allowed to grow for 72 hours. After that cell viability was assessed with the CellTiter-Glo luminescence assay (Promega, Madison, WI, USA). Cell response to drug treatment was determined based on normalizing the luminescence signal in the treated wells as compared to controls.

For the 2D sprouting assay, HUVEC were mixed in methylcellulose containing medium (70% RPMI, 20% Methocel™/RPMI-1640 (Sigma-Aldrich, St. Louis, MO, USA) and 10% human serum).¹² Drops of 1000 cells in 25 μl were deposited on the lid of a petri dish, which was then flipped to allow spheroid formation in hanging drops, and incubated overnight. After 24 hours, a collagen gel mixture was prepared using PureCol® (Sigma), 0.2M NaOH and M199 medium (Sigma), new-born calf serum (NBCS), heparin and bFGF (50ng/ml;). Spheroids were collected by flushing the lid with PBS, spun (400g for 5'), gently mixed with the collagen gel solution and placed in pre-warmed Ibidi (Martinsreid, Germany) culture slides. Images of spheroids were taken after overnight incubation using a Leica DMI3000 microscope (Leica, Rijswijk, Netherlands). Image-based quantification was preformed using ImageJ software (62).

Cell migration assay

ECRF24 (30×10^3 cells/well) or HUVEC (15×10^3 cells/well) were seeded in 96-well cell culture plates and grown overnight to confluence. A uniform scratch was made using a sterile scratch tool (Peira Scientific Instruments, Beerse, Belgium) and treatment was

administered immediately after. The wells were imaged using a Leica DMI3000 microscope (Leica) at x5 magnification using Universal Grab 6.3 software (DCILabs, Keerbergen, Belgium). Imaging was performed immediately (T=0) and 6 hours (T=6) after scratching. The size of the scratch was automatically quantified and analyzed using Scratch Assay 6.2 (DCILabs) by calculating the absolute wound closure (initial minus final scratch surface) and values were presented as the percentage normalized to the CTRL (0.1% DMSO in cell culture medium).

Endothelial-Pericyte co-culture network formation assay

Adherent HUVEC and primary pericytes were labeled with 1 μM CellTracker Orange CMRA548 (Thermo Fisher Scientific, Waltham, MA, USA) and 1 μM CellTracker Green CMFDA488 (Thermo Fisher Scientific) dyes, respectively, in serum-free M199 medium for 30 minutes at 37°C. When premixed with growth factor-reduced Matrigel (Corning, New York, NY, USA) both HUVEC and pericytes were then harvested by trypsinization and counted. 2.5×10^3 HUVEC and 5×10^3 pericytes were added to the polymerized Matrigel in each well, and cultured in complete M199 for up to 10 hours. The co-cultures were analyzed by live-cell time-lapse imaging using Nikon A1R confocal microscope (see Supplementary Methods).

3.2

Flow cytometry

Analysis of cellular DNA content using propidium iodide was performed using flow cytometry (63). Cells were seeded at $20\text{-}40 \times 10^3$ cells/well and incubated for 24 hours. Medium with or without or crenolanib was applied and cells were incubated for an additional 72 hours. Cells were harvested by trypsinization and fixated in 70% ethanol for 2 hours at -20°C. Cell pellets were then resuspended in DNA extraction buffer (90 parts 0.05 M Na_2HPO_4 , 10 parts 0.025 M citric acid, 1 part 10% Triton-X100, pH 7.4) and incubated for 20 min at 37°C. Propidium iodide (PI, 20 $\mu\text{g}/\text{ml}$) was added and cells were analyzed with a FACSCalibur flow cytometer (BD Biosciences, Franklin Lakes, NJ, USA). DNA content was quantified with CellQuest Pro software (BD Biosciences).

Mitosis live-cell imaging

To visualize the effect of crenolanib on mitosis, live-cell imaging was performed for 24 hours at 37°C on a Ti widefield microscope (Nikon) equipped with an environmental chamber (5% CO_2) using a 60 \times 1.3 NA oil objective, a Cy5 filter, a CoolSNAP HQ camera (Roper Scientific, Vianen, Netherlands) at a sampling rate of 3 min, recording at each time point 9 z-stacks separated by 2 μm . ECRF24 were maintained as described above. HUVECs were maintained in M199 medium (Thermo Fisher Scientific) supplemented with 10% fetal calf serum (FCS), 1% penicillin/streptomycin (Thermo Fisher Scientific), 1% endothelial cell growth supplement (Millipore), 0.1 mg/mL heparin sodium salt (Sigma), 0.1 μM hydrocortisone (Sigma), and 10 $\mu\text{g}/\text{mL}$ L-ascorbic acid (Sigma). The day before,

the cells were seeded in an Ibidi μ -Slide 8 Well culture plate (Vitaris, Baar, Switzerland). 4 hours prior to the start of imaging, 50 nM SiR-Tubulin (SpiroChrome AG, Switzerland) was added on the cells to stain microtubules in addition with 10 μ M Verapamil (SpiroChrome AG, Stein am Rein, Switzerland) to keep the dye inside the cells. Neither treatment affected mitosis, nor the efficacy of crenolanib. Crenolanib was added just before the start of image acquisition. Time-lapse movies were analyzed using NIS Elements AR Software.

Immunofluorescence

In ECRF24, HUVEC, A2780 and HDFa F-actin and cell nuclei were visualized by a combination of phalloidin-Alexa488 (A12379, Invitrogen) and DAPI (D9542, Sigma). Separately, HUVEC were stained for VE-cadherin and DAPI (detailed in Supplementary Material).

3.2

Human ovarian carcinoma grown and photodynamic therapy (PDT) on the chicken chorioallantoic membrane (CAM)

Fertilized chicken eggs were incubated in a hatching incubator (relative humidity 65%, 37°C). On embryo development day (EDD) 8, 25 μ L hanging drops containing 10^6 A2780 cells in 20% Methocel™ (Sigma) and 80% serum free RPMI-1640 medium were prepared. 3 hours later the spheroids were transplanted onto the surface of the CAM (63, 64). Vascularized three-dimensional tumors were visible and eggs were randomized on EDD 11. Crenolanib, freshly dissolved in 0.9% NaCl, was administered on EDD 11 and 12 (referred to as treatment day 1 and 2) in 100 μ l i.v. injections. The injected doses (52 μ g/kg/day and 260 μ g/kg/day) were adjusted to the normalized embryo weight at EDD 11 and 12. Control tumors were treated with vehicle (0.1% DMSO in 0.9% NaCl). Tumors were monitored daily for 8 days and tumor size was calculated with the formula: volume = [large diameter] x [perpendicular diameter]² x 0.52. At the last experiment day, embryos were sacrificed and weighed. Tumors were resected and fixed in zinc-fixative for additional analysis. *In vivo* angiogenic sprouting on the CAM was induced by photodynamic therapy (PDT) as and visualised on EDD11 (65). Directly after PDT, 20 μ l crenolanib at a dose of 25 μ M (corresponding to 63.5 μ g/kg) was administered intravenously. Fluorescence images were taken 24 hours later using a pco.1300 12-bit CCD camera (Gloor Instruments AG, Usler, Switzerland) run by Micro-Manager 1.4 (NIH, Bethesda, MD, USA) (63, 66).

Immunohistochemistry

Immunohistochemical staining of A2780 CAM tumors was performed to detect blood vessels (CD31) and proliferating cells (Ki67; Supplementary Methods). Microvessel density (MVD; number of CD31+ structures per microscopic field) and the frequency of Ki67 positive cells in CAM tumors was assessed by ImageJ quantification of representative images (20x objective) using the color deconvolution plugin, as previously described (67).

In silico analysis of crenolanib target proteins

Crenolanib target proteins were retrieved from proteomicsDB (www.proteomicsdb.org), an online repository on the human proteome. Using the 'Analytics Toolbox' function, dose-dependent protein-drug interactions can be mined. We used a concentration of 5 μM crenolanib to search for target proteins, and proteins reported with an effective inhibition of $\geq 50\%$ with this concentration of crenolanib were subsequently included for further analysis. More details are provided in Supplementary Methods.

Statistics and data correction

The data are presented as the mean of multiple independent experiments (\pm SEM). In the MVD analysis, statistical outliers were removed from the dataset using the modified thompson Tau test. Statistical significance was determined using the one-way or two-way ANOVA test with post-hoc Dunnett's multiple comparison test or an unpaired t-test (Graphpad Prism). * P values lower than 0.05 and ** P lower than 0.01 were considered statistically significant and are indicated versus the control in unless noted otherwise.

RESULTS

Crenolanib inhibits cell viability, cell migration and sprouting in vitro

The activity of crenolanib was investigated in immortalized human endothelial cells (ECRF24), freshly isolated primary human umbilical vein endothelial cells (HUVEC), human A2780 ovarian carcinoma cells and adult human dermal fibroblasts (HDFa). Cell viability was dose-dependently and significantly (ECRF24 2 - 10 μM ; HUVEC 7.5 - 10 μM and A2780 5 - 10 μM) inhibited in ECRF24, HUVEC and A2780 cells after exposure to crenolanib for 72 hours, with comparable IC_{50} values (i.e. 5.1 μM for A2780, 4.6 μM for ECRF24 and 8.4 μM for HUVEC, Fig. 1A). In contrast, crenolanib did not affect HDFa cell viability.

Cell migration, evaluated using the wound-healing assay, was significantly and dose-dependently inhibited in ECRF24, HUVEC and HDFa (Fig. 1B). Interestingly, crenolanib administered at lower doses (0.5 – 2 μM) tended to stimulate (not significantly) rather than inhibit EC migration, particularly in HUVEC (Fig. 1B). Of note, the inability of A2780 cells to form confluent monolayers precluded us to investigate this trait in these cells. Furthermore, we confirmed absence of viability inhibition during the time frame of the assay, indicating that a direct effect on cell migration was found (data not shown).

Strikingly, when we addressed the expression of the main targets of crenolanib, i.e. PDGFR- α and PDGFR- β , we noted that their expression was almost undetectable in A2780, ECRF24 and HUVEC (Fig. 1C and Suppl. Fig. 1), whereas HDFa showed marked expression. This seemingly counterintuitive observation urged us to further investigate the mode of action of crenolanib in these different cells.

In the next step, the effect of crenolanib was investigated in a collagen-based three-dimensional endothelial cell sprouting model (Fig. 1D). Average sprout length and total

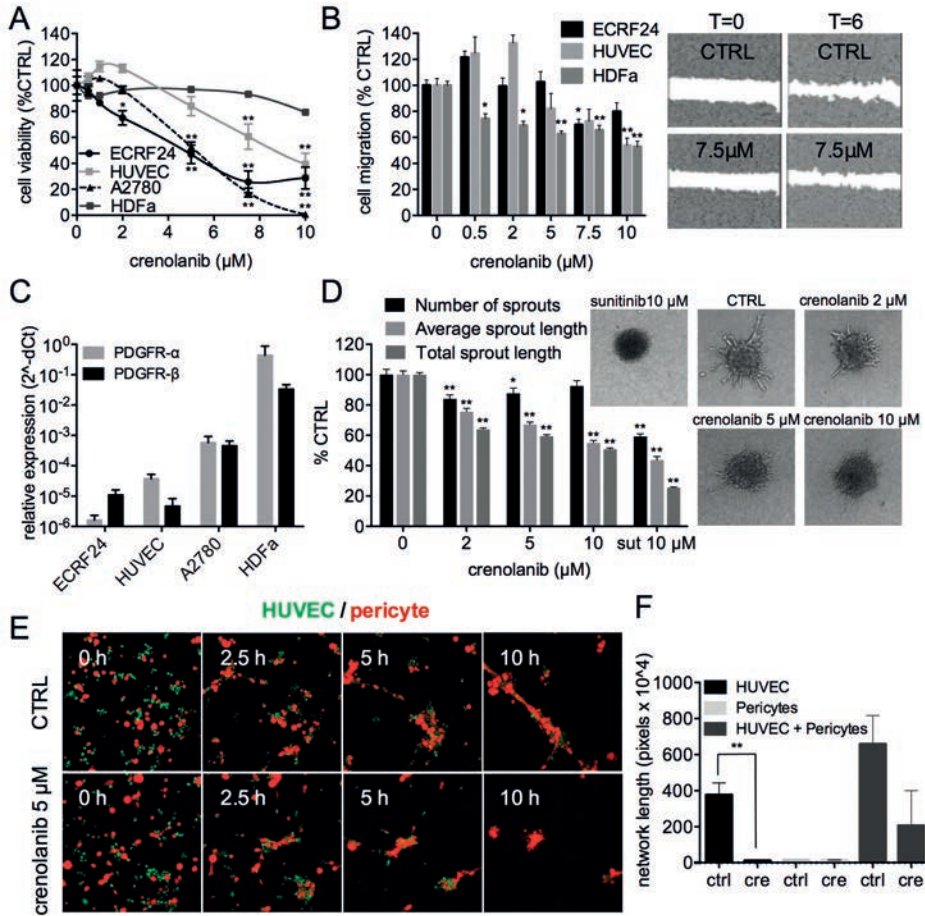


Figure 1. Activity of crenolanib on cell viability, migration and sprouting. (A) Cell viability dose response curves of crenolanib in endothelial cells (immortalized ECRF24 and primary human umbilical vein endothelial cells (HUVEC), ovarian cancer cells (A2780) and adult human dermal fibroblasts (HDFa). Cell viability was assessed after 72 hours of exposure to crenolanib and represented as a percentage of untreated controls. Significance is indicated versus untreated cells. (B) Endothelial cell migration in response to crenolanib. Cell migration was assessed after 6 hours drug treatment using a scratch assay. (C) PDGFR- α and - β expression in ECRF24, HUVEC, A2780 and HDFa determined by qPCR. (D) Activity of crenolanib on HUVEC sprouting. The number of sprouts and the average sprout length were quantified. (E) Representative images of HUVEC (green) and human pericyte (red) co-cultures. Co-cultures were established in 3D Matrigel matrices and allowed to randomly co-assemble over 10 hours in the presence of DMSO or crenolanib (5 μ M) at 0, 2.5, 5 and 10 hours. Scale bars represent 200 μ m. (F) Quantification of the network length of capillary-like structures in HUVEC alone, pericyte alone and HUVEC/pericyte co-culture in the presence or absence of crenolanib (5 μ M) at 10 hours. All values shown are presented as percentage of the CTRL and represent the mean of at least two experiments performed in triplicate. Cells treated with 0.1% DMSO were used as a control (CTRL). Error bars indicate SEM. Significance (* P < 0.05, ** P < 0.01) is indicated as compared to control.

sprout length were decreased dose-dependently by crenolanib, whereas the number of sprouts was only minimally affected and decreased only at a dose of 2 μM ($16 \pm 2.7\%$ as compared to CTRL). These results suggest that a reduced sprout length is due to inhibition of endothelial cell proliferation and sprout elongation. To further investigate this, we analyzed the effect of crenolanib on the percentage of tip cells by flow cytometry using CD34 as a marker in HUVEC (30, 68). Crenolanib administered at 5 μM for 72 hours resulted in a significant increase in the number of CD34⁺ tip cells (Suppl. Fig. 2A). Next, to assess whether crenolanib acts differentially on CD34⁺ tip cells versus non-tip cells, we immunolabeled cells with antibodies for Annexin-V (for apoptotic cells) and CD34 (for tip cells) and analyzed the cells by FACS. No differences were found in the percentage of apoptotic cells between CD34⁺ and CD34⁻ cells (Suppl. Fig. 2B).

To investigate further the anti-angiogenic mechanism of action of crenolanib, qPCR analysis was performed in HUVEC after crenolanib treatment (Suppl. Fig. 2C). A panel of tip cell genes was included in the analysis to test if crenolanib stimulates the expression of genes corresponding to the observed increase in tip cells. This panel included CD34, vascular endothelial cell growth factor receptors (VEGFR2-3), the endothelial cell Notch ligand Dll4, angiopoietin 2 (ANGPT2), CXC chemokine receptor 4 (CXCR4), netrin receptor UNC5B and insulin like growth factor 2 (IGF2) (68). Administration of crenolanib at 5 μM in HUVEC resulted in an increase in mRNA levels of 3 out of 8 tip cell specific genes, including CD34 mRNA. This indicates that the effect of crenolanib may not be tip cell specific. Expression of VEGFR2 and is significantly decreased as a result of crenolanib treatment, whereas VEGFR3 mRNA levels are not affected.

Crenolanib regulates pericyte recruitment *in vitro* and affects cell morphology

In angiogenesis, endothelial cells of newly formed blood vessels produce PDGF to attract pericytes, a process that results in vessel stabilization and maturation (69). In order to assess the role of crenolanib in pericyte recruitment, an *in vitro* endothelial-pericyte co-culture assay was applied to mimic pericyte recruitment and attachment to endothelial cells *in vivo* (70, 71). Human pericytes (labeled with red cell tracker) were cultured with or without HUVEC (labeled with green cell tracker) on Matrigel (Fig. 1F and Suppl. Fig. 3). During a 10-hour incubation, HUVEC alone aligned to form capillary-like cords in the control condition while they did not efficiently align in the presence of crenolanib (5 μM) (Suppl. Fig. 3A and Suppl. Videos 1, 2). Pericytes alone were not able to align to form capillary-like cords in either control or crenolanib conditions (Suppl. Fig. 3B and Suppl. Videos 3, 4). Time-lapse imaging of capillary-like assembly revealed that after 10 hours of co-culture, pericytes were tightly associated with endothelial cells in the control conditions (Fig. 1E and Suppl. Video 5). Strikingly, pericytes that were co-cultured with HUVEC in the presence of crenolanib did not closely associate and extended away from the cords in certain regions (Fig. 1E and Suppl. Video 6). Measurement of

the length of the capillary-like networks confirmed the observed differences between cultures of HUVEC and/or pericytes in the presence or absence of crenolanib (Fig. 1F.)

To further investigate the cellular morphology and integrity in response to crenolanib treatment, ECRF24, HUVEC, A2780 and HDFa were stained for F-actin (phalloidin) and DNA (DAPI; Suppl. Fig. 4A). The actin cytoskeleton consists of a membrane supporting component, a cortical actin rim and actomyosin based stress fibers (72). In non-treated cells, especially in ECRF24 and HUVEC, the stress fibres and cortical rim can clearly be observed. Treatment with crenolanib 5 μM results in cell border retraction and gap formation. In all cell lines, treatment with increasing crenolanib dose led to the formation of micronuclei which may be indicative of genomic instability and chromosomal damage (Fig. 2A) (73). In addition, undivided cell nucleus doublets can be observed that may imply a halt in cell division and thus cell proliferation (Fig. 2A). Quantification revealed a significant increase of the total number of micronuclei and undivided cell nucleus doublets (Fig. 2B and 2C). Interestingly, this result was most profound in A2780 cells.

Next, HUVEC were also stained for the adherens junction molecule VE-cadherin (VE-cad) and DNA (DAPI). Treatment with crenolanib resulted in a decrease of adherens junctions that have a ruffled appearance and formation of intercellular gaps (indicated by white arrowheads; Suppl. Fig. 4B) in accordance to the activity observed in F-actin staining that suggests cell traction (Suppl. Fig. 4A).

Crenolanib induces apoptosis in both endothelial and ovarian cancer cells before mitotic entry

To study the mechanism of crenolanib-induced suppression of cell viability in EC and ovarian cancer cells, DNA profiles of crenolanib treated cells were assessed by flow cytometry analysis of sub-diploid cells, after staining with propidium iodide (PI). Sunitinib (10 μM) was used as a positive control in these assays (61). Crenolanib induced apoptosis in ECRF24, HUVEC and A2780 (Fig. 2D-E and Suppl. Fig. 5). Ovarian cancer cells were more sensitive to apoptosis induction by crenolanib than EC.

To investigate in more detail how crenolanib affects cell proliferation and induces apoptosis in endothelial cells, we performed live-cell imaging of ECRF24 and HUVEC cells treated with increasing doses of crenolanib. To monitor mitotic events in particular, and the behaviour of the mitotic spindle, cells were stained with the live-cell dye SiR-tubulin that stains microtubules (74). Our analysis revealed that crenolanib affected the cell cycle and mitosis at several levels. First, crenolanib prevented mitotic entry, as with increasing doses a smaller percentage of ECRF24 and HUVEC entered mitosis over the period of 24 hours (Fig. 3A). In particular, at 5 μM crenolanib, mitotic entry was completely blocked in both cell types. Second, crenolanib significantly increased the duration between mitotic entry and mitotic exit (mitotic timing) in both cell types (Fig. 3B-C). Since mitotic timing is mostly determined by the ability of cells to attach all chromosomes on kinetochores and satisfy the spindle assembly checkpoint (75), this implied that crenolanib partially impairs

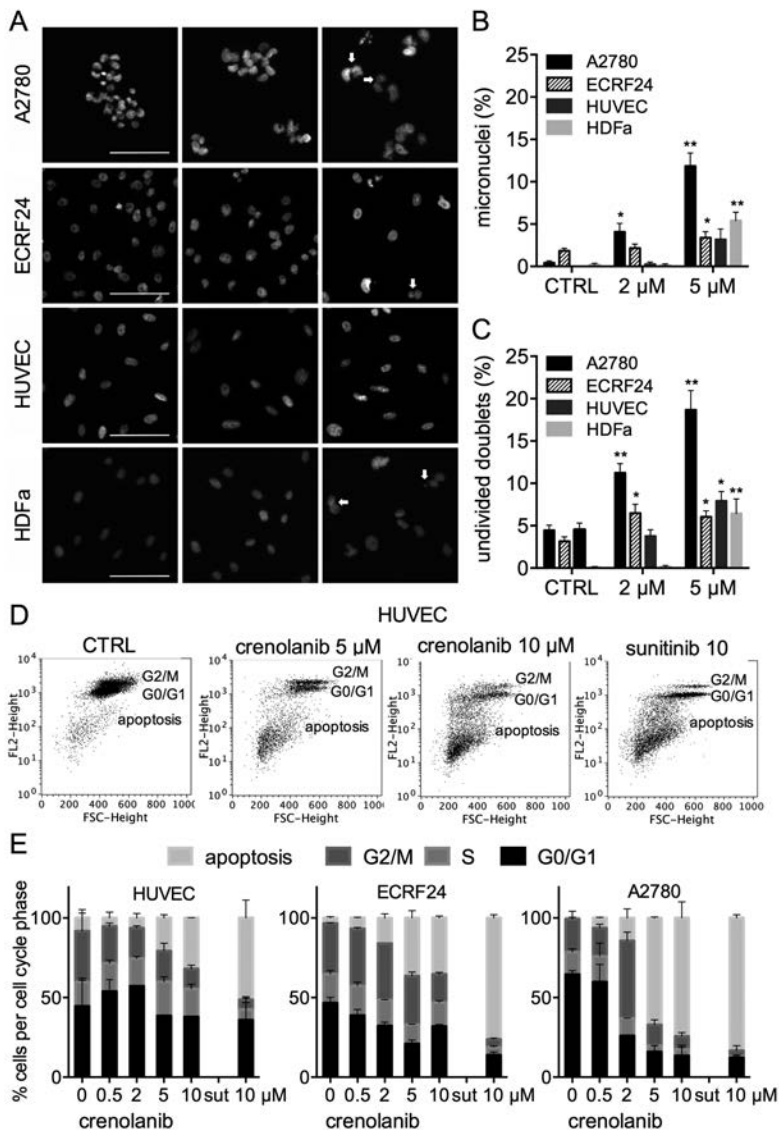


Figure 2. Crenolanib induces nuclear aberrations and apoptosis. (A) DAPI staining of A2780, ECRF24, HUVEC and HDFa after treatment with crenolanib for 72 hours. In cells treated with crenolanib 5 μ M white arrowheads indicate either micronuclei or undivided nuclear doublets. (B, C) Quantification of the percentage of micronuclei (B) and undivided nuclear doublets (C) based on images of DAPI staining. Values shown represent the percentage aberrations of the total amount of cell nuclei per image field. (D) Propidium-iodide staining of HUVEC treated with crenolanib for 72 hours using flow cytometry. Cellular DNA content in permeabilized cells is proportional to fluorescence intensity (FL2-H; y-axis), and allows for the distinction of cells containing diploid DNA (G0/G1), tetraploid DNA (G2/M) and subdiploid DNA (apoptotic fraction). (E) Quantification of cellular DNA distribution over cell cycle phases as indicated in HUVEC, ECRF24 and A2780 cells after crenolanib treatment. All values shown are presented as percentage of the CTRL and represent the mean of at least two experiments. Error bars indicate SEM.

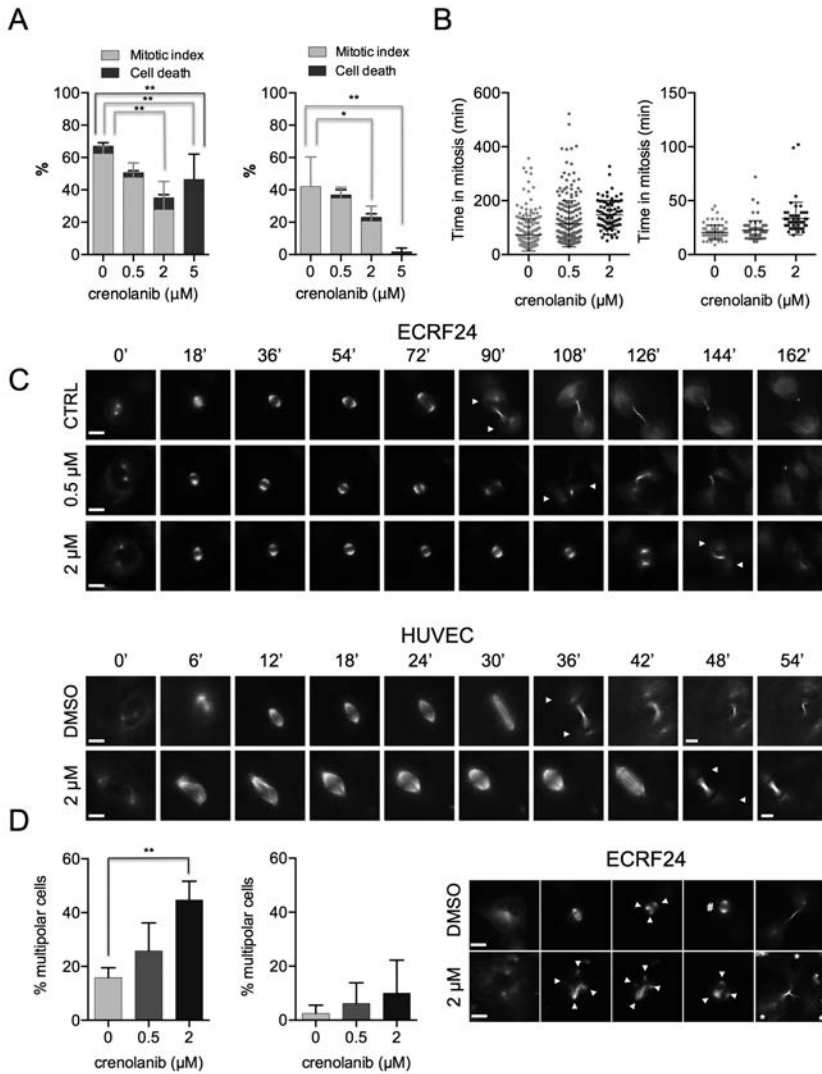


Figure 3. Crenolanib impairs mitosis and prevents centrosome clustering. (A) Percentage of ECRF24 and HUVEC cells entering mitosis during the 24hr live cell imaging movies (mitotic index) and the percentage of cell death after treatment with 0.5, 2 and 5 μM of crenolanib or DMSO. (B) Plots for the timing between nuclear envelope breakdown and anaphase onset in minutes (mitotic timing). Number of cells are ECRF24: 0 μM $n=230$, 0.5 μM $n=229$, 2 μM $n=84$; HUVEC: 0 μM $n=81$, 0.5 μM $n=80$, 2 μM $n=54$. (C) Representative live cell imaging stills over time of mitotic ECRF24 (top) and HUVEC cells stained with SiR-tubulin (microtubule marker), and treated with indicated doses of crenolanib. The arrows indicate the two daughter cells. Scale bars = 10 μm . (D) Quantification of multipolar spindles in mitosis in ECRF24 and HUVEC cells treated with indicated crenolanib concentrations. On the right, representative images of a mitotic ECRF24 cell (CTRL and crenolanib 2 μM) displaying multipolar spindles (indicated by arrows) are shown. The hashtag symbol indicates the centrosome clustering event and the asterisks the daughter cells resulting from the asymmetric division. Scale bars = 10 μm . Significance (* $P < 0.05$, ** $P < 0.01$) is indicated as compared to control (0.1% DMSO) and error bars indicate SD.

chromosome attachment by the mitotic spindle. Third, crenolanib has been previously reported to prevent the clustering of spindle poles (centrosome clustering) in cancer cells in the presence of multipolar spindles (76). Consistent with this study, 2 μM crenolanib prevented centrosome clustering in ECRF24 cells, as we observed an increased percentage of mitotic cells with multipolar spindles; HUVEC cells had much fewer multipolar spindles to start with and we did not see a significant increase after crenolanib treatment (Fig. 3D). Finally, despite these mitotic defects, we observed that crenolanib induced cell death mostly independently of mitosis, as the occurrence of cell death did not correlate with any mitotic outcome. In particular, 5 μM crenolanib induced massive cell death in ECRF24 cells (0 μM = 4.5% \pm 2.0 vs. 5 μM = 46.5% \pm 15.6%) despite the absence of mitosis (Fig. 3A). We further note that in this assay, HUVEC cells appeared to be less sensitive to crenolanib induced cell-death (Fig. 3A).

Taken together, we show that crenolanib induces apoptosis at increasing dose levels. Furthermore, despite partial impairment of mitotic progression, crenolanib mostly affects ECRF24 and HUVEC cells before cell division by preventing mitotic entry and inducing a cell division-independent cell death.

Crenolanib inhibits tumor growth, microvessel density and vascular sprouting in the CAM model

Finally, the vascular and anti-tumor activity of crenolanib was investigated in the CAM model. First, the activity of crenolanib was assessed on human A2780 ovarian carcinoma grown on the CAM. Crenolanib treatment was performed once daily for two days (EDD11-12) at doses of 52 $\mu\text{g}/\text{kg}/\text{day}$ and 260 $\mu\text{g}/\text{kg}/\text{day}$ (corresponding to 5 μM and 25 μM of crenolanib in 100 μL saline, respectively). Daily injections were performed mimicking the clinical use of crenolanib considering its short *in vivo* half-life of 8 hours (77). A 2-day treatment of i.v. administration of crenolanib resulted in significant tumor growth inhibition up to 57.4 \pm 9.4% (260 $\mu\text{g}/\text{kg}/\text{day}$; Fig. 4A-B).

During tumor growth of A2780 ovarian carcinoma on the CAM, the endothelial mRNA levels of PDGFR- α and β were considerably increased (Suppl. Fig. 6), consistent with on-going angiogenesis. To investigate the effect of crenolanib treatment on the tumor vasculature, microvessel density (MVD) was quantified by staining for the endothelial cell marker CD31 in tumor sections (Fig. 4E). Administration of crenolanib (260 $\mu\text{g}/\text{kg}/\text{day}$) resulted in a significant decrease in MVD up to 55.6 \pm 7.0%. Additionally, tumor sections were also stained for the proliferation marker Ki67. Quantification revealed a significant decrease in the amount of Ki67 positive cell nuclei in crenolanib (260 $\mu\text{g}/\text{kg}/\text{day}$) treated tumors (Fig. 4F).

Next, *in vivo* vascular sprouting was assessed following vaso-occlusive VisudyneTM-photodynamic therapy (PDT) (65). Application of PDT to the CAM vasculature leads to occlusion of blood vessels, which subsequently induces an angiogenic switch leading to the revascularization of the treated CAM areas.¹⁴ The administration of crenolanib

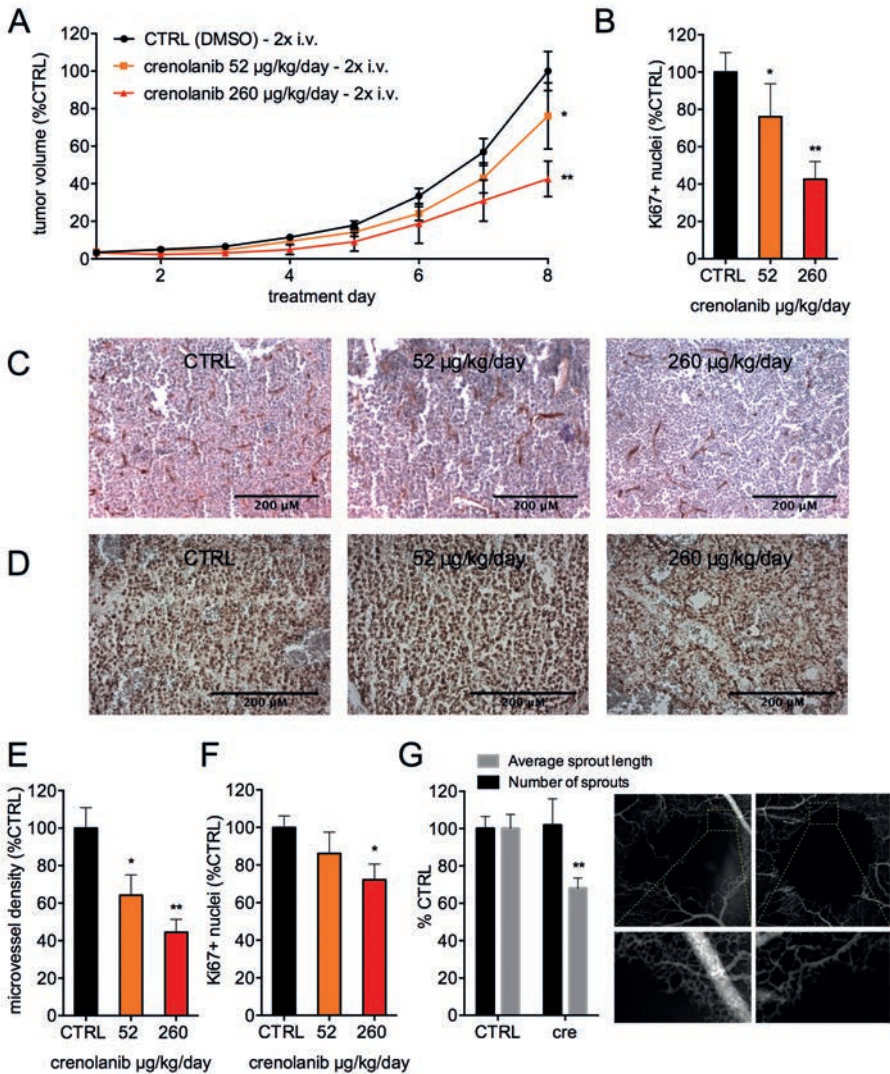


Figure 4. Crenolanib inhibits A2780 tumor growth and PDT-induced sprouting in the CAM model. (A) Tumor growth curves of A2780 spheroids xenografted on the CAM. Tumor volume is represented as the percentage of control tumor volume in respect to treatment days. N = 41 in the control group and N = 12-27 in the treatment groups. Eggs were treated with vehicle (0.1% DMSO) or crenolanib (52 µg/kg/day and 260 µg/kg/day) 2x daily i.v. injections. (B) Final tumor volume at the day of tumour resection. (C) Representative images of tumor sections stained for CD31. (D) Representative images of tumor sections stained for Ki67. (E) Microvessel density analysis of tumor sections stained for the endothelial cell marker CD31. (F) Analysis of the fraction of Ki67 positive cell nuclei presented as the percentage of stained cells per image field. (G) Effect of crenolanib at a dose of 63.5 µg/kg on PDT-induced vascular sprouting in the CAM. Quantification of the number of sprouts and the average sprout length are shown as percentage of control. Significance (*P < 0.05, **P < 0.01) is indicated as compared to control (0.1% DMSO treated cells) and error bars indicate SEM. Representative images 24h after PDT are shown. The bottom panel indicates zoomed areas corresponding to yellow boxes in the upper panel.

directly after PDT on EDD11 resulted in a decrease of the average sprout length, but not the number of sprouts, 24 hours after PDT as compared to the control (Fig. 4G). Strikingly, this result strongly resembles the effect of crenolanib seen in EC sprouting *in vitro* where the number of sprouts was not affected in contrast to the average sprout length (Fig. 1C).

In summary, crenolanib inhibits tumor growth in a dose dependent manner, which, at least in part, is caused by MVD inhibition. Furthermore, a decrease in the length of vascular sprouts is observed while the number of sprouts is not affected. These results in the CAM model confirm the strong anti-angiogenic activity observed in previous experiments.

***In silico* analysis of alternative mechanism of action of crenolanib**

In order to explain the observed phenotypic effects of crenolanib in cells that do not express the target receptors, we mined ProteomicsDB repository for additional protein targets of crenolanib. Using a drug concentration of 5 μ M and an effective inhibition score of $\geq 50\%$, 63 proteins were retrieved. Pathway enrichment analysis of these proteins clearly demonstrate their involvement in cell division organization (Fig. 5A and Suppl. Fig 7). Furthermore, protein interaction analysis using STRING identifies tight clustering and multi-level interactions between cell cycle related proteins, whereas the main targets of crenolanib (i.e. PDGFR- β and FLT3) are present in an unconnected cluster (Fig. 5B). As such, these data support and explain our observations on the predominant effects on mitosis and apoptosis by crenolanib.

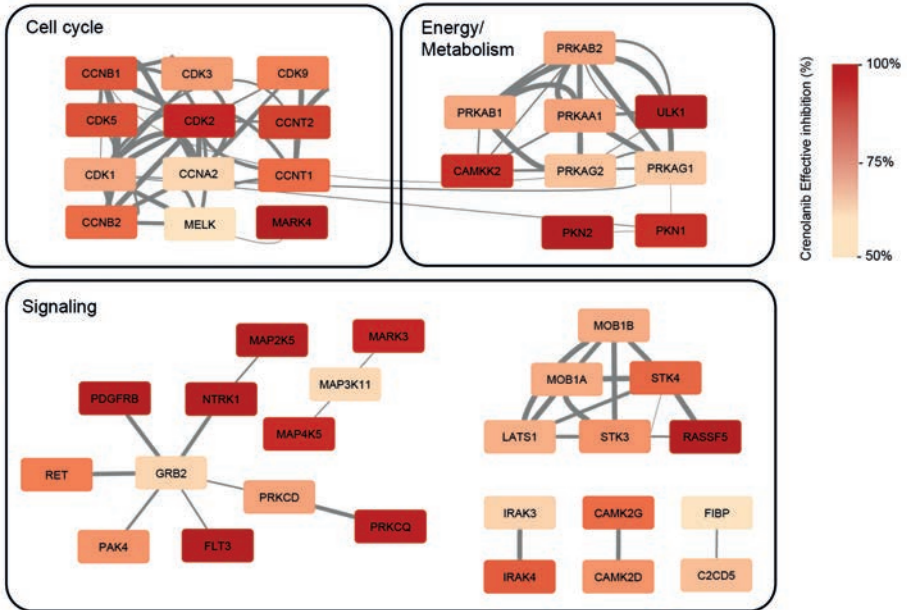
DISCUSSION

Angiogenesis inhibition is currently a widely used treatment strategy for patients with cancer. Although many angiogenesis-targeted drugs are currently limited in their ability to prolong overall patient survival, many novel therapeutic targets and combination-based strategies are being developed with the aim of improving angiogenesis suppression and overcoming limitations associated with angiogenesis inhibition, such as toxicity and resistance (78, 79).

The results presented in this study show that crenolanib exerts strong anti-angiogenic activity in both *in vitro* and *in vivo* angiogenesis models, as well as direct anti-cancer activity. Analysis of PDGFR expression in the included cell lines (ECRF24, HUVEC, A2780) revealed that PDGFR expression barely exceeded detection levels as compared to positive control cell line HDFa. Thus, crenolanib appears to act on both endothelial cells and cancer cells independent of PDGFR expression. It should be noted that crenolanib is a type I inhibitor which means the drug only acts on active receptor conformations (i.e. binding of PDGF to its receptor). Consequently, PDGF ligand must be present for crenolanib to exert its effect. In our assays however we did not evaluate conditions with excess PDGF ligand.

Since the activity of crenolanib cannot be explained as a result of PDGFR receptor targeting in EC, it is likely that there are other mechanisms at play that account for

A



B

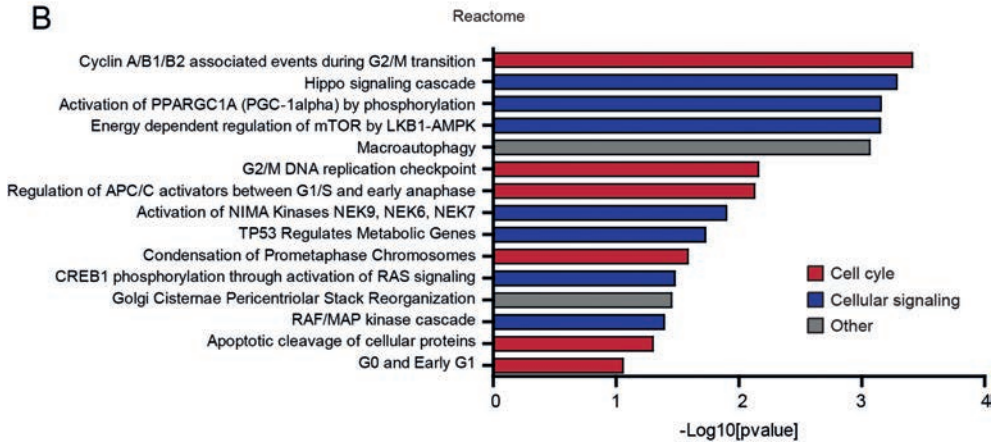


Figure 5. *In silico* analysis of crenolanib target proteins. Crenolanib target proteins with an effective inhibition (EI%) of $\geq 50\%$ with 5 μM crenolanib were retrieved from proteomicsDB (<https://www.proteomicsdb.org>) and subject to network analysis via STRING (A) and enrichment analysis using DAVID (B) as described in materials and methods. (A) Protein-protein interaction data from STRING were visualized in Cytoscape where the node colors reflect the EI% and the thickness of the edges indicate confidence levels of the interaction. (B) Enrichment of functional clusters for the Reactome database.

the activity of crenolanib. First, we showed that crenolanib reduces cell viability and cell migration of HUVEC and ECRF24 cells in a dose-dependent manner (Fig. 1A and 1B). Studying the effect of crenolanib on HUVEC sprouting in a 3D collagen-based model revealed that only the sprout length was affected and not the number of sprouts (Fig. 1D). This was confirmed by analysis of vascular sprouting in the CAM model after PDT induced angiogenesis (Fig. 4G). In our previous work we have demonstrated that the PDT CAM angiogenesis is much more sensitive (10-fold as compared to the angiogenesis inhibitors used in the cited study) than the developmental CAM model and resembles better the tumor microenvironment (65).

The observation that EC viability, migration and sprout length, but not sprout initiation was inhibited prompted us to study variable activity of crenolanib on different EC phenotypes. Specifically, ECs can differentiate into tip cells and non-tip cells (mainly existing of stalk cells, but also phalanx cells and quiescent cells). The EC tip cell phenotype is characterized by long filopodia and migratory activity whereas the stalk cell phenotype is characterized by proliferative activity and sprout stabilization (80). Thus, the strong anti-proliferative effect of crenolanib may be primarily due to activity on the proliferative stalk cells, accounting for a significant decrease in sprout length without a reduction in the overall number of sprouts (30).

Studying cell morphology in response to crenolanib revealed that crenolanib significantly affects the actin cytoskeleton resulting in cell contraction and ultimately gap formation (Suppl. Fig. 4A). Staining for adherens junction molecule VE-cadherin revealed a decrease and loosening of adherens junctions which may contribute to the observed gap formation (Suppl. Fig. 4B). Both a loss of adherens junctions and actin cytoskeleton structure may lead to increased vascular permeability (81). Furthermore, after visualization of cell nuclei with DAPI we observed the appearance of micronuclei and undivided doublets. The appearance of micronuclei may be indicative of genomic instability, chromosomal damage and apoptosis (Fig. 2B-C) (73). We described this phenomenon previously as a result of an angiostatic combination therapy (82).

Due to the observation of micronuclei and undivided doublets we hypothesized that crenolanib may halt or affect mitosis. Crenolanib was found to increase mitotic timing in ECRF24 and HUVEC and to prevent centrosome clustering in ECRF24 cells (Fig. 3). Crenolanib was previously described to prevent centrosome clustering in cancer cells but this has not been described for other cell types (76). The authors demonstrated that crenolanib induced 'activation of the actin-severing protein cofilin, leading to destabilization of the cortical actin network' and found that this activity was unrelated to PDGFR- β expression (76). Nevertheless, here we find that crenolanib mostly affected cell viability and cell proliferation of endothelial cells before or independently of cell division, as we observed a dose-dependent block in mitotic entry, and an increase in apoptosis independent of mitotic events.

To further assess the mechanism of action of crenolanib we searched for crenolanib target proteins in an online proteomics database and found a total of 63 proteins (Suppl. Table 1) that were reported to have an effective inhibition of $\geq 50\%$ by 5 μM of crenolanib. Subsequent gene ontology analysis showed considerable enrichment for cell cycle and cell division related proteins, in line with the results presented here (Fig. 5B and Suppl. Fig. 7). Various proteins of the Hippo pathway were also identified as targets of crenolanib. Together, these data point to a more complex mechanism of action of crenolanib that is not only mediated by inhibition of PDGFR and FLT3, but which is also heavily relying on disruption of normal cellular proliferation.

The anti-angiogenic activity of crenolanib observed in various *in vitro* assays described here was confirmed *in vivo* in tumors grown on the CAM. Here we report that crenolanib inhibits tumor growth at doses of 52 $\mu\text{g}/\text{kg}/\text{day}$ and 260 $\mu\text{g}/\text{kg}/\text{day}$ (Fig. 4A-B). Tumor growth inhibition was found to correlate to a decrease in MVD based on CD31 staining (Fig. 4E) and to a decrease in the density of proliferating cells, assessed by quantification of Ki67 staining (Fig. 4F).

In summary, we present a thorough analysis of the anti-angiogenic activity of the crenolanib. Since the effects of crenolanib presented in this study appear unrelated to PDGFR expression, we propose several other mechanisms that account for the observed activity. Based on our findings, we propose crenolanib for further investigations in other solid tumor types and application against solid cancers in clinical studies.

ADDITIONAL INFORMATION

Ethical Approval and Consent to Participate

The study was performed in accordance with the Declaration of Helsinki. Dutch legislation does not necessitate the acquisition of approval from institutional or licensing committee for experiments on the CAM terminated before hatching of the chicken embryo. Immortalized human vascular endothelial cells (ECRF24) were immortalized at the VU Medical Center Amsterdam from HUVEC cells. Human umbilical vein endothelial cells (HUVEC) were harvested from umbilical cords obtained from obtained from the Department of Gynecology, Amsterdam University Medical Center, using generalized consent approval of the local ethical review committee of VU University Hospital (Amsterdam, The Netherlands) through the code of anonymized usage. Human ovarian carcinoma cells (A2780) were purchased from European Collection of Authenticated Cell Cultures (ECACC 93112519), Human Dermal Fibroblasts adult (HDFa) from ATCC (ATCC PCS-201-012). Human pericytes were purchased from ScienCell Research Laboratories.

Data availability

All the data generated or analyzed in this study are included in the manuscript or the supplementary information.

Conflict of interest

The authors declare no conflict of interests.

FUNDING

European Research Council (ERC-StG-2015-680209 to PNS), Swiss National Science foundation (31003A-179413 to PM), the University of Geneva (to PM), and the Dutch Cancer Society (VU 2012-5480 to JRvB and VU 2014-7234 to PNS).

ACKNOWLEDGMENTS

We thank the European Research Council and the Dutch Cancer Society for financial support. We thank Prof. Dr. Arjan W. Griffioen for helpful discussions and material support and Tse Wong for performing the experiments.

Supplementary information is available here:

<https://www.nature.com/articles/s41416-019-0498-2>

REFERENCES

1. Folkman J. Tumor angiogenesis: therapeutic implications. *N Engl J Med.* 1971;285(21):1182-6.
2. Carmeliet P, Jain RK. Angiogenesis in cancer and other diseases. *Nature.* 2000;407(6801):249-57.
3. Gonzalez-Angulo AM, Hortobagyi GN, Ellis LM. Targeted therapies: peaking beneath the surface of recent bevacizumab trials. *Nature reviews Clinical oncology.* 2011;8(6):319-20.
4. Gerlinger M, Rowan AJ, Horswell S, Larkin J, Endesfelder D, Gronroos E, et al. Intratumor heterogeneity and branched evolution revealed by multiregion sequencing. *N Engl J Med.* 2012;366(10):883-92.
5. Hoey T. Drug resistance, epigenetics, and tumor cell heterogeneity. *Science translational medicine.* 2010;2(28):28ps19.
6. Hayman SR, Leung N, Grande JP, Garovic VD. VEGF inhibition, hypertension, and renal toxicity. *Current oncology reports.* 2012;14(4):285-94.
7. Ebos JM, Lee CR, Cruz-Munoz W, Bjarnason GA, Christensen JG, Kerbel RS. Accelerated metastasis after short-term treatment with a potent inhibitor of tumor angiogenesis. *Cancer cell.* 2009;15(3):232-9.
8. Loges S, Schmidt T, Carmeliet P. Mechanisms of resistance to anti-angiogenic therapy and development of third-generation anti-angiogenic drug candidates. *Genes Cancer.* 2010;1(1):12-25.
9. Griffioen AW, Molema G. Angiogenesis: potentials for pharmacologic intervention in the treatment of cancer, cardiovascular diseases, and chronic inflammation. *Pharmacological reviews.* 2000;52(2):237-68.
10. Lignet F, Calvez V, Grenier E, Ribba B. A structural model of the VEGF signalling pathway: emergence of robustness and redundancy properties. *Mathematical biosciences and engineering : MBE.* 2013;10(1):167-84.
11. Misale S, Arena S, Lamba S, Siravegna G, Lallo A, Hobor S, et al. Blockade of EGFR and MEK intercepts heterogeneous mechanisms of acquired resistance to anti-EGFR therapies in colorectal cancer. *Science translational medicine.* 2014;6(224):224ra26.
12. Sen B, Peng S, Tang X, Erickson HS, Galindo H, Mazumdar T, et al. Kinase-impaired BRAF mutations in lung cancer confer sensitivity to dasatinib. *Science translational medicine.* 2012;4(136):136ra70.
13. Lehar J, Krueger AS, Avery W, Heilbut AM, Johansen LM, Price ER, et al. Synergistic drug combinations tend to improve therapeutically relevant selectivity. *Nature biotechnology.* 2009;27(7):659-66.
14. Bozic I, Reiter JG, Allen B, Antal T, Chatterjee K, Shah P, et al. Evolutionary dynamics of cancer in response to targeted combination therapy. *eLife.* 2013;2:e00747.
15. Sequist LV, Waltman BA, Dias-Santagata D, Digumarthy S, Turke AB, Fidias P, et al. Genotypic and histological evolution of lung cancers acquiring resistance to EGFR inhibitors. *Science translational medicine.* 2011;3(75):75ra26.
16. Feldman DR, Baum MS, Ginsberg MS, Hassoun H, Flombaum CD, Velasco S, et al. Phase I trial of bevacizumab plus escalated doses of sunitinib in patients with metastatic renal cell carcinoma. *J Clin Oncol.* 2009;27(9):1432-9.
17. Spreafico A, Chi KN, Sridhar SS, Smith DC, Carducci MA, Kavsak P, et al. A randomized phase II study of cediranib alone versus cediranib in combination with dasatinib in docetaxel resistant, castration resistant prostate cancer patients. *Invest New Drugs.* 2014.
18. Mayer LD, Janoff AS. Optimizing combination chemotherapy by controlling drug ratios. *Molecular interventions.* 2007;7(4):216-23.
19. Pritchard JR, Lauffenburger DA, Hemann MT. Understanding resistance to combination chemotherapy. *Drug resistance updates : reviews and commentaries in antimicrobial and anticancer chemotherapy.* 2012;15(5-6):249-57.

20. Wong PK, Yu F, Shahangian A, Cheng G, Sun R, Ho CM. Closed-loop control of cellular functions using combinatory drugs guided by a stochastic search algorithm. *Proceedings of the National Academy of Sciences of the United States of America*. 2008;105(13):5105-10.
21. Price KV, Storn RM, Lampinen JA. *Differential evolution : a practical approach to global optimization*. Berlin ; New York: Springer; 2005. xix, 538 p. p.
22. Calzolari D, Bruschi S, Coquin L, Schofield J, Feala JD, Reed JC, et al. Search algorithms as a framework for the optimization of drug combinations. *PLoS computational biology*. 2008;4(12):e1000249.
23. Dancey JE, Chen HX. Strategies for optimizing combinations of molecularly targeted anticancer agents. *Nature reviews Drug discovery*. 2006;5(8):649-59.
24. Feala JD, Cortes J, Duxbury PM, Piermarocchi C, McCulloch AD, Paternostro G. Systems approaches and algorithms for discovery of combinatorial therapies. *Wiley interdisciplinary reviews Systems biology and medicine*. 2010;2(2):181-93.
25. Park M, Nassar M, Vikalo H. Bayesian active learning for drug combinations. *IEEE transactions on bio-medical engineering*. 2013;60(11):3248-55.
26. Marshall J. Clinical implications of the mechanism of epidermal growth factor receptor inhibitors. *Cancer*. 2006;107(6):1207-18.
27. Adhireksan Z, Davey GE, Campomanes P, Groessl M, Clavel CM, Yu H, et al. A ligand distinction between two ruthenium-cymen anticancer agents determines protein versus DNA targeting. *Nature Communications*. 2014;5:3462.
28. Garber K. Targeting mTOR: something old, something new. *J Natl Cancer Inst*. 2009;101(5):288-90.
29. van Beijnum JR, Nowak-Sliwinska P, van den Boezem E, Hautvast P, Buurman WA, Griffioen AW. Tumor angiogenesis is enforced by autocrine regulation of high-mobility group box 1. *Oncogene*. 2013;17(32):363-74.
30. Siemerink MJ, Klaassen I, Vogels IM, Griffioen AW, Van Noorden CJ, Schlingemann RO. CD34 marks angiogenic tip cells in human vascular endothelial cell cultures. *Angiogenesis*. 2012;15(1):151-63.
31. Nowak-Sliwinska P, van Beijnum JR, van Berkel M, van den Bergh H, Griffioen AW. Vascular regrowth following photodynamic therapy in the chicken embryo chorioallantoic membrane. *Angiogenesis*. 2010;13(4):281-92.
32. Tsutsui H, Valamehr B, Hindoyan A, Qiao R, Ding X, Guo S, et al. An optimized small molecule inhibitor cocktail supports long-term maintenance of human embryonic stem cells. *Nat Commun*. 2011;2:167.
33. Yu F, Al-Shyoukh I, Feng J, Li X, Liao CW, Ho CM, et al. Control of Kaposi's sarcoma-associated herpesvirus reactivation induced by multiple signals. *PLoS One*. 2011;6(6):e20998.
34. Price KV, Storn RM, Lampinen JA. *Differential evolution : a practical approach to global optimization*. Berlin: Springer; 2005. xix, 538 p. p.
35. Weiss A, van Beijnum JR, Bonvin D, Jichlinski P, Dyson PJ, Griffioen AW, et al. Low-dose angiostatic tyrosine kinase inhibitors improve photodynamic therapy for cancer: lack of vascular normalization. *J Cell Mol Med*. 2014;18:480-91.
36. Ding X, Sanchez DJ, Shahangian A, Al-Shyoukh I, Cheng G, Ho CM. Cascade search for HSV-1 combinatorial drugs with high antiviral efficacy and low toxicity. *International journal of nanomedicine*. 2012;7:2281-92.
37. Al-Shyoukh I, Yu F, Feng J, Yan K, Dubinett S, Ho CM, et al. Systematic quantitative characterization of cellular responses induced by multiple signals. *BMC systems biology*. 2011;5:88.

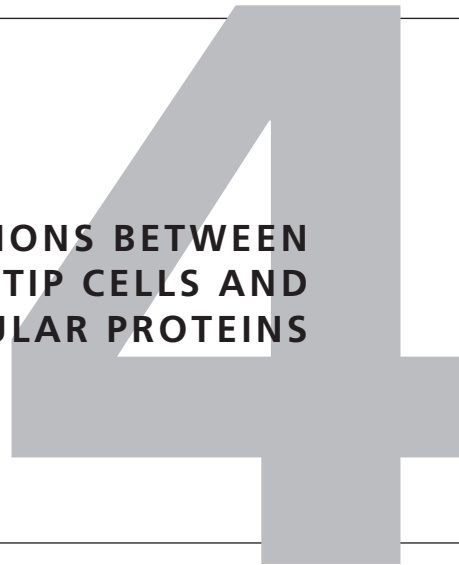
38. Wood K, Nishida S, Sontag ED, Cluzel P. Mechanism-independent method for predicting response to multidrug combinations in bacteria. *Proceedings of the National Academy of Sciences of the United States of America*. 2012;109(30):12254-9.
39. Bhargava P, Robinson MO. Development of second-generation VEGFR tyrosine kinase inhibitors: current status. *Current oncology reports*. 2011;13(2):103-11.
40. Adhireksan Z, Davey GE, Campomanes P, Groessl M, Clavel CM, Yu H, et al. Ligand substitutions between ruthenium-cymene compounds can control protein versus DNA targeting and anticancer activity. *Nature communications*. 2014;5:3462.
41. Martin M, Potente M, Janssens V, Vertommen D, Twizere JC, Rider MH, et al. Protein phosphatase 2A controls the activity of histone deacetylase 7 during T cell apoptosis and angiogenesis. *Proceedings of the National Academy of Sciences of the United States of America*. 2008;105(12):4727-32.
42. Hellebrekers DM, Castermans K, Vire E, Dings RP, Hoebbers NT, Mayo KH, et al. Epigenetic regulation of tumor endothelial cell anergy: silencing of intercellular adhesion molecule-1 by histone modifications. *Cancer Res*. 2006;66(22):10770-7.
43. Rossig L, Li H, Fisslthaler B, Urbich C, Fleming I, Forstermann U, et al. Inhibitors of histone deacetylation downregulate the expression of endothelial nitric oxide synthase and compromise endothelial cell function in vasorelaxation and angiogenesis. *Circulation research*. 2002;91(9):837-44.
44. Bianco R, Garofalo S, Rosa R, Damiano V, Gelardi T, Daniele G, et al. Inhibition of mTOR pathway by everolimus cooperates with EGFR inhibitors in human tumours sensitive and resistant to anti-EGFR drugs. *Br J Cancer*. 2008;98(5):923-30.
45. Rao RD, Mladek AC, Lamont JD, Goble JM, Erlichman C, James CD, et al. Disruption of parallel and converging signaling pathways contributes to the synergistic antitumor effects of simultaneous mTOR and EGFR inhibition in GBM cells. *Neoplasia*. 2005;7(10):921-9.
46. Bauman JE, Arias-Pulido H, Lee SJ, Fekrazad MH, Ozawa H, Fertig E, et al. A phase II study of temsirolimus and erlotinib in patients with recurrent and/or metastatic, platinum-refractory head and neck squamous cell carcinoma. *Oral oncology*. 2013;49(5):461-7.
47. Wen PY, Chang SM, Lamborn KR, Kuhn JG, Norden AD, Cloughesy TF, et al. Phase I/II study of erlotinib and temsirolimus for patients with recurrent malignant gliomas: North American Brain Tumor Consortium trial 04-02. *Neuro-oncology*. 2014;16(4):567-78.
48. Hinow P, Gerlee P, McCawley LJ, Quaranta V, Ciobanu M, Wang S, et al. A spatial model of tumor-host interaction: application of chemotherapy. *Mathematical biosciences and engineering* : MBE. 2009;6(3):521-46.
49. Reardon DA, Cheresch D. Cilengitide: a prototypic integrin inhibitor for the treatment of glioblastoma and other malignancies. *Genes Cancer*. 2011;2(12):1159-65.
50. Almokadem S, Belani CP. Volociximab in cancer. *Expert opinion on biological therapy*. 2012;12(2):251-7.
51. Bergers G, Benjamin LE. Tumorigenesis and the angiogenic switch. *Nature Reviews Cancer*. 2003;3(6):401-10.
52. Andrae J, Gallini R, Betsholtz C. Role of platelet-derived growth factors in physiology and medicine. *Genes & development*. 2008;22(10):1276-312.
53. Griffioen AW, Molema G. Angiogenesis: Potentials for Pharmacologic Intervention in the Treatment of Cancer, Cardiovascular Diseases, and Chronic Inflammation. *Pharmacological Reviews*. 2000;52(2):237.
54. Abramsson A, Lindblom P, Betsholtz C. Endothelial and nonendothelial sources of PDGF-B regulate pericyte recruitment and influence vascular pattern formation in tumors. *The Journal of clinical investigation*. 2003;112(8):1142-51.
55. Otrock ZK, Mahfouz RA, Makarem JA, Shamseddine AI. Understanding the biology of angiogenesis: review of the most important molecular mechanisms. *Blood Cells Mol Dis*. 2007;39(2):212-20.

56. Griffioen Arjan W, Weiss A, Berndsen Robert H, Abdul UK, te Winkel Marije T, Nowak-Sliwinska P. The emerging quest for the optimal angiostatic combination therapy. *Biochemical Society Transactions*. 2014;42(6):1608.
57. Karaman MW, Herrgard S, Treiber DK, Gallant P, Atteridge CE, Campbell BT, et al. A quantitative analysis of kinase inhibitor selectivity. *Nature Biotechnology*. 2008;26(1):127-32.
58. Lewis NL, Lewis LD, Eder JP, Reddy NJ, Guo F, Pierce KJ, et al. Phase I study of the safety, tolerability, and pharmacokinetics of oral CP-868,596, a highly specific platelet-derived growth factor receptor tyrosine kinase inhibitor in patients with advanced cancers. *Journal of clinical oncology : official journal of the American Society of Clinical Oncology*. 2009;27(31):5262-9.
59. Smith CC, Lasater EA, Lin KC, Wang Q, McCreery MQ, Stewart WK, et al. Crenolanib is a selective type I pan-FLT3 inhibitor. *P Natl Acad Sci USA*. 2014;111(14):5319-24.
60. van Beijnum JR, van der Linden E, Griffioen AW. Angiogenic profiling and comparison of immortalized endothelial cells for functional genomics. *Exp Cell Res*. 2008;314(2):264-72.
61. Nowak-Sliwinska P, Alitalo K, Allen E, Anisimov A, Aplin AC, Auerbach R, et al. Consensus guidelines for the use and interpretation of angiogenesis assays. *Angiogenesis*. 2018.
62. Schulkens IAE, Kleibeuker EA, Castricum KCM, Griffioen AW, Thijssen VLJL. Examination of the Role of Galectins and Galectin Inhibitors in Endothelial Cell Biology. In: Stowell SR, Cummings RD, editors. *Galectins: Methods and Protocols*. New York, NY: Springer New York; 2015. p. 285-91.
63. Nowak-Sliwinska P, Alitalo K, Allen E, Anisimov A, Aplin AC, Auerbach R, et al. Consensus guidelines for the use and interpretation of angiogenesis assays. *Angiogenesis*. 2018;21(3):425-532.
64. Nowak-Sliwinska P, Segura T, Iruela-Arispe ML. The chicken chorioallantoic membrane model in biology, medicine and bioengineering. *Angiogenesis*. 2014;17(4):779-804.
65. Nowak-Sliwinska P, Weiss A, van Beijnum JR, Wong TJ, Ballini JP, Lovisa B, et al. Angiostatic kinase inhibitors to sustain photodynamic angio-occlusion. *J Cell Mol Med*. 2012;16(7):1553-62.
66. Edelstein AD, Tsuchida MA, Amodaj N, Pinkard H, Vale RD, Stuurman N. Advanced methods of microscope control using μ Manager software. *J Biol Methods*. 2014;1(2):e10.
67. Kleibeuker EA, Ten Hooven MA, Castricum KC, Honeywell R, Griffioen AW, Verheul HM, et al. Optimal treatment scheduling of ionizing radiation and sunitinib improves the antitumor activity and allows dose reduction. *Cancer Med*. 2015;4(7):1003-15.
68. Dallinga MG, Yetkin-Arik B, Kayser RP, Vogels IMC, Nowak-Sliwinska P, Griffioen AW, et al. IGF2 and IGF1R identified as novel tip cell genes in primary microvascular endothelial cell monolayers. *Angiogenesis*. 2018;21:823-36.
69. Bergers G, Song S. The role of pericytes in blood-vessel formation and maintenance. *Neuro Oncol*. 2005;7(4):452-64.
70. Stratman AN, Malotte KM, Mahan RD, Davis MJ, Davis GE. Pericyte recruitment during vasculogenic tube assembly stimulates endothelial basement membrane matrix formation. *Blood*. 2009;114(24):5091-101.
71. Tigges U, Welser-Alves JV, Boroujerdi A, Milner R. A novel and simple method for culturing pericytes from mouse brain. *Microvasc Res*. 2012;84(1):74-80.
72. Prasain N, Stevens T. The actin cytoskeleton in endothelial cell phenotypes. *Microvasc Res*. 2009;77(1):53-63.
73. Leibowitz ML, Zhang C-Z, Pellman D. Chromothripsis: A New Mechanism for Rapid Karyotype Evolution. *Annual Review of Genetics*. 2015;49(1):183-211.
74. Lukinavičius G, Blaukopf C, Pershagen E, Schena A, Reymond L, Derivery E, et al. SiR-Hoechst is a far-red DNA stain for live-cell nanoscopy. *Nature communications*. 2015;6:8497-.
75. Meraldi P, Draviam VM, Sorger PK. Timing and checkpoints in the regulation of mitotic progression. *Dev Cell*. 2004;7(1):45-60.

76. Konotop G, Bausch E, Nagai T, Turchinovich A, Becker N, Benner A, et al. Pharmacological Inhibition of Centrosome Clustering by Slingshot-Mediated Cofilin Activation and Actin Cortex Destabilization. *Cancer Res.* 2016;76(22):6690.
77. Galanis A, Ma H, Rajkhowa T, Ramachandran A, Small D, Cortes J, et al. Crenolanib is a potent inhibitor of FLT3 with activity against resistance-conferring point mutants. *Blood.* 2014;123(1):94-100.
78. van Beijnum JR, Nowak-Sliwinska P, Huijbers EJM, Thijssen VL, Griffioen AW. The Great Escape; the Hallmarks of Resistance to Antiangiogenic Therapy. *Pharmacological Reviews.* 2015;67(2):441.
79. Nowak-Sliwinska P. Optimization for multidrug combinations: Challenges and perspectives in complex disorders. *Pharmacol Res.* 2019:104165.
80. Gerhardt H, Golding M, Fruttiger M, Ruhrberg C, Lundkvist A, Abramsson A, et al. VEGF guides angiogenic sprouting utilizing endothelial tip cell filopodia. *J Cell Biol.* 2003;161(6):1163-77.
81. Bogatcheva NV, Verin AD. The role of cytoskeleton in the regulation of vascular endothelial barrier function. *Microvasc Res.* 2008;76(3):202-7.
82. Berndsen RH, Weiss A, Abdul UK, Wong TJ, Meraldi P, Griffioen AW, et al. Combination of ruthenium(II)-arene complex [Ru(η (6)-p-cymene)Cl₂(pta)] (RAPTA-C) and the epidermal growth factor receptor inhibitor erlotinib results in efficient angiostatic and antitumor activity. *Scientific reports.* 2017;7:43005-.



**IDENTIFICATION OF INTERACTIONS BETWEEN
ENDOTHELIAL TIP CELLS, NON-TIP CELLS AND
EXTRACELLULAR PROTEINS**



Margriet M. Palm¹,
Marchien G. Dallinga²,
Erik van Dijk¹,
Ingeborg Klaassen²,
Reinier O. Schlingemann²,
Roeland M.H. Merks^{1,3,*}

¹ Life Sciences Group, Centrum Wiskunde & Informatica,
Amsterdam, the Netherlands

² Ocular Angiogenesis Group, Academic Medical Center,
Amsterdam, the Netherlands

³ Mathematical Institute, Leiden University, Leiden, the Netherlands



**COMPUTATIONAL SCREENING OF TIP AND
STALK CELL BEHAVIOR PROPOSES A ROLE FOR
APELIN SIGNALING IN SPROUT PROGRESSION**

INTRODUCTION

Angiogenesis, the formation of new blood vessels from existing vessels, is important in numerous mechanisms in health and disease, including wound healing and tumor development. As a natural response to hypoxia, normal cells and tumor cells secrete a range of growth factors, including vascular endothelial growth factors (VEGFs) and fibroblast growth factors (FGFs). These activate quiescent endothelial cells to secrete proteolytic enzymes, to migrate from the blood vessel and organize into an angiogenic sprout. Angiogenic sprouts are led by tip cells, a highly migratory, polarized cell type that extends numerous filopodia (1). Tip cells express high levels of the VEGF receptor VEGFR2 (1), Delta-like ligand 4 (Dll4) (2) and, *in vitro*, CD34 (3). The tip cells are followed by stalk cells (1), a proliferative and less migratory type of endothelial cell, which expresses low levels of Dll4 (2) and, *in vitro*, have undetectable levels of CD34 (3).

4.1

The behavior of tip and stalk cells during angiogenic sprouting has been well characterized in mouse retina models and in endothelial spheroids (4, 5). From a mechanistic point of view, however, it is not well understood why two types of endothelial cells are involved in angiogenesis. Experimental and computational lines of evidence suggest that in absence of tip and stalk cell differentiation, endothelial cells can form blood-vessel like structures, albeit with abnormal morphological parameters. In cell cultures, endothelial cells organize into network-like structures, without obvious differentiation into tip and stalk cells (6, 7), although the individual endothelial cells were found to vary in other aspects of their behavior, e.g., their tendency to occupy the nodes of vascular networks (8). Computational models have suggested a range of biologically-plausible mechanisms, by which populations of identical endothelial cells can self-organize into vascular network-like structures (9-15) and sprout-like structures can form in endothelial spheroids (11, 12, 16). Experimental interference with tip and stalk cell differentiation modifies, but does not stop the endothelial cells' ability to form networks. In mouse retinal vascular networks, inhibition of Notch signaling increases the number of tip cells and produces denser and more branched vascular networks (17-19), while in gain-of-function experiments of Notch the fraction of stalk cells is increased, producing less extensive branching (17). *In vitro*, similar effects of altered Notch signaling are observed (20-22). Taken together, these observations suggest that differentiation between tip and stalk cells is not required for vascular network formation or angiogenic sprouting. Instead they may fine-tune angiogenesis, e.g., by regulating the number of branch points in vascular networks.

The exact mechanisms that regulate the differentiation of tip and stalk cell fate are subject to debate. Activation of the VEGFR2 by VEGF-A, which is secreted by hypoxic tissue, upregulates Dll4 expression (19, 23-25). Dll4 binds to its receptor Notch in adjacent endothelial cells, where it induces the stalk cell phenotype (26), which includes downregulation of Dll4. The resulting lateral inhibition mechanism, together with increased VEGF signaling close to the sprout tip, may stimulate endothelial cells located

at the sprout tip to differentiate into tip cells “in place”. Detailed fluorescent microscopy of growing sprouts *in vitro* and *in vivo* shows that endothelial cells move along the sprout and “compete” with one another for the tip position (4, 5). Endothelial cells expressing a lower amount of VEGFR2, and therefore producing less Dll4, are less likely to take the leading tip cell position, while cells that express less VEGFR1, which is a decoy receptor for VEGFR2 (27, 28), are more likely to take the tip cell position (4). These results suggest that the VEGF-Dll4-Notch signaling loop is constantly re-evaluated and thereby tip cell fate is continuously reassigned. A series of recent observations, however, support an opposing view in which tip cells differentiate more stably. Tip cells express the sialomucin CD34, making it possible to produce “tip cell” (CD34⁺) and “stalk cell” (CD34⁻) cultures using fluorescence-activated cell sorting (FACS) (3). CD34⁺ cells have a significantly lower proliferation rate than CD34⁻ cultures during the first 48 hours, suggesting that during this time they do not redifferentiate into stalk cells. In cultures of CD34-negative endothelial cells (stalk cells), the wild-type ratio of tip and stalk cells reestablishes only after around ten days. Thus within the time frame of *in vitro* vascular network formation of around 24 to 48 hours (29) cross-differentiation between tip and stalk cells is relatively rare. These data suggest that the differentiation between tip and stalk cells depends on a balance between (a) lateral inhibition via the Dll4-Notch pathway (17-19, 30), and (b) a stochastically “temporary stabilized” tip or stalk cell fate, potentially correlated with CD34 expression (3).

To develop new hypotheses on the role of tip and stalk cell differentiation during angiogenesis, we developed an explorative approach inspired by Long *et al.* (31) who used a genetic algorithm to identify the transition rules between endothelial cell behaviors that could best reproduce *in vitro* sprouting. Here we use a cell-based, computational model of angiogenesis (11) that is based on the Cellular Potts model (CPM) (32, 33). We extend the model with tip and stalk cell differentiation, and systematically vary the parameters of the tip cells to search for properties that make the “tip cells” behave in a biologically realistic manner: i.e., they should move to the sprout tip and affect the overall branching morphology. We consider both a “pre-determined” model in which ECs are stably differentiated into tip and stalk cells throughout the simulation time of the model, and a “lateral inhibition” model, in which tip and stalk cells cross-differentiate rapidly via Dll4-Notch signaling. We compare the tip cell properties that our model predicts with differential gene expression data, and perform initial experimental tests for the resulting gene candidate *in vitro*.

RESULTS

To develop new hypotheses on the role of tip cells during angiogenesis, we took the following “agnostic” approach that combines bottom-up modeling, bioinformatical analysis and experimental validation. We started from a previously published computational model of de novo vasculogenesis and sprouting angiogenesis (11). Briefly,

the model simulates the formation of sprouts and vascular networks from a spheroid of identical “endothelial cells”, driven by an autocrine, diffusive chemoattractant that drives endothelial cells together (see Ref. (11) and methods section for details). In the first step, we assumed that a fraction of the cells are “tip cells” (tip cell fraction) and the remaining cells are “stalk cells”, hence assuming that cross-differentiation between tip and stalk cells does not occur over the course of the simulation. We next systematically varied the model parameters of the tip cells to look for cell behavior that (a) takes the tip cells to the sprout tips, and (b) changes the morphology of the simulated vascular networks formed in the model. The predicted differences between tip cell and stalk cell behavior were then expressed in gene ontology terms, so as to compare them with published gene expression differences between tip and stalk cells (3). The analysis yielded a gene candidate that was further tested in an *in vitro* model of spheroid sprouting.

As a computational model for angiogenesis, we used our previous cell-based model of de novo vasculogenesis and sprouting angiogenesis (11). The model assumes that endothelial cells secrete an autocrine, diffusive chemoattractant to attract one another. Due to the resulting attractive forces between the endothelial cells, the cells aggregate into a spheroid-like configuration. If the chemoattractant sensitivity of the endothelial cells is restricted to the interfaces between the endothelial cells and the surrounding ECM by means of a contact inhibition mechanism, the spheroids sprout in microvascular-network-like configurations. Although our group (12, 15, 34) and others (9, 10, 13, 35-37) have suggested numerous plausible alternative mechanisms for de novo vasculogenesis and sprouting, in absence of a definitive explanatory model of angiogenesis we have selected the contact inhibition model for pragmatic reasons: It agrees reasonably well with experimental observation (11, 38), it focuses on a chemotaxis mechanism amenable to genetic analysis, and it has a proven applicability in studies of tumor angiogenesis (39), age-related macular degeneration (40), and toxicology (41).

The computational model is based on a hybrid, cellular Potts and partial differential equation model (32, 33, 42). The cellular Potts model (CPM) represents biological cells as patches of connected lattice sites on a finite box Λ of a regular 2D lattice $Z \subset Z^2$ with each lattice site $\vec{x} \in \Lambda$ containing a *cell identifier* $\sigma \in Z^{+0}$ that uniquely identifies each cell. Each cell σ is also associated with a cell type $\tau(\sigma) \in \{tip, stalk, ECM\}$. To mimic amoeboid cell motility the method iteratively attempts to move the interfaces between adjacent cells, depending on the amplitude of active membrane fluctuations (expressed as a “cellular temperature” (43) $\mu(\tau)$) and on a force balance of the active forces the cells exert on their environment (e.g. due to chemotaxis or random motility) and the reactive adhesive, cohesive and cellular compression forces. Assuming overdamped motility, the CPM solves this force balance as a Hamiltonian energy minimization problem (see Methods section for details).

The angiogenesis model includes the following endothelial cell properties and behaviors: cell-cell and cell-matrix adhesion, volume conservation, cell elasticity, and

chemotaxis at cell-ECM interfaces. To describe cell-cell adhesion we define a contact energy $J(\tau, \tau')$ that represents the interfacial tension between cells of type τ and τ' . This term lumps contributions due to cell-cell adhesion (44) and cortical tensions (45). We assume that cells resist compression and expansion by defining a resting area $A(\tau)$. In practice the cells fluctuate slightly around their resting area depending on the elasticity parameter $\lambda(\tau)$. The cells secrete a diffusive chemoattractant c at a rate $\alpha(\tau)$, with $\frac{\partial c}{\partial t} = D\nabla^2 c - \epsilon(\tau)c + \alpha(\tau)$, where D is a diffusion coefficient, ϵ is a degradation rate, which is zero inside cells, and $\alpha(ECM) = 0$. Chemotaxis at cell-ECM interfaces is incorporated by biasing active cell extension and retractions up chemoattractant with a factor $\chi(\tau)$, which is the chemoattractant sensitivity.

We start the analysis from the set of nominal parameters listed in Table 1; these yield the nominal collective cell behavior shown in Figure 1A. The parameters are set according to experimental values as far as possible. The cross-sectional area of the endothelial cells in the cell cultures was $360 \pm 100 \mu\text{m}^2$ (see Methods for detail), based on which we set the target area of the cells, $A(\text{tip})$ and $A(\text{stalk})$, to 100 lattice sites, corresponding with $400 \mu\text{m}^2$. The diffusion coefficient, secretion rate and degradation rate of the chemoattractant were set equal to those used in our previous work (11); note that the diffusion coefficient is set to a value lower than the one, e.g., reported for VEGF in watery conditions ($10^{-11} \text{m}^2/\text{s}$; see Ref. [36]) because of its binding to ECM proteins (46). In absence of detailed experimental data on EC cell-cell and cell-ECM adhesive forces, cell stiffness, and the chemotactic response, for the corresponding parameters we used the values from Ref. (11); the exact values of these parameters do not qualitatively affect the results of the model, and have modest quantitative impact; for a detailed sensitivity analysis see Refs. (11, 47).

Table 1. Parameter values for the angiogenesis and tip cell selection model. Underlined parameters are varied in the screen for tip cell behavior

Symbol	Description	value
$\mu(\text{tip}), \mu(\text{stalk})$	cell motility	50
$J(\text{tip}, \text{stalk}), J(\text{tip}, \text{tip}), J(\text{stalk}, \text{stalk})$	cell-cell adhesion	40
$J(\text{tip}, \text{ECM}), J(\text{stalk}, \text{ECM})$	cell-ECM adhesion	20
$A(\text{tip}), A(\text{stalk})$	target area	$400 \mu\text{m}^2$
$\lambda(\text{tip}), \lambda(\text{stalk})$	elasticity parameter	25
$\chi(\text{tip}), \chi(\text{stalk})$	chemoattractant sensitivity	500
$\alpha(\text{tip}), \alpha(\text{stalk})$	chemoattractant secretion rate	10^{-3}s^{-1}
$\epsilon(\text{ECM})$	chemoattractant decay rate in ECM	10^{-3}s^{-1}
$\epsilon(\text{tip}), \epsilon(\text{stalk})$	chemoattractant decay rate below cells	0s^{-1}
D	chemoattractant diffusion coefficient	$10^{-13} \text{m}^2 \text{s}^{-1}$

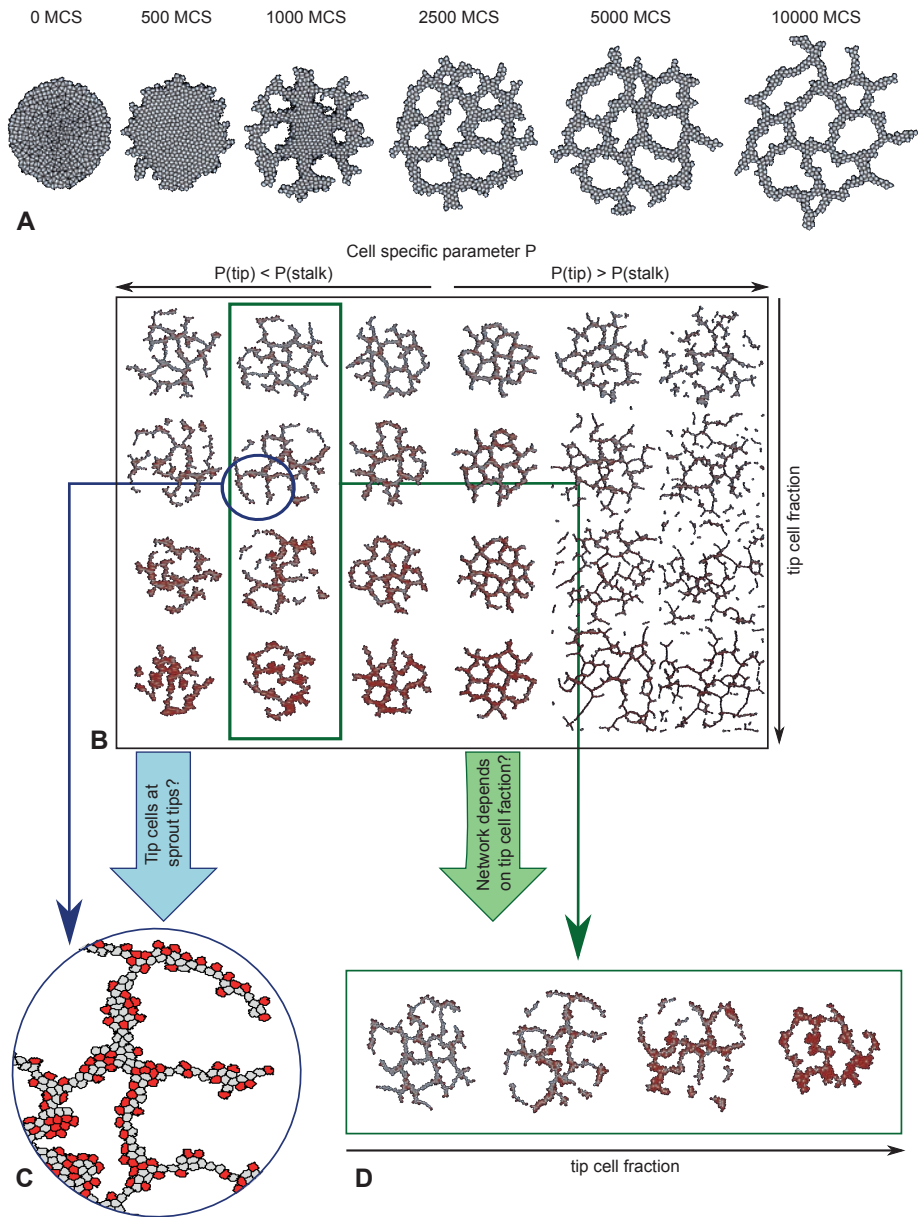


Figure 1. Overview of the angiogenesis model and the parameter search. **A** Time-lapse of angiogenesis model behavior **B** For each parameter P that is tested in the parameter search a morphospace is created to compare the different parameter values for different tip cell fractions. **C** Each morphology is studied in detail to see if the sprout tips are occupied by tip cells (red). **D** Each row of morphologies is studied to find rows in which the morphologies change, indicating that network formation depends on the tip cell fraction.

Computational screening for putative tip cell behavior

We set up a screen for differences in the parameters of tip cells and stalk cells that affect the outcome of the model. In particular, we looked for parameters for which the tip cells lead sprouts in such a way that it affects the network morphology. In the angiogenesis model, a fraction (F_{tip}) of the endothelial cells is assumed to be the “tip cell”, $\tau(\sigma) = tip$, and the remaining fraction $1 - F_{tip}$ is set to $\tau(\sigma) = stalk$. We assigned the nominal parameters shown in Table 1 to both “tip cells” ($\tau(\sigma) = tip$) and “stalk cells” ($\tau(\sigma) = stalk$). We varied the underlined parameters in Table 1 to change the behavior of “tip cells” and ran the simulation for 10 000 time steps for a series of tip cell fractions and a series of parameters. The behavior of “stalk cells” was fixed because the nominal parameters, which were thoroughly studied in our previous work (11), are based on *in vitro* experiments in which no stalk cells were observed.

To keep this initial analysis computationally feasible, we tested only one parameter at a time instead of searching through the complete parameter space (see Ref. (47) for more systematic parameter study of the initial, single-cell-type model, based on a SOBOL-analysis). Also, in this initial screening we have limited the analysis to parameters that we could possibly associate directly with differentially expressed genes in tip and stalk cells. For this reason, we have omitted cell size differences, and we fixed the tip-tip cell adhesion strength. Figure 1B illustrates a typical range of morphologies, or *morphospace*, that we obtained in this way. We analyzed the position of tip cells in each morphology (Figure 1C) and analyzed the morphology of the vascular network in function of the tip cell fraction, F_{tip} .

To evaluate whether tip cells occupy sprout tips, we simulated the model with a tip cell fraction of $F_{tip} = 0.2$, in accordance with published observations: 11.9% in a HUVEC monolayer (3) and ~30% in the growing of the retinal vasculature (17). Because we assume that tip cell fate is strongly inhibited in a monolayer and tip cells are overexpressed in the growing front, we set the tip cell fraction at 20%, which is roughly the average of the two. At the end of each simulation we detected sprouts with tip cells on the tip using an automated method, as detailed in the methods section. We then counted the percentage of sprouts with at least one tip cell at the sprout tip. If more sprout tips were occupied by a tip cell than in the control experiment with identical tip and stalk cells, the parameter values were retained for further analysis.

Figure 2 shows the percentage of sprout tips occupied by one or more tip cells for all parameters tested. More sprouts are occupied by tip cells that: (a) are less sensitive to the autocrine chemoattractant than stalk cells ($\chi(tip) < \chi(stalk)$), (b) adhere more strongly to the ECM than stalk cells ($J(tip, ECM) < J(stalk, ECM)$), (c) adhere stronger to stalk cells than stalk cells to stalk cells ($J(tip, stalk) < J(stalk, stalk)$), (d) secrete the chemoattractant at a lower rate than stalk cells ($\alpha(tip) < \alpha(stalk)$), or (e) have a higher active motility than stalk cells ($\mu(tip) > \mu(stalk)$). For the parameters associated with cell-cell and cell-ECM adhesion, we observed a non-monotonic trend in Figure 2. A slight

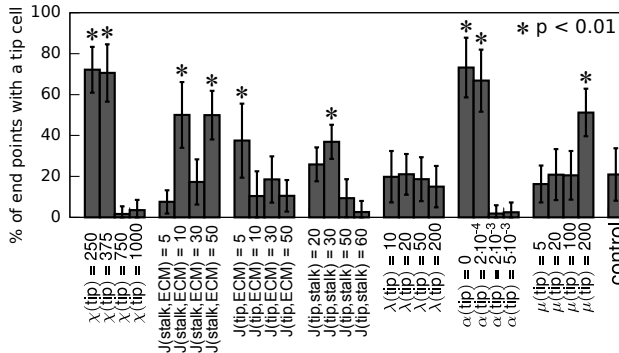


Figure 2. Differences in cell properties can enable cells of one type to occupy sprout tips. The percentage of sprout tips occupied by at least one tip cell was calculated at 10 000 MCS and averaged over 50 simulations (error bars depict the standard deviation). In each simulation 20% of the cells were predefined as tip cells. For each simulation one tip cell parameter was changed, except for the control experiment where the nominal parameters were used for both tip and stalk cells. p-values were obtained with a one sided Welch’s t-test for the null hypothesis that the number of tip cells at the sprout tips is not larger than in the control simulation.

change in an adhesion parameter would affect the relative positions of tip and stalk cells, whereas a larger change can completely change the morphology of the network. For example, if the tip cells adhere slightly more strongly to the ECM than the stalk cells, the tip cells tend to be pushed to the sprout tip (A). The stalk cells surround the tip cells if they adhere much more strongly to the ECM than the tip cells do (B), an effect that differential chemotaxis counteracts. In these simulations, the tip cells tended to cluster together. Because tip cells do not cluster together (1), we excluded reduced stalk-ECM adhesion from further analysis.

Out of the cell behaviors that turned out to make cells move to the sprout tips, we next selected cell behaviors that also affect network morphology. We quantified network morphology using two measures. The *compactness*, $C = A_{cluster} / A_{hull}$ is the ratio of the area of the largest cluster of connected cells, $A_{cluster}$, and the area of the convex hull enclosing the connected cluster, A_{hull} (11). It approaches $C = 1$ for a disk and tends to $C \rightarrow 0$ for a sparse network. We also counted the number of “gaps” in the network, or lacunae, $N_{lacunae}$. For details see the Methods section.

Figures 3A-F takes a selection of the tip cell parameters identified in the previous section, and then plots the compactness C (black curves) and the number of lacunae $N_{lacunae}$ (blue curves) as a function of the tip cell fraction. The results for the remaining parameter value are shown in (S1 Fig). For each tip cell fraction tested, the outcome is then compared with simulations in which the tip cells were identical to the stalk cells (i.e., as in Figure 1A). Closed symbols indicate a significant difference with the respective reference simulation (Welch’s t-test, $p < 0.05$, $n = 10$). Tip cell parameters that affected

network morphologies for at least half of the tip cell fractions tested were kept for further analysis.

The screening selected three ways in which tip cells could differ from stalk cells to change network morphology: reduced chemoattractant sensitivity ($\chi(\text{tip}) < \chi(\text{stalk})$; see Figure 3A), reduced chemoattractant secretion by tip cells ($\alpha(\text{tip}) < \alpha(\text{stalk})$; see Figure 3E), and increased tip-ECM adhesion ($J(\text{stalk}, \text{ECM}) > J(\text{tip}, \text{ECM})$; see Figures 3B-C). It turned out that increased ECM adhesion by tip cells was best modeled by reducing the adhesion of stalk cells with the ECM instead ($J(\text{stalk}, \text{ECM})$), because for $J(\text{tip}, \text{ECM}) = 5$ (Figure 3C) networks could not form with too many tip cells (see).

The results of the screening held for the other parameter values tested (S1 Fig) with two exceptions: (1) the networks disintegrated if tip cells did not respond sufficiently strongly to the chemoattractant ($\chi(\text{tip}) < 100$ (J)), and (2) the tip cells spread out over the stalk cells to cover the whole network for $J(\text{stalk}, \text{ECM}) > 70$ (K). Also, the conclusions were confirmed in a screening relative to three additional nominal parameter sets (and).

Altogether, the computational screening presented in this section identified three tip cell parameters that affect tip cell position in the sprout and the morphology of the networks formed in our computational model: reduced secretion of the chemoattractant, reduced sensitivity to the chemoattractant, and increased tip-ECM adhesion. It is possible, however, that these effects are due to spatial or temporal averaging of tip and stalk cell parameters, not due to interaction of two different cell types. The next section will introduce a control for such effects.

Comparison with control model selects “reduced chemoattractant sensitivity” scenario for further analysis

The computational screening highlighted three tip cell parameters that affected both the position of tip cells in the sprouts and the morphology of the networks: (1) increased tip-cell ECM adhesion, (2) reduced chemoattractant secretion by tip cells, and (3) reduced chemoattractant sensitivity of tip cells. Because it was unsure whether these effects were due to (a) the differential cell behavior of tip and stalk cells, or (b) due to temporal or spatial averaging of the parameters differentially assigned to tip and stalk cells, we compared the results against a control model that had only one cell type with “averaged” parameters: $P(\text{cell}) = (1 - F_{\text{tip}}) \cdot P(\text{stalk}) + F_{\text{tip}} \cdot P(\text{tip})$, with $P(\text{tip})$ the tip cell parameter value and $P(\text{stalk})$ the stalk cell parameter value.

For each of the three parameters identified in the first step of the computational screening, we compared the morphologies formed in the control model after 10000 MCS with the morphologies formed in the original model with mixed cell types (Figure 4). Figures 4A,F, and K show example configurations formed in the original model, in comparison with example configuration formed in the corresponding “averaged” model (Figures 4B,G, and L). In the “mixed” model the tip cells (red) tend to move to the periphery of the branches, in contrast to the “averaged” model in which all cells have the same parameter values.

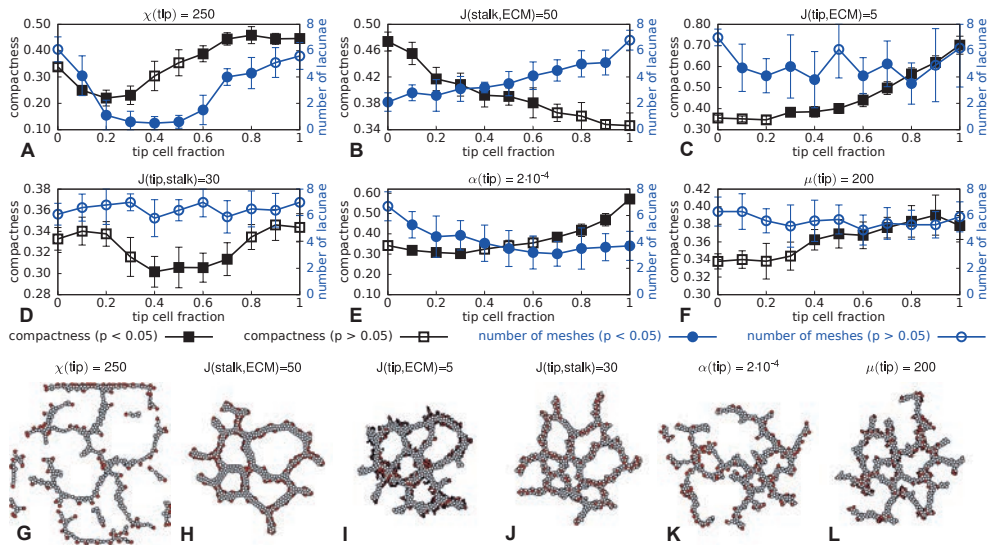


Figure 3. Effects of different tip and stalk cell properties on network morphology. **A-F** Trends of compactness (black rectangles) and number of lacunae (blue circles) calculated with the morphologies at 10 000 MCS. For each data point 10 morphologies were analyzed and the error bars represent the standard deviation. p-values were obtained with a Welch’s t-test for the null hypothesis that the mean of the sample is identical to that of a reference with the nominal parameters listed in Table 1. For **B** this reference is the data for tip cell fraction 1 and for all other graphs this is the data for tip cell fraction 0. **G-L** Morphologies after 10 000 MCS for each tested parameter value with $F_{\text{tip}} = 0.2$.

We next tested if networks formed in the “mixed” model differed from those formed in the corresponding “averaged” model for tip cell fractions ranging from 0 (no tip cells) to 1 (only tip cells). Although the measures differed for individual morphometrics and tip cell fractions in all three scenarios (Figure 4C-E, H-J, M-O), only in the model where tip cells had reduced chemoattractant sensitivity all morphometrics differed significantly for practically all tip cell fractions tested (Figure 4M-O). The analysis was repeated for three additional parameter values per scenario (S5 Fig); although in all three scenarios the morphometrics differed between the “mixed” and “averaged” models for a number of tip cell fractions, only in the “reduced chemoattractant sensitivity” scenario the differential behavior of tip and stalk cells consistently affected the morphometrics. We thus retained only this model for further analysis.

Heterogeneous chemoattractant sensitivity increases direction persistence of migrating tip and stalk cell pairs

The parameter screening indicated that tip cells that are less sensitive to the chemoattractant than stalk cells tend to move to the front of the sprouts, affecting in this way the network morphology. To better understand now such differential chemoattractant sensitivity can affect angiogenic sprouting, we analyzed the migration of a cell pair consisting of one

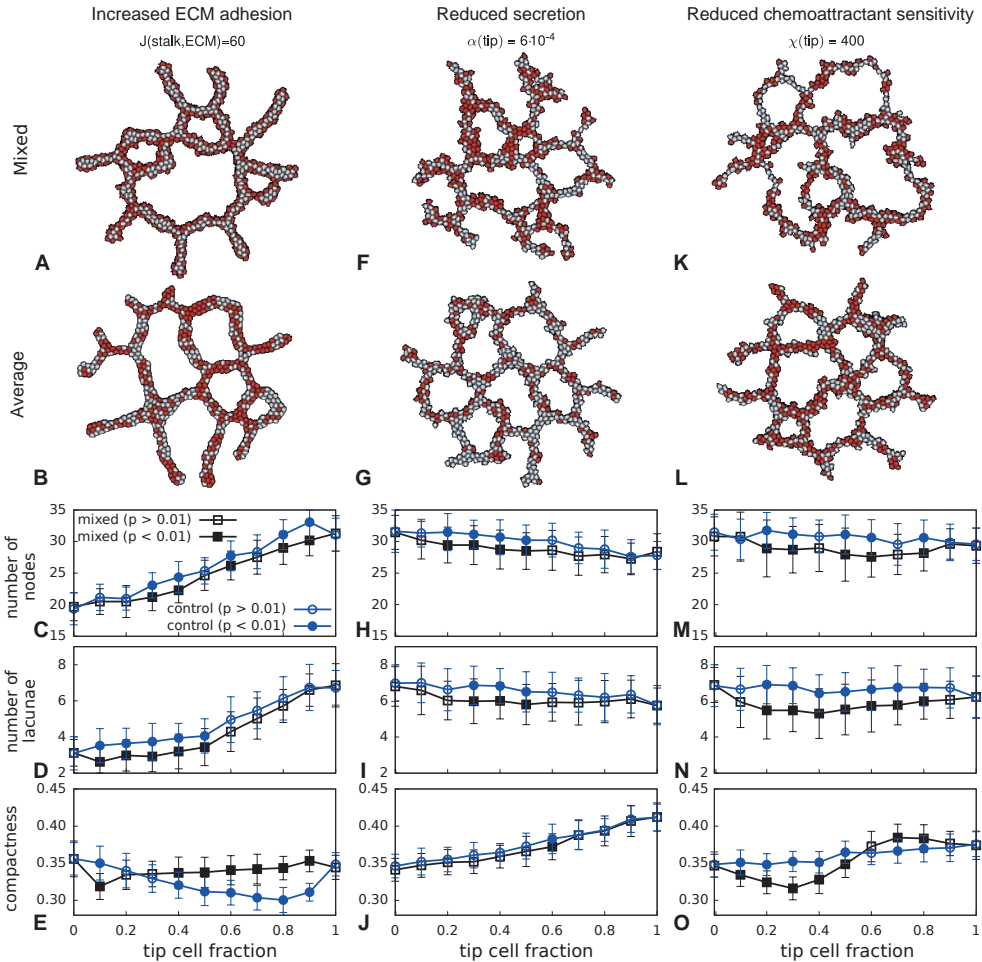


Figure 4. Comparison of networks formed with mixed cells and cells with average properties. **A, F,** and **K** morphologies for mixed tip (red) and stalk (gray) cells ($F_{\text{tip}} = 0.5$). **B, G,** and **L** morphologies for averaged cells ($F_{\text{tip}} = 0.5$). **C-E, H-J,** and **M-O** morphometrics for a range of tip cell fractions for both the control and mixed model. The morphometrics were calculated for 50 simulations at 10 000 MCS (error bars represent the standard deviation). p -values were obtained with a Welch's t -test for the null hypothesis that the mean of mixed model and the control model are identical.

tip cell and one stalk cell. As shown in Figure 5A-C, cell pairs with a large difference in the chemoattractant sensitivity migrated much further than cell pairs with a smaller or no difference in chemoattractant sensitivity. To quantify this observation, we used the McCutcheon index (48), which is the ratio of the distance between the initial and final position, and the total path length. As shown in Figure 5D, the McCutcheon index decreases as the tip cell's chemoattractant sensitivity approaches that of the stalk cell. Indicating that a strong difference in chemotaxis causes the cell pair to move along a straighter path. These results suggest that, in a self-generated gradient, heterogeneous

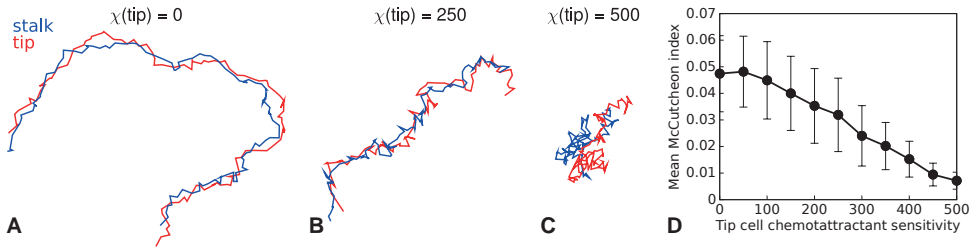


Figure 5. Migrating cell pair consisting of a stalk cell and a tip cell with a reduced chemoattractant sensitivity. **A-C** Trajectories of the tip and stalk cell during 10 000 MCS with $\chi(\text{stalk})=500$ and respectively $\chi(\text{tip})=0$, $\chi(\text{tip})=250$, and $\chi(\text{tip})=5000$. **D** McCutcheon index as a function of the tip cell chemoattractant sensitivity. The values were averaged over 100 simulations and error bars depict the standard deviation.

chemoattractant sensitivity improves migration speed and persistence. In the context of angiogenesis, this effect speeds sprouting and sprout elongation.

Local tip cell selection regularizes network morphology

In the parameter screenings presented in the previous sections, to a first approximation we assumed that a subpopulation of endothelial cells are “predetermined” to become tip cells, e.g., due to prior expression of CD34 (3). It is likely, however, that tip cell fate is continuously “re-evaluated” in a Dll4-Notch-VEGFR2 signaling loop (17-19, 30). Tip cells express Dll4 on their cell membranes (2), which binds to the Notch receptor on adjacent cell membranes. This leads to the release of the Notch intracellular domain (NICD), activating the stalk cell phenotype (17, 30). Via this lateral inhibition mechanism, cells adjacent to tip cells tend to differentiate into stalk cells. To simulate such “dynamic tip cell selection”, a simplified genetic regulatory network (GRN) model of Dll4-Notch signaling was added to each simulated cell, as described in detail in section Methods. Briefly, the level of NICD in each cell is a function of the amount of Dll4 expressed in adjacent cells, weighed according to the proportion of the cell membrane shared with each adjacent cells. If the concentration of NICD $N(\sigma)$ of a tip cell σ exceeds a threshold $N(\sigma) > \Theta_{NICD}$, the cell cross-differentiates into a stalk cell; conversely, if in a stalk cell $N(\sigma) \leq \Theta_{NICD}$ it differentiates into a tip cell (17, 18, 30).

Figure 6 shows the behavior of the initial ‘static model’ (Figures 6A-F) in comparison with the ‘dynamic tip cell selection’ model (Figures 6G-L). In the dynamic model the tip cell fraction was set using the values of Θ_{NICD} , such that the exact tip cell fractions depended on the local configurations. In comparison with the initial, ‘static’ model (Figure 6A-F), the model with ‘dynamic’ selection (Figure 6G-L and) seems to form more compact and regular networks. To quantify this difference in network regularity, we determined the variation of the areas of the lacunae of the networks at the final time step of a simulation. Figure 6M shows this measurement averaged over 50 simulations for a range of tip cell fractions. Lacunae in networks formed from mixtures of stalk cells and

10% to 60% 'static' tip cells have more variable sizes than lacunae in networks formed by the 'dynamic tip cell' model.

To further analyze how dynamic tip cell selection regularized network morphologies in our model, we studied in detail how tip cells contributed to network formation in the 'static' and 'dynamic' tip cell models. Figure 6N-Q shows the evolution of a part of a network formed with 20% 'static tip cells'. At first, some tip cells locate at sprout tips and others are located adjacent to or within the branches (Figure 6N). The chemoattractant gradually accumulates 'under' the branches, with a curvature effect producing slightly higher concentrations at the side of the lacunae. This attracts the stalk cells (Figure 6O), 'squeezing' the tip cells out of the branch and away from the lacuna, due to their reduced chemoattractant sensitivity (Figure 6P and). The resulting layered configuration with tip cells at the outer rim drives a drift away from the lacuna (Figure 6Q): Due to their stronger chemoattractant sensitivity, the stalk cells attempt to move to the center of the configuration, pushing the tip cells away, thus leading to directional migration driven by the mechanism outlined in the previous section (see also Ref. (49)).

In the 'dynamic tip cell selection' mechanism, the persistent migration will be confined to the sprout tips. The model thus suggests that tip cells could assist in producing a local, self-generated gradient mechanism that directs the migration of sprouts, a mechanism that requires tip cells to differentiate only at sprout tips. For tip cells to "drag" just the sprouts, only a limited number of tip cells must be present in the network. To test this idea, we compared network morphologies for the 'dynamic' and the 'static' tip cell models for a range of tip cell fractions (Figure 6R-T). Indeed, the network morphologies were practically identical for high tip cell fractions, whereas they differed significantly for all three morphometrics for tip cell fractions between 0.1 and 0.3: In the dynamic selection model the networks become more disperse (Figure 6R) and formed more branches (Figure 6S) and lacunae (Figure 6T) than in the 'static' model.

To validate the 'dynamic' tip cell model, we compared the effect of the tip cell fraction on network morphology with published experimental observations. The *in vivo*, mouse retinal angiogenesis model is a good and widely used model for tip/stalk cell interactions during angiogenesis (4, 5, 17-19, 23, 44, 50, 51). Networks formed with an increased abundance of tip cells become more dense and form a larger number of branches (17-19, 23) than wild type networks. Our computational model is consistent with this trend for tip cell fractions between 0 and up to around 0.2 (Figure 6R-T), but for tip cell fractions >0.2 the vascular morphologies become less branched (Figure 6S-T). To investigate in more detail to what extent our model is consistent with these experimental observations, we tested the effect of the tip cell fraction in the 'dynamic' tip cell selection model in more detail. In particular we were interested in how the difference in chemoattractant sensitivity between tip and stalk cells affected network morphology. Figure 7 shows the effect of the NICD threshold (increasing the NICD threshold is comparable to inhibiting Dll4 expression or Notch signaling, and hence controls the tip cell fraction) for a range of tip cell chemoattractant sensitivities. When the difference

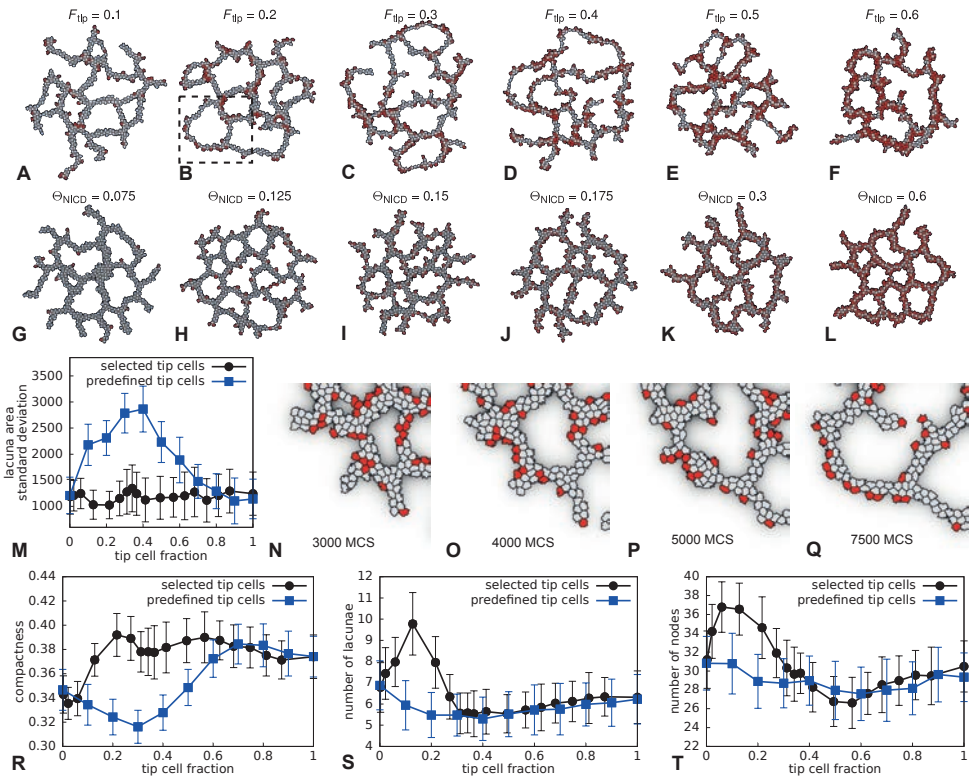


Figure 6. Effects of tip cell selection on network formation. **A-F** Networks formed with varying fractions of predefined tip cells (F_{tip}) with $\chi(\text{tip})=400$ at 10 000 MCS. **G-L** Networks formed with the tip cell selection model for varying NICD thresholds ($\sim \Theta_{NICD}$) at 10 000 MCS. **M** Standard deviation of lacuna area in a network after 10 000 MCS. **N-Q** Close up of the evolution of a network with 20% predefined tip cells (marked area in **B**). **R-T** Comparison of the morphometrics for networks formed with predefined and selected tip cells with reduced chemoattractant sensitivity ($\chi(\text{tip})=400$) and network at 10 000 MCS. For the simulations with tip cell selection, the average tip cell fraction was calculated for each NICD threshold. For all plots (**M** and **R-T**) the values were averaged over 50 simulations and error bars depict the standard deviation.

in the chemoattractant sensitivity between tip and stalk cells is relatively small ($\chi(\text{tip}) \geq 300$), increasing the NICD threshold results in the formation of denser network with fewer lacunae. In contrast, when the difference in chemoattractant sensitivity between tip and stalk cells is larger ($\chi(\text{tip}) \leq 200$), there exists an intermediate state in which the networks are both compact and have a large number of branch points (Figure 7A4 and 7B4). This intermediate state resembles the dense, highly connected networks that are observed when tip cells are abundant in the mouse retina (17-19, 23). Thus, when the difference in the chemoattractant sensitivity of tip and stalk cells is sufficiently large, the model can reproduce both normal angiogenesis and the excessive angiogenic branching observed for an abundance of tip cells (17).

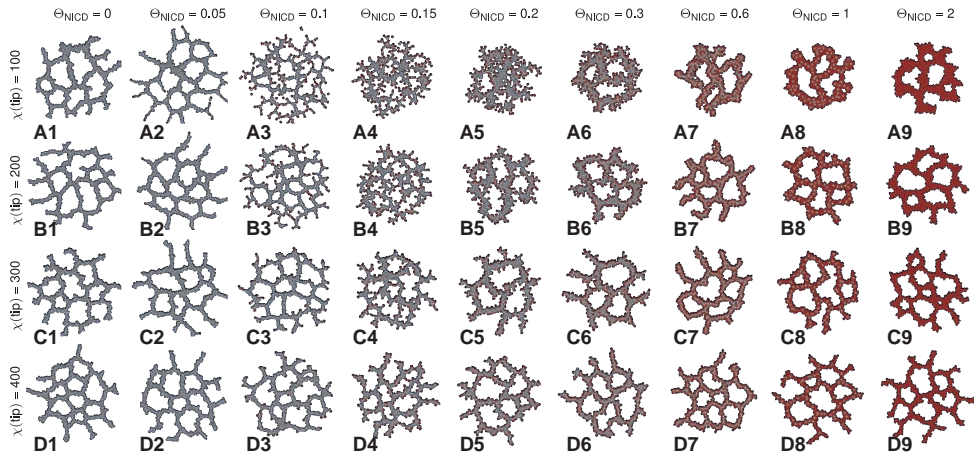


Figure 7. Effects of reducing tip cell chemoattractant sensitivity for varying NICD thresholds. Morphospace of the final morphologies (10 000 MCS) with varying tip cell chemoattractant sensitivities ($\chi(\text{tip})$) and NICD thresholds (θ_{NICD}).

4.1

Survey for chemoattractant receptors reduced in tip cells suggests Apelin as candidate

The comparative, computational model analysis of the role of tip cells in angiogenesis, predicted that—among the models tested—a model where tip cells show reduced sensitivity to an autocrine chemoattractant best matches tip cell phenomenology: The tip cells lead the sprouts, and facilitate the formation of vascular networks of regular morphology for tip cell fractions of up to around 0.2. Could a chemoattractant with these, or very similar properties be involved in vascular development? To answer this question, we evaluated four comparative studies of gene expression in tip and stalk cells (3, 52-54). These studies identified three receptors involved in endothelial chemotaxis that were differentially expressed in tip cells and stalk cells: VEGFR2, CXCR4, and APJ. VEGFR2 is upregulated in tip cells (3, 44, 52). VEGFR2 is a receptor for the chemoattractant VEGF that is secreted by hypoxic tissue (55). Whether or not VEGF is secreted at sufficiently high levels to act as an autocrine chemoattractant between ECs has been under debate (11, 56, 57), with the emerging being that it is most likely a long-range guidance cue of angiogenic sprouts secreted by hypoxic tissues ((1); reviewed in Ref. (58)). The chemokine CXCL12 and its receptor CXCR4 (59) are both upregulated in tip cells (3, 52, 54), suggesting that tip cells would have higher, not lower sensitivity to CXCL12 signaling than stalk cells. Interestingly, CXCL12 and CXCR4 are key components of a self-generated gradient mechanism for directional tissue migration in the lateral line primordium mechanisms (49). Because of the key role of CXCL12/CXCR4 in angiogenesis (see, e.g., (60)) it is therefore tempting to speculate that CXCL12/CXCR4 may be part of a similar, self-generated gradient mechanism during angiogenesis.

However, because CXCL12 expression is upregulated in tip cells relative to stalk cells, not downregulated, we will focus here on a third receptor/ligand pair differentially expressed in tip and stalk cells: APJ and Apelin. APJ is a receptor for the endothelial chemoattractant Apelin (61-63) that is secreted by endothelial cells (62, 63). Apelin expression is upregulated in tip cells (3, 53, 54), whereas its receptor APJ is not detected in tip cells (53). Thus the expression pattern of Apelin and its receptor APJ fits with our model prediction: Apelin is an endothelial chemoattractant that is secreted by endothelial cells and tip cells are less responsive to Apelin than stalk cells. In our model the chemoattractant is secreted at the same rate by tip and stalk cells, whereas Apelin is preferentially expressed in tip cells. The next section will therefore add preferential secretion of Apelin by tip cells to the model, and test if and how this changes the predictions of our model.

Model refinement to mimic role of Apelin/APJ more closely

The computational analyses outlined in the previous sections suggest that Apelin and its receptor APJ might act as an autocrine chemoattractant in the way predicted by our model: Both stalk cells and tip cells secrete Apelin and APJ (62, 63) and the tip cells do not express the APJ receptor (53). Gene expression analyses (3, 53) also suggest that tip cells secrete Apelin at a higher rate than stalk cells. We therefore tested if the simulation results still held if we changed the model assumptions accordingly: In addition to a reduced chemoattractant sensitivity in tip cells ($\chi(\text{tip})=100$), we assumed tip cells secrete chemoattractant at a higher rate than stalk cells: $\alpha(\text{tip}) > \alpha(\text{stalk})$. Although the absence of APJ expression in tip cells suggests that tip cells are insensitive to the chemoattractant, $\chi(\text{tip})=0$, to reflect the phenomenological observation that ECs are attracted to one another, we set $\chi(\text{stalk}) > \chi(\text{tip}) > 0$. Such intercellular attraction could, e.g., be mediated by cell-cell adhesion, by alternative chemoattractant-receptor pairs (e.g., CXCR4-CXCL12 (64)), or by means of mechanical EC interactions via the extracellular matrix (65). Figure 8 shows how the Apelin secretion rate in tip cells ($\alpha(\text{tip})$) affects the morphology of the vascular networks formed in our model, as expressed by the compactness. For tip cell secretion rates of up to around $\alpha(\text{tip})=0.01$ the model behavior does not change. The networks became more compact and exhibit thicker branches for tip cell chemoattractant secretion rates of $\alpha(\text{tip}) > 0.01$. This result does not agree with the observation that Apelin promotes vascular outgrowth (62, 66). The increased compactness for $\alpha(\text{tip}) > 0.01$ is a model artifact: stalk cells were so strongly attracted to tip cells that they engulfed the tip cells and thereby inhibited the tip cell phenotype. A similar increase in compactness and branch thickness is observed in a model where tip cells are not sensitive to the chemoattractant (S6 Fig), which indicates that a too large Apelin secretion rate of tip cells destabilizes sprout elongation. Altogether, these results suggest that, if the Apelin secretion rate of tip cells does not become more than ten times larger than that of stalk cells, our model produces similar results independent of the tip cell secretion rate of Apelin.

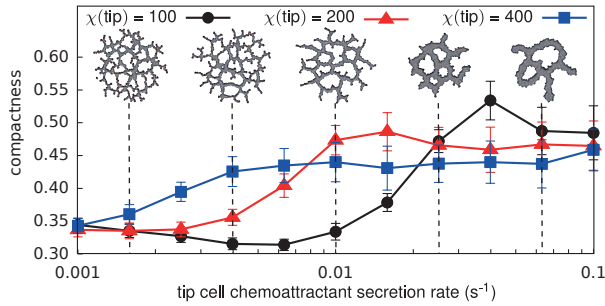


Figure 8. Effects of increasing tip cell Apelin secretion rate for varying levels of tip cell chemotaxis. Compactness of the final network (10 000 MCS) with the morphologies for $\chi(\text{tip})=100$ for tip cell Apelin secretion rates of $\alpha(\text{tip})=1.6 \cdot 10^{-3}$, $\alpha(\text{tip})=4.0 \cdot 10^{-3}$, $\alpha(\text{tip})=1 \cdot 10^{-2}$, $\alpha(\text{tip})=2.5 \cdot 10^{-2}$, and $\alpha(\text{tip})=6.3 \cdot 10^{-2}$ as insets. Except for $\alpha(\text{tip})$, all parameters have the values listed in Table 1. Data points show average values for $n = 50$ simulations with error bars giving the standard deviation.

Apelin or APJ silencing inhibits sprouting *in vitro* and *in silico*

Previous studies have shown that Apelin promotes angiogenesis of retinal endothelial cells seeded on Matrigel (62), as well as *in vivo* systems such as the mouse retina, *Xenopus* embryo, and chick chorioallantoic membrane (66). Furthermore, *in vivo* inhibition of Apelin or APJ reduced sprouting in *Xenopus* embryos (66), zebrafish (67), and the mouse retina (53, 68). To assess the relation between tip-stalk cell interaction and Apelin signaling, we inhibited Apelin signaling in an *in vitro* model of angiogenic sprouting in which the fraction of CD34⁺ (“stalk”) cells could be controlled. Spheroids of immortalized human microvascular endothelial cells (HMEC-1s) were embedded in collagen gels and in collagen enriched with VEGF. After culturing the spheroids for 24 hours at 37 degrees Celsius under 5% CO_2 , the cultures were photographed (Figure 9A-F and). The spheroids did not form network structures within the culturing time, whereas the computational model simulated both angiogenic sprouting and subsequent vascular plexus formation (Figure 1A). In order to assess the effect of Apelin and APJ silencing on sprouting in the *in vitro* and *in silico* models, we assess the morphologies formed by the *in silico* model after 750 MCS. For each model the degree of sprouting was assessed by counting the number of sprouts using the semi-automated image analysis software ImageJ. We compared sprouting in a “mixed” spheroid of HMEC-1s with a population enriched in “stalk cells”, i.e., a population of CD34⁺ HMEC-1s sorted using FACS. To inhibit Apelin signaling, the spheroids were treated with an siRNA silencing translation of Apelin (siAPLN) or of its receptor (siAPJ).

Figures 9A-F and K-L show how the number of sprouts per spheroid changes, relative to the treatment with non-translating siRNA (siNT), due to the silencing RNA treatments. To determine significance, ANOVA was performed on each data set, one for the “mixed” spheroids and one the “stalk cell” spheroids, and followed up by pairwise comparisons

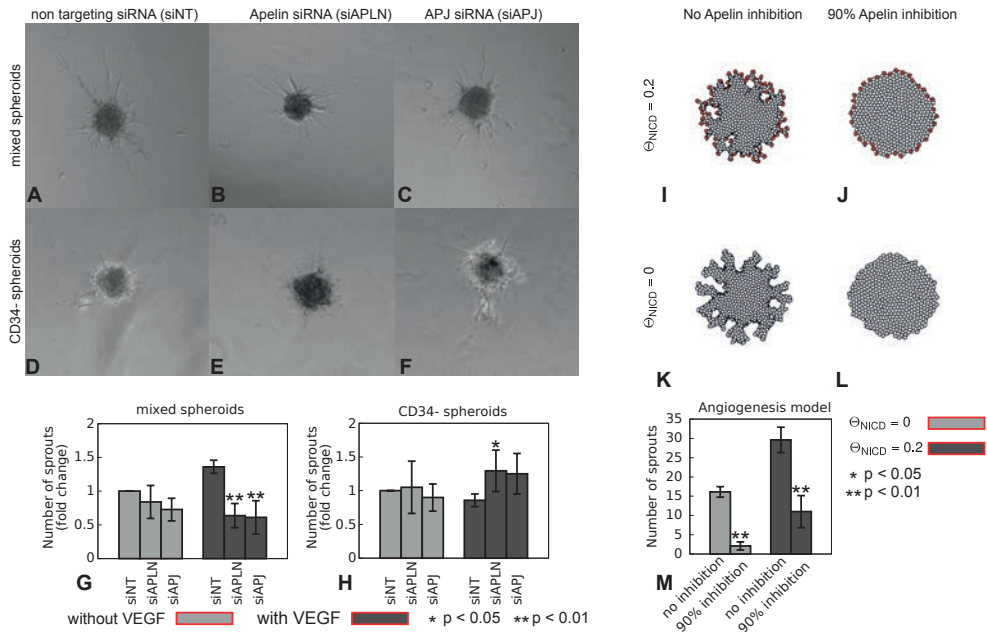


Figure 9. Effects of Apelin or APJ silencing in spheroid sprouting assays. **A-F** Microscopy images of the WT and CD34⁺ spheroids in VEGF-enriched collagen after 24 hours. **G-H** Number of sprouts, relative to siNT treatment, after 24 hours for spheroids with mixed cells and CD34⁺ spheroids. These metrics are the mean of the normalized, average number of sprouts of each replicate with the error bars depicting standard deviation. The * denotes $p < 0.05$, see the methods section for details of the normalization and statistical analysis. **I-L** Example morphologies formed in the computational angiogenesis model (750 MCS); **(I-J)** model including tip cells ($\theta_{NICD=0.2}$ in absence **(I)** and $\theta_{NICD}=0$ in presence **(J)** of chemoattractant inhibition; **(K-L)** model with reduced tip cell number ($\theta_{NICD}=0$) in presence **(K)** and in absence **(M)** of chemoattractant inhibition. **M** Number of sprouts after 750 MCS for $n = 20$ simulations; error bars show the standard deviation; asterisks denote $p < 0.05$ for p-values obtained with Welch's t-test in comparison with controls (no inhibition).

using Tukey's range test (see Methods for detail). Relative to a control model with non-translating siRNA (siNT), "mixed" spheroids in VEGF enriched collagen formed fewer sprouts (Figure 9 **A-C** and **G**,) when treated with siAPJ or siAPLN. Interestingly, when the collagen gels are not enriched with VEGF, siAPJ or siAPLN did not significantly affect the number of sprouts. Since VEGF can induce tip cell fate (51, 69), this may suggest that without VEGF there are too few tip cells present to observe the effects of inhibiting Apelin signaling. In "stalk cell" spheroids siRNA treatments interfering with Apelin treatments slightly improved sprouting in some replicates and had no clear effect in others (S5 Fig). Thus these results suggest that Apelin signaling requires a mix of sufficient CD34⁺ ("tip") and CD34⁻ ("stalk") cells, in support of our hypothesis that differential chemotaxis of stalk and tip cells to Apelin drives the sprout forward.

We next asked if the observed reduction of sprouting associated with inhibition of Apelin-signaling also occurred in the computational model. To mimic application of siAPLN in the computational model, we reduced the secretion of the chemoattractant both in tip and stalk cells to $\alpha(\text{tip})=10^{-3}$ and $\alpha(\text{stalk})=10^{-4}$. To mimic wild-type spheroids we used $\Theta_{\text{NICD}}=0.2$, which yields a mix of CD34⁺ and CD34⁻ cells. To mimic spheroids enriched in stalk cells, we reduced the NICD-levels to $\Theta_{\text{NICD}}=0$ in which case all ECs became stalk cells. Figure 9I-L and show how the model responds to the inhibition of Apelin-signaling, showing reduced sprouting after inhibiting the chemoattractant. To quantify these observations, we repeated the simulations ten times for 750 MCS. We converted the resulting images to gray scale images (see) and counted the number of sprouts using ImageJ, thus using the same quantification procedure as that used for the *in vitro* cultures. In both the *in silico* “wild type” spheroids ($\Theta_{\text{NICD}}=0.2$) and in the *in silico* “stalk cell” spheroids ($\Theta_{\text{NICD}}=0$), inhibition of Apelin-signaling reduced sprouting. However, the simulations did not reproduce the experimental observation that in “stalk cell” spheroids silencing of Apelin signaling had little effect in absence of VEGF and slightly promoted sprouting in VEGF-treated CD34⁻ cultures.

DISCUSSION

In this work we asked how and by what mechanisms tip cells can participate in angiogenic sprouting. We employed a suitable computational model of angiogenic network formation (11), which was extended with tip and stalk cell differentiation. In the extended model, the behavior of tip and stalk cells could be varied independently by changing the model parameters. Instead of testing preconceived hypotheses on tip and stalk cell behavior, we took a “reversed approach” in which we could rapidly compare series of alternative parameter settings, each representing different tip cell behavior: We systematically searched for parameters that led tip cells to occupy the sprouts tips, and that changed the morphology of the angiogenic networks relative to a nominal set of simulations in which tip and stalk cells have identical behavior. We studied two cases, reflecting the two extremes in the range of known molecular mechanisms regulating tip and stalk cell differentiation. In the first case, we assumed that endothelial cells are differentiated stably between a tip and stalk cell phenotype within the characteristic time scale of angiogenic development (approximately 24 to 48 hours). In the second case, we assumed a much more rapidly-acting lateral inhibition mechanism, mediated by Dll4 and Notch. Here endothelial cells can switch back and forth between tip and stalk cell fate at time scales of the same order of cell motility. Our analysis showed that in a model driven by contact-inhibited chemotaxis to a growth factor secreted by ECs, tip cells that respond less to the chemoattractant move to the tips of the sprouts and speed up sprout extension. Under the same conditions, more regular and more dense networks formed if ECs switched between tip and stalk cell fate due to lateral inhibition. This limits tip cells to growing sprouts; due to their stronger chemoattractant sensitivity the stalk cells push

the tip cells forwards leading to faster sprout extension in a mechanism reminiscent of a “self-generated gradient mechanism” (49).

We next asked if a growth factor with the predicted properties is involved in angiogenic sprouting. To this end we looked for matching, differential gene expression patterns in published data sets of gene expression in tip and stalk cells. In particular the Apelin-APJ ligand-receptor pair turned out to be a promising candidate: Apelin is a chemoattractant for endothelial cells that is secreted by endothelial cells and the receptor APJ is only detected in stalk cells. In agreement with our simulations, *in vitro* experiments on endothelial spheroids showed that inhibition of Apelin or its receptor APJ reduced *in vitro* spheroid sprouting. Thus the reversed bottom-up simulation approach employed in this study helped identify a candidate molecule mediating the interaction between tip and stalk cells during angiogenesis.

Our approach was inspired by a recent study that used a computational model to identify what cell behavior changed when endothelial cells were treated with certain growth factors (31). This study used an agent-based, 3D model of angiogenesis in which sprouts extend from a spheroid. With a genetic algorithm the parameters for which the model reproduces experimental results are derived. In this way Long *et al.* (31) could hypothesize what changes in cell behavior the growth factors caused and successfully derived how certain growth factors affect cell behavior in 3D sprouting assays. Here, we used a similar approach to study what behavior makes tip cells lead sprouts and affect network formation, using high-throughput parameter studies instead of objective optimization approaches. Tip-stalk cell interactions have been studied before with several hypothesis-driven models where specific behavior was assigned to the tip cells based on experimental observations, and tip cells were either defined as the leading cell (70-75) or tip cell selection was modeled such that the tip cell could only differentiate at the sprout tip (41, 76, 77). These models have been used to study how extracellular matrix (ECM) density (70), ECM degradation (70), ECM inhomogeneity (71, 72), a porous scaffold (73, 74), cell migration and proliferation (75, 76), tip cell chemotaxis (77) and toxins (41) affect sprouting and angiogenesis. Thus these studies asked how a specific hypothesis of tip cell behavior and tip cell position affected the other mechanisms and observables in the simulation. Our approach aims to develop new models for the interaction between tip and stalk cells that can reproduce biological observation. These new hypotheses can be further refined in hypothesis-driven model studies, as we do here, e.g., in Figure 8.

In order to make this “reversed’ approach possible, we have simplified the underlying genetic regulatory networks responsible for tip-stalk cell differentiation. These molecular networks, in particular Dll4-Notch signaling, have been modeled in detail by Bentley *et al.* (78, 79). Their model describes a strand of endothelial cells, and was used to study how lateral inhibition via Dll4-Notch signaling in interaction with VEGF signaling participates in tip cell selection. With this model Bentley and coworkers predicted that the shape of the VEGF gradient determines the rate of tip cell selection, and that for very

high levels of VEGF the intracellular levels of Dll4 and VEGFR2 oscillate. Based on their experimental observations that tip cells migrate within a sprout, cell movement has been added to the model by allowing cells to switch positions along the sprout (4). Bentley and coworkers reproduced tip cell migration in the sprout and showed that the VEGFR2 levels in a cell determine the chance of that cell to become a tip cell. The migration of tip cells in a sprout was further studied using a model that included a cell migration model (44). Bentley and coworkers (44) thus showed that the differences in VE-cadherin expression between tip and stalk cells could cause tip cell migration to the sprout tip. Altogether, these models gave useful insights in the role of Dll4-Notch signaling and VEGF signaling in tip cell selection in a growing sprout. Here, instead of focusing at single sprouts, we focused on the scale of a vascular network. By combining a tip cell selection model with a cell based model of angiogenesis, we showed that tip cell selection can aid the development of dense networks by limiting the destabilizing effects of tip cells.

The model prediction that tip cells respond less to a chemoattractant secreted by all endothelial cells fits with the expression pattern of the chemoattractant Apelin, which is secreted by all endothelial cells and of which the receptor is not detected in tip cells. Previous studies indicated that Apelin induces angiogenesis *in vitro* (62, 63). Apelin-APJ signaling is necessary for vascular development in *in vivo* systems such as in the mouse retina (68), frog embryo (63, 66), and chicken chorioallantoic membrane (66). Furthermore, high levels of vascularization in human glioblastoma are correlated with high expression levels of Apelin and APJ (63). Based on these observations Apelin is considered to be a pro-angiogenic factor. Similar to other pro-angiogenic factors such as VEGF (80), Apelin is expressed near areas where blood vessels develop and Apelin expression is induced by hypoxia (67). The pro-angiogenic role of Apelin is linked to its role as a chemoattractant [66,67] and mitogenic factor (66, 67). However, the role of Apelin in proliferation may be disputed because Apelin did not promote proliferation in a series of sprouting assays with human umbilical vein endothelial cells, human umbilical arterial endothelial cells, and human dermal microvascular endothelial cells (63). Our models propose a scenario where Apelin can promote angiogenesis as an autocrine chemoattractant, in contrast to the previous studies where the source of Apelin was external. Such a mechanism would fit with the observation that the Apelin receptor APJ is only expressed in stalk cells.

Inhibition of sprouting is manifested as a decrease in the number of sprouts. As mentioned previously, Apelin may promote proliferation, and thus inhibition of Apelin signaling may result in a reduced proliferation rate. A reduced proliferation rate could result in a reduced sprout length, but, a reduced number of sprouts is an unlikely effect of a decreased proliferation rate. This indicates that the mechanism that drives sprouting is affected by the inhibition of Apelin signaling. However, whereas in the model inhibition of Apelin signaling inhibits sprouting for all tested cases, in the experimental assays the effects of Apelin or APJ inhibition depended on the fraction of tip cells and the environment. In mixed spheroids, Apelin and APJ inhibition reduced sprouting in spheroids embedded in VEGF-enriched collagen. In CD34⁺ spheroids, i.e., spheroids

enriched with stalk cells, Apelin or APJ inhibition has no effect in plain collagen and slightly enhances sprouting in a VEGF rich environment. This suggests that, in a VEGF rich environment, Apelin-APJ signaling inhibits sprouting by stalk cells. VEGF has been shown to induce tip cell fate (51, 69), as well as APJ expression (81, 82). However, it remains unclear how the combination of a VEGF rich environment and Apelin signaling could inhibit sprouting and therefore further experiments studying the interaction between VEGF and Apelin signaling in vascular sprouting are needed. Further *in vitro* experiments are also needed to study the effects of Apelin signaling on network formation, that follows the initial sprouting phase. Our model predicts that inhibition of Apelin signaling would also block the network formation. However, because the 3D sprouting assay does not mimic vascular network formation, this prediction could not be verified experimentally.

The importance of VEGF in our validation experiments suggests that we cannot ignore VEGF in our tip cell selection model. As mentioned above, VEGF may interact with Apelin-APJ signaling. Furthermore, VEGF (55) and Apelin (66, 67) are both involved in endothelial cell proliferation. Besides the link between VEGF and Apelin, VEGF is also involved in tip cell selection. Dll4-Notch signaling and VEGF signaling interact directly in two ways. First, Dll4 is upregulated by signaling between VEGF and VEGF receptor 2 (VEGFR2) (50, 69). Second, Dll4-Notch signaling downregulates VEGFR2 (18, 21, 52, 83) and upregulates VEGF receptor 1 (VEGFR1) (52, 84), which acts as a decoy receptor for VEGF (85). Because *in vivo* VEGF acts as an external guidance cue for angiogenesis, the interplay between VEGF signaling and Dll4-Notch signaling could promote tip cell selection in the growing sprouts. The expression levels of VEGFR2 also directly reduce adhesion between cells because VEGFR2-VEGF binding causes endocytosis of VE-cadherin (86). This reduced adhesion may enable cells with high VEGFR2 levels, such as tip cells, to migrate to the sprout tip (44). Because of this complex interplay between cell behavior and Dll4, Notch, VEGF, and the VEGF receptors, future studies will replace the simplified tip cell selection model for a tip cell selection model with explicit levels of Dll4, Notch, VEGF, VEGFR1 and VEGFR2, and link those levels directly to tip and stalk cell behaviors. Furthermore, future studies should include explicit levels of Apelin and APJ to study if and how VEGF-induced Apelin secretion affects network formation. Such an extended model will provide more insight into how the interaction between stalk cell proliferation (1, 87), ECM association of VEGF (88), and pericyte recruitment and interaction (87, 89), which all have been linked to Apelin signaling and/or VEGF signaling, affects angiogenesis.

MATERIALS AND METHODS

Cellular Potts model

In the cellular Potts model (32, 33) cells are represented on a finite box $\Lambda \subset \mathbb{Z}^2$ within a regular square lattice. Each lattice site $\vec{x} \in \Lambda$ represents a $2\mu\text{m} \times 2\mu\text{m}$ portion of a cell or the extracellular matrix. They are associated with a cell identifier $\sigma \in \mathbb{Z}^{\{+,0\}}$. Lattice sites with $\sigma = 0$ represent the extracellular matrix (ECM) and groups of lattice sites with

the same $\sigma > 0$ represent one cell. Each cell σ has a cell type $\tau(\sigma) \in \{ECM, tip, stalk\}$. The balance of adhesive, propulsive and compressive forces that cells apply onto one another is described using a Hamiltonian,

$$H = \sum_{(\bar{x}, \bar{x}')} J(\tau, \tau') (1 - \delta(\sigma, \sigma')) + \sum_{\sigma} \lambda(\tau(\sigma)) (a(\sigma) - A(\tau(\sigma)))^2,$$

with (\bar{x}, \bar{x}') a set of adjacent lattice sites, $\tau = \tau(\sigma(\bar{x}))$ and $\tau' = \tau(\sigma(\bar{x}'))$, $\sigma = \sigma(\bar{x})$ and $\sigma' = \sigma(\bar{x}')$, $J(\tau, \tau')$ the contact energy, the Kronecker delta: $\delta(x, y) = \{1, x = y; 0, x \neq y\}$, the elasticity parameter $\lambda(\tau)$, and the target area $A(\tau)$. To mimic random pseudopod extensions the CPM repeatedly attempts to copy the state of a randomly chosen lattice site \bar{x} , into an adjacent lattice site \bar{x}' selected at random among the eight nearest and next-nearest neighbors of \bar{x} . The copy attempt is accepted with probability,

$$P_{accept}(\Delta H) = \{1 \text{ if } \Delta H \leq 0; e^{\frac{-\Delta H}{f(\tau, \tau')}} \text{ if } \Delta H > 0;$$

with

$$f(\bar{x}, \bar{x}') = \{min(\mu(\tau), \mu(\tau')) \text{ if } \sigma > 0 \text{ and } \sigma' > 0; max(\mu(\tau), \mu(\tau')) \text{ otherwise.}$$

Here $\mu(\tau)$ is the cell motility and $\tau = \tau(\sigma(\bar{x}))$ and $\tau' = \tau(\sigma(\bar{x}'))$ are shorthand notations. One Monte Carlo step (MCS)—the unit time step of the CPM—consists of $|\Lambda|$ random copy attempts; i.e., in one MCS as many copy attempts are performed as there are lattice sites in the simulation box.

The endothelial cells secrete a chemoattractant at rate $\alpha(\tau)$ that diffuses and decays in the ECM,

$$\frac{\partial c(\bar{x}, t)}{\partial t} = D \nabla^2 c(\bar{x}, t) + \alpha(\tau(\sigma(\bar{x}))) (1 - \delta(\sigma(\bar{x}), 0)) - \varepsilon \delta(\sigma(\bar{x}), 0) c(\bar{x}, t),$$

with c the chemoattractant concentration, D the diffusion coefficient, and ε the decay rate. After each MCS equation [eq:diffusion] is solved numerically with a forward Euler scheme using 15 steps of $\Delta t = 2s$ and a lattice spacing coinciding with the Cellular Potts lattice of $\Delta x = 2\mu m$ with absorbing boundary conditions ($c = 0$ at the boundaries of Λ); thus one MCS corresponds with 30 seconds. Chemotaxis is modeled with a gradient dependent term in the change of the Hamiltonian [42] associated to a copy attempt from \bar{x} to \bar{x}' :

$$\Delta H_{chemotaxis} = -\chi(\tau, \tau') \left(\frac{c(\bar{x}')}{1 + sc(\bar{x}')} - \frac{c(\bar{x})}{1 + sc(\bar{x})} \right),$$

with $\chi(\tau, \tau')$ the chemoattractant sensitivity of a cell of type τ towards a cell of type τ' and vice versa, and $\ll Eqn00148.eps \gg$ the receptor saturation. In the angiogenesis model we assumed that chemotaxis only occurs at cell-ECM interfaces (contact-inhibited chemotaxis; see (11) for detail); hence we set $\chi(\tau) = 0$ if $\tau \neq ECM$ and $\tau' \neq ECM$. For the remaining, non-zero chemoattractant sensitivities we use the shorthand notation $\chi(\tau)$.

Tip cell selection model

The differentiation between tip and stalk cells is regulated by a simplified tip and stalk cell selection model. The model is based on lateral inhibition via Dll4-Notch signaling: If Dll4 binds to Notch on a adjacent cell it causes the dissociation of Notch, resulting in the release of Notch intracellular domain (NICD) (90). We assume that tip cells express Notch at a permanent level of $N(tip)$ and Delta at a level of $D(tip)$; stalk cells express Delta and Notch at permanent levels of $N(stalk)$ and $D(stalk)$. The level of NICD in a cell, $I(\sigma)$, is given by,

$$I(\sigma) = \frac{N(\tau(\sigma))}{a(\sigma)} \sum_{n \in neighbors} D(\tau(n)) L_{\sigma \cap n},$$

in which $N(\tau)$ and $D(\tau)$ are the levels of Notch and Delta in a cell of type τ , and $L_{\sigma \cap n}$ is the length of the interface between cells σ and n . To model differentiation between the stalk and tip cell type in response to the release of NICD [17,30] the cell type is a function of the cell's NICD level,

$$\tau(\sigma) = \{tip \text{ if } I(\sigma) \leq \Theta_{NICD}; stalk \text{ if } I(\sigma) > \Theta_{NICD},$$

with Θ_{NICD} threshold representing the NICD-level above which the cell differentiates into a stalk cell. To prevent rapid cell type changes, we introduced a hysteresis effect by setting the Notch levels to: $N(tip) = 0.3$ and $N(stalk) = 0.5$. The Dll4 levels are set according to the experimental observation that tip cells express more membrane bound Dll4 than stalk cells (2)[2]: $D(tip) = 4$ and $D(stalk) = 1$.

Morphometrics

To quantify the results of the sprouting simulations we calculated the compactness of the morphology and detect the lacunae, branch points and end points. The compactness C is defined as $C = A_{\text{cell}} / A_{\text{hull}}$, with A_{cell} the total area of a set of cells and A_{hull} the area of the convex hull around these cells. For the compactness we used the largest connected component of lattice sites with $\sigma > 0$. This connected component was obtained using a standard union-find with path compression (91). The convex hull around these lattice sites is the smallest convex polygon that contains all lattice sites which is obtained using the Graham scan algorithm (92).

4.1

Lacunae are defined as connected components of lattice sites with $\sigma(\vec{x}) = 0$ (ECM) completely surrounded by lattice sites with $\sigma(\vec{x}) > 0$. These areas are detected by applying the *label* function of Mahotas on the binary image $\{\vec{x} \in \Lambda, \mathbf{1}_{\sigma(\vec{x})=0}\}$, i.e., the image obtained if medium pixels are set to 1 and all other pixels are set to 0. The number of labels areas in this image is the number of lacuna, and the number of lattice sites in a labeled area is the area of a lacuna.

To identify the branch points and end points, the morphology is reduced to a single pixel morphological skeleton (93). For this, first the morphology is obtained as the binary image $\{\vec{x} \in \Lambda, \mathbf{1}_{\sigma(\vec{x})>0}\}$. Rough edges are removed from the binary image by applying a morphological closing (94) with a disk of radius 3. Then, 8 thinning steps are performed in which iteratively all points that are detected by a hit-and-miss operator are removed from the image (94). In the skeleton, pixels with more than two first order neighbors are branch points and pixels with only one first order neighbor are end points. The skeleton may contain superfluous nodes. Therefore, all sets of nodes that are within a radius of 10 lattice units are collected and replaced by a single node at: $\vec{n}_{\text{merged}} = \langle \vec{x} \rangle_{\{\vec{x} \in \text{nodes}; |\vec{n} - \vec{x}| < 10\}}$.

All morphological operations are performed using the Python libraries Mahotas (95) and Pymorph (96). Mahotas implements standard morphological operations, except for the closing and thinning operations required for skeleton generation. For these we use Pymorph, that implements a more complete set of morphological operation than Mahotas. However, as it is implemented in pure Python it is computationally less efficient than Mahotas.

Tip cell detection

Cells at the sprout tips were automatically detected in two steps: (1) detection of the sprouts in the network; (2) detection of the cells on the sprout tip. For the first step, detecting sprouts, a sprout is defined as a connection between a branch point, \vec{B} , and an end point, \vec{E} . To find the branch point \vec{B} that is connected to end point \vec{E} , all nodes, except \vec{E} , are removed from the morphological skeleton (Figure 10B). In the resulting image one part of the skeleton is still connected to \vec{E} , this is the branch. Then, all nodes are superimposed on the image with the branch (Figure 10C) and the node connected to \vec{E} is the branch point \vec{B} . Next, we search for the cells at the tip

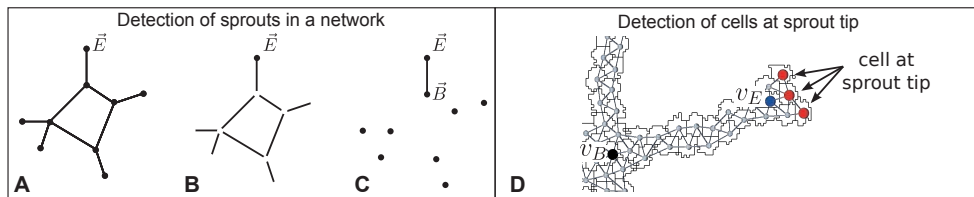


Figure 10. Detection of cells at the tips of sprouts. **A-C** detection of sprouts in a network. **A** Skeleton with branch points and end points. **B** Skeleton from which all nodes except \bar{E} are removed. **C** The union of the nodes and the connected component in **B** that contains \bar{E} . The node that, in **C**, is part of the same connected component as \bar{E} is the branch point \bar{B} . **D** detection of cells at the sprout tip (red vertices), which are farthest away from the branch point v_B (black vertex).

of the sprout, which are the cells in the sprout furthest away from σ_B . To find these cells we use a graph representation of the morphology. In this graph, $G(v, r)$, each vertex v represented a cell and vertices of neighboring cells shared an edge (Figure 10D). Now, we calculate the shortest path between each vertex v and the vertex belonging to the cell at the branch point v_B using Dijkstra's algorithm (97). Then, we iteratively search for vertices with the longest shortest path to v_B starting at the vertex associated to σ_E (v_E). To limit the search to the a single sprout, the search is stopped when v_B is reached. When the search is finished, the node or nodes with the longest shortest path to v_B represent the cells or cells that are at the sprout tip.

Model implementation and parameter sweeps

The simulations were implemented using the cellular Potts modeling framework *CompuCell3D* (98) which can be obtained from <http://www.compuCell3D.org>. The simulation script is deposited in . File also includes two extensions to *CompuCell3D*, called steppables, which we developed for the simulations presented in this paper. Steppable *RandomBlobInitializer* is used to initialize the simulations with a blob of cells, and steppable *TCS* contains the tip cell selection model. To efficiently set up, run and analyze large parameters sweeps including the ones presented in this paper, we have developed a pipeline to set up, run, and analyze large numbers of simulations of cell-based models on parallel hardware using software like *CompuCell3D*, described in detail elsewhere (99). Briefly, the pipeline automatically generate simulation scripts for a list of parameters values, run the simulations on a cluster, and analyze the results using the morphometric methods described in sections Morphometrics and Tip Cell Detection.

In vitro sprouting assay

Immortalized human dermal endothelial cells (HMEC-1s) were cultured in 2% gelatin-coated culture flask at 37 °C under 5% CO_2 with a M199 medium (Gibco, Grand Island, NY, USA) supplemented with 10% foetal calf serum (Biowhittaker, Walkersville, MD,

USA), 5% human serum and 1% Penicillin-streptomycin-glutamine (Gibco). The HMEC-1 cells used in this study were a kind gift of Prof. Dr. P. Hordijk (Sanquin, Amsterdam, the Netherlands). Cell suspensions were obtained from the cultures by TrypLE (Gibco) treatment of adherent endothelial cell monolayers. After the cells were extracted from the culture they were seeded in methylcellulose (Sigma-Aldrich) containing medium to allow spheroid formation(100). After 18 hours, the spheroids were embedded in a collagen gel containing human serum. In the period that these experiments were performed, the lab had to change collagen gels because of availability issues. Therefore, the following three gels were used: Purecol bovine collagen (Nutacon, Leimuident, the Netherlands), Nutacon bovine collagen (Nutacon, Leimuident, the Netherlands), and Cultrex rat collagen I (R&D Systems, Abingdon, United Kingdom). The gels may be supplemented with VEGF-A (25 ng/ml). After 24h images of the sprouts were obtained using phase-contrast microscopy. Using ImageJ (100) with the NeuronJ plugin (101) the number of sprouts and the length of the sprouts in the image were counted. To compare the *in silico* simulations with the *in vitro* experiments, *in silico* morphologies at 750 MCS were analyzed following the same method. To prevent biases in this manual analysis due to prior knowledge, black and white images in which tip and stalk cells were indistinguishable (see) were counted by a technician.

To study sprouting in absence of tip cells, CD34 negative HMEC-1s (3) were extracted using Fluorescence-activated cell sorting (FACS). For this the cells were washed in PBS containing 0.1% bovine serum albumin. Cells were incubated with anti-CD34-phycoerythrin (anti-CD34-PE; clone QBend-10) and analyzed by flow cytometry on a FACSCalibur (Becton Dickinson, Franklin Lakes, NJ, USA) with FlowJo 6.4.7 software (Tree Star, San Carlos, CA, USA).

To inhibit Apelin signaling HMEC-1s were transfected with a silencing RNA (siRNA) against Apelin (siAPLN) or against the Apelin receptor APJ (siAPJ), and a non-translating siRNA (siNT) was used as a control. For each siRNA the HMEC-1s were transfected with 25 nM siRNA (Dharmacon, Lafayette, CO, USA) final concentration and 2.5 nM Dharmafect 1 (Dharmacon) for 6 hours using the reversed transfection method (102). Transfection efficiency was evaluated with qPCR and a knockdown of RNA expression above 70% was considered as an effective transfection.

For both the unsorted HMEC-1s and the CD34 negative HMEC-1s the experiments were repeated several times, resulting in 4 biological replicates for the unsorted HMEC-1s and 5 biological replicates for the CD34 negative HMEC-1s. To combine the results of the biological replicates, the number of sprouts n_R^i of spheroid i in replicate R was normalized: $N_R^i = \frac{n_R^i}{n_R^{-siNT}}$, with n_R^{-siNT} the average number of sprouts formed with the non-translating siRNA treatment in biological replicate R . Next, we computed the average number of sprouts per replicate: $N_{-R} = \frac{\sum_{i=1}^{m_R} N_R^i}{m_R}$, with m_R the number of spheroids in replicate R . This resulted in four data points for the unsorted HMEC-1s and five data points for the CD34 negative HMEC-1s. Then, significance of each treatment was analyzed

in a two-step procedure. First, groups in which the means differ significantly were identified with analysis of variance (ANOVA). Second, to identify which means in a group differ, we used Tukey's range test (103, 104) to compare the results of the treatments in plain collagen with the siNT treatment in plain collagen and the treatments in VEGF-enriched collagen with the siNT treatment in VEGF-enriched collagen. All experimental measurements are included in S1 Dataset together with the python script used to perform the statistical analysis. An archive containing the photographs of the HMEC spheroids used for the image analysis is included as .

Estimation of endothelial cell cross-sectional area

The spheroid assay was performed as described above. Gels were fixed with 4% paraformaldehyde for 15 min at room temperature and blocked with blocking buffer containing 1% FBS, 3% triton x-100 (sigma), 0.5% tween-20 (sigma), 0.15% natriumazide for 2 hours. Cells were incubated with antibodies directed against F-actin (Phalloidin, Life technologies, Carlsbad, CA, USA). Three-dimensional image stacks were recorded using confocal microscopy. Within those, images containing the largest cross-section were selected visually, and measurements were obtained using the ImageJ polygonal selection tool. The image stacks and measurements are included as .

4.1

ACKNOWLEDGMENTS

This work was financed by the Netherlands Consortium for Systems Biology (NCSB) which is part of the Netherlands Genomics Initiative/Netherlands Organization for Scientific Research (NWO). The investigations were in part supported by the Division for Earth and Life Sciences (ALW) with financial aid from the Netherlands Organization for Scientific Research (NWO). The *in vitro* work was supported by grants from the following Dutch eye funds: Algemene Nederlandse Vereniging ter Voorkoming van Blindheid (ANVVB), Stichting Blinden-Penning, Landelijke Stichting voor Blinden en Slechtienden (LSBS), Stichting MD fonds (all together cooperated by UitZicht, project # UitZicht2012-17), Nederlandse Vereniging ter Verbetering van het Lot der Blinden, Rotterdamse Stichting Blindenbelangen, Stichting voor Ooglijders and the Stichting Nederlands Oogheelkundig Onderzoek. The authors thank the IU and the Biocomplexity Institute for providing the CC3D modeling environment (www.compuCell3d.org) [98] and SARA for providing access to The National Compute Cluster LISA (www.sara.nl).

Supplementary information can be found here:

<https://journals.plos.org/plosone/article?id=10.1371/journal.pone.0159478#sec019>

Marchien G. Dallinga¹,
Alinda W.M. Schimmel²,
Ingeborg Klaassen¹,
Geesje M. Dallinga-Thie²,
Cornelis J.F. Van Noorden^{1,3},
Reinier O. Schlingemann^{1,4}

¹ Ocular Angiogenesis Group, Departments of Ophthalmology and Medical Biology, Amsterdam Cardiovascular Sciences, Cancer Center Amsterdam, Amsterdam UMC, University of Amsterdam, Meibergdreef 9, Amsterdam, The Netherlands.

² Department of Experimental Vascular Medicine, Amsterdam UMC, University of Amsterdam, Amsterdam, The Netherlands.

³ Department of Genetic Toxicology and Cancer Biology, National Institute of Biology, Ljubljana, Slovenia.

⁴ Department of Ophthalmology, University of Lausanne, Jules Gonin Eye Hospital, Fondation Asile des Aveugles, Lausanne, Switzerland.



**ROLE OF HEPARAN SULFATE AND
NEUROFILIN 2 IN VEGFA SIGNALING IN
HUMAN ENDOTHELIAL TIP CELLS AND
NON-TIP CELLS IN ANGIOGENESIS**

INTRODUCTION

Sprouting angiogenesis is the complex process of blood vessel growth from the existing vasculature. It is characterized by differentiation of endothelial cells (ECs) into subtypes with distinct functions: **tip cells** are non-proliferating and highly migratory, and lead the growing vessel sprout towards a source of growth factors. Tip cells induce the adjacent cells into the proliferative phenotype of the **stalk cell** that starts forming a lumen, and further down the sprout are **phalanx cells** that initiate vessel maturation (1, 105). Vascular endothelial growth factor isoform A (VEGFA) is the main initiator of sprouting angiogenesis (1). The main receptor for angiogenic signaling by VEGFA is VEGFR2, and its stimulation induces tip cell migration, expression of tip cell genes, proliferation of stalk cells, EC survival and more (1, 106). Binding of VEGFA to VEGFR2 is affected by a number of factors, which include binding to extracellular matrix (ECM) components such as heparan sulfate proteoglycans (HSPGs), or simultaneous binding of VEGFA to one of its neuropilin (NRP) co-receptors (NRP1 or NRP2) (107-109).

4.2

HSPGs are present in the extracellular matrix (ECM), in particular in the basal lamina (110). Binding of VEGFA to the HSPGs in the ECM is essential for vascular network development. This is illustrated by the lack of complexity in vascular networks in mice that only express VEGFA isoform 121 (VEGFA₁₂₁), which lacks the heparan sulfate (HS)-binding domain of the most common VEGFA isoform VEGFA₁₆₅ (88). The importance of VEGFA binding to extracellular proteins in the ECM has also been investigated using *in silico* modeling (111), which showed that vascular networks, in which an ECM-binding signal was present, were more stable over time, and that binding of VEGFA to the ECM allowed cells to elongate towards a source of VEGFA (111). HSPGs are also located in the glycocalyx on the apical membrane domain of ECs, including human umbilical vein endothelial cells (HUVECs) *in vitro*. The glycocalyx is a negatively charged, organized mesh of membranous glycoproteins, proteoglycans and glycosaminoglycans (112-114) which affects internalization of VEGFR2 after VEGFA binding, thus modulating VEGF signaling outcome (115).

The specific types of sulfate groups in HS molecules are important for the degree of VEGFA₁₆₅ binding. It has been shown that ECs surrounded by HSPGs in the glycocalyx that selectively contain 6-O sulfate groups on their HS molecules are less angiogenic, and that binding to and subsequent phosphorylation of VEGFR2 by VEGFA₁₆₅ is reduced (116). Moreover, zebrafish with genetic defects in specific 6-O sulfotransferases have defective vascular development (117). Sulfatase 2 (SULF2) is an extracellular enzyme that selectively removes 6-O sulfate groups from HS chains on HSPG molecules (118). A major role of SULF2 in post-prandial regulation of serum triglycerides has been described, whereas a role of SULF2 in angiogenesis via alteration of VEGFA binding to HSPGs has been proposed (119), but not reported as far as we know. SULF2 has also been shown to inhibit HSPG-mediated uptake of very low density lipoprotein (VLDL) by ECs (120). This may affect angiogenesis, since VLDL cargo is used for biosynthesis by proliferating

cells, and VLDL has been shown to activate several pro-angiogenic pathways such as phosphatidylinositol 3-kinase (PI3K) and PPAR- γ (121-125). Taken together, the literature suggests a role of HSPGs in regulating angiogenesis, but exact mechanisms and possible differential regulation of tip cells and non-tip endothelial cells are unknown.

In addition to binding to HSPGs, binding to VEGFR2 co-receptors may also affect the outcome of VEGFA signaling in specific subtypes of ECs during angiogenesis. Since microarray data showed that mRNA expression of *NRP2* was significantly higher in CD34⁺ tip cells than in CD34⁻ non-tip cells in an *in vitro* model of tip cells (3), *NRP2* may have a differential role in such regulation.

Therefore, in the present study we investigated whether modulation of binding of VEGFA to VEGFR2 by knockdown of *SULF2* or *NRP2* affects sprouting angiogenesis, tip cell formation, proliferation of non-tip cells and EC survival, and uptake of VLDL, employing *in vitro* models of angiogenic tip cells and vascular sprouting.

MATERIALS & METHODS

Cell cultures

Primary HUVECs were isolated from umbilical cords (obtained from the Department of Gynecology, Amsterdam University Medical Center (Amsterdam UMC), location Academic Medical Center (AMC), Amsterdam, The Netherlands), as described previously (126). Subjects gave informed consent for the use of tissues and/or serum and samples were stored anonymously. HUVECs were cultured in M199 basal medium (Gibco, Grand Island, NY, USA) supplemented with 10% heat-inactivated human serum (obtained from the Department of Oncology, Amsterdam UMC, location AMC, Amsterdam, The Netherlands), 10% fetal bovine serum (Gibco), and 1% penicillin-streptomycin-glutamine (Gibco). HUVEC cultures were incubated with antibodies directed against CD31/PECAM-1 (1:100; eBioscience, Vienna, Austria) to check the purity of the ECs. HUVECs were cultured in 2% gelatin-coated (Millipore, Billerica, MA, USA) T75 culture flasks at 37°C and 5% CO₂. Experiments were performed with confluent HUVECs at passage 3 of at least 3 donors. HUVECs were treated for 24 h with VEGFA₁₆₅ (R&D Systems, Minneapolis, MN, USA), VEGFA₁₂₁ (Prospec, Rehovot, Israel) in a final concentration of 25 ng/mL, or insulin-like growth factor 1 (IGF1; Prospec) in a final concentration of 50 ng/mL.

Flow cytometric analysis

Cell suspensions were obtained after treatment of adherent HUVEC monolayers with TrypLE (Gibco). Cells were fixed in 2% paraformaldehyde in PBS for 15 min at room temperature and incubated with anti-CD34-phycoerythrin antibody (anti-CD34-PE; clone QBend-10, Thermo Scientific, Waltham, MA, USA) without permeabilization of the cells. Cells were analyzed using a FACSCalibur (Becton Dickinson, Franklin Lakes, NJ, USA) and FlowJo 6.4.7 software (Tree Star, San Carlos, CA, USA). Non-stained, non-

treated cells were used as negative controls. Cell proliferation was assessed by measuring incorporation of 5-ethynyl-2'-deoxyuridine (EdU) and propidium iodide (PI) using flow cytometry, following manufacturer's instructions (Molecular Probes, Eugene, OR, USA).

Spheroid-based *in vitro* angiogenesis assay

Seven hundred and fifty cells per spheroid were seeded in methylcellulose (Sigma-Aldrich, Buchs, Switzerland)-containing medium in the presence of 2% human serum to allow spheroid formation using the hanging drop method (100, 127). After 18 h, the spheroids were embedded in collagen gels containing IGF1 (50 ng/mL) and when indicated VEGFA₁₆₅ (25 ng/mL), VEGFA₁₂₁ (25 ng/mL), or VLDL (25 µg/mL), and were allowed to sprout for 24 h. Images were taken using a phase-contrast microscope and the number of sprouts and average sprout length per spheroid were analyzed using the Neuron-J plug-in package for Image-J software (128). For siRNA experiments, HUVECs were transfected with siRNA as described below at 48 h before spheroids were made.

4.2

siRNA knockdown experiments

HUVECs were transfected with 25 nM *SULF2* and/or *NRP2* siRNA or a non-targeting control siRNA (Dharmacon, Lafayette, CO, USA), in the presence of 2.5 µg/mL Dharmafect 1 (Dharmacon). The cells were transfected for 6 h using the reversed transfection method as described by the manufacturer. The transfection efficiency was verified by measuring mRNA levels of the target genes and considered acceptable when expression was reduced by at least 70% after 72 h.

VLDL isolation and labeling

VLDL was isolated from human plasma using gradient ultracentrifugation as described (129). VLDL-Apo B was analyzed in the VLDL fraction using a nephelometric assay (Diasys, Wixom, MI, USA) on a Selectra system (Sopachem, Ochten, The Netherlands). VLDL was labeled with DyLight 680 according to the manufacturer's protocol (Thermo Scientific) and dialyzed extensively and stored at 4 °C.

Immunohistochemistry

Cells were treated with siNT or siSULF2 as mentioned above and cultured on gelatin-coated coverslips (Thermo Scientific) for 72 h before treatment with DyLight-680-labeled VLDL (25 µg/mL) for 120 min in the presence or absence of heparanase (7.5 mU/mL Sigma Aldrich, St Louis, MO, USA). Heparanase hydrolyses HS selectively whereas heparins are poor substrates for heparanases (110). Cells were fixed in freshly-prepared 4% paraformaldehyde in PBS for 15 min at room temperature, and then nonspecific binding was blocked and cells were permeabilized in PBS containing 10% bovine serum albumin (BSA; Sigma-Aldrich, St. Louis, MO, USA) and 0.5% Triton X-100 (Sigma) for 1 h at room temperature. Next, cells were incubated with a monoclonal primary

antibody against CD34 (clone MD34.2; Sanquin, Amsterdam, The Netherlands) and a rabbit anti-early endosome antibody (EEA1, 1:500 dilution; Thermo Scientific) for 2 h and a secondary anti-mouse Alexa488-conjugated antibody and anti-rabbit Alexa568-conjugated antibody (Life Technologies, Carlsbad, CA, USA) for 1 h. Cells were mounted in Vectashield containing DAPI (Vector Laboratories, Burlingame, CA, USA). Images were captured using a Leica confocal microscope (Leica Microsystems, Wetzlar, Germany) using a 63x objective. Quantification was performed using Matlab (MathWorks B.V., Eindhoven, The Netherlands) and images of EEA1-positive endosomes were compared with images of VLDL staining to assess endosomal uptake of VLDL using a custom script.

RNA isolation and quantitative PCR

Total RNA was isolated from cells using the TRIzol method (Invitrogen, Carlsbad, CA, USA). A total amount of 1 μ g total RNA was used for DNase-I treatment (amplification grade; Invitrogen, Carlsbad, CA, USA) and reversed transcribed into first strand cDNA using the Maxima First Strand cDNA Synthesis Kit (Thermo Scientific). Primer details are available in Supplemental Table 1. NCBI BLAST confirmed the specificity of the primers. The presence of a single PCR product was verified by both the presence of a single melting temperature peak and detection of a single band of the expected size on agarose gels. Non-template controls were included as control. Real-time quantitative PCR was performed using a CFX96 real-time PCR detection system (Bio-Rad Laboratories, Hercules, CA, USA) as described previously (3). Expression data were normalized to glyceraldehyde-3-phosphate dehydrogenase (GAPDH) mRNA levels for PCR data after *SULF2* knockdown or tyrosine 3-monooxygenase/tryptophan 5-monooxygenase activation protein zeta (YWHAZ) mRNA levels after siNRP2 knockdown. Microarray data were obtained from a previous study (3).

Statistics and data correction

To correct for differences between donors, data from flow cytometry and spheroid experiments were corrected using factor correction as described previously (130). For single column comparisons an unpaired T-test was used, for multiple comparisons a Two-way ANOVA was used. A P value of <0.05 was considered to indicate statistically significant differences.

RESULTS

Differential effects of VEGFA₁₂₁ and VEGFA₁₆₅ on tip cell formation and sprouting vessel formation

VEGFA₁₆₅ has a HS-binding domain which VEGFA₁₂₁ lacks. We tested whether the differences in HS-binding of these two VEGFA variants lead to differences in tip cell formation and sprouting of new vessels *in vitro*. Flow cytometric analyses showed that stimulation of HUVECs with VEGFA₁₂₁ and VEGFA₁₆₅ resulted in a 1.5- and 1.6-fold increased percentage

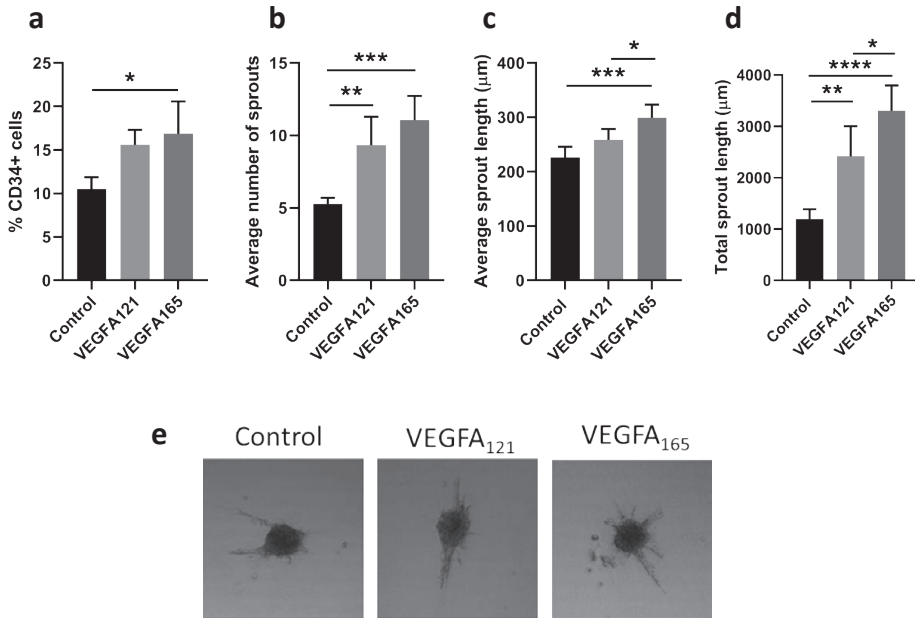


Figure 1. Effect of VEGFA₁₂₁ and VEGFA₁₆₅ on tip cell formation and sprouting. HUVECs were cultured in the presence of VEGFA₁₆₅ or VEGFA₁₂₁ or untreated as a control. **a** Flow cytometric analysis of CD34⁺ cells (% of total number of cells). Average number (**b**), average length in μm (**c**) and total length in μm (**d**) of sprouts per HUVEC spheroid. **e** Representative images of sprout formation from HUVEC spheroids. Results are presented as mean ± standard deviation (n=5). One-way ANOVA with multiple comparison was used to calculate statistical differences (* $P < 0.05$, ** $P < 0.01$, *** $P < 0.001$, **** $P < 0.0001$).

of tip cells, respectively (Fig. 1a). The number of sprouts per HUVEC spheroid increased 1.8-fold after stimulation with VEGFA₁₂₁, and 2.1-fold after stimulation with VEGFA₁₆₅ (Fig. 1b). Sprout length increased modestly more with VEGFA₁₆₅ than with VEGFA₁₂₁ ($P < 0.05$) (Fig. 1c). For total sprout length, VEGFA₁₂₁ and VEGFA₁₆₅ showed a 2.0- vs. a 2.8-fold increase ($p < 0.05$) (Fig. 1d). All together, these results show a clear trend that the effects of VEGFA₁₆₅ on tip cell formation and sprouting are more pronounced than that of VEGFA₁₂₁.

Role of SULF2 in VLDL uptake by HUVECs

VLDL uptake, which is regulated by SULF2, mainly occurred in CD34⁻ non-tip cells rather than in CD34⁺ tip cells (Fig 2a). We further investigated whether HSPGs had an effect on VLDL uptake by CD34⁻ cells. Figs 2 b-d show that siSULF2 treatment stimulated endosomal but not non-endosomal uptake of VLDL in non-tip cell HUVECs. The effect of siSULF2 treatment was annihilated by heparanase activity that cleaves HS. These findings suggest that VLDL is specifically needed by proliferating stalk cells during angiogenesis, and that VLDL uptake may be a marker for CD34⁻ stalk cells *in vitro*.

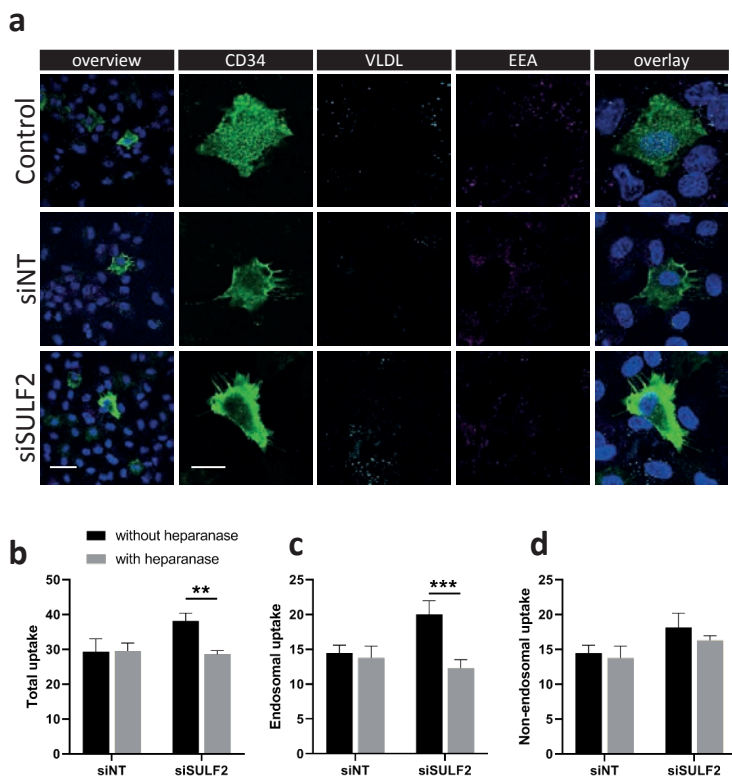


Figure 2. Knockdown of *SULF2* leads to increased uptake of VLDL. **a** Analysis of endosomal uptake of fluorescently-labeled VLDL by CD34⁺ but not CD34⁻ cells. Staining of CD34 (green), VLDL (light blue), endosomes (EEA, pink) and nuclei (DAPI, blue) in HUVECs and overlay images at low (bar = 50 μ m) and higher (bar = 20 μ m) magnification. **b-d** Quantification of total, endosomal and non-endosomal uptake of fluorescently-labeled VLDL by HUVECs after siRNA-mediated knockdown of *SULF2*. Heparanase was used as a control as it removes all HS chains from HSPG proteins. Cells were stained with DAPI and EEA1 for nuclei and endosomes. Number of VLDL particles per cell were counted using Matlab and overlap with EEA1 staining was considered as endosomal uptake. Students' T-tests were used to calculate statistical differences (** $P < 0.01$, *** $P < 0.001$).

Role of *SULF2* in VEGFA₁₆₅ and VEGFA₁₂₁ stimulation of HUVECs

SULF2 gene expression was twice as high in CD34⁺ tip cells than in CD34⁻ cells (Fig. 3a). *SULF2* siRNA-mediated knockdown resulted in a 90% decrease in *SULF2* mRNA levels (Fig. 3b). Knockdown of *SULF2* did not affect the percentage of tip cells in untreated HUVECs or in HUVECs treated with VEGFA₁₂₁ or VEGFA₁₆₅ (Fig. 3c). In HUVEC spheroids, inhibition of *SULF2* did not affect the number of sprouts of spheroids in the presence or absence of VEGFA₁₂₁ or VEGFA₁₆₅, and sprout length was marginally reduced by 1.2-fold ($p=0.02$) (Fig. 3d-e). Specific assays were performed to exclude major effects of apoptosis or proliferation confounding the final percentage of tip cells in these experiments (131, 132). No significant differences in proliferation were found in HUVECs treated with

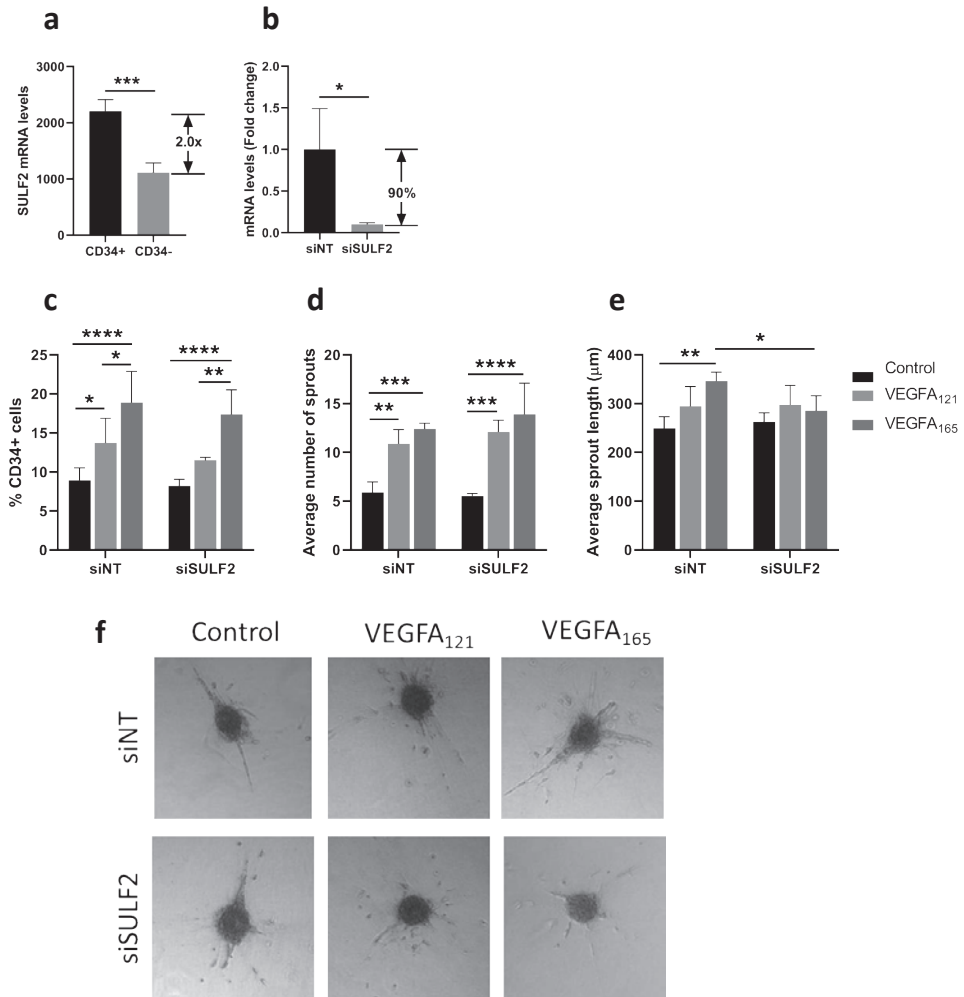


Figure 3. Effect of *SULF2* knockdown on VEGFA₁₂₁- and VEGFA₁₆₅- induced tip cell formation and sprouting. **a** Microarray analysis showed enrichment of *SULF2* mRNA in CD34⁺ cells as compared to CD34⁻ cells. HUVECs were cultured in the presence or absence of VEGFA₁₆₅ or VEGFA₁₂₁ after treatment with siINT or siSULF2. **b** Treatment of cells with siSULF2 resulted in a significant reduction in mRNA levels of more than 70% as compared to treatment with siINT. **c** Flow cytometric analysis of CD34⁺ cells (% of total number of cells). Average number (**d**) and length in µm (**e**) of sprouts per HUVEC spheroid. **f** Representative images of sprout formation from HUVEC spheroids. Results are presented as mean ± standard deviation (n=3). Unpaired T-tests (a,b), two-way ANOVA (c) or two-way mixed ANOVA (d,e) were used to calculate statistical differences (* $P < 0.05$, ** $P < 0.01$, *** $P < 0.001$, **** $P < 0.0001$).

siSULF2 as compared to HUVECs treated with siINT (Fig. 4a-c). Addition of VEGFA₁₆₅ and, to a lesser extent, VEGFA₁₂₁, reduced apoptosis in CD34⁺ tip cells but not in CD34⁻ HUVECs (Fig. 4d,e). siSULF2 treatment did not affect apoptosis in both CD34⁺ and CD34⁻

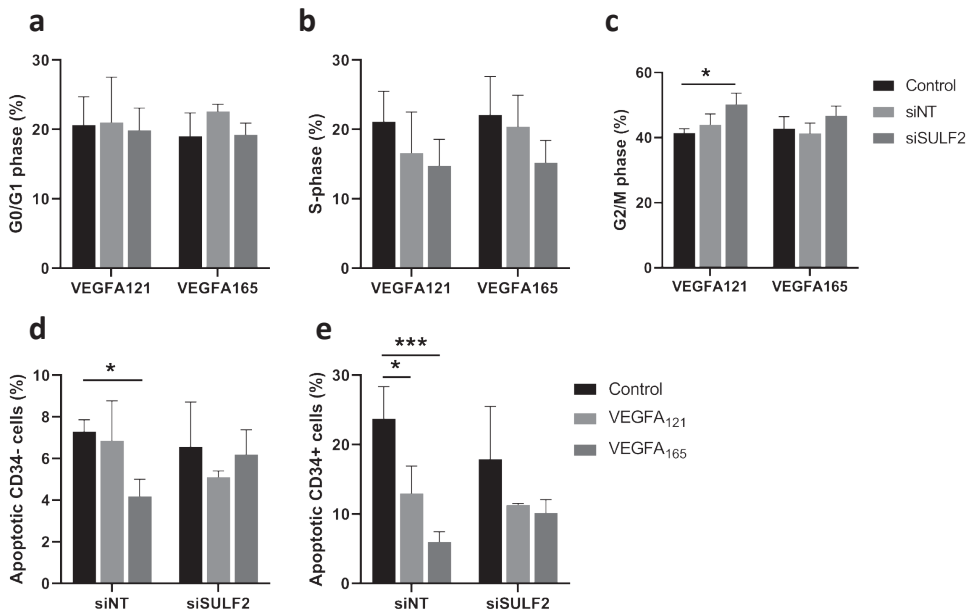


Figure 4. Effect of *SULF2* knockdown on VEGFA₁₂₁ and VEGFA₁₆₅ induced cell proliferation and apoptosis. HUVECs were cultured in the presence or absence of VEGFA₁₆₅ or VEGF₁₂₁ or no VEGF (Control) after treatment with siNT or siSULF2. Flow cytometric analysis determined the percentage of cells in G0/G1 phase (a), S-phase (b) and in G2/M phase (c). FACS analysis with annexin-5 and CD34 labeling determined the percentage of CD34⁻ non-tip cells (d) and CD34⁺ tip cells (e). Results are presented as mean ± standard deviation (n=3). Two-way ANOVA was used to calculate statistical differences (* *P* < 0.05, *** *P* < 0.001).

HUVECs. Taken together, although *SULF2* is preferentially expressed by tip cells, it does not seem to have a major role in their formation, survival or function as leading cells of sprouts.

NRP2 is a VEGFR2 co-receptor involved in VEGFA-induced sprouting, but not in tip cell formation

NRP2 promotes EC survival, and plays a role in angiogenesis (133, 134). NRP2 is mainly expressed in tip cells (Fig 5a). Therefore, we tested whether siRNA-mediated knockdown of *NRP2* affects VEGFA₁₆₅-induced tip cell formation and vessel sprouting. An efficient reduction of 78% in *NRP2* mRNA levels was found after siRNA-mediated knockdown of *NRP2* (Fig. 5b). Knockdown of *NRP2* did not affect the percentage of CD34⁺ tip cells in the presence or absence of VEGFA (Fig. 5c). The VEGFA₁₂₁ and VEGFA₁₆₅-induced increase in the number of sprouts was abolished after knockdown of *NRP2* (Fig. 5d). There was no change in sprout length after knockdown of *NRP2* in the presence or absence of VEGFA₁₂₁ and VEGFA₁₆₅ (Fig. 5e). Together, we found that NRP2, which is mainly expressed by tip cells, plays a role in sprout initiation, but not tip cell formation.

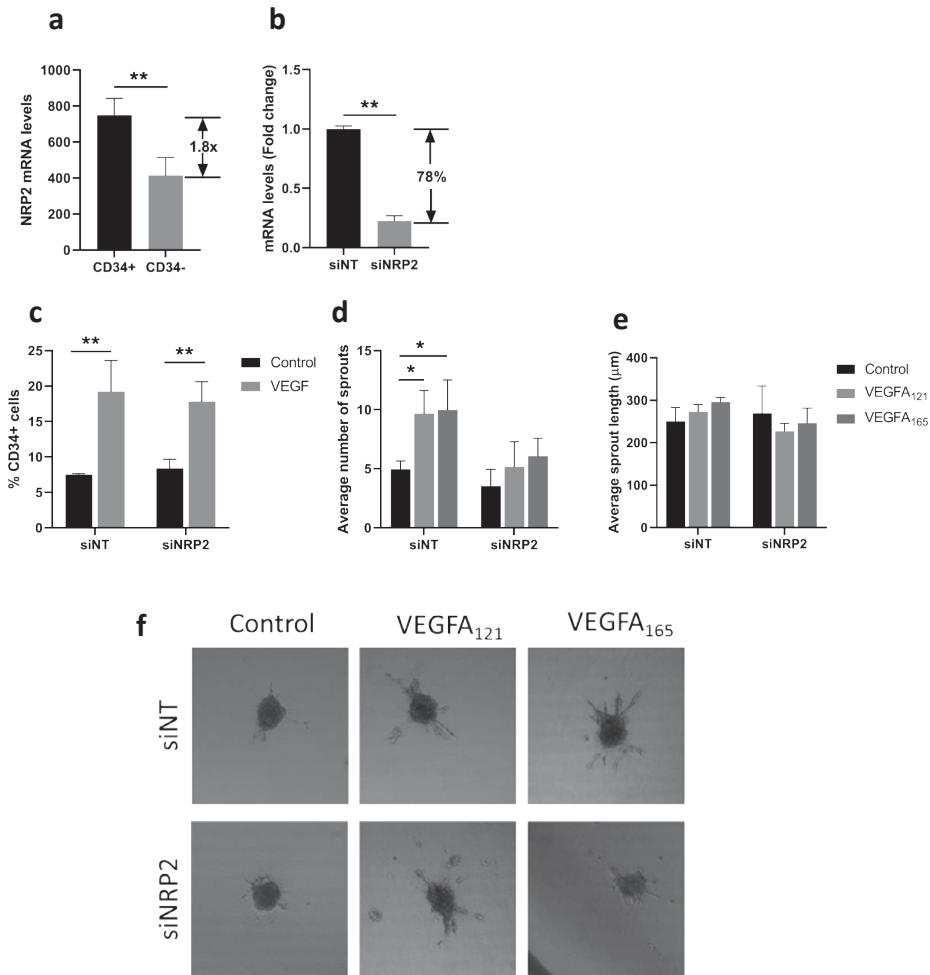


Figure 5. Effect of *NRP2* knockdown on VEGF-induced tip cell formation and sprouting. **a** Microarray analysis showed enrichment of *NRP2* mRNA in CD34⁺ cells as compared to CD34⁻ cells. HUVECs were cultured in the presence or absence of VEGFA₁₂₁ and/or VEGFA₁₆₅ or after treatment with siNT or siNRP2. **b** Treatment of cells with siNRP2 resulted in a significant reduction in mRNA levels of more than 70% as compared to treatment with siNT. **c** Flow cytometric analysis of CD34⁺ cells (% of total number of cells). Average number (**d**) and length in µm (**e**) of sprouts per HUVEC spheroid. **f** Representative images of sprout formation from HUVEC spheroids. Results are presented as mean ± standard deviation (n=3). Unpaired T-tests (a,b) or Two-way ANOVA analyses (c-e) were used to calculate statistical differences (* $P < 0.05$, ** $P < 0.01$).

VLDL uptake does not affect the tip cell percentage but enhances the number of sprouts

VLDL uptake is involved in angiogenesis as provider of biomass for proliferating stalk cells, and is inhibited by SULF2 (Fig 2) (135). We tested the possible consequences of VLDL uptake on tip cell percentage and on vessel sprouting. There was a modest but

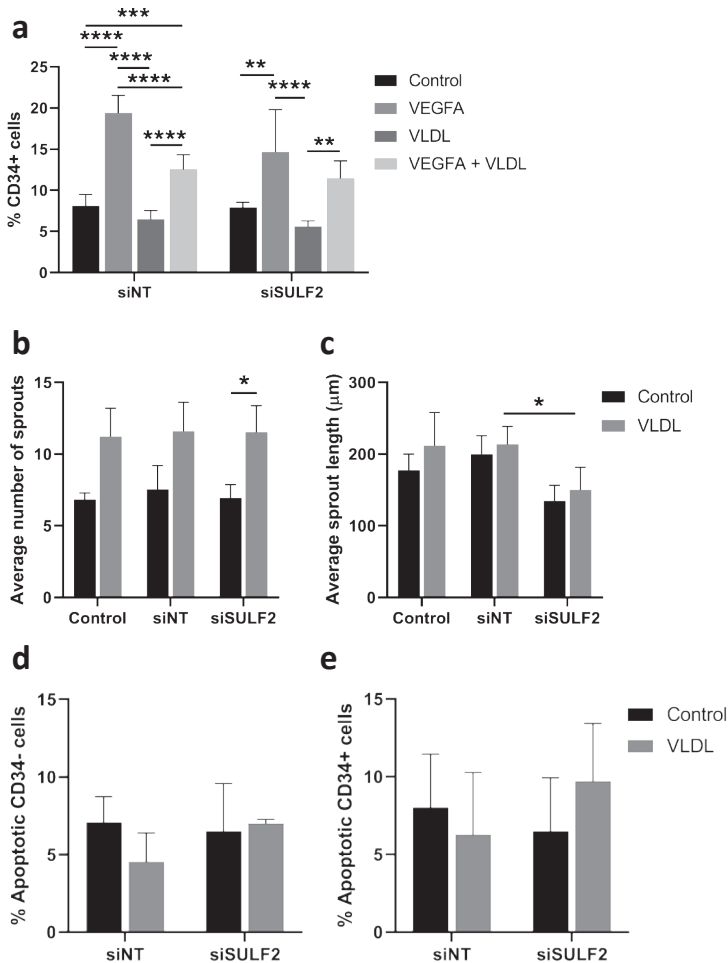


Figure 6. Effect of VLDL on tip cell formation, sprouting and apoptosis. HUVECs were cultured in the presence or absence of VEGFA₁₆₅ and/or VLDL or after treatment with siNT or siSULF2. **a** Flow cytometric analysis of CD34⁺ cells (% of total number of cells). Average number (**b**) and length in μm (**c**) of sprouts per HUVEC spheroid. Relative amount of apoptotic CD34⁻ (**d**) and CD34⁺ cells (**e**). Results are presented as mean ± standard deviation (n=3). Two-way ANOVA was used to calculate statistical differences (* $P < 0.05$, ** $P < 0.01$, *** $P < 0.001$, **** $P < 0.0001$).

significant inhibitory effect of exogenous VLDL on VEGFA-induced tip cell formation, whereas the addition of VLDL did not affect the percentage of tip cells after *siSULF2* treatment (Fig. 6a). Addition of VLDL to HUVEC spheroids resulted in an increased number of sprouts per spheroid (Fig. 6b), but did not change sprout length (Fig. 6c), whereas *siSULF2* inhibited sprout length to some extent (Fig. 6c). Apoptosis of CD34⁻ or CD34⁺ cells was not changed upon addition of VLDL or knockdown of *SULF2* (Fig. 6d-e). Taken together, we found that exogenous VLDL induces sprouting in cultured HUVECs but does not induce tip cell formation.

DISCUSSION

This study shows that VEGFA₁₆₅ is a stronger inducer of tip cell formation and angiogenesis *in vitro* than VEGFA₁₂₁, by an unknown mechanism, as modulation of VEGFA-HSPG binding by knockdown of *SULF2* only modestly reduces sprout length, and does not affect the number of sprouts in spheroids, or tip cell formation. Uptake of VLDL, which is regulated by *SULF2*, is limited to non-tip cells. It increases upon knockdown of *SULF2* and induces sprouting but not tip cell formation. Finally, sprout initiation by VEGFA is affected by simultaneous binding of the VEGFR2 co-receptor NRP2.

4.2 VEGFA is the main driving force for sprouting angiogenesis (1). Its binding to VEGFR2 induces a cascade of signaling processes resulting in increased migration of tip cells, increased proliferation of stalk cells (3, 136), and inhibition of apoptosis in both tip and stalk cells (1, 106). We have shown that VEGFA₁₆₅ consistently induces sprouting and CD34⁺ tip cell formation, whereas VEGFA₁₂₁ has less potent effects. One of the main differences between VEGFA₁₆₅ and VEGFA₁₂₁ is HS binding. It has been reported that binding of VEGFA₁₆₅ to extracellular HSPGs alters the activation of downstream signaling pathways in ECs *in vitro*: extracellular protein binding of VEGFA₁₆₅ caused elevated activation of AKT serine/threonine kinase 1 (AKT), whereas unbound VEGFA₁₆₅ mainly activated p38 (137). Activation of p38 induces migratory signals, whereas activated AKT causes proliferative and survival signals in ECs (138-140). The migratory signaling cascade is relevant for tip cells during angiogenesis, whereas the latter signaling cascade is relevant for stalk cells. Moreover, excessive amounts of 6-O sulfate groups on HSPGs have been shown to reduce binding of VEGFA to VEGFR2 (116). As *SULF2* removes 6-O sulfate groups, knockdown of *SULF2* is expected to result in an excess of 6-O sulfate groups on HSPGs and reduced sprouting. This is in agreement with the results shown in **Fig 3e** and **6a**, which suggest that binding to HSPGs by VEGFA₁₆₅ has a modest enhancing effect on sprout elongation. In transgenic mice expressing only VEGFA₁₂₁, which does not bind to HSPGs, this may also be the underlying mechanism of disturbed vascular development leading to irregular vascular networks (88).

Binding of the VEGFR2 co-receptor NRP2 only affected VEGFA-induced sprouting *in vitro*, and not tip cell formation. NRP2 has mainly been associated with EC survival (133), but has been less studied than its family member NRP1, which is involved in tip cell regulation during angiogenesis, and in neuronal development (141, 142). NRP1 and NRP2 have been shown to bind VEGFA₁₆₅, but whether they also bind VEGFA₁₂₁ has been subject of debate (108, 143, 144). Since we found that *NRP2* is mainly expressed in CD34⁺ tip cells, it may play a role in tip cells during initiation of sprouting. Here, we show that knockdown of *NRP2* affects VEGF₁₂₁- as well as VEGF₁₆₅-signaling during sprouting, indicating that there is a functional interaction between NRP2 and VEGF₁₂₁. It seems that NRP2 is not involved in induction of the tip cell phenotype by VEGFA, but supports formation of new vessel sprouts by VEGFA in another manner.

Besides altering growth factor binding to ECM, *SULF2* also regulates uptake of VLDL particles by endothelial cells (119). VLDL provides fatty acids as a source for energy

and biomass for proliferating cells and is therefore important for sprout elongation by proliferation of stalk cells. Angiogenesis is mainly driven by glycolysis (145-147), whereas tip cells have a flexible energy metabolism, which fits with their role as pioneers moving into tissues during angiogenesis, where availability of substrates and oxygen may vary greatly (146, 147). We show here that tip cells do not take up VLDL particles, whereas non-tip cells do. This process is regulated by SULF2-induced alteration of HSPGs, as was shown by abolition of these effects by heparanase which removes all extracellular HS chains (110). Our *in vitro* experiments show that VLDL itself affects sprouting: addition of exogenous VLDL does not induce stalk cell proliferation or sprout elongation, but it increases the number of sprouts. This is consistent with previous studies which have shown that VLDL can elicit activation of several pro-angiogenic pathways such as PI3K and PPAR- γ (125, 148). The inhibitory effects on VEGF-induced formation of tip cells seem to be contradictory in this case but could be the result of a decreased number of HSPG molecules on the cell surface because they are endocytosed along with the VLDL molecules (149).

Our study is limited because the *in vitro* environment is different from angiogenic sprouting *in vivo*. In our experiments, HUVECs are seeded on gelatin-coated plastic, and are covered by medium supplemented with VEGFA or VLDL which is probably mainly in contact with the ECs on the side of the medium, which could be interpreted as the luminal side of ECs. During sprouting *in vivo*, tip cells, which lack a luminal side or glycocalyx, penetrate the ECM. The ECM consists of a large number of proteins, including HSPGs. In our experiments, we cannot discriminate between effects of our interventions on HSPG in the glycocalyx of the cultured ECs (114), which is present *in vivo* on the luminal side (112, 150), versus HSPGs in the ECM, i.e. in the basal lamina deposited by the cells on the plastic. Nevertheless, since we have shown that expression of *SULF2* is stronger in these CD34⁺ tip cells compared to CD34⁻ cells, a finding recently confirmed by others (151), sulfation of HSPGs in the ECM may well play a role in vessel sprouting during angiogenesis *in vivo*.

CONCLUSION

We conclude that co-binding of the VEGFR2 co-receptor and HSPGs by VEGFA₁₆₅ plays an only marginal role in the elongation of angiogenic sprouts, and does not affect the initiation of the sprouts or tip cell formation. Uptake of VLDL is limited to non-tip cells, regulated by HSPG binding, and induces sprouting but not tip cell formation, all suggesting that VLDL has a role in sprouting by providing biomass for stalk cell proliferation. Finally, the other VEGFA-VEGFR2 co-receptor NRP2 plays a role in sprout initiation by tip cells.

Marchien G Dallinga¹,
Geesje M Dallinga-Thie²

¹Ocular angiogenesis group, Department of Ophthalmology, Academic Medical Center Amsterdam, University of Amsterdam, The Netherlands.

²Departments of Vascular and Experimental Vascular Medicine, Academic Medical Center Amsterdam, University of Amsterdam, The Netherlands.

4.3

**ROLE OF SULFATASE 2 IN LIPOPROTEIN
METABOLISM AND ANGIOGENESIS**

INTRODUCTION

Subject with type 2 diabetes and the metabolic syndrome frequently have the atherogenic dyslipidemic phenotype, reflected by increased levels of fasting plasma very low density lipoprotein (VLDL) particles and elevated postprandial levels of triglyceride-rich lipoproteins (TRL) remnants (152). The increased prevalence of obesity, the metabolic syndrome and Type 2 Diabetes in Western Societies has further emphasized the need of understanding the pathophysiology underlying this atherogenic phenotype, since plasma TRL-cholesterol levels were causally associated with increased risk for coronary vascular disease (CVD) in the population (153, 154). Important determinants in TRL homeostasis are LPL-mediated lipolysis and hepatic TRL clearance. A key role has been proposed for Heparan Sulfate Proteoglycans (HSPGs), macromolecular components of the extracellular matrix that are involved TRL uptake and are as such indispensable for lipid metabolism. HSPGs also influence growth factor signaling, enabling them to influence pathological processes like atherosclerosis and angiogenesis in multiple ways (155). Concomitantly, endothelial cells excessively exposed to TRL are prone to abnormal behavior underlying pathologies like atherosclerosis, but also abnormal blood vessel growth (angiogenesis), which has recently become evident (155).

This review will highlight current evidence for the role of SULF2, an extracellular sulfatase that targets the 6-O-sulfate residue of HSPG, in TRL metabolism and growth factor signaling, providing arguments for how these pathways may be involved in the pathophysiology of atherosclerosis and angiogenesis.

HEPARAN SULFATE PROTEOGLYCANS AND SULF2

Heparan Sulfate Proteoglycans (HSPGs) are large molecules that are present on the cell surface of mammalian endothelial cells and, together with other macromolecules, form the extracellular matrix. HSPGs operate in a large number of different organs such as the heart, pancreas, liver and the vascular system and participate in pathophysiological processes such as angiogenesis and TRL metabolism. HSPGs are structurally different between tissues as represented by unique disaccharide repeats and modifications of heparan sulfate chains (HS chains) (149, 156). These structural changes are necessary to enable HSPGs to differentially bind proteins and lipoprotein particles in order to perform varied functions including: 1) co-receptors for growth factor signaling 2) allow adhesion of cells to the extracellular matrix (ECM) and consequently aiding migration of cells 3) binding of microbial pathogens and 4) uptake of triglycerides (TG) for energy use or storage (109).

The HSPG are composed of a “backbone” core protein consisting of either syndecans, which are transmembrane proteins or glypicans, which are attached to the cell membrane by a glycosyl-phosphatidyl-inositol anchor. The HS chains are covalently attached to the serine residues present in the core proteins and consist of large unique polysaccharides of up to 200 repeating disaccharides units consisting of N-acetyl glucosamine and D-glucuronic

acid (149, 156). The synthesis of HS chains involves a plethora of different proteins, such as Exostosin Glycosyltransferase 1 and 2 (EXT1 and EXT2) involved in chain elongation, Heparan Sulfotransferases involved in the sulfation of the carbon at the position 2, 3 and 6 and N-deacetylase/N-Sulfotransferase 1 (NDST1) involved in the sulfation of N residue. Altogether, more than 25 different proteins are involved (109).

A number of proteins, such as Heparanase and Sulfatase 1 and 2 (SULF1 and SULF2), are involved in the extracellular remodeling of HSPGs, which interferes with the biological functions of HSPG. In this respect it has been shown that SULF2 can greatly diminish binding of Vascular Endothelial Growth Factor A (VEGF-A) and Fibroblast Growth factor 1 (FGF-1) (157). Interestingly, SULF2 can also actively interfere with proteins already immobilized to HSPG. In diabetes, cancer or dysregulation of the coagulation system, uncontrolled HSPG remodeling is therefore expected to partly underlie the pathobiology (158). Heparanase cleaves HSPG at the cell surface and in the ECM (for review see (158)). SULF1 and SULF2 modify the 6-O-sulfate group on tri-sulfated glucosamine residues in an environment of neutral pH (156, 158, 159). SULF1 and SULF2 share 60% sequence identity. They are synthesized as pre-pro-protein with a molecular weight of 125 kDa. The signal peptide is removed and the pro-protein is then cleaved by a furin-type proteinase into 2 fragments of 75 and 50 kDa which both exhibit extracellular sulfatase activity (160). The gene for *SULF2* is located on chromosome 20 and for *SULF1* on chromosome 8.

HSPG AND LIPOPROTEIN METABOLISM

TRL metabolism involves a sequence of steps involving hydrolysis of triglycerides (TG) and subsequent uptake of the remnant particles in the liver (161, 162). The first rate-limiting step is the hydrolysis of triglycerides by the enzyme Lipoprotein Lipase (LPL) facilitating uptake of free fatty acids for energy use or storage as TG in adipose tissue, muscle and heart. Lipoprotein Lipase is synthesized in parenchymal cells. Upon maturation by Lipase Maturation Factor 1 (LMF1) LPL is secreted and then transported to the surface of vascular endothelial cells (163). To date, how LPL reaches the cell surface is still under investigation. It was thought that LPL was anchored to the endothelial cell surface by binding to HSPG (164). Interestingly, patients with a mutation in Collagen XVIII (*COL18A1*), an HSPG present in basement membranes, have increased plasma TG levels and decreased LPL activity and mass, endorsing a role for HSPG in LPL translocation (165). However, the identification of GPIHBP1 as the platform for LPL-mediated triglyceride lipolysis at the endothelial cell surface has fundamentally changed this concept (166). In the heart LPL is synthesized by the cardiomyocytes. After reaching the myocyte cell surface, LPL binds to HSPG and is transported across the interstitial space where LPL binds to glycosyl-phosphatidyl-inositol HDL binding protein 1 (GPIHBP1) which facilitates further transport of LPL across the cell to the apical endothelial cell surface where LPL will hydrolyze TG (167, 168). To date, patients with a complete loss-of function of GPIHBP1 have a severe hypertriglyceridemic phenotype comparable to that observed in patients with *LPL* or *APOC2* deficiency (169).

Hepatic TRL clearance in mice involves, to date, 3 different receptors, Low-density lipoprotein receptor (LDLR), LDLR-related protein 1 (LRP1) and HSPG, which are expressed on the cell surface of the hepatocytes and are able to bind TRL particles. Early evidence was obtained by generation of a murine model with a hepatic deletion of Syndecan 1 (*Sdc1*), which invariably showed delayed TRL clearance (170). Concomitantly, the role of syndecan-1 was further elucidated using human primary hepatocytes showing that syndecan-1 mediates the binding and uptake of TRL (171, 172). Shedding of syndecan-1 from human hepatocytes using phorbol myristic acid (PMA) leads to impaired TRL clearance which further establishes the concept of HSPG involvement in hepatic TRL metabolism. To date, injection of lipopolysaccharide (LPS) results in the shedding of hepatic Sdc1, resulting in impaired TRL clearance and hypertriglyceridemia (171). The role of different receptors in TRL clearance was further addressed in studies using different genetically modified mouse models i.e. *Ldlr*^{-/-}, liver-specific *Ndst1*^{-/-} and *Lrp1*^{-/-}, showing that the LDL receptor and the sulfation pattern of HSPG are fundamental in the clearance of TRL by the liver, whereas *Lrp1* only plays an essential role in the absence of the *Ldlr* and validated the concept that sulfation of both syndecan-1 and specific sulfation patterns of the HS chain are crucial for TRL binding and uptake (173). The importance of HSPG chain length was illustrated using mice deficient in *Ext1*, which also exhibited moderate increased plasma TG levels (174).

The interplay between Low-density lipoprotein receptor (LDLR), LDLR-related protein 1 (LRP1) and HSPG in hepatic TRL metabolism in humans is not fully elucidated. Patients with a homozygous complete loss-of-function mutation in *LDLR* (Familial Hypercholesterolemia, FH) have at best moderately elevated plasma TG levels (175, 176). Interestingly, genetic variations (SNPs) in glucuronic acid epimerase (*GLCE*), an enzyme involved in the synthesis of the HS chain were associated with increased plasma TG levels in Turkish families (177). To further address this issue we measured postprandial TRL clearance in subjects with heterozygous FH and matched controls and were able to confirm an important contribution for the LDLR in postprandial hepatic TRL clearance reflected by increased incremental area under the curve (iAUC) for both TG and retinylesters, a marker for intestinal lipid uptake (174). However, postprandial TRL clearance in subjects with a heterozygous loss-of-function mutation in *EXT1* or *EXT2*, who have a defect in HSPG chain length, was not different from that in matched controls, suggesting that HSPG chain length in human, unlike mice, only has a marginal impact in human TRL metabolism and that a second hit (like LDL deficiency) is needed (174).

SULF2 AND HEPATIC CLEARANCE OF TRL

SULF2 modifies the HS chain sulfation *in vivo* and may influence TRL uptake and clearance. This was demonstrated in a murine model of diabetes (*db/db mice*), where hepatic *Sulf2* expression was strongly upregulated and was associated with decreased HSPG sulfation and increased plasma TG levels (178). Inhibition of hepatic *Sulf2* expression with an

allele-specific oligo (ASO) was able to correct the fasting and postprandial TG levels and normalizes postprandial TRL metabolism by improving the 6-O-sulfation of the HS chain (120). Hepatocytes isolated from *db/db* mice exhibited impaired VLDL binding and uptake which could be reversed by *Sulf2*-ASO, and was a proof of concept that 6-O-sulfation of HSPG plays an essential role in HSPG mediated TRL metabolism in mouse hepatocytes.

In humans it was demonstrated that liver *SULF2* mRNA expression levels were significantly associated with fasting plasma TG in obese subjects (135). Next, 7 tagging SNPs in *SULF2* were analyzed for association with fasting and postprandial plasma TG levels in subjects with type 2 diabetes. *SULF2* rs2281279 reproducibly associated with TRL parameters. Individuals with the minor allele predispose for significant lower postprandial TRL levels but also improved Hba1C and plasma glucose, which may suggest that regulation of *SULF2* depends upon the insulin resistant state. In accordance, Matikainen et al (179) demonstrated that in healthy individuals the minor allele of rs2281279 was associated with lower hepatic *SULF2* mRNA levels and improved postprandial TRL clearance. Collectively, these data support an important role for HSPG 6-O-sulfation in human TRL metabolism and indicate that *SULF2* may be an attractive target for therapeutic intervention to decrease the atherogenic lipoprotein phenotype in type 2 diabetes.

SULF2 AND ANGIOGENESIS

Atherogenic dyslipidemia affects vascular endothelium and may also modulate other endothelial processes like angiogenesis (180). Angiogenesis is the highly coordinated process of vessel sprouts originating from the pre-existing vasculature, which can exacerbate many diseases including cancer and proliferative retinopathies (105). Endothelial cells receiving pro-angiogenic signals will differentiate into angiogenic phenotypes. The tip cells are leading the newly formed vessel sprout towards the source of pro-angiogenic growth factors. The proliferating, lumen-forming stalk cells are elongating the sprout, and further down the sprout are the Phalanx cells, which stabilize cell junctions and recruit supporting cells such as pericytes (105, 181). Tip and stalk cells each depends on different metabolic pathways. Tip cells that migrate towards tissues with low oxygen concentrations use anaerobic glycolysis for ATP production which allows the tip cells to generate a large amount of ATP molecules within a short time frame resulting in a vast sprouting process (155, 182). Stalk cells, on the other hand, stimulate fatty acid oxidation pathways to supply carbon sources for synthesis of intermediates necessary for proliferation (180). HSPGs have been implicated in angiogenesis since they bind most of the angiogenic growth factors, wherein the sulfation patterns of HSPG are important to allow binding of the different molecules. *SULF2* has been identified in a microarray comparing mRNA transcriptome in tip cells to that of other endothelial cells (3). Herein, it was found that tip cells, in contrast to stalk cells, do not express *SULF2* mRNA, implying a role for *SULF2* in stalk cells rather than tip cells. As mentioned above,

stalk cells are very proliferative, and require fatty acids to supply biomass for cell division. TRL are an important source for fatty acid supply to the endothelial cells and HSPGs facilitates binding and uptake. SULF2, by regulating the 6-O sulfation of HSPG, could therefore be essential for sprouting stalk cells by facilitating TRL uptake. Alternatively, SULF2 can interfere with angiogenesis by influencing growth factor-HSPG-interactions. Many pro-angiogenic growth factors such as vascular endothelial growth factor (VEGF) and fibroblast growth factor (FGF) have an HSPG-binding site, which can be influenced by SULF2 (157). Interaction of growth factors with HSPGs can modify receptor binding and induce differential signals for cells. A recent study shows that SULF2 influences growth factor signaling in a highly vascularized malignancy (glioblastoma) and reveals its role in Pericyte-derived Growth Factor Receptor- α (PDGFR- α) signaling. Ablation of SULF2 in mouse models resulted in a reduction in PDGFR- α signaling and consequently

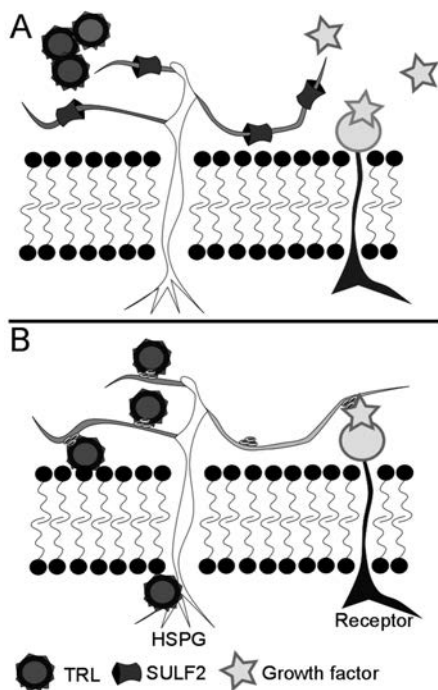


Figure 1. SULF2 on HSPGs. Schematic representation of the action of SULF2 on cell membranes. A. SULF2 removes negatively charged 6-O-sulfate groups from the HS chains linked to the transmembrane Syndecan-1 core protein. Removal of sulfate groups prevents binding of TRL (left), hereby preventing uptake into the cell. Growth factor binding to the HS chains is prevented by SULF2-mediated removal of sulfate groups (right) which alters receptor binding and consequent downstream signaling. B. Absence of SULF2 allows binding of TRLs to the negatively charged HS chains, which enables uptake into the cell for storage and processing of TRL content (left). Growth factors also bind negatively charged HS chains, which influences receptor binding and consequent downstream signaling.

a reduction in cell and tumor growth (183). Whether these reductions could be due to changes in the growth of the tumor vasculature remains unclear.

VEGF signaling, which is essential for vessel growth, is also modified by SULF2 mediated changes of the HSPGs. It has been shown that SULF2 can impede in binding of VEGF to immobilized heparin (157). Furthermore, downstream signaling of VEGF-receptor 2 (VEGFR2) is influenced by the binding-state of VEGF (178). Binding of VEGF results in more migratory downstream signaling through the phosphorylation of P38, whilst unbound VEGF stimulated a more proliferative signal through Akt phosphorylation (178). These modifications, influenced by SULF2, may be essential for differential tip and stalk cell signaling, enabling them to perform their angiogenic role. In summary, whilst SULF2 is necessary for normal angiogenesis, whether this effect is established through modifications of growth factor-HSPG-interactions or an effect on stalk cell fatty acid metabolism has yet to be revealed.

4.3

In summary, HSPGs are instrumental for normal TRL metabolism but also play an essential role in angiogenesis by facilitating TRL uptake and allowing VEGF-mediated cell signaling. SULF2, by removing the 6-O- sulfation group, is an important regulator of HSPG function in TRL homeostasis and angiogenesis. Future studies are required to investigate whether SULF2 can be used as antisense based therapeutic target.

REFERENCES

1. Gerhardt H, Golding M, Fruttiger M, Ruhrberg C, Lundkvist A, Abramsson A, et al. VEGF guides angiogenic sprouting utilizing endothelial tip cell filopodia. *J Cell Biol.* 2003;161(6):1163-77.
2. Claxton S, Fruttiger M. Periodic Delta-like 4 expression in developing retinal arteries. *Gene Expr Patterns.* 2004;5(1):123-7.
3. Siemerink MJ, Klaassen I, Vogels IM, Griffioen AW, Van Noorden CJ, Schlingemann RO. CD34 marks angiogenic tip cells in human vascular endothelial cell cultures. *Angiogenesis.* 2012;15(1):151-63.
4. Jakobsson L, Franco CA, Bentley K, Collins RT, Ponsioen B, Aspalter IM, et al. Endothelial cells dynamically compete for the tip cell position during angiogenic sprouting. *Nat Cell Biol.* 2010;12(10):943-53.
5. Arima S, Nishiyama K, Ko T, Arima Y, Hakozaki Y, Sugihara K, et al. Angiogenic morphogenesis driven by dynamic and heterogeneous collective endothelial cell movement. *Development.* 2011;138(21):4763-76.
6. Folkman J, Haudenschild C. angiogenesis *in vitro*. *Nature.* 1980;288:551-6.
7. Califano JP, Reinhart-King CA. A Balance of Substrate Mechanics and Matrix Chemistry Regulates Endothelial Cell Network Assembly. *Cellular and Molecular Bioengineering.* 2008;1(2-3):122-32.
8. Parsa H, Upadhyay R, Sia SK. Uncovering the behaviors of individual cells within a multicellular microvascular community. *Proc Natl Acad Sci U S A.* 2011;108(12):5133-8.
9. Manoussaki D, Lubkin SR, Vernon RB, Muiray JD. A mechanical model for the formation of vascular networks *in vitro*. *Acta biotheoretica.* 1996;44:271-82.
10. Serini G, Ambrosi D, Giraudo E, Gamba A. Modeling the early stages of vascular network assembly. *EMBO J.* Preziosi, L. Bussoline, F.;22(8):1771-9.
11. Merks RM, Perryn ED, Shirinifard A, Glazier JA. Contact-inhibited chemotaxis in de novo and sprouting blood-vessel growth. *PLoS Comput Biol.* 2008;4(9):e1000163.
12. van Oers RF, Rens EG, LaValley DJ, Reinhart-King CA, Merks RM. Mechanical cell-matrix feedback explains pairwise and collective endothelial cell behavior *in vitro*. *PLoS Comput Biol.* 2014;10(8):e1003774.
13. Szabo A, Perryn ED, Czirok A. Network formation of tissue cells via preferential attraction to elongated structures. *Phys Rev Lett.* 2007;98(3):038102.
14. Szabo A, Mehes E, Kosa E, Czirok A. Multicellular sprouting *in vitro*. *Biophys J.* 2008;95(6):2702-10.
15. Merks RM, Brodsky SV, Goligorsky MS, Newman SA, Glazier JA. Cell elongation is key to *in silico* replication of *in vitro* vasculogenesis and subsequent remodeling. *Dev Biol.* 2006;289(1):44-54.
16. Szabo A, Czirok A. The Role of Cell-Cell Adhesion in the Formation of Multicellular Sprouts. *Math Model Nat Phenom.* 2010;5(1):106.
17. Hellstrom M, Phng LK, Hofmann JJ, Wallgard E, Coultas L, Lindblom P, et al. Dll4 signalling through Notch1 regulates formation of tip cells during angiogenesis. *Nature.* 2007;445(7129):776-80.
18. Suchting S, Freitas C, le Noble F, Benedito R, Breant C, Duarte A, et al. The Notch ligand Delta-like 4 negatively regulates endothelial tip cell formation and vessel branching. *Proc Natl Acad Sci U S A.* 2007;104(9):3225-30.
19. Lobov IB, Renard RA, Papadopoulos N, Gale NW, Thurston G, Yancopoulos GD, et al. Delta-like ligand 4 (Dll4) is induced by VEGF as a negative regulator of angiogenic sprouting. *Proc Natl Acad Sci U S A.* 2007;104(9):3219-24.
20. Sainson RCA, Aoto J, Nakatsu MN, Holderfield MT, Conn E, Koller E, et al. Cell-autonomous notch signaling regulates endothelial cell branching and proliferation during vascular tubulogenesis. *FASEB J.* 2005;19:1027-9.
21. Williams CK, Li JL, Murga M, Harris AL, Tosato G. Up-regulation of the Notch ligand Delta-like 4 inhibits VEGF-induced endothelial cell function. *Blood.* 2006;107(3):931-9.

22. Scehnet JS, Jiang W, Kumar SR, Krasnoperov V, Trindade A, Benedito R, et al. Inhibition of Dll4-mediated signaling induces proliferation of immature vessels and results in poor tissue perfusion, hemostasis, thrombosis and vascular biology. *2007;109(11):4753-60.*
23. Ridgway J, Zhang G, Wu Y, Stawicki S, Liang WC, Chantry Y, et al. Inhibition of Dll4 signalling inhibits tumour growth by deregulating angiogenesis. *Nature. 2006;444(7122):1083-7.*
24. Patel NS, Li JL, Generali D, Poulsom R, Cranston DW, Harris AL. Up-regulation of delta-like 4 ligand in human tumor vasculature and the role of basal expression in endothelial cell function. *Cancer Res. 2005;65(19):8690-7.*
25. Hainaud P, Contreres JO, Villemain A, Liu LX, Plouet J, Tobelem G, et al. The role of the vascular endothelial growth factor-Delta-like 4 ligand/Notch4-ephrin B2 cascade in tumor vessel remodeling and endothelial cell functions. *Cancer Res. 2006;66(17):8501-10.*
26. Jakobsson L, Bentley K, Gerhardt H. VEGFRs and Notch: a dynamic collaboration in vascular patterning. *Biochem Soc Trans. 2009;37(Pt 6):1233-6.*
27. Hiratsuka S, Minowa O, Kuno J, Noda T, Shibuya M. Flt-1 lacking the tyrosine kinase domain is sufficient for normal development and angiogenesis in mice. *Proc Natl Acad Sci USA. 1998;95:9349-54.*
28. Rahimi N, Dayanir V, Lashkari K. Receptor chimeras indicate that the vascular endothelial growth factor receptor-1 (VEGFR-1) modulates mitogenic activity of VEGFR-2 in endothelial cells. *J Biol Chem. 2000;275(22):16986-92.*
29. Arnaoutova I, George J, Kleinman HK, Benton G. The endothelial cell tube formation assay on basement membrane turns 20: state of the science and the art. *Angiogenesis. 2009;12(3):267-74.*
30. Siekmann AF, Lawson ND. Notch signalling limits angiogenic cell behaviour in developing zebrafish arteries. *Nature. 2007;445(7129):781-4.*
31. Long BL, Rekhi R, Abrego A, Jung J, Qutub AA. Cells as state machines: cell behavior patterns arise during capillary formation as a function of BDNF and VEGF. *J Theor Biol. 2013;326:43-57.*
32. Graner F, Glazier JA. Simulation of Biological Cell Sorting Using a Two-Dimensional Extended Potts Model. *physical review letters. 1992;69(13):2013-6.*
33. Glazier JA. Dynamics of cellular patterns. *physical review letters. 1992;47(3):2013-6.*
34. Palm MM, Merks RM. Vascular networks due to dynamically arrested crystalline ordering of elongated cells. *Phys Rev E Stat Nonlin Soft Matter Phys. 2013;87(1):012725.*
35. Tranqui L, Tracqui P. Mechanical signalling and angiogenesis. The integration of cell-extracellular matrix couplings. *Comptes Rendus de l'Académie des Sciences - Series III - Sciences de la Vie. 2000;323(1):31-47.*
36. Gamba A, Ambrosi D, Coniglio A, de Candia A, Di Talia S, Giraudo E, et al. Percolation, morphogenesis, and burgers dynamics in blood vessels formation. *Phys Rev Lett. 2003;90(11):118101.*
37. Namy P, Ohayon J, Tracqui P. Critical conditions for pattern formation and *in vitro* tubulogenesis driven by cellular traction fields. *J Theor Biol. 2004;227(1):103-20.*
38. Gory-Faure S, Prandini MH, Pointu H, Roullot V, Pignot-Paintrand I, Vernet M, et al. Role of vascular endothelial-cadherin in vascular morphogenesis. *development. 1999;126:2093-102.*
39. Shirinifard A, Gens JS, Zaitlen BL, Poplawski NJ, Swat M, Glazier JA. 3D multi-cell simulation of tumor growth and angiogenesis. *PLoS One. 2009;4(10):e7190.*
40. Shirinifard A, Glazier JA, Swat M, Gens JS, Family F, Jiang Y, et al. Adhesion failures determine the pattern of choroidal neovascularization in the eye: a computer simulation study. *PLoS Comput Biol. 2012;8(5):e1002440.*
41. Kleinstreuer N, Dix D, Rountree M, Baker N, Sipes N, Reif D, et al. A computational model predicting disruption of blood vessel development. *PLoS Comput Biol. 2013;9(4):e1002996.*
42. Savill NJ, Hogeweg P. Modelling morphogenesis: from single cells to crawling slugs. *Journal of Theoretical Biology. 1997;184:229-35.*

43. Angelini TE, Hannezo E, Trepas X, Marquez M, Fredberg JJ, Weitz DA. Glass-like dynamics of collective cell migration. *Proc Natl Acad Sci U S A*. 2011;108(12):4714-9.
44. Bentley K, Franco CA, Philippides A, Blanco R, Dierkes M, Gebala V, et al. The role of differential VE-cadherin dynamics in cell rearrangement during angiogenesis. *Nat Cell Biol*. 2014;16(4):309-21.
45. Krieg M, Arboleda-Estudillo Y, Puech PH, Kafer J, Graner F, Muller DJ, et al. Tensile forces govern germ-layer organization in zebrafish. *Nat Cell Biol*. 2008;10(4):429-36.
46. Kohn-Luque A, de Back W, Yamaguchi Y, Yoshimura K, Herrero MA, Miura T. Dynamics of VEGF matrix-retention in vascular network patterning. *Phys Biol*. 2013;10(6):066007.
47. Boas SE, Merks RM. Tip cell overtaking occurs as a side effect of sprouting in computational models of angiogenesis. *BMC Syst Biol*. 2015;9:86.
48. McCutcheon M. chemotaxis in leukocytes. *physiological reviews*. 1946;26(3):319-35.
49. Dona E, Barry JD, Valentin G, Quirin C, Khmelinskii A, Kunze A, et al. Directional tissue migration through a self-generated chemokine gradient. *Nature*. 2013;503(7475):285-9.
50. Benedito R, Rocha SF, Woeste M, Zamykal M, Radtke F, Casanovas O, et al. Notch-dependent VEGFR3 upregulation allows angiogenesis without VEGF-VEGFR2 signalling. *Nature*. 2012;484(7392):110-4.
51. Benedito R, Roca C, Sorensen I, Adams S, Gossler A, Fruttiger M, et al. The notch ligands Dll4 and Jagged1 have opposing effects on angiogenesis. *Cell*. 2009;137(6):1124-35.
52. Harrington LS, Sainson RC, Williams CK, Taylor JM, Shi W, Li JL, et al. Regulation of multiple angiogenic pathways by Dll4 and Notch in human umbilical vein endothelial cells. *Microvasc Res*. 2008;75(2):144-54.
53. del Toro R, Prahst C, Mathivet T, Siegfried G, Kaminker JS, Larrivee B, et al. Identification and functional analysis of endothelial tip cell-enriched genes. *Blood*. 2010;116(19):4025-33.
54. Strasser GA, Kaminker JS, Tessier-Lavigne M. Microarray analysis of retinal endothelial tip cells identifies CXCR4 as a mediator of tip cell morphology and branching. *Blood*. 2010;115(24):5102-10.
55. Ferrara N, Hillan KJ, Gerber HP, Novotny W. Discovery and development of bevacizumab, an anti-VEGF antibody for treating cancer. *Nat Rev Drug Discov*. 2004;3(5):391-400.
56. Seghezzi G, Patel S, Ren CJ, Gualandris A, Pintucci G, Robbins ES, et al. Fibroblast growth factor-2 (FGF-2) induces vascular endothelial growth factor (VEGF) expression in the endothelial cells of forming capillaries: an autocrine mechanism contributes to angiogenesis. *the journal of cell biology*. 1998;141:1659-73.
57. Franco M, Roswall P, Cortez E, Hanahan D, Pietras K. Pericytes promote endothelial cell survival through induction of autocrine VEGF-A signaling and Bcl-w expression. *Blood*. 2011;118(10):2906-17.
58. Geudens I, Gerhardt H. Coordinating cell behaviour during blood vessel formation. *Development*. 2011;138(21):4569-83.
59. Gupta SK, Lysko PG, Pillarisetti K, Ohlstein E, Stadel JM. Chemokine receptors in human endothelial cells. *the journal for biochemistry and molecular biology*. 1998;273(7):4282-7.
60. Salcedo R, Oppenheim JJ. Role of chemokines in angiogenesis: CXCL12/SDF-1 and CXCR4 interaction, a key regulator of endothelial cell responses. *Microcirculation*. 2003;10(3-4):359-70.
61. Tatemoto K, Hosoya M, Habata Y, Fujii R, Kakegawa T, Zou MX, et al. Isolation and characterization of a novel endogenous peptide ligand for the human APJ receptor. *Biochem Biophys Res Commun*. 1998;251:471-6.
62. Kasai A, Shintani N, Oda M, Kakuda M, Hashimoto H, Matsuda T, et al. Apelin is a novel angiogenic factor in retinal endothelial cells. *Biochem Biophys Res Commun*. 2004;325(2):395-400.
63. Kalin RE, Kretz MP, Meyer AM, Kispert A, Heppner FL, Brandli AW. Paracrine and autocrine mechanisms of apelin signaling govern embryonic and tumor angiogenesis. *Dev Biol*. 2007;305(2):599-614.

64. Salvucci O, Yao L, Villalba S, Sajewicz A, Pittaluga S, Tosato G. Regulation of endothelial cell branching morphogenesis by endogenous chemokine stromal-derived factor-1. *chemokines*. 2002;99(8):2703-11.
65. Reinhart-King CA, Dembo M, Hammer DA. Cell-cell mechanical communication through compliant substrates. *Biophys J*. 2008;95(12):6044-51.
66. Cox CM, D'Agostino SL, Miller MK, Heimark RL, Krieg PA. Apelin, the ligand for the endothelial G-protein-coupled receptor, APJ, is a potent angiogenic factor required for normal vascular development of the frog embryo. *Dev Biol*. 2006;296(1):177-89.
67. Eyries M, Siegfried G, Ciumas M, Montagne K, Agrapart M, Lebrin F, et al. Hypoxia-induced apelin expression regulates endothelial cell proliferation and regenerative angiogenesis. *Circ Res*. 2008;103(4):432-40.
68. Kasai A, Shintani N, Kato H, Matsuda S, Gomi F, Haba R, et al. Retardation of retinal vascular development in apelin-deficient mice. *Arterioscler Thromb Vasc Biol*. 2008;28(10):1717-22.
69. Caolo V, van den Akker NM, Verbruggen S, Donners MM, Swennen G, Schulten H, et al. Feed-forward signaling by membrane-bound ligand receptor circuit: the case of NOTCH DELTA-like 4 ligand in endothelial cells. *J Biol Chem*. 2010;285(52):40681-9.
70. Milde F, Bergdorf M, Koumoutsakos P. A hybrid model for three-dimensional simulations of sprouting angiogenesis. *Biophys J*. 2008;95(7):3146-60.
71. Bauer AL, Jackson TL, Jiang Y. A cell-based model exhibiting branching and anastomosis during tumor-induced angiogenesis. *Biophys J*. 2007;92(9):3105-21.
72. Bauer AL, Jackson TL, Jiang Y. Topography of extracellular matrix mediates vascular morphogenesis and migration speeds in angiogenesis. *PLoS Comput Biol*. 2009;5(7):e1000445.
73. Artel A, Mehdizadeh H, Chiu YC, Brey EM, Cinar A. An agent-based model for the investigation of neovascularization within porous scaffolds. *Tissue Eng Part A*. 2011;17(17-18):2133-41.
74. Mehdizadeh H, Sumo S, Bayrak ES, Brey EM, Cinar A. Three-dimensional modeling of angiogenesis in porous biomaterial scaffolds. *Biomaterials*. 2013;34(12):2875-87.
75. Jackson T, Zheng X. A cell-based model of endothelial cell migration, proliferation and maturation during corneal angiogenesis. *Bull Math Biol*. 2010;72(4):830-68.
76. Qutub AA, Popel AS. Elongation, proliferation & migration differentiate endothelial cell phenotypes and determine capillary sprouting. *BMC Syst Biol*. 2009;3:13.
77. Travasso RD, Corvera Poire E, Castro M, Rodriguez-Manzanique JC, Hernandez-Machado A. Tumor angiogenesis and vascular patterning: a mathematical model. *PLoS One*. 2011;6(5):e19989.
78. Bentley K, Gerhardt H, Bates PA. Agent-based simulation of notch-mediated tip cell selection in angiogenic sprout initialisation. *J Theor Biol*. 2008;250(1):25-36.
79. Bentley K, Mariggi G, Gerhardt H, Bates PA. Tipping the balance: robustness of tip cell selection, migration and fusion in angiogenesis. *PLoS Comput Biol*. 2009;5(10):e1000549.
80. Bautch VL. VEGF-directed blood vessel patterning: from cells to organism. *Cold Spring Harb Perspect Med*. 2012;2(9):a006452.
81. Kidoya H, Ueno M, Yamada Y, Mochizuki N, Nakata M, Yano T, et al. Spatial and temporal role of the apelin/APJ system in the caliber size regulation of blood vessels during angiogenesis. *EMBO J*. 2008;27(3):522-34.
82. Hara C, Kasai A, Gomi F, Satooka T, Sakimoto S, Nakai K, et al. Laser-induced choroidal neovascularization in mice attenuated by deficiency in the apelin-APJ system. *Invest Ophthalmol Vis Sci*. 2013;54(6):4321-9.
83. Taylor KL, Henderson AM, Hughes CC. Notch activation during endothelial cell network formation *in vitro* targets the basic HLH transcription factor HESR-1 and downregulates VEGFR-2/KDR expression. *Microvasc Res*. 2002;64(3):372-83.
84. Funahashi Y, Shawber CJ, Vorontchikhina M, Sharma A, Outtz HH, Kitajewski J. Notch regulates the angiogenic response via induction of VEGFR-1. *J Angiogenes Res*. 2010;2(1):3.

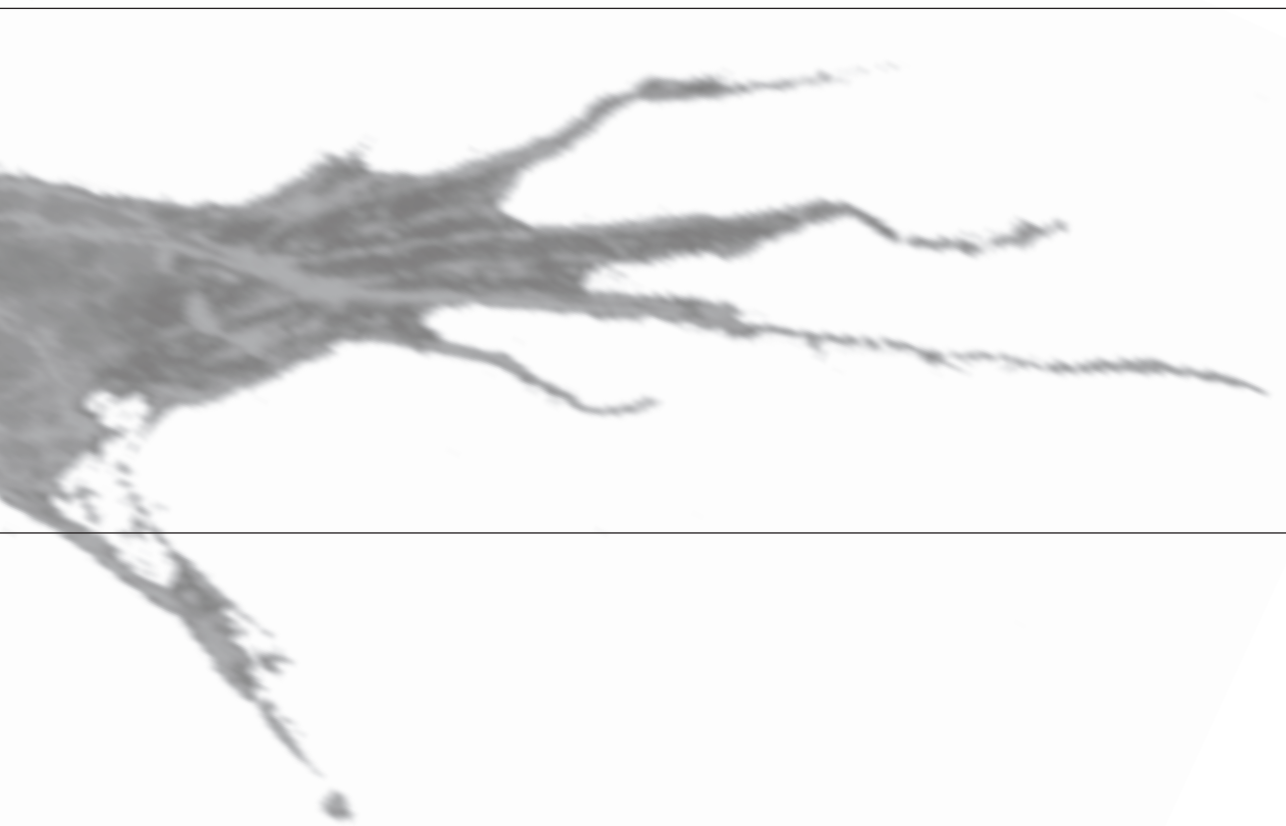
85. Park JE, Chen HH, Winer J, Houck KA, Ferrara N. Placenta growth factor. *The Journal of Biological Chemistry*. 1994;269(41):25646-54.
86. Gavard J, Patel V, Gutkind JS. Angiopoietin-1 prevents VEGF-induced endothelial permeability by sequestering Src through mDia. *Dev Cell*. 2008;14(1):25-36.
87. Kasai A, Ishimaru Y, Higashino K, Kobayashi K, Yamamuro A, Yoshioka Y, et al. Inhibition of apelin expression switches endothelial cells from proliferative to mature state in pathological retinal angiogenesis. *Angiogenesis*. 2013;16(3):723-34.
88. Ruhrberg C. Spatially restricted patterning cues provided by heparin-binding VEGF-A control blood vessel branching morphogenesis. *Genes & Development*. 2002;16(20):2684-98.
89. Ribatti D, Nico B, Crivellato E. The role of pericytes in angiogenesis. *Int J Dev Biol*. 2011;55(3):261-8.
90. Bray SJ. Notch signalling: a simple pathway becomes complex. *Nat Rev Mol Cell Biol*. 2006;7(9):678-89.
91. Galler BA, Fisher MJ. An improved equivalence algorithm. *Communications of the ACM*. 1964;7(5):301-3.
92. Graham RL. An efficient algorithm for determining the convex hull of a finite planar set. *Information processing letters*. 1972;1.
93. Guidolin D, Vacca A, Nussdorfer GG, Ribatti D. A new image analysis method based on topological and fractal parameters to evaluate the angiostatic activity of docetaxel by using the Matrigel assay *in vitro*. *Microvasc Res*. 2004;67(2):117-24.
94. Dougherty ER, Lotufo RA. Hands-on morphological image processing. press S, editor2003.
95. Coelho LP. Mahotas: Open source software for scriptable computer vision. *Journal of Open Research Software*. 2013;1(1).
96. Polymorph [15-7-2014]. Available from: <http://luispedro.org/software/pymorph>.
97. Dijkstra EW. A note on two problems in connexion with graphs. *Numerische Mathematik*. 1959;1:269-71.
98. Swat MH, Thomas GL, Belmonte JM, Shirinifard A, Hmeljak D, Glazier JA. Multi-scale modeling of tissues using CompuCell3D. *Methods Cell Biol*. 2012;110:325-66.
99. Palm MM, Merks RM. Large-Scale Parameter Studies of Cell-Based Models of Tissue Morphogenesis Using CompuCell3D or VirtualLeaf. *Methods in molecular biology*. 1189: MIMB; 2014.
100. Korff T, Augustin HG. Integration of endothelial cells in multicellular spheroids prevents apoptosis and induces differentiation. *J Cell Biol*. 1998;143(5):1341-52.
101. Meijering E, Jacob M, Sarría JC, Steiner P, Hirling H, Unser M. Design and validation of a tool for neurite tracing and analysis in fluorescence microscopy images. *Cytometry A*. 2004;58(2):167-76.
102. reverse transcription siRNA [15-7-2014]. Available from: <http://www.thermoscientificbio.com/uploadedfiles/resources/reverse-transfection-of-sirna-protocol.pdf>.
103. Tukey JW. Comparing individual means in the analysis of variance. *Biometrics*. 1949;5(2):99-114.
104. Williams AH, Newman-Keuls, Tukey JW. *Encyclopedia of research design*2010. 897-904 p.
105. Dallinga MG, Boas SEM, Klaassen I, Merks RHM, van Noorden CJF, Schlingemann RO. Tip cells in angiogenesis. *eLS*. 2015:1-10.
106. Yang Z, Mo X, Gong Q, Pan Q, Yang X, Cai W, et al. Critical effect of VEGF in the process of endothelial cell apoptosis induced by high glucose. *Apoptosis*. 2008;13(11):1331-43.
107. Geretti E, Shimizu A, Klagsbrun M. Neuropilin structure governs VEGF and semaphorin binding and regulates angiogenesis. *Angiogenesis*. 2008;11(1):31-9.
108. Sarabipour S, Mac Gabhann F. VEGF-A121a binding to Neuropilins - A concept revisited. *Cell Adh Migr*. 2018;12(3):204-14.
109. Billings PC, Pacifici M. Interactions of signaling proteins, growth factors and other proteins with heparan sulfate: mechanisms and mysteries. *Connect Tissue Res*. 2015;56(4):272-80.

110. Smorenburg S, van Noorden CJF. The complex effects of heparins on cancer progression and metastasis in experimental studies. *Pharmacological reviews*. 2001;53:93-105.
111. Kohn-Luque A, de Back W, Starruss J, Mattiotti A, Deutsch A, Perez-Pomares JM, et al. Early embryonic vascular patterning by matrix-mediated paracrine signalling: a mathematical model study. *PLoS One*. 2011;6(9):e24175.
112. Pries AR, Secomb TW, Gaetgens P. The endothelial surface layer. *Pflugers Arch*. 2000;440(5):653-66.
113. Gouverneur M, Berg B, Nieuwdorp M, Stroes E, Vink H. Vasculoprotective properties of the endothelial glycocalyx: effects of fluid shear stress. *J Intern Med*. 2006;259(4):393-400.
114. Möckl L, Hirn S, A.A. T, Uhl B, Bräuchle CF, Krombach F. The glycocalyx regulates the uptake of nanoparticles by human endothelial cells *in vitro*. *Nanomedicine*. 2017;12(3):207-17.
115. LeBlanc ME, Saez-Torres KL, Cano I, Hu Z, Saint-Geniez M, Ng YS, et al. Glycocalyx regulation of vascular endothelial growth factor receptor 2 activity. *FASEB J*. 2019;33(8):9362-73.
116. Avizienyte E, Cole CL, Rushton G, Miller GJ, Bugatti A, Presta M, et al. Synthetic Site-Selectively Mono-6-O-Sulfated Heparan Sulfate Dodecasaccharide Shows Anti-Angiogenic Properties *In Vitro* and Sensitizes Tumors to Cisplatin *In Vivo*. *PLoS One*. 2016;11(8):e0159739.
117. Chen E, Stringer SE, Rusch MA, Selleck SB, Ekker SC. A unique role for 6-O sulfation modification in zebrafish vascular development. *Developmental Biology*. 2005;284(2):364-76.
118. Dai Y, Yang Y, MacLeod V, Yue X, Rapraeger AC, Shriver Z, et al. HSulf-1 and HSulf-2 are potent inhibitors of myeloma tumor growth *in vivo*. *J Biol Chem*. 2005;280(48):40066-73.
119. Dallinga MG, Dallinga-Thie GM. Role of sulfatase 2 in lipoprotein metabolism and angiogenesis. *Curr Opin Lipidol*. 2016;27(2):181-6.
120. Hassing HC, Mooij H, Guo S, Monia BP, Chen K, Kulik W, et al. Inhibition of hepatic sulfatase-2 *in vivo*: a novel strategy to correct diabetic dyslipidemia. *Hepatology*. 2012;55(6):1746-53.
121. Teuwen LA, Draoui N, Dubois C, Carmeliet P. Endothelial cell metabolism: an update anno 2017. *Curr Opin Hematol*. 2017;24(3):240-7.
122. Nakamura MT, Yudell BE, Loor JJ. Regulation of energy metabolism by long-chain fatty acids. *Prog Lipid Res*. 2014;53:124-44.
123. Norata G. Gene expression and intracellular pathways involved in endothelial dysfunction induced by VLDL and oxidised VLDL. *Cardiovascular Research*. 2003;59(1):169-80.
124. Graupera M, Potente M. Regulation of angiogenesis by PI3K signaling networks. *Exp Cell Res*. 2013;319(9):1348-55.
125. Kotlinowski J, Jozkowicz A. PPAR Gamma and Angiogenesis: Endothelial Cells Perspective. *J Diabetes Res*. 2016;2016:8492353.
126. van der Schaft DWJ, Toebe EAH, Haseman JR, Mayo KH, Griffioen AW. Bactericidal/permeability-increasing protein (BPI) inhibits angiogenesis via induction of apoptosis in vascular endothelial cells. *Blood*. 2000;96(1):176-81.
127. Nowak-Sliwinska P, Alitalo K, Allen E, Anisimov A, Aplin AC, Auerbach R, et al. Consensus guidelines for the use and interpretation of angiogenesis assays. *Angiogenesis*. 2018;21(3):425-532.
128. Chieco P, Jonker A, De Boer BA, Ruijter JM, Van Noorden CJ. Image cytometry: protocols for 2D and 3D quantification in microscopic images. *Prog Histochem Cytochem*. 2013;47(4):211-333.
129. Rezaee F, Casetta B, Levels JH, Speijer D, Meijers JC. Proteomic analysis of high-density lipoprotein. *Proteomics*. 2006;6(2):721-30.
130. Ruijter JM, Thygesen HH, Schoneveld OJ, Das AT, Berkhout B, Lamers WH. Factor correction as a tool to eliminate between-session variation in replicate experiments: application to molecular biology and retrovirology. *Retrovirology*. 2006;3:2.
131. Dallinga MG, Yetkin-Arik B, Kayser RP, Vogels IMC, Nowak-Sliwinska P, Griffioen AW, et al. IGF2 and IGF1R identified as novel tip cell genes in primary microvascular endothelial cell monolayers. *Angiogenesis*. 2018;21:823-36.

132. Berndsen RH, Castrogiovanni C, Weiss A, Rausch M, Dallinga MG, Miljkovic-Licina M, et al. Anti-angiogenic effects of crenolanib are mediated by mitotic modulation independently of PDGFR expression. *Br J Cancer*. 2019;121(2):139-49.
133. Favier B, Alam A, Barron P, Bonnin J, Laboudie P, Fons P, et al. Neuropilin-2 interacts with VEGFR-2 and VEGFR-3 and promotes human endothelial cell survival and migration. *Blood*. 2006;108(4):1243-50.
134. Kim WH, Lee SH, Jung MH, Seo JH, Kim J, Kim MA, et al. Neuropilin2 expressed in gastric cancer endothelial cells increases the proliferation and migration of endothelial cells in response to VEGF. *Exp Cell Res*. 2009;315(13):2154-64.
135. Hassing HC, Surendran RP, Derudas B, Verrijken A, Francque SM, Mooij HL, et al. SULF2 strongly predisposes to fasting and postprandial triglycerides in patients with obesity and type 2 diabetes mellitus. *Obesity (Silver Spring)*. 2014;22(5):1309-16.
136. Ausprunk DH, Folkman J. Migration and proliferation of endothelial cells in preformed and newly formed blood vessels during tumor angiogenesis. *Microvasc Res*. 1977;14(1):53-65.
137. Chen L, Jiang W, Huang J, He BC, Zuo GW, Zhang W, et al. Insulin-like growth factor 2 (IGF-2) potentiates BMP-9-induced osteogenic differentiation and bone formation. *J Bone Miner Res*. 2010;25(11):2447-59.
138. Ho FM, Lin WW, Chen BC, Chao CM, Yang CR, Lin LY, et al. High glucose-induced apoptosis in human vascular endothelial cells is mediated through NF-kappaB and c-Jun NH2-terminal kinase pathway and prevented by PI3K/Akt/eNOS pathway. *Cell Signal*. 2006;18(3):391-9.
139. Rousseau S. Vascular Endothelial Growth Factor (VEGF)-driven Actin-based Motility Is Mediated by VEGFR2 and Requires Concerted Activation of Stress-activated Protein Kinase 2 (SAPK2/p38) and Geldanamycin-sensitive Phosphorylation of Focal Adhesion Kinase. *Journal of Biological Chemistry*. 2000;275(14):10661-72.
140. Shiojima I. Role of Akt Signaling in Vascular Homeostasis and Angiogenesis. *Circulation Research*. 2002;90(12):1243-50.
141. Fantin A, Maden CH, Ruhrberg C. Neuropilin ligands in vascular and neuronal patterning. *Biochem Soc Trans*. 2009;37(Pt 6):1228-32.
142. Fantin A, Vieira JM, Plein A, Denti L, Fruttiger M, Pollard JW, et al. NRP1 acts cell autonomously in endothelium to promote tip cell function during sprouting angiogenesis. *Blood*. 2013;121(12):2352-62.
143. Kazemi M, Carrer A, Moimas S, Zandona L, Bussani R, Casagrande B, et al. VEGF121 and VEGF165 differentially promote vessel maturation and tumor growth in mice and humans. *Cancer Gene Ther*. 2016;23(5):125-32.
144. Ferrara N, Gerber HP, LeCouter J. The biology of VEGF and its receptors. *nature Medicine*. 2003;9(6):669-76.
145. Eelen G, de Zeeuw P, Treps L, Harjes U, Wong BW, Carmeliet P. Endothelial Cell Metabolism. *Physiol Rev*. 2018;98(1):3-58.
146. Yetkin-Arik B, Vogels IMC, Nowak-Sliwinska P, Weiss A, Houtkooper RH, Van Noorden CJF, et al. The role of glycolysis and mitochondrial respiration in the formation and functioning of endothelial tip cells during angiogenesis. *Sci Rep*. 2019;9(1):12608.
147. Yetkin-Arik B, Vogels IMC, Neyazi N, van Duinen V, Houtkooper RH, van Noorden CJF, et al. Endothelial tip cells *in vitro* are less glycolytic and have a more flexible response to metabolic stress than non-tip cells. *Sci Rep*. 2019;9(1):10414.
148. Lu CW, Lo YH, Chen CH, Lin CY, Tsai CH, Chen PJ, et al. VLDL and LDL, but not HDL, promote breast cancer cell proliferation, metastasis and angiogenesis. *Cancer Lett*. 2017;388:130-8.
149. Christianson HC, Belting M. Heparan sulfate proteoglycan as a cell-surface endocytosis receptor. *Matrix Biol*. 2014;35:51-5.
150. Barker AL, Konopatskaya O, Neal CR, Macpherson JV, Whatmore JL, Winlove CP, et al. Observation and characterisation of the glycocalyx of viable human endothelial cells using confocal laser scanning microscopy. *Phys Chem Chem Phys*. 2004;6(5):1006-11.

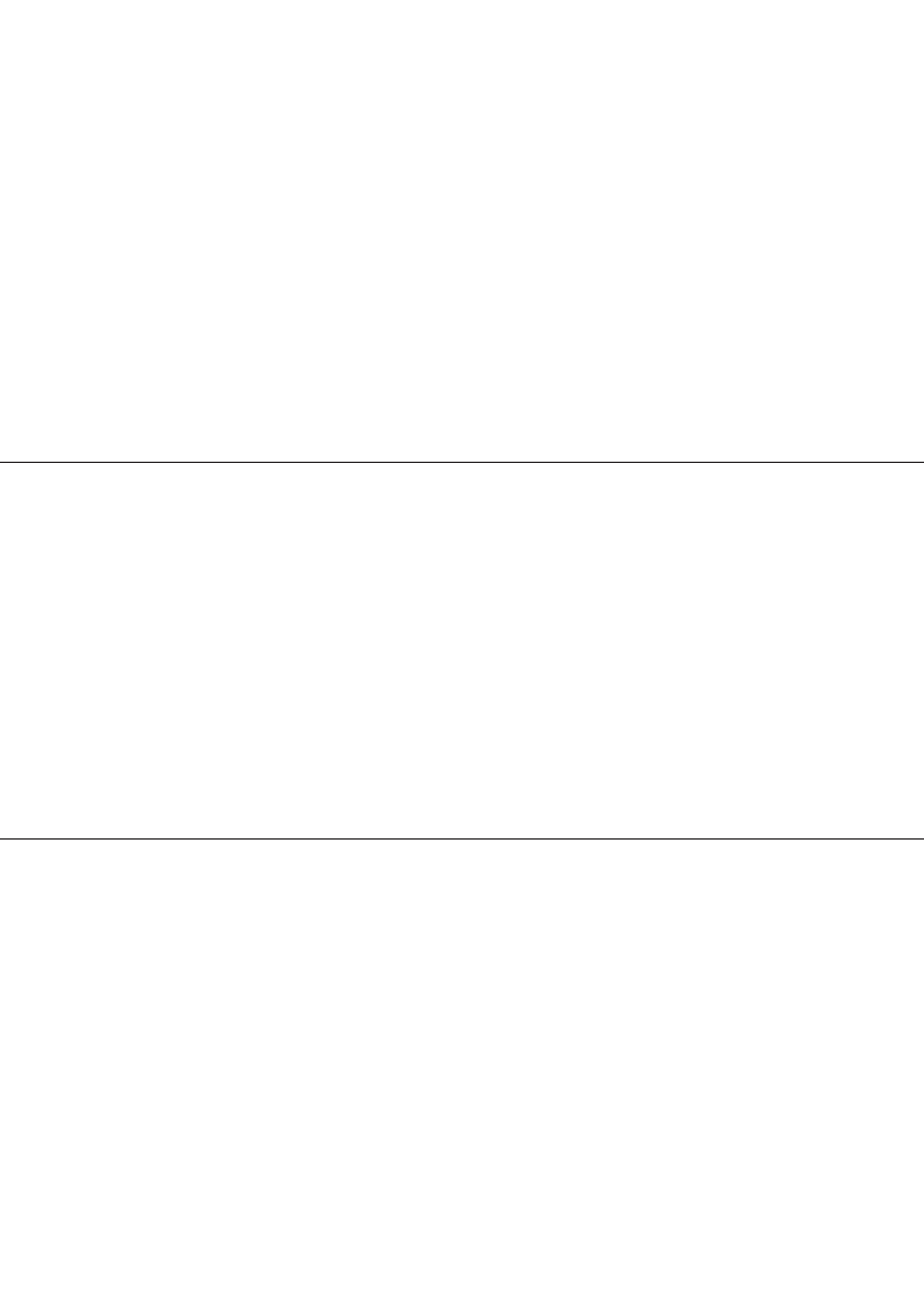
151. Goveia J, Rohlenova K, Taverna F, Treps L, Conradi LC, Pircher A, et al. An Integrated Gene Expression Landscape Profiling Approach to Identify Lung Tumor Endothelial Cell Heterogeneity and Angiogenic Candidates. *Cancer Cell*. 2020;37(1):21-36 e13.
152. Taskinen MR, Boren J. New insights into the pathophysiology of dyslipidemia in type 2 diabetes. *Atherosclerosis*. 2015;239(2):483-95.
153. Nordestgaard BG, Varbo A. Triglycerides and cardiovascular disease. *The Lancet*. 2014;384(9943):626-35.
154. Varbo A, Benn M, Smith GD, Timpson NJ, Tybjaerg-Hansen A, Nordestgaard BG. Remnant cholesterol, low-density lipoprotein cholesterol, and blood pressure as mediators from obesity to ischemic heart disease. *Circ Res*. 2015;116(4):665-73.
155. Vandekeere S, Dewerchin M, Carmeliet P. Angiogenesis Revisited: An Overlooked Role of Endothelial Cell Metabolism in Vessel Sprouting. *Microcirculation*. 2015;22(7):509-17.
156. Lindahl U, Kjellen L. Pathophysiology of heparan sulphate: many diseases, few drugs. *J Intern Med*. 2013;273(6):555-71.
157. Uchimura K, Morimoto-Tomita M, Bistrup A, Li J, Lyon M, Gallagher J, et al. HSulf-2, an extracellular endoglucosamine-6-sulfatase, selectively mobilizes heparin-bound growth factors and chemokines: effects on VEGF, FGF-1, and SDF-1. *BMC Biochem*. 2006;7:2.
158. Wang F, Wan A, Rodrigues B. The function of heparanase in diabetes and its complications. *Can J Diabetes*. 2013;37(5):332-8.
159. Morimoto-Tomita M, Uchimura K, Bistrup A, Lum DH, Egeblad M, Boudreau N, et al. Sulf-2, a Proangiogenic Heparan Sulfate Endosulfatase, Is Upregulated in Breast Cancer. *Neoplasia*. 2005;7(11):1001-10.
160. Rosen SD, Lemjabbar-Alaoui H. Sulf-2: an extracellular modulator of cell signaling and a cancer target candidate. *Expert Opin Ther Targets*. 2010;14(9):935-49.
161. Williams KJ, Chen K. Recent insights into factors affecting remnant lipoprotein uptake. *Curr Opin Lipidol*. 2010;21(3):218-28.
162. Lewis GF, Xiao C, Hegele RA. Hypertriglyceridemia in the genomic era: a new paradigm. *Endocr Rev*. 2015;36(1):131-47.
163. Peterfy M. Lipase maturation factor 1: a lipase chaperone involved in lipid metabolism. *Biochim Biophys Acta*. 2012;1821(5):790-4.
164. Merkel M, Eckel RH, Goldberg IJ. Lipoprotein lipase: genetics, lipid uptake, and regulation. *J Lipid Res*. 2002;43(12):1997-2006.
165. Bishop JR, Passos-Bueno MR, Fong L, Stanford KI, Gonzales JC, Yeh E, et al. Deletion of the basement membrane heparan sulfate proteoglycan type XVIII collagen causes hypertriglyceridemia in mice and humans. *PLoS One*. 2010;5(11):e13919.
166. Young SG, Zechner R. Biochemistry and pathophysiology of intravascular and intracellular lipolysis. *Genes Dev*. 2013;27(5):459-84.
167. Wang Y, Rodrigues B. Intrinsic and extrinsic regulation of cardiac lipoprotein lipase following diabetes. *Biochim Biophys Acta*. 2015;1851(2):163-71.
168. Goulbourne CN, Gin P, Tatar A, Nobumori C, Hoenger A, Jiang H, et al. The GPIHBP1-LPL complex is responsible for the margination of triglyceride-rich lipoproteins in capillaries. *Cell Metab*. 2014;19(5):849-60.
169. Surendran RP, Visser ME, Heemelaar S, Wang J, Peter J, Defesche JC, et al. Mutations in LPL, APOC2, APOA5, GPIHBP1 and LMF1 in patients with severe hypertriglyceridaemia. *J Intern Med*. 2012;272(2):185-96.
170. MacArthur JM, Bishop JR, Stanford KI, Wang L, Bensadoun A, Witztum JL, et al. Liver heparan sulfate proteoglycans mediate clearance of triglyceride-rich lipoproteins independently of LDL receptor family members. *J Clin Invest*. 2007;117(1):153-64.
171. Deng Y, Foley EM, Gonzales JC, Gordts PL, Li Y, Esko JD. Shedding of syndecan-1 from human hepatocytes alters very low density lipoprotein clearance. *Hepatology*. 2012;55(1):277-86.

172. Fuki IV, Kuhn KM, Lomazov IR, Rothman VL, Tuszyński GP, Iozzo RV, et al. The syndecan family of proteoglycans. Novel receptors mediating internalization of atherogenic lipoproteins *in vitro*. *J Clin Invest*. 1997;100(6):1611-22.
173. Foley EM, Gordts P, Stanford KI, Gonzales JC, Lawrence R, Stoddard N, et al. Hepatic remnant lipoprotein clearance by heparan sulfate proteoglycans and low-density lipoprotein receptors depend on dietary conditions in mice. *Arterioscler Thromb Vasc Biol*. 2013;33(9):2065-74.
174. Mooij HL, Bernelot Moens SJ, Gordts PL, Stanford KI, Foley EM, van den Boogert MA, et al. Ext1 heterozygosity causes a modest effect on postprandial lipid clearance in humans. *J Lipid Res*. 2015;56(3):665-73.
175. Carneiro MM, Miname MH, Gagliardi AC, Pereira C, Pereira AC, Krieger JE, et al. The removal from plasma of chylomicrons and remnants is reduced in heterozygous familial hypercholesterolemia subjects with identified LDL receptor mutations: study with artificial emulsions. *Atherosclerosis*. 2012;221(1):268-74.
176. Tremblay AJ, Lamarche B, Ruel I, Hogue JC, Bergeron J, Gagne C, et al. Lack of evidence for reduced plasma apo B48 catabolism in patients with heterozygous familial hypercholesterolemia carrying the same null LDL receptor gene mutation. *Atherosclerosis*. 2004;172(2):367-73.
177. Hodoglugil U, Williamson DW, Yu Y, Farrer LA, Mahley RW. Glucuronic acid epimerase is associated with plasma triglyceride and high-density lipoprotein cholesterol levels in Turks. *Ann Hum Genet*. 2011;75(3):398-417.
178. Chen K, Liu ML, Schaffer L, Li M, Boden G, Wu X, et al. Type 2 diabetes in mice induces hepatic overexpression of sulfatase 2, a novel factor that suppresses uptake of remnant lipoproteins. *Hepatology*. 2010;52(6):1957-67.
179. Matikainen N, Burza MA, Romeo S, Hakkarainen A, Adiels M, Folkersen L, et al. Genetic variation in SULF2 is associated with postprandial clearance of triglyceride-rich remnant particles and triglyceride levels in healthy subjects. *PLoS One*. 2013;8(11):e79473.
180. Schoors S, Bruning U, Missiaen R, Queiroz KC, Borgers G, Elia I, et al. Fatty acid carbon is essential for dNTP synthesis in endothelial cells. *Nature*. 2015;520(7546):192-7.
181. Siemerink MJ, Klaassen I, Van Noorden CJ, Schlingemann RO. Endothelial tip cells in ocular angiogenesis: potential target for anti-angiogenesis therapy. *J Histochem Cytochem*. 2013;61(2):101-15.
182. De Bock K, Georgiadou M, Schoors S, Kuchnio A, Wong BW, Cantelmo AR, et al. Role of PFKFB3-driven glycolysis in vessel sprouting. *Cell*. 2013;154(3):651-63.
183. Phillips JJ, Huillard E, Robinson AE, Ward A, Lum DH, Polley MY, et al. Heparan sulfate sulfatase SULF2 regulates PDGFR α signaling and growth in human and mouse malignant glioma. *J Clin Invest*. 2012;122(3):911-22.



SUMMARY AND DISCUSSION





5

SUMMARY AND DISCUSSION

.

1

SUMMARY AND DISCUSSION

The aim of this thesis was to use CD34 as a marker for tip cells *in vitro* to further characterize growth factors and pathways involved in regulation of the tip cell phenotype. The use of three different approaches to study tip cells resulted in the following conclusions:

- » CD34⁺ tip cells *in vitro* can be used to identify novel tip cell-specific genes.
- » The effects of anti-angiogenic compounds on CD34⁺ tip cells *in vitro* provide valuable information about their effectiveness and mechanisms of action *in vivo*.
- » CD34⁺ tip cells express specific proteins that regulate interactions with stalk cells and extracellular matrix to enhance sprouting.

This discussion provides a review of the results in a broader pathophysiological and clinical perspective.

Tip cell-specific genes as therapeutic targets

Targeting tip cell-specific proteins may increase efficacy and reduce side effects of anti-angiogenic therapies used to treat blinding retinal diseases and cancer. To study tip cells, we used CD34, which was previously shown to be a specific marker for tip cells *in vitro*. *In vivo*, CD34 is not only expressed on tip cells but also on the luminal side of blood vessels, and we investigated if CD34 has a role in angiogenesis *in vivo*. We found that CD34 is not essential for physiological angiogenesis, but plays a role in pathological angiogenesis in the hypoxic mouse retina (**chapter 2.1**). We then compared mRNA expression of CD34⁺ tip cells and CD34⁻ cells using a microarray to identify candidate tip cell-specific genes. The success of this microarray-based approach, highlighted by the identification of IGF2, IGF1R, and IGFBP3 and 4 (**chapter 2.2 and 2.3**), provides evidence that *in vitro* research on tip cells forms a platform to screen for novel tip cell-specific genes without the need of animal models. IGF2 was identified as an essential growth factor that allows tip cells to maintain their phenotype. Inhibition of IGF2 protein levels led to a dramatic decrease in sprouting in the models that we studied, which highlights the robustness of the results. Live cell imaging of sprouting EC spheroids showed that proper maintenance of the tip cell phenotype is essential for sprouting, since both spheroids lacking IGF2 as well as spheroids cultured in the presence of excess IGF2, exhibit disturbed sprouting. We observed strong inhibition of sprouting occurs when IGF2 is inhibited, whereas inhibition of sprout persistence, and lack of sprout elongation occur when there is excess IGF2. A current hypothesis is that the best fitted cell takes on the tip cell phenotype and leads the growing vessel sprout (1, 2). We can now state that not only the best fitting cell takes on the tip cell phenotype, but that tip cells also express proteins that serve to maintain the phenotype for long enough to ensure proper sprouting. This mechanism highlights the challenge of angiogenesis inhibition: inhibition of one cell type often leads to a phenotypic switch that enables the other, “better suited”, cell to take over and continue guiding the growth of the vessel sprout. Inhibition of the IGF2-IGF1R signaling axis

provides an alternative approach, and would allow cells to take on the tip cell phenotype but would inhibit their efficacy, because of failure to maintain the phenotype. There are several clinical trials ongoing that are studying the effects of IGF/IGF1R inhibitors, as described in **chapter 2.4** (3, 4). Further studies are required to elucidate more details of the cellular and molecular mechanisms of IGF2 signaling in angiogenesis and to establish the therapeutic efficacy of IGF2 inhibition.

Implications of differential effects of anti-angiogenic compounds on tip cells

Anti-angiogenic treatment of retinal diseases currently relies on intra-ocular injection of compounds that inhibit a single growth factor, VEGF. Although the treatment has successfully prevented blindness in many patients, it still needs improvement: reduction of the number of injections is needed, and longer-acting compounds may greatly reduce infection risks for patients and improve their quality of life. Furthermore, there is a need for alternative treatments for patients that do not respond to VEGF-inhibitors (5-8). Our studies of several anti-angiogenic compounds that inhibit a number of pro-angiogenic proteins and receptors revealed a variable effect on the percentage of CD34⁺ tip cells *in vitro* (**chapter 3**). In **chapter 3.1**, we present an algorithm to rapidly optimize combinations of anti-angiogenic compounds. **Chapter 3.2** describes our study on a specific drug designed to inhibit PDGFR, in which we show that it has a broader mechanism of action independent of PDGFR. This drug reduces angiogenesis by inhibiting stalk cell proliferation rather than tip cell migration, amongst other effects. In these studies, we used several models to study angiogenesis and tip cells in particular, including CD34 as a marker for tip cells and to measuring changes in their numbers as a model for tip cell formation. Since no other markers of tip cells *in vitro* than CD34 have been identified as yet, we are aware that the results need to be interpreted with caution. Therefore, we combined as much as possible different methods, including assays that measure proliferation, migration and apoptosis, and methods to detect effects on tip cell-specific target genes, to exclude confounders which may affect the measured percentages of tip cells in this model. Recently, indirect support was reported for the validity of our *in vitro* model by Goveia et al., who demonstrated that the markers of the tip cell phenotype were conserved across species in tumor endothelial cells and in *in vivo* and *in vitro* models, in contrast to other tumor endothelial cell phenotypes (9). Our studies show that there are many alternative angiogenic pathways that induce ECs to become tip cells, as supported by van Beijnum and colleagues (10). It also shows the importance of the phenotype for angiogenesis, as only combinations of drugs were capable of reducing tip cell activities such as migration and sprout formation in spheroid assays. Since the emergence of tip cells to lead growing vessel sprouts is the common final pathway of many pro-angiogenic pathways, we hypothesize that inhibition of tip cells may dampen the effects of multiple pro-angiogenic pathways and that this approach may therefore be more effective as a therapeutic

strategy in cancer and retinal diseases. Furthermore, since the effects of these theoretical anti-tip cell compounds would be specific for tip cells, the existing vasculature should remain unaffected, thereby limiting side effects. Screening of candidate compounds for their effects on CD34⁺ tip cells is, therefore, a valuable additional assessment tool of their potential therapeutic efficacy in patients.

Tip cell microenvironment

Interactions between ECs and their microenvironment are vital for cell differentiation and angiogenic sprouting efficiency. The ECM provides a reservoir of growth factors, such as IGF2 and VEGF, and regulates the downstream effects of these growth factors. In addition, communication between tip cells and stalk cells is crucial for proper sprouting (11-14). The use of CD34⁺ tip cells to study these interactions are presented in **chapter 4**. Initial *in silico* modeling of cell-cell adhesion revealed that tip cells are less adherent to other cells than stalk cells, which allows them to reach the leading tip of the growing vessel sprout. An analysis of mRNA expression data identified cell adhesion molecule apelin (APLN) and its receptor APJ (15), which are differentially expressed in CD34⁺ tip cells and CD34⁻ cells, as candidate proteins involved in this phenomenon (**chapter 4.1**). Subsequent *in vitro* experiments confirmed that reduced expression of APJ by tip cells allowed them to migrate to the sprout tip to lead the growing sprout.

Tip cells also interact with the extracellular matrix in their microenvironment. Experiments using 2 different VEGFA splice variants revealed that VEGFA₁₆₅, the most common variant that has a HSPG-binding domain, is a stronger inducer of tip cells and angiogenesis than VEGFA₁₂₁, a variant lacking the HSPG-binding domain. Knockdown of VEGFR2 co-receptor *NRP2* demonstrated that it has a role in sprouting but not in tip cell formation (**chapter 4.2**). Knockdown of *SULF2*, an extracellular modifier of HSPGs which alters its growth factor-binding capacity, revealed that binding of VEGF to HSPGs is not pivotal for angiogenesis, but may play a marginal role in sprout elongation, suggesting that the observed differential effects of the two VEGF isoforms on tip cell induction and angiogenesis may be regulated by other mechanisms than HSPG binding. Furthermore, we found that uptake of very low-density lipoproteins (VLDL) is limited to non-tip cells and enhances angiogenesis without affecting tip cell formation. These intercellular and cell-matrix interactions are crucial for proper signaling during angiogenesis, and numerous genes and proteins have been described that affect angiogenesis through these interactions. Examples are signaling via DLL4 and NOTCH1 that allows tip cells to induce the stalk cell phenotype in their neighboring cells (11-13), binding of VEGF to HSPGs that alters its signaling outcome and thus its pro-angiogenic effects (16, 17), and altered binding of growth factors to HSPGs that has been proposed as an attractive therapeutic strategy because pro-angiogenic pathways often rely on extracellular binding of pro-angiogenic growth factors (18). Future research may reveal whether inhibition

or alteration of the pro-angiogenic ECM created by tip cells affect sprouting and thus disease outcome.

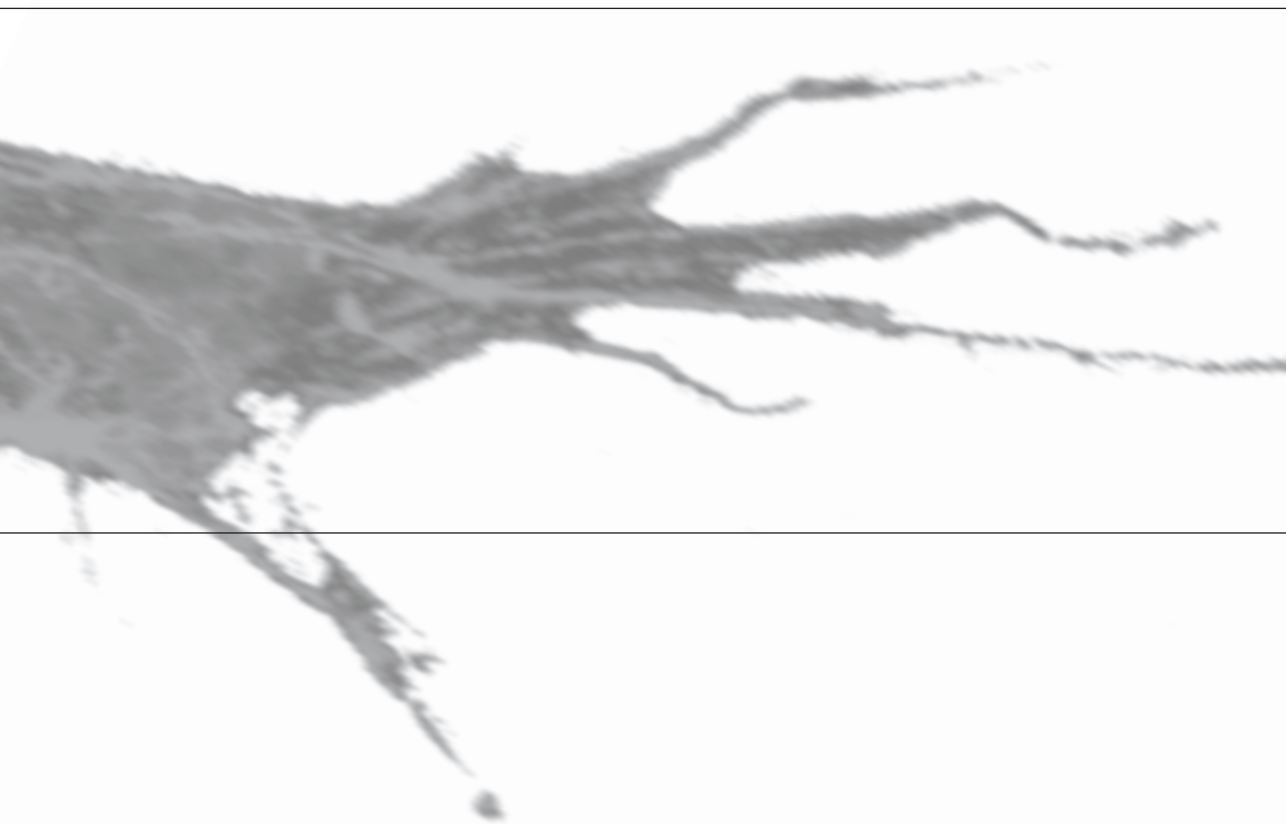
CONCLUDING REMARKS

Studying tip cells in culture has enabled us to identify new aspects of this highly specialized endothelial phenotype without the use of animal models. The results shown in this thesis have given many new insights into the cellular and molecular mechanisms involved in tip cell biology *in vitro* and *in vivo*. One of the main findings is that the tip cell phenotype is induced and maintained by specific proteins and by cell-cell and cell-matrix interactions. Future efforts should make the translational step to the clinic and show whether these efforts could lead to the development of new therapies. Hopefully, tip cell-inhibitory drugs will lead to improved therapeutic outcomes and better quality of life for patients with retinal diseases and cancer.

5.1

REFERENCES

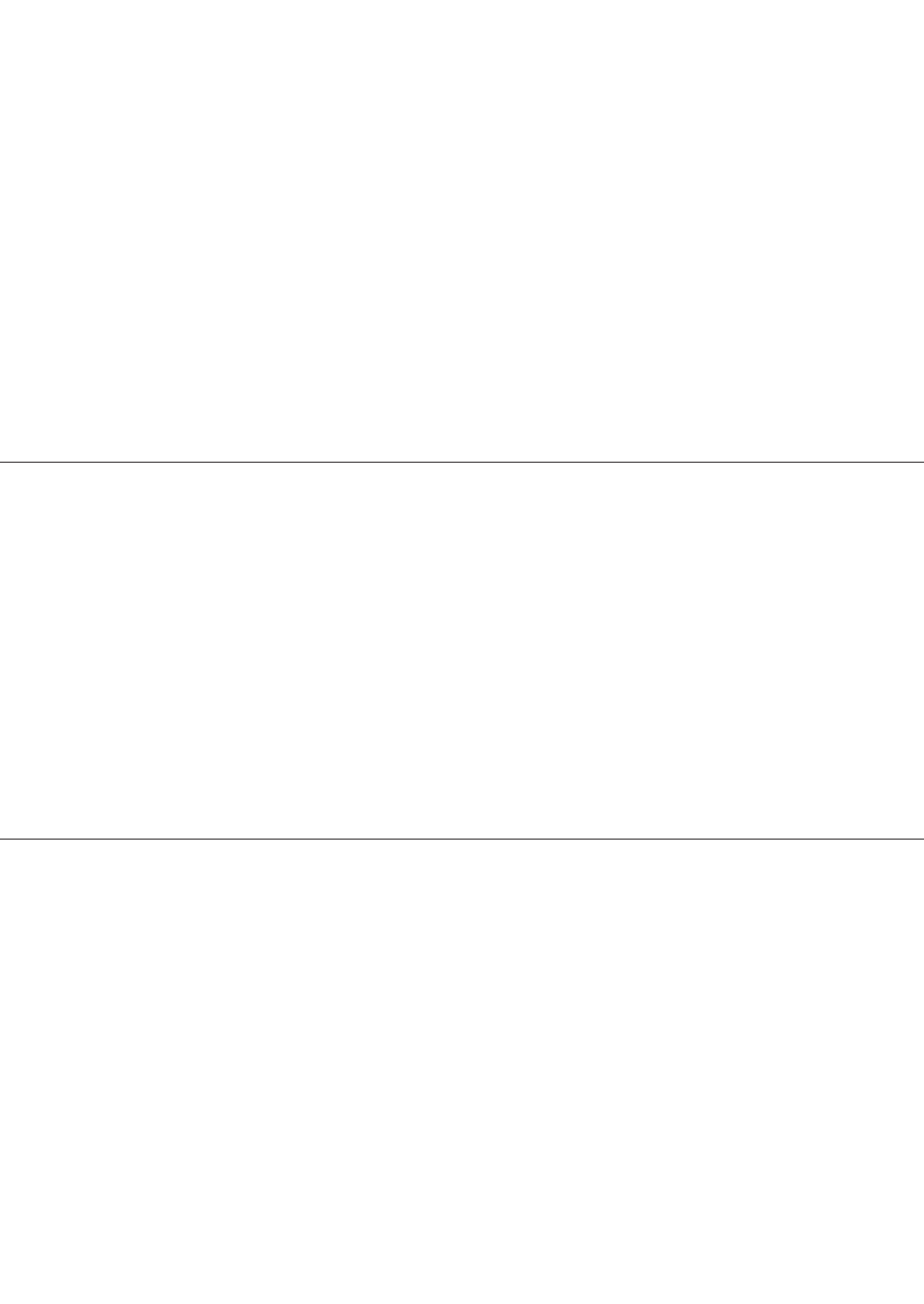
1. Eelen G, de Zeeuw P, Treps L, Harjes U, Wong BW, Carmeliet P. Endothelial Cell Metabolism. *Physiol Rev.* 2018;98(1):3-58.
2. Jakobsson L, Franco CA, Bentley K, Collins RT, Ponsioen B, Aspalter IM, et al. Endothelial cells dynamically compete for the tip cell position during angiogenic sprouting. *Nat Cell Biol.* 2010;12(10):943-53.
3. Gao J, Chesebrough JW, Cartlidge SA, Ricketts SA, Incognito L, Veldman-Jones M, et al. Dual IGF-III-neutralizing antibody MEDI-573 potentially inhibits IGF signaling and tumor growth. *Cancer Res.* 2011;71(3):1029-40.
4. Chen HX, Sharon E. IGF-1R as an anti-cancer target - trials and tribulations. *Chin J Cancer.* 2013;32(5):242-52.
5. Suzuki M, Nagai N, Izumi-Nagai K, Shinoda H, Koto T, Uchida A, et al. Predictive factors for non-response to intravitreal ranibizumab treatment in age-related macular degeneration. *Br J Ophthalmol.* 2014;98(9):1186-91.
6. Maksys S, Richter-Muksch S, Weingessel B, Vecsei-Marlovits PV. Short-term effect of aflibercept on visual acuity and central macular thickness in patients not responding to ranibizumab and bevacizumab. *Wien Klin Wochenschr.* 2017;129(9-10):351-7.
7. Hussain RM, Ciulla TA. Treatment strategies for refractory diabetic macular edema: switching anti-VEGF treatments, adopting corticosteroid-based treatments, and combination therapy. *Expert Opin Biol Ther.* 2016;16(3):365-74.
8. Mantel I, Gillies MC, Souied EH. Switching between ranibizumab and aflibercept for the treatment of neovascular age-related macular degeneration. *Surv Ophthalmol.* 2018;63(5):638-45.
9. Goveia J, Rohlenova K, Taverna F, Treps L, Conradi LC, Pircher A, et al. An Integrated Gene Expression Landscape Profiling Approach to Identify Lung Tumor Endothelial Cell Heterogeneity and Angiogenic Candidates. *Cancer Cell.* 2020;37(1):21-36 e13.
10. van Beijnum JR, Nowak-Sliwinska P, Huijbers EJM, Thijssen VL, Griffioen AW. The Great Escape; the Hallmarks of Resistance to Antiangiogenic Therapy. *Pharmacological Reviews.* 2015;67(2):441.
11. Suchting S, Freitas C, le Noble F, Benedito R, Breant C, Duarte A, et al. The Notch ligand Delta-like 4 negatively regulates endothelial tip cell formation and vessel branching. *Proc Natl Acad Sci U S A.* 2007;104(9):3225-30.
12. Hellstrom M, Phng LK, Hofmann JJ, Wallgard E, Coultas L, Lindblom P, et al. Dll4 signalling through Notch1 regulates formation of tip cells during angiogenesis. *Nature.* 2007;445(7129):776-80.
13. Lobov IB, Renard RA, Papadopoulos N, Gale NW, Thurston G, Yancopoulos GD, et al. Delta-like ligand 4 (Dll4) is induced by VEGF as a negative regulator of angiogenic sprouting. *Proc Natl Acad Sci U S A.* 2007;104(9):3219-24.
14. Palm MM, Dallinga MG, van Dijk E, Klaassen I, Schlingemann RO, Merks RM. Computational Screening of Tip and Stalk Cell Behavior Proposes a Role for Apelin Signaling in Sprout Progression. *PLoS One.* 2016;11(11):e0159478.
15. Cheng J, Luo X, Huang Z, Chen L. Apelin/APJ system: A potential therapeutic target for endothelial dysfunction-related diseases. *J Cell Physiol.* 2019;234(8):12149-60.
16. Vempati P, Popel AS, Mac Gabhann F. Extracellular regulation of VEGF: isoforms, proteolysis, and vascular patterning. *Cytokine Growth Factor Rev.* 2014;25(1):1-19.
17. Chen TT, Luque A, Lee S, Anderson SM, Segura T, Iruela-Arispe ML. Anchorage of VEGF to the extracellular matrix conveys differential signaling responses to endothelial cells. *J Cell Biol.* 2010;188(4):595-609.
18. Chiodelli P, Bugatti A, Urbinati C, Rusnati M. Heparin/Heparan sulfate proteoglycans glycomic interactome in angiogenesis: biological implications and therapeutical use. *Molecules.* 2015;20(4):6342-88.





6

APPENDICES



6

SAMENVATTING



SAMENVATTING

Groei van bloedvaten vanuit een bestaand bloedvatnetwerk, ofwel angiogenese, is een fysiologisch proces dat overal in het lichaam plaats kan vinden als onderdeel van een wondgenezingsreactie, maar ook in specifieke processen, zoals in het ovarium en endometrium als onderdeel van de menstruele cyclus. Aangezien het oog het orgaan is met de hoogste zuurstofvraag en de hoogste bloeddorstomring per hoeveelheid weefsel is het niet verbazingwekkend dat ziektes die bloedvaten beschadigen, bijvoorbeeld in het netvlies (retina), tot verlies van zicht kunnen leiden. Voorbeelden hiervan zijn diabetische retinopathie, leeftijdsgebonden maculadegeneratie en prematurenretinopathie. Als de retinale bloedvaten de benodigde zuurstof niet kunnen leveren ontstaat hypoxie, ofwel zuurstoftekort. De retina reageert hierop door groeifactoren aan te maken die angiogenese stimuleren zodat de bloedtoevoer kan worden hersteld. Dit is een fysiologisch reactie om het weefsel te doen herstellen, maar het heeft vaak negatieve consequenties omdat onrijpe nieuwe bloedvaten voor langere tijd lekkage van stoffen uit het bloed veroorzaken, en tot de vorming van littekenweefsel leiden. Hierdoor wordt de functie van de retina aangetast en ontstaat verlies van gezichtsvermogen. Rijpe bloedvaten zijn gevoerd met een enkele laag endotheelcellen die stevig aan elkaar vast zitten door intercellulaire verbindingen. De endotheelcellen worden ondersteund door andere celtypes zoals pericyten, gliale cellen en door extracellulaire matrix. In de gezonde retina vormt dit samen de bloedretina barrière. In tegenstelling tot deze rijpe bloedvaten zijn angiogene vaatspruiten onrijp en aangepast aan het wondgenezingsmilieu, zonder intercellulaire verbindingen, maar omgeven door geactiveerde pericyten en een aangepaste extracellulaire matrix. Dit stelt de vaatspruiten in staat om te groeien en het wondhelingsproces te stimuleren.

Angiogene vaatspruiten bestaan uit specifieke subtypes van endotheelcellen. Een gedetailleerde introductie van deze endotheliale subtypes is te vinden in **hoofdstuk 1.2**. In het kort: een vaatspruit wordt geleid door een “tipcel”, gevolgd door “stalk” cellen en “phalanx” cellen. De tipcellen hebben uitsteeksels die filopodia worden genoemd die helpen bij migratie richting de zuurstofarme (hypoxische) gebieden. De stalkcellen delen en zorgen zo voor verlenging van het vaatspruitje, terwijl phalanxcellen zorgen voor rijping van het vat. Door hun leidende rol en specifieke functies tijdens angiogenese, en door hun unieke eiwitexpressie vormen tipcellen een aantrekkelijk doelwit voor selectieve anti-angiogenese therapie. Het gevolg hiervan is dat tipcellen onderwerp zijn van preklinische studies om nieuwe specifieke eiwitten of mechanismen te ontdekken waartegen therapeutica ontwikkeld kunnen worden om ziektes van het netvlies en aandoeningen met angiogenese buiten het oog, zoals kanker, te behandelen.

Tot nu toe werd onderzoek naar tipcellen vooral uitgevoerd in diermodellen, maar deze dienen zo veel mogelijk te worden vermeden vanwege ethische bezwaren. Onze onderzoeksgroep heeft voor het eerst aangetoond dat tipcellen ook voorkomen in gekweekte endotheelcellen, en dat deze te herkennen zijn omdat ze het eiwit CD34 op hun oppervlak dragen. Een uitgebreide introductie over deze onderzoeksmethode wordt

gegeven in **hoofdstuk 1.3**. In dit proefschrift hebben we drie aspecten van tipcellen in gekweekte endotheelcel populaties onderzocht:

- » Identificatie van tipcel-specifieke eiwitten
- » Effecten van bestaande angiogeneseremmers op tip cellen
- » Interacties tussen tipcellen en andere celtypen en extracellulaire eiwitten in hun omgeving.

Tipcel-specifieke eiwitten

Een eiwit dat specifiek in een tipcel tot expressie komt, en tegelijkertijd ook essentieel is voor het fenotype van de tipcel, of het gen dat voor dit eiwit codeert, kunnen aantrekkelijk zijn als therapeutisch doelwit zijn om angiogenese te remmen. Aangezien andere cellen het eiwit niet, of in mindere mate, tot expressie brengen, worden bijwerkingen zo veel mogelijk vermeden. In het eerste deel van dit proefschrift hebben we een aantal van dergelijke tipcel-genen bestudeerd. In **Hoofdstuk 2.1** onderzochten we de rol van het eiwit CD34, in een model van door hypoxie gedreven retinale angiogenese in muizen. We vonden dat dit eiwit, dat tot expressie komt aan de binnenzijde (luminale kant) van alle bloedvaten in het lichaam, en op de filopodia van tipcellen, zelf niet essentieel is voor angiogenese. In **Hoofdstuk 2.2** beschrijven we de identificatie van insuline-achtige groeifactor 2 (insulin-like growth factor 2, IGF2) en IGF-1 receptor (IGF1R) als tipcel-specifieke eiwitten. Beide eiwitten komen sterk verhoogd tot expressie in tipcellen in verhouding tot andere endotheelcellen. We vonden dat IGF2 er via binding aan IGF1R voor zorgt dat de tipcel zijn fenotype kan behouden. Dit is essentieel voor angiogenese *in vivo*, zoals we hebben aangetoond in zebrafissen en kippen embryo's: bij remming van *Igf2* was angiogenese in zebrafissen verstoord. In **hoofdstuk 2.3** onderzoeken we de rol van IGF2 en IGF1R tijdens het onderhouden van het tipcel-fenotype *in vitro* en laten we zien dat andere leden van de IGF eiwit familie waaronder de IGF bindingseiwitten (IGF binding proteins 3 en -4, IGFBP3 en -4) ook een rol spelen in angiogenese. IGFBP3 faciliteert binding van IGF2 en IGF1R en stimuleert zo angiogenese. IGFBP4 daarentegen is een remmer van IGF2 die waarschijnlijk door tipcellen wordt geproduceerd om te zorgen voor regulering van de lokale concentraties van IGF2. **Hoofdstuk 2.4** is een review van de bestaande literatuur over de IGF familie waarin we beschrijven dat IGF2 via meerdere signaaltrajecten zorgt voor behoud van het tipcel-fenotype.

Angiogeneseremmers

Angiogenese is een van de voorwaarden voor de groei van kanker en is uitgebreid onderzocht als therapeutisch doelwit om kanker te bestrijden. Als een tumor groter wordt dan één à twee mm is de toevoer van zuurstof en nutriënten en afvoer van koolstofdioxide en afvalproducten via diffusie in en uit de tumor niet meer voldoende. Hierdoor ontstaat hypoxie en wordt angiogenese geïnduceerd om dit op te heffen door middel van het creëren van een bloedvatnetwerk in de tumor. Het idee om deze angiogenese te remmen

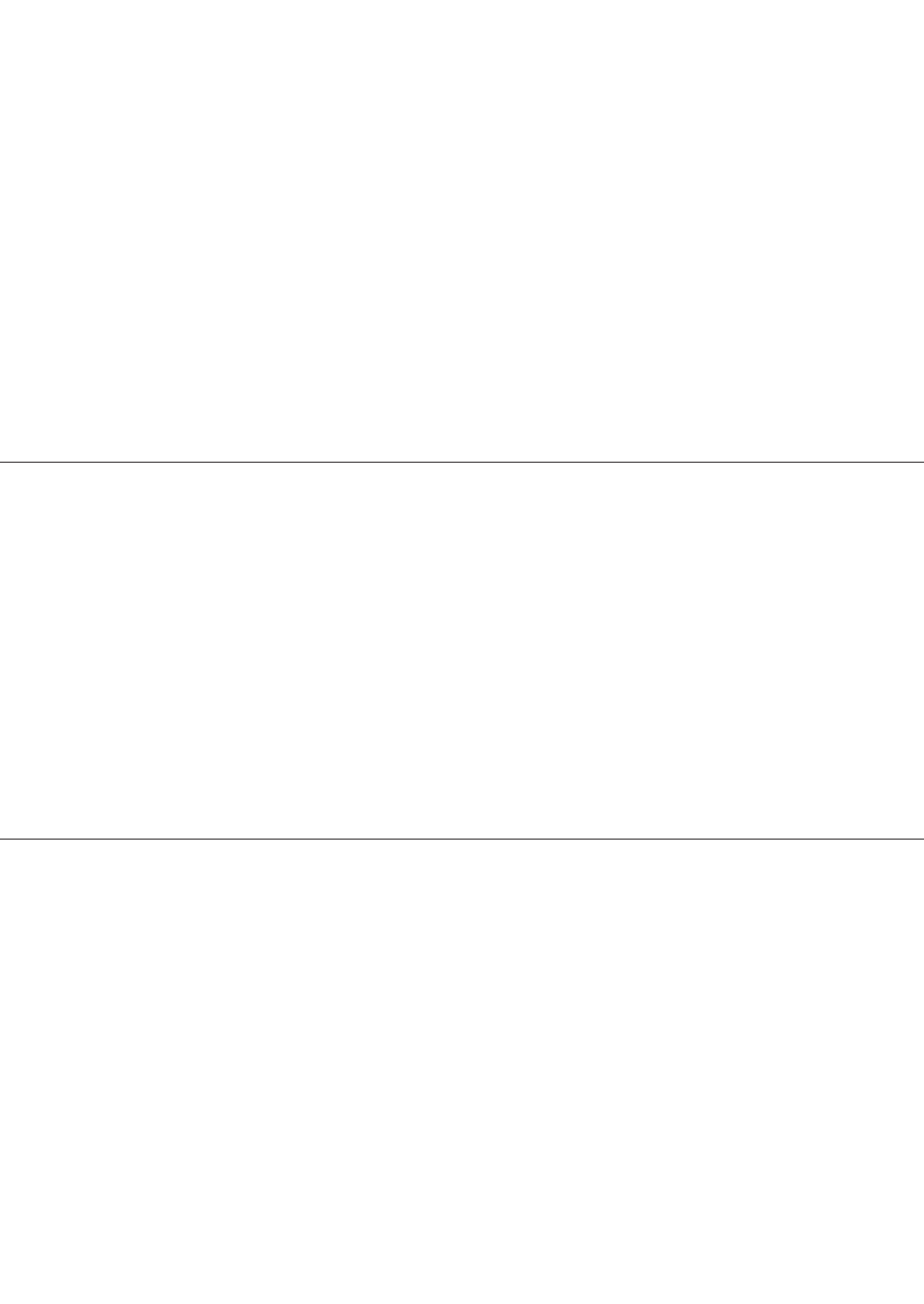
zodat de tumor niet verder kan groeien is geïntroduceerd door Judah Folkman en zijn collega's als een aantrekkelijke behandelingsstrategie in de oncologie. Helaas heeft deze strategie niet de therapeutische impact gehad die was verwacht en zijn er met angiogeneseremmers slechts marginale successen behaald in de kliniek. Mogelijk komt dit door compensatoire mechanismen zoals vasculaire mimicrie door kankercellen en gebruik van alternatieve angiogene signaaltrajecten. Angiogenese remmers zijn vaak uitgebreid getest om hun effecten op het gehele angiogenese proces te analyseren, maar hun directe en specifieke effecten op tipcellen zijn tot nu toe onderbelicht gebleven door gebrek aan adequate experimentele modellen. **Hoofdstuk 3** van dit proefschrift richt zich op de effecten van angiogenese remmers op tipcellen *in vitro*. In **hoofdstuk 3.1** wordt een algoritme beschreven om optimale combinaties van angiogenese remmers te bepalen. We vonden dat de optimale combinatie wat betreft remming van angiogenese ook een krachtige remming van het tipcel-fenotype gaf. **Hoofdstuk 3.2** beschrijft een preklinische studie naar crenolanib, een nieuwe angiogeneseremmer. We vonden dat crenolanib niet de tipcellen maar juist de non-tipcellen remt. Remming van celdeling van stalkcellen zorgt er dus waarschijnlijk voor dat de vaatspruit niet langer kan worden, waardoor angiogenese verstoord raakt.

Interacties tussen tipcellen en hun omgeving

De tipcel en stalkcel fenotypes zijn dynamisch, reversibel en onderling uitwisselbaar. De best uitgeruste cel dirigeert de vaatspruit als tipcel en deze dwingt de volgende endotheelcellen om stalkcel te worden. Dit maakt het hele angiogenese-proces efficiënter, omdat er te veel kleine vaatspruiten zouden worden gemaakt als er te veel tipcellen zouden zijn. Interacties tussen de endotheliale subtypes en hun omgeving spelen dus een belangrijke rol bij het bepalen welk fenotype een cel aanneemt. Door gebruik te maken van gekweekte endotheelcellen kunnen we tipcellen en stalkcellen scheiden, om eiwitten in de omgeving en op het celoppervlak te bestuderen die differentiatie in endotheliale subtypes of eigenschappen van subtypes bewerkstelligen. Dit wordt beschreven in **Hoofdstuk 4**. **Hoofdstuk 4.1** beschrijft een gecombineerde *in vitro* en *in silico* studie naar de aantrekking tussen tipcellen en andere cellen via het eiwit apeline en de receptor ervan. Apeline is een signaleiwit dat de onderlinge aantrekkingskracht van cellen vergroot als het bindt aan de receptor. We vonden dat tipcellen minder gevoelig zijn voor Apeline door verminderde expressie van de Apeline receptor. Hierdoor zijn ze minder aangetrokken tot andere cellen en kunnen ze gemakkelijker de groei van de vaatspruit dirigeren. In **Hoofdstuk 4.2** worden de effecten van binding van de pro-angiogene groeifactor vasculaire endotheliale groeifactor (vascular endothelial growth factor, VEGF) op tipcellen en non-tipcellen beschreven. Door expressie van co-receptor neuropiline 2 (NRP2) en Sulfatase 2, een modulator van heparan sulfaat proteoglycanen (HSPGs), te remmen vonden we dat binding aan co-receptoren de signalering van VEGF in tipcellen en stalkcellen door complexvorming met VEGFA en VEGF receptor 2

(VEGFR2) stimuleert. **Hoofdstuk 4.3** is een review over het eiwit Sulfatase 2, een enzym dat extracellulaire matrix eiwitten zoals heparan sulfaat moduleert en zo de binding van groeifactoren beïnvloedt.

Concluderend: dit proefschrift beschrijft ons onderzoek naar CD34-positieve tipcellen *in vitro*. Het laat zien dat onderzoek naar tipcellen in celkweken van menselijke endotheelcellen verschillende belangrijke voordelen heeft boven het gebruik van diermodellen, en aanvullend is op deze diermodellen. Voordelen zijn onder andere: 1) lagere kosten en grotere efficiëntie, 2) superieure vergelijkbaarheid met menselijke ziektes, en 3) ontbreken van de ethische bezwaren die gelden voor het gebruik van proefdieren. Het bestuderen van tipcellen *in vitro* heeft onze kennis van tipcel-regulatie vergroot. Voortzetting van het onderzoek dat beschreven is in dit proefschrift kan resulteren in tipcel-specifieke doelwitten voor toekomstige anti-angiogenese therapieën bij patiënten, en daardoor hopelijk een betere en effectievere behandeling van ziektes van het oog en daarbuiten waarbij angiogenese een rol speelt.



6.2

PUBLICATIONS

PUBLICATIONS

Bennett BJ, Orozco L, Kostem E, Erbilgin A, Dallinga M, Neuhaus I, et al. High-resolution association mapping of atherosclerosis loci in mice. *Arterioscler Thromb Vasc Biol.* 2012;32(8):1790-8.

Dallinga MG, Boas SEM, Klaassen I, Merks RHM, van Noorden CJF, Schlingemann RO. Tip cells in angiogenesis. *eLS.* 2015:1-10.

Weiss A, Ding X, van Beijnum JR, Wong I, Wong TJ, Berndsen RH, Dormond O, Dallinga MG, Shen L, Schlingemann RO, Pili R, Ho C-M, Dyson PJ, van den Bergh H, Griffioen AW, Nowak-Sliwinska P. Rapid optimization of drug combinations for the optimal angiostatic treatment of cancer. *Angiogenesis.* 2015;18(3):233-44.

Palm MM, Dallinga MG, van Dijk E, Klaassen I, Schlingemann RO, Merks RM. Computational screening of tip and stalk cell behavior proposes a role for apelin signaling in sprout progression. *PLoS One.* 2016;11(11):e0159478.

Siemerink MJ, Hughes MR, Dallinga MG, Gora T, Cait J, Vogels IM, et al. CD34 promotes pathological epi-retinal neovascularization in a mouse model of oxygen-induced retinopathy. *PLoS One.* 2016;11(6):e0157902.

Dallinga MG, Dallinga-Thie GM. Role of sulfatase 2 in lipoprotein metabolism and angiogenesis. *Curr Opin Lipidol.* 2016;27(2):181-6.

Dallinga MG, Yetkin-Arik B, Kayser RP, Vogels IMC, Nowak-Sliwinska P, Griffioen AW, et al. IGF2 and IGF1R identified as novel tip cell genes in primary microvascular endothelial cell monolayers. *Angiogenesis.* 2018;21:823-36.

Berndsen RH, Castrogiovanni C, Weiss A, Rausch M, Dallinga MG, Miljkovic-Licina M, Klaassen I, Meraldi P, van Beijnum JR, Nowak-Sliwinska P. Anti-angiogenic effects of crenolanib are mediated by mitotic modulation independently of PDGFR expression. *Br J Cancer.* 2019;121(2):139-49.

Dallinga MG, Habani YI, Kayser RP, Van Noorden CJF, Klaassen I, Schlingemann RO. IGF-binding proteins 3 and 4 are regulators of sprouting angiogenesis. *Mol Biol Rep.* 2020;47:2561-72.

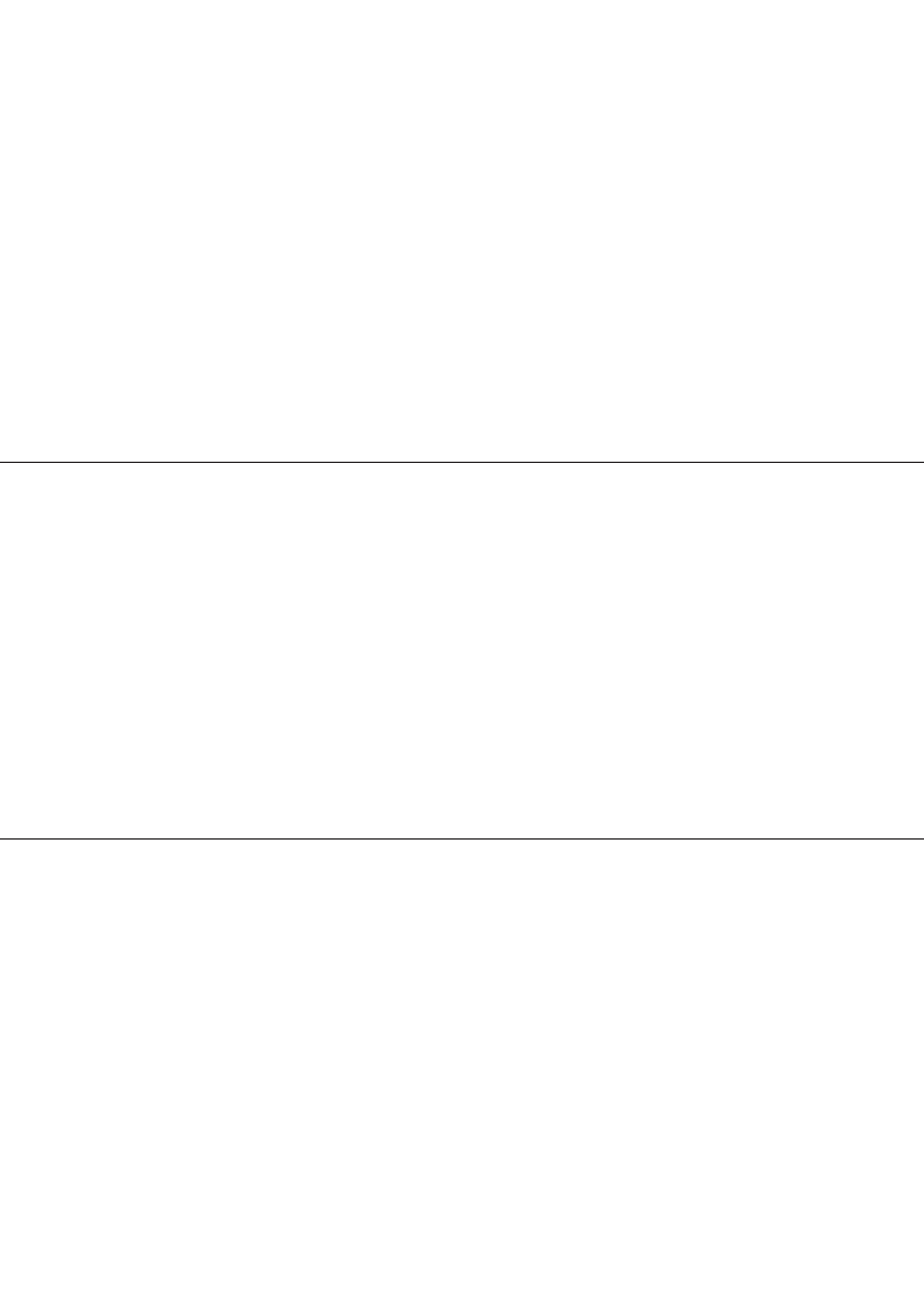
Submitted

Dallinga, M.G., Bolhuis, K., Bins, A., de Hoog, J. Bilateral diffuse uveal melanocyte proliferation in a patient with metastatic renal cell carcinoma.. *BMJ case reports*

In preparation

M.G. Dallinga, I. Klaassen, C.J.F. van Noorden, R.O. Schlingemann, The role of the insulin-like growth factor family in endothelial tip and stalk cell biology in angiogenesis. *IJMS*

M. G. Dallinga, Alinda W.M. Schimmel, Ingeborg Klaassen, Geesje M. Dallinga-Thie, Cornelis J.F. Van Noorden, Reinier O. Schlingemann. Role of heparan sulfate and neuropilin 2 in VEGFA signaling in human endothelial tip cells and non-tip cells in angiogenesis. *Cells*



6.3

AUTHORS AND CONTRIBUTIONS

AUTHORS AND CONTRIBUTIONS

Chapter 1

- 1.2. All authors contributed to writing this review.

Chapter 2

- 2.1. MJS and MRH wrote the manuscript. TG, MGD and MJS performed and collected data for *in vitro* experiments, with assistance of IMCV. MJS, MRH and JC performed and collected data for *in vivo* retinal angiogenesis experiments. HLH and JHEB performed the angioreactor experiments and analysis. MJS, MRH, MGD, CJFvN, IK, AIM, BMM, FMVR, KMM and ROS designed experiments. CJFvN, IK, KMM and ROS were involved in critical analysis and drafting of the manuscript. KMM and ROS initiated and supervised the project
- 2.2. MGD, BYA, RPK IMCV and PNS performed the experiments, MGD, PN-S, IK, CJFvN and ROS designed the experiments, MGD, BYA, PN-S, AWG, CJFvN, IK and ROS wrote the manuscript.
- 2.3. MGD and RPK performed the experiments, MGD, IK, CJFvN and ROS designed the experiments and wrote the manuscript.
- 2.4. All authors contributed to writing this review.

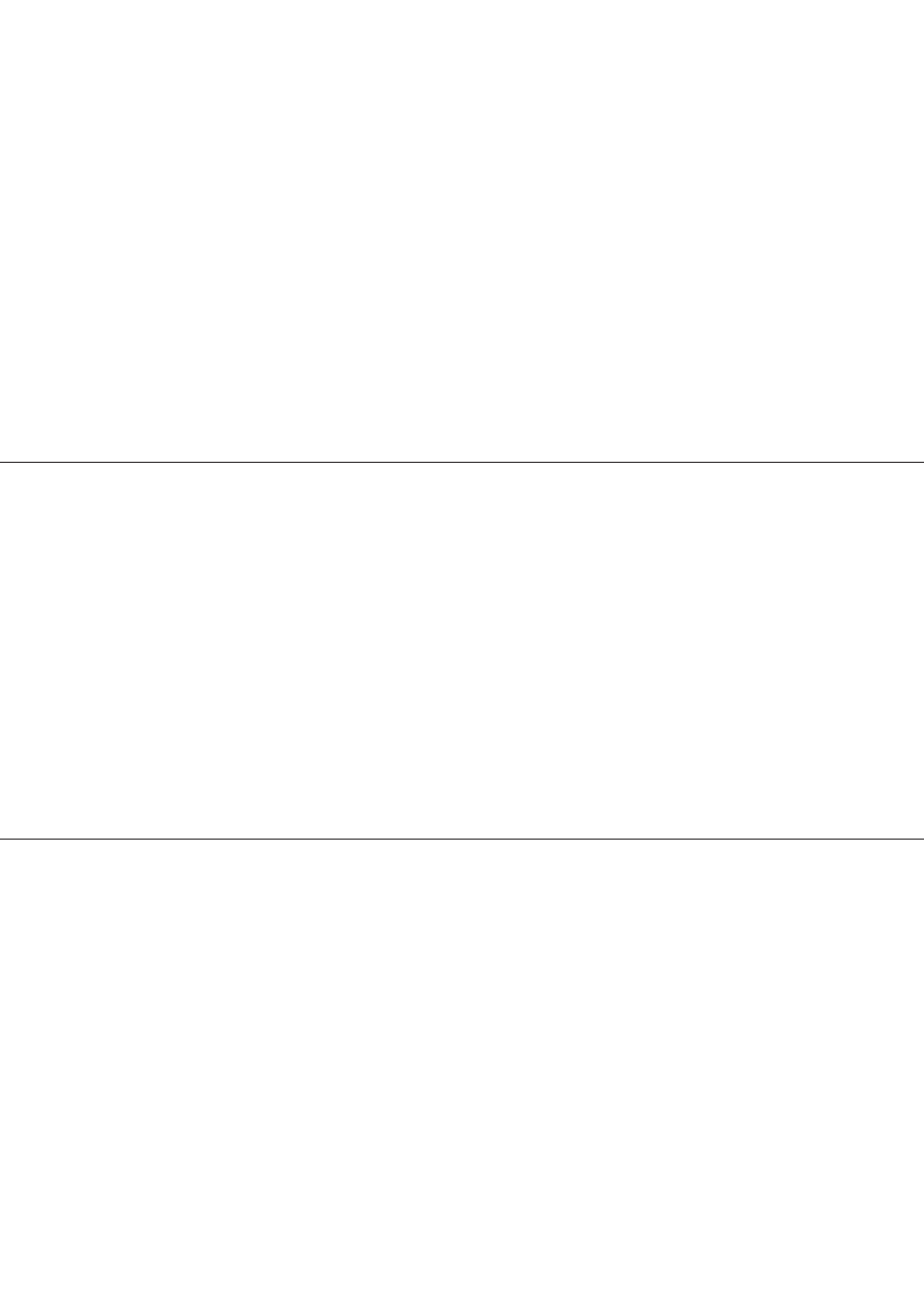
Chapter 3

- 3.1. AW performed *in vitro* and *in vivo* studies and statistical analyses, interpreted the data, and wrote the manuscript. BHB performed apoptosis, CAM studies, image analysis. JRvB participated in migration experiments, data interpretation and writing the manuscript. XD, IW and CMH participated in data modeling, data interpretation and writing the manuscript. TJW performed part of *in vitro* experiments. PJD participated in data interpretation and writing the manuscript. OD performed part of *in vitro* experiments and edited the manuscript. MD and ROS performed the tip cell study. RP and LS performed *in vivo* studies. HvdB conceived the study, participated in data interpretation and in writing the manuscript. AWG designed the study, analyzed and interpreted the data, and contributed in writing the manuscript. PNS conceived and designed the study, obtained permission for animal experiments, performed and coordinated the *in vitro* and *in vivo* experiments, and wrote the manuscript
- 3.2. RHB and AW performed the experiments, analyzed the data and wrote the manuscript. MGD, CC, MM-L and IK performed experiments and interpreted the data. JRvB and PM designed experiments and interpreted the data. PN-S

designed and supervised the study, edited the manuscript and interpreted the data. All authors edited the paper.

Chapter 4

- 4.1. MMP, ED and RMHM conceived the computational model. MMP performed the model simulations and analyzed their results. MGD, IK, and ROS conceived the experimental model. MGD performed the experiments and the image analysis. MMP performed the statistical analysis of the experimental results. MMP, MGD, and RMHM wrote the manuscript.
- 4.2. MGD, AWS and RPK performed *in vitro* and *in vivo* experiments , MGD, IK, CJFvN, ROS, GMD-T designed experiments and wrote the manuscript.
- 4.3. MGD and GMD-T wrote this manuscript.



6

.

4

PORTFOLIO

PORTFOLIO

Name PhD student: Marchien Geesje Dallinga

University of Amsterdam, Faculty of Medicine

Ocular Angiogenesis Group, department of Ophthalmology, Amsterdam Medical Center

PhD period: March 2012 – June 2016

Names PhD supervisors: Prof. dr. R.O. Schlingemann & Prof. dr. C.J.F. van Noorden

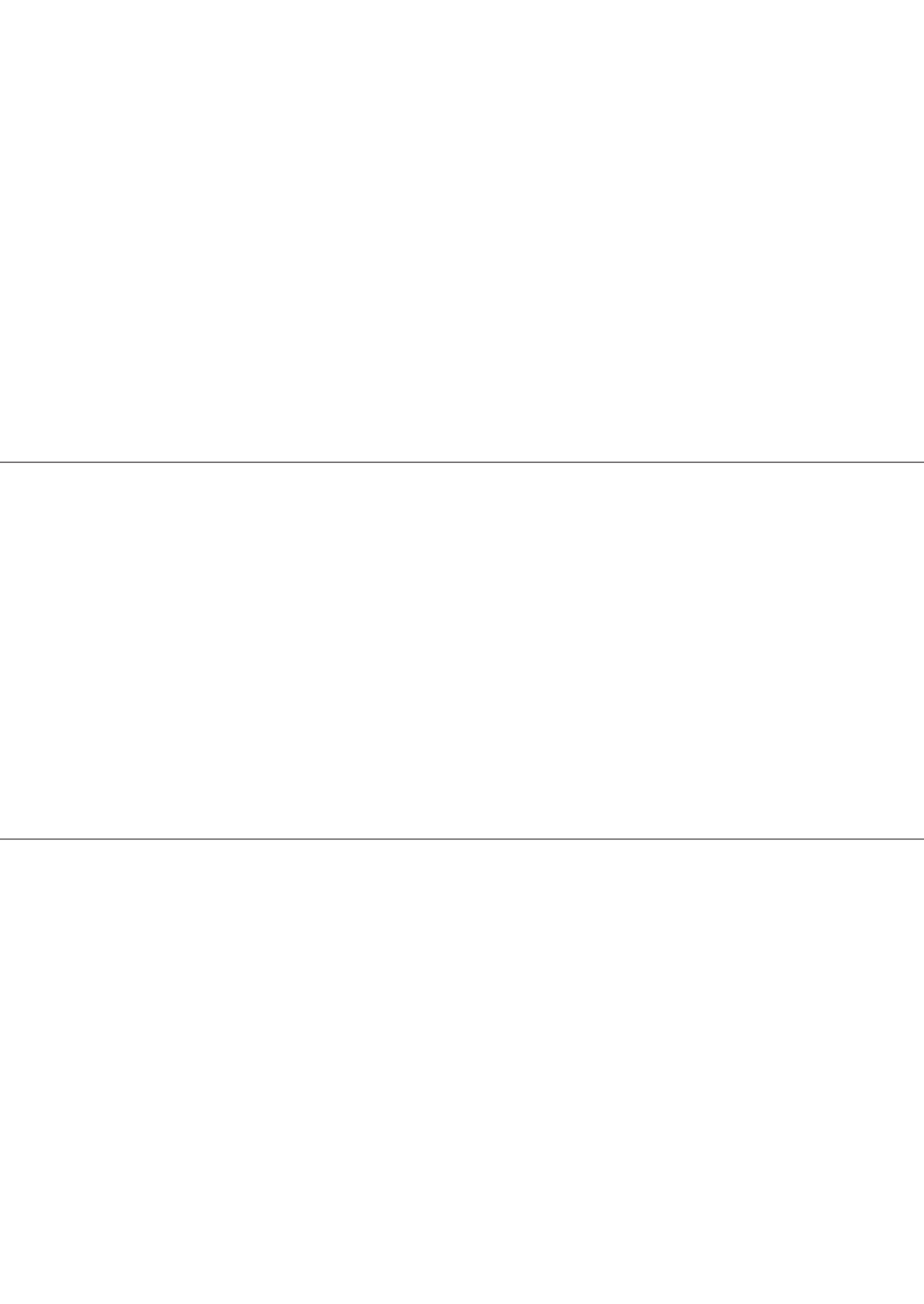
PhD training

General courses	Year	Workload (ECTS*)
Basic laboratory safety	2012	0.4
Laboratory animals	2012	3.9
Practical biostatistics	2012	1.1
Oral presentation	2013	0.8
Specific courses		
Microscopy course	2012	1.6
VR in a day	2014	0.4
Seminars, workshops and master classes		
Lorentz training workshop "Interdisciplinary Life Sciences"	2013	1
Minisymposium "Angiogenesis"	2013	0.2
Minisymposium "Biological Pattern Formation"	2014	0.2
Minisymposium "Angiogenesis and vascular permeability. Is there a link?"	2014	0.2
Rembrandt symposium	2014	0.2
Symposium "Combination Therapy of Cancer"	2015	0.2
Amsterdam Cardiovascular Research Institute symposium	2015	0.2
(Inter)national conferences		
Dutch Ophthalmology PhD Symposium	2012	1
Cell Symposia: Angiogenesis, Metabolic Regulation and Cancer Biology	2012	0.75
Amsterdam retina debate	2012	0.25
Dutch Ophthalmology PhD Symposium	2013	1
NOG annual meeting	2013	0.75
EASDEC	2013	0.75
Dutch Ophthalmology PhD Symposium	2014	1
Vth International Meeting on Angiogenesis	2014	0.75
Amsterdam retina debate	2014	0.25
ARVO annual meeting	2015	1.25
Joint Dutch-German Microcirculation Meeting	2015	0.75

Portfolio (continued)

Presentations	Year	Workload (ECTS*)
Oral presentations:		
Dutch Ophthalmology PhD Symposium	2013	
Minsymposium "Biological Pattern Formation"	2013	0.5
EASDEC conference	2013	0.5
The Bayer Ophthalmology Research Award	2015	0.5
Poster presentations		
Vth International Meeting on Angiogenesis	2014	0.5
Rembrandt symposium	2014	0.5
ARVO	2015	0.5
Joint Dutch-German Microcirculation meeting	2015	0.5
Amsterdam Cardiovascular Research Institute meeting	2015	0.5
Other		
UCL Institute of Ophthalmology (London) various lectures and symposia	2013/2014	2
Organizing committee Dutch Ophthalmology PhD Symposium	2013/2014	1
Teaching		
Lectures		
Werkcollege "Bindweefsel" - September 2014	2014	0.3
Werkcollege "De cel" - September 2015	2015	0.3
Werkcollege "Bindweefsel" - September 2015	2015	0.3
Supervision		
Richelle Kayser - Master internship	2012	3
Maik Brouwer - Bachelor internship	2013	1
Konstantin Ivanov - Master internship	2015	1
Esmee Engelman - Bachelor thesis	2015	0.4
Clinical Cell Biology Course - Ocular Angiogenesis	2013	1
Clinical Cell Biology Course - Ocular Angiogenesis	2014	1
Other		
Linde Lanting - post-master internship	2015	1
Parameters of Esteem		
Grants		
Uitzicht 2013-12 "What is the role of IGF-2 in retinopathy of prematurity?"	2013	
Awards and Prizes		
The Bayer Ophthalmology Research Award - Finalist	2015	
Cellular Imaging image contest - Winner	2016	

* 1 ECTS (European Credit Transfer System) equals a workload of 28 hours.



6

.

5

DANKWOORD

DANKWOORD

8 jaar, dat is best lang voor promotieonderzoek, zeggen ze. Vind ik ook wel. Maar het verhaal is compleet en mijn proefschrift is af. In 2012 begon het allemaal. Als broekie, vers uit de geneeskunde opleiding en geïnspireerd door mijn wetenschapsstage in het lab in Los Angeles wilde ik promotie onderzoek doen. Liefst in een lab, lekker bezig zijn. In het AMC was een plekje en daar ging ik, op zoek naar de werking van tipcellen. Cellen kweken, proefjes doen, resultaten bekijken en weer nieuwe proefjes bedenken. Zonder specifieke opleiding stond ik in het lab, alleen pipetteer-les gehad van Han. En toch heb ik het kunnen doen allemaal. Maar niet zonder hulp natuurlijk.

Ingeborg, jij eerst. Co-promotor en mentor in het lab, we bespraken elke week mijn plannen voor de experimenten, we keken naar de resultaten en probeerden te bedenken wat het zou kunnen betekenen. Geduldig als ik iets niet begreep, enthousiast als jij ook de waarde van een bevinding zag, en liefde voor het vak en voor de tipcellen. Maar ook de verbinder van ons kleine groepje en degene die iedereen even goed leek te begrijpen. Reinier en Ron boffen maar met jou erbij.

Reinier, de grote baas. Jij bent degene die het zag zitten om mij onderzoek naar de tip cellen te laten doen. Jij bent ook degene die de kleinste details altijd weer naar een groter mechanisme weet te vertalen. Heel knap en onmisbaar in het geheel van de groep.

Ron, ook de grote baas, maar dan anders. Het celbiologisch brein in de groep. Anders dan Reinier weet jij juist weer de details die de experimenten met elkaar verbinden. De eigenschappen van cellen en eiwitten waar anderen niet aan denken. Jij bent dan ook degene die in de teksten de meeste eisen stelt en de details eruit pikt die niet kloppen. En dat zullen we weten ook, anders wordt het nooit beter. De laatste promotor in Nederland die teksten met de hand corrigeert?

Dan mijn lieve paranimfen. Richelle: eerst student, daarna collega, wat was ik blij dat jij na je stage bij de groep mocht blijven als analist. Alle experimenten die je hebt gedaan. Alle cellen die je hebt geïsoleerd. Het blinderen van de sferoid-experimenten was altijd een hoogtepunt. Ik heb ze nog eens even teruggekeken: acteurs, Nederlandstalige muziek, sprookjes, alle categorieën kwamen voorbij. En dan achteraf raden wat wat was, altijd fout natuurlijk. We leven voort als team van Nieuwland. Ik vind nog steeds dat je oogarts moet worden, dan kunnen we mooi weer samenwerken. Meta: vriendin, de beste net-niet olympische keepster van Nederland en voorbeeld wat je promotie betreft. Jij moest ook je promotie nog afmaken toen je contract klaar was. maar dat kwam wel, net als bij mij. Eerst die andere baan beginnen. Jou is het ook gelukt. Toen dacht ik: dan kan ik het ook, moet gewoon lukken. En nu is het voor ons beide klaar en kunnen we lekker op pad met de kindjes en naar de bios-met-bediening. Allebei heel erg bedankt voor jullie steun.

Op de afdeling celbiologie bestaan we als de OAG, de Ocular Angiogenesis Group. Behalve Ingeborg als rots in de branding is er het nodige veranderd. Promovendi komen en gaan, natuurlijk, maar ook Ilse, onze vast analist en skyradio-fan is inmiddels lekker met pensioen. Ik denk nog altijd aan je als ik smeerkaas zie, vaste prik bij de lunch. Zonder jou had onze groep het nooit zo goed gedaan. Martin, grondlegger van het hele project door het identificeren van de tipcellen en het uitvoeren van de microarray waardoor ik veel kandidaat-genen had om te bestuderen. Dank voor je hulp bij het opstarten! Bahar, Anne-Eva en Joanna, de andere promovendi in de OAG: dank voor de gezelligheid en hulp. Kosyo en Maik, stagiairs, zeldzame mannen in onze vrouwenclub op het lab. Ook jullie erg bedankt voor je hulp en succes met wat jullie verder allemaal gaan uitspoken in de toekomst.

Iedereen van de vasculaire: Bedankt dat ik als “dochter-van-Geesje” mocht aansluiten bij het jaarlijkse bowling toernooi en de gezellige borrels. En fijn dat ik jullie apparaten mocht gebruiken als de onze stuk waren, ideaal!

6.5

Mike and Marcus at the institute of ophthalmology in London. Thanks so much for your help and allowing me to visit your lab. It's been a real eye-opener and I've had a great time. Alle co-auteurs en iedereen met wie ik heb samengewerkt: bedankt, ik vond het heel leuk om bij jullie allemaal in het lab te kijken en met jullie samen te werken.

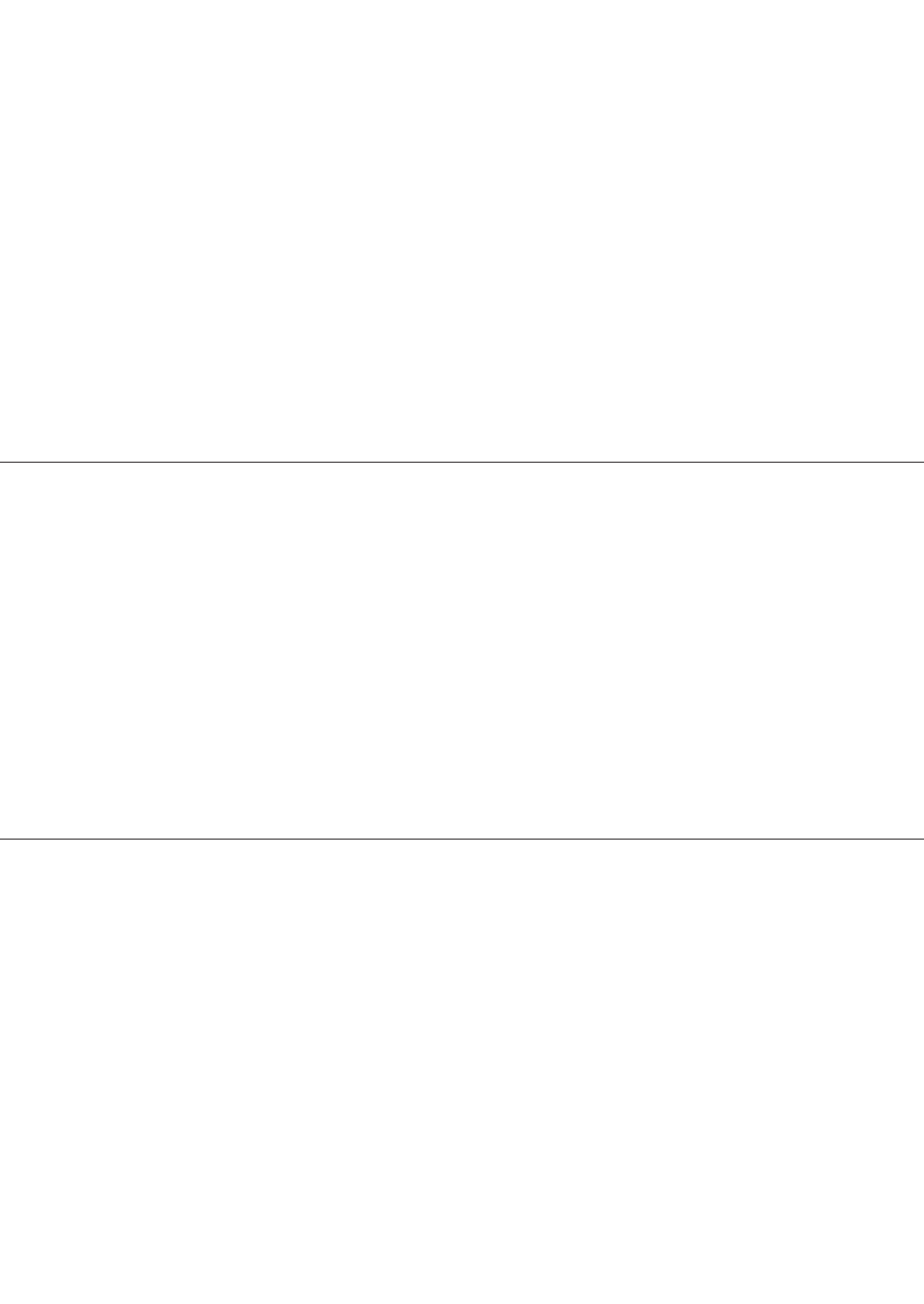
AIOS oogheelkunde: jullie zijn geweldig! Ann-Sofie: nu jij! Minions: nu hebben we tijd voor onze cornea-kliniek.

Musketiers: Sinds de eerste dag van de introductie van geneeskunde hebben we elkaar vast en laten we niet meer los. Bedankt voor de mentale support en bezoeken aan de sauna etc. ter afleiding.

Mam, pap, Onne, Wiecher: Zonder familie wordt het niets. Mam: bedankt voor het nakijken van de manuscripten. Hoe makkelijk is het als je moeder precies begrijpt waar je tegenaan loopt en waar je mee bezig bent. En nog leuker dat we 2 mooie papers in dit boekje samen hebben kunnen maken. Bedankt voor je hulp. Pap: als ik het boekje af kan maken kun jij het ook!

En natuurlijk als laatste mijn liefdes thuis: Arnoud en Fiene. Arnoud, jij begon ongeveer tegelijk met mij begonnen met je promotie en we kwamen elkaar tegen in het begin. Ik ben zo blij dat ik je tegenkwam bij de pubquiz in Utrecht en ik hou van je. Kleine Fiene, jij snapt er nog niet veel van, maar je vrolijke schaterlach kan iedereen smelten en vrolijkt me zo weer op als iets tegen zit. Kus van mama.

Alle typfouten in dit proefschrift wijdt ik aan onze kat, Japie, die tijdens zijn liefdevolle ondersteuning over het toetsenbord loopt.



6

CURRICULUM VITAE



6

CURRICULUM VITAE

Marchien Dallinga was born on February 8th, 1988 in Wageningen, the Netherlands. After completing her secondary school (VWO-certificate, Nature and Health) at the “Pantarijn Scholengemeenschap” in Wageningen, she started medical school at the Rijksuniversiteit Groningen in 2005. During her final year of medical school, she spent 5 months in Los Angeles (University of California, Los Angeles, USA) in the laboratory of prof. A.J. Lusis for her research internship on the role of TMAO in atherosclerosis. Upon returning to the Netherlands, Marchien started to pursue a career in ophthalmology by spending her final internship at the Department of Ophthalmology at the Erasmus Medical Center, under supervision of prof C.C.W. Klaver. She started her PhD project on tip cells in endothelial cell cultures in March 2012 at the University of Amsterdam under supervision of Prof R.O. Schlingemann and Prof C.J.F. van Noorden. In 2013 she spent 6 months in the laboratory of dr. M. Fruttiger (University College London, Moorfields Eye Hospital, London, UK) to perform in situ hybridization on mouse retinas. Marchien has been working as a resident in Ophthalmology in the Department of Ophthalmology at the Academic Medical Center in Amsterdam since July 2016.

